Metallo-Supramolecular Complexes and their Interactions with Biomolecules and Cells

UNIVERSITY OF BIRMINGHAM

SUKRAJ KAUR BANWAIT

A thesis submitted in partial fulfilment of the requirements for the degree of Doctor of Philosophy in Chemistry

September 2009

Acknowledgements

I wish to express my heartfelt gratitude to the following people who have helped make this thesis possible:

First and foremost, I would like to thank my Guru ji for never leaving my side and for guiding me and blessing me so much. I am also grateful to Sati and my family for their patience and love throughout my PhD. In particular, I want to thank my mum and dad for their unwavering support and encouragement throughout my studies, my brother, Jas, and my sisters, Rav, Suky and Kam, and true friends who pushed me to succeed and were always there to lift my spirits.

I would like to thank my supervisor Professor Mike Hannon for giving me the opportunity to carry out this research in his group and for providing me with a stimulating research project.

I am grateful to Professor Kevin Chipman for allowing me to use his laboratories and Nik Hodges for guiding me through the comet assay experiments. A special thank you to Shrikant Jondhale for letting me take over his bench for days at a time and for helping me with the Ames tests and of course for the routine pub lunches! I would also like to thank Dr. Felix Zamora and his group for making me feel so very welcome at the Universidad Autonoma de Madrid where I carried out the AFM experiments. I am especially thankful to Lorena for teaching me so much about AFM and everything Spanish!

I am grateful to all the people who have carried out analyses on my behalf: Dr. Benson Kariuki and Dr. Louise Male for X-ray analysis, Dr. Peter Ashton and Nick May for mass spectrometry, Dr. Neil Spencer for NMR experiments and Lianne Hill for elemental analysis.

Finally, I would like to thank Katia Ryabova, Anna Hotze and Carlos Sanchez-Cano for their contributions to this work, Lexi and Anna for their meticulous proof-reading and the rest of the Hannon group, past and present, for their support and friendship and for teaching me so much about everything! I am truly grateful to you all.

Abstract

Chapter 1 introduces the field of supramolecular chemistry and reviews examples of supramolecular architectures. Applications of these assemblies are outlined with a focus on DNA recognition.

In chapter 2 the synthesis and characterisation of an array of palladium(II) and platinum(II) tetra-stranded, dinuclear complexes is described. The synthesis of two palladium(II) triangles and a palladium(II) pyramid are also presented.

Chapter 3 investigates the biological activities of four of the tetra-stranded palladium(II) complexes described in chapter 2. The results show that while all of them bind to DNA, only two show good cytotoxic activities in an MTT assay. Toxicological studies were conducted on the two active cylinders and excitingly, the preliminary results indicate that they are not genotoxic or mutagenic.

In chapter 4 the interaction of two novel single-stranded palladium(II) and platinum(II) complexes with B-DNA is probed by circular and linear dichroism and gel electrophoresis. The study confirms that the complexes bind to DNA, causing it to kink and bend.

Chapter 5 presents the synthesis and crystallographic characterisation of four new silver(I) supramolecular polymers.

In chapter 6 a new pyridylazo ligand system is described and the coordination chemistry of this ligand with silver(I), copper(I) and palladium(II) investigated.

Abbreviations

Å	Angstroms ($1x10^{-10}$ m)
AFM	Atomic Force Microscopy
br	Broad
CD	Circular dichroism
CD_3CN	Deuterated acetonitrile
CD_3OD	Deuterated methanol
$CDCl_3$	Deuterated chloroform
cr	Cis-platin resistant
ct-DNA	Calf thymus DNA
d	NMR- doublet
DMEM	Dulbecco's Modified Eagle's Medium
DMSO	Dimethylsulfoxide
d_6-DMSO	Deuterated dimethylsulfoxide
DNA	Deoxyribonucleic acid
ε	Extinction coefficient (mol^{-1} dm^{-3} cm^{-1})
EI	Mass spectrometry- electron impact
ESI	Mass spectrometry- electrospray ionisation
Et	Ethyl
EtOH	Ethanol
IR	Infrared
J	NMR- coupling constant
K	Kelvin
LD	Linear dichroism

LMPA	Low melting point agarose
m	Infrared- medium
m	NMR- multiplet
M	Molar (mol dm^{-3})
MeCN	Acetonitrile
MeOH	Methanol
m/z	Mass spectrometry- mass/charge
Me	Methyl
mM	milli-molar concentration ($1x10^{-3}$ mol dm^{-3})
NMPA	Normal melting point agarose
NMR	Nuclear magnetic resonance
NS	Negatively supercoiled DNA
OC	Open circular DNA
Ph	Phenyl
Ppm	parts per million
PS	Positively supercoiled DNA
$r_{(c)}$	number of cylinders bound per plasmid
RPMI-1640	Roswell Park Memorial Institute
σ	Superhelicity constant
s	Infrared- strong
s	NMR- singlet
t	NMR- triplet
TAE	Tris-acetate-EDTA
TFA	Trifluoroacetic acid
THF	Tetrahydrofuran

μM	micro-molar concentration ($1x10^{-6}$ mol dm^{-3})
UV/vis	Ultraviolet/ visible
w	Infrared- weak
δ	NMR- chemical shift
ϕ	Unwinding Angle

Declaration

The experimental work, observations and recommendations reported in this thesis are those of the author unless specifically stated and have not previously been submitted as part of a degree at the University of Birmingham, or any other institution.

Contents

Chapter 1

Introduction

1.1 Overview

Since the discovery of the leading anti-cancer drug cis-platin, metal complexes that bind to DNA have attracted a great deal of attention. In the Hannon group, research has been focused on non-covalent DNA recognition by metallo-supramolecular complexes. The supramolecular methodology has allowed the construction of large synthetic agents that have been shown to bind non-covalently to DNA and cause remarkable and unprecedented effects on its structure. Advances in this field have shown that the supramolecular approach is a valuable tool for the design of new DNA recognition agents. In this introduction, the principles of supramolecular chemistry will be discussed and some examples of the types of architectures formed will be presented.

1.2 Supramolecular Chemistry

Molecular chemists have developed a large collection of reliable procedures for preparing complex molecules and materials from atoms connected by covalent bonds.[1] Beyond the molecule, supramolecular chemistry has been described by one of its pioneers, Jean-Marie Lehn, as the 'chemistry of molecular assemblies and of the intermolecular bond'.[2] In broader terms it is the self-assembly of small molecular subunits into larger arrays via non-covalent, intermolecular interactions. The simple self-assembly process rules out the need for complicated, multi-step organic synthesis and is the key driving force in the formation of supramolecular structures. The interactions involved in the self-assembly process include metal ion coordination, aromatic π-π stacking, solvent effects, hydrogen bonding and host-guest interactions, each one varying in its binding strength. The controlled utilisation of one or more of these

interactions has enabled the design and synthesis of a multitude of supramolecular architectures.[3]

1.3 Metallo-Supramolecular Architectures

The successful synthesis of supramolecular assemblies is reliant on the careful selection of the starting materials and the reaction conditions, thus permitting self-assembly to occur in a controlled manner. Metallo-supramolecular chemistry is a term used to describe metal-mediated self-assembly. In this field, the emphasis lies in the careful design of the organic ligands and the appropriate selection of the metal ions.[4] The metal ions are used as templates in the organisation of the molecular building blocks and are thus chosen for their coordination numbers and stereochemical preferences. The ligands are designed with the appropriate features required for the formation of the synthetic target i.e. with the appropriate use of spacer groups and the correct number and spatial arrangement of the donor sites. Metal-directed self-assembly plays a key role in supramolecular chemistry and has led to the development of an array of highly sophisticated architectures including boxes,[5] helicates,[6] triangles[7] and grids.[8] Some examples of these are discussed in more detail in the following sections.

1.4 Supramolecular Helicates

First introduced by Jean-Marie Lehn in 1987, the term helicate is used to describe supramolecular structures in which ‘one or more covalent organic strands are wrapped about and coordinated to a series of metal ions defining the helical axis’.[9] Helicates are formed by self-assembly, therefore the subunits

must be pre-designed so that they are complementary in the formation of the helical structure. The metal ions are chosen for their coordination number and geometry preferences which should be closely matched to the properties of the ligand. The ligands are designed with two or more binding sites that are capable of coordinating to the chosen metal ion(s). The spacer group between the binding sites should be flexible enough to allow the ligand to wrap about the helical axis, but also rigid enough to prevent multiple binding sites of that ligand from coordinating to the same metal centre.

Helicates can be classified as homotopic or heterotopic. If the coordinated ligand strands contain similar binding sites along their length, they will form homotopic helicates. If the ligand strands possess dissimilar binding sites, the resulting helicates will be heterotopic. As shown in Scheme 1.1, heterotopic helicates exist in two isomeric forms.[10]

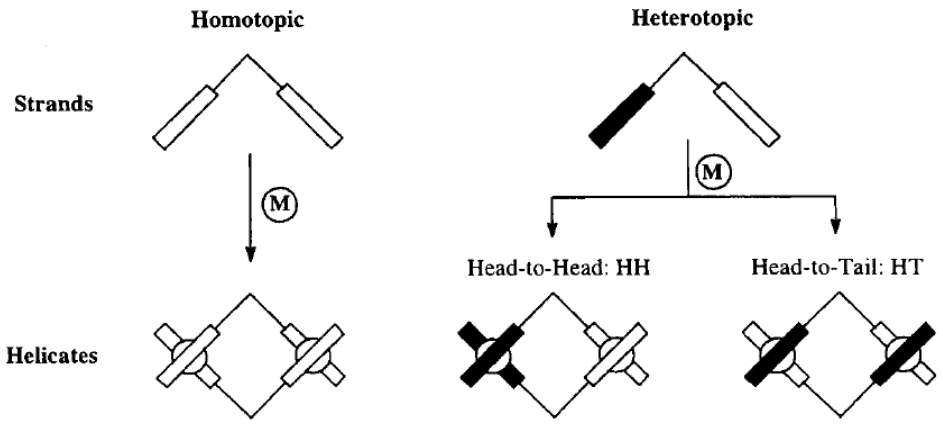

Scheme.1.1. A schematic representation of homotopic and heterotopic helicates (Taken from reference 10).

A number of helical structures have been reported. The majority of these structures contain either one, two, three or four ligand strands. Some interesting examples of supramolecular helicates are discussed in the following section.

1.4.1 Single-Stranded Helicates

Single-stranded helicates can be formed by employing a metal ion which is too small to fit the cavity of a multi-dentate ligand. A small twist is induced in the ligand to minimise the steric interactions between the two ends of the strand.

In 1988 Constable *et al.* reported the formation of a single-stranded helicate from the reaction of silver(I) acetate with 2,2’:6’,2”:6”,2”’:6”’,2””-quinquepyridine (**La**). Constable found that the silver(I) ion was too small for the gap between the pyridine rings. Therefore, when the five nitrogen donors bind to the metal ion the ligand is forced to wrap around it with a slight helical twist (Figure 1.1). [11]

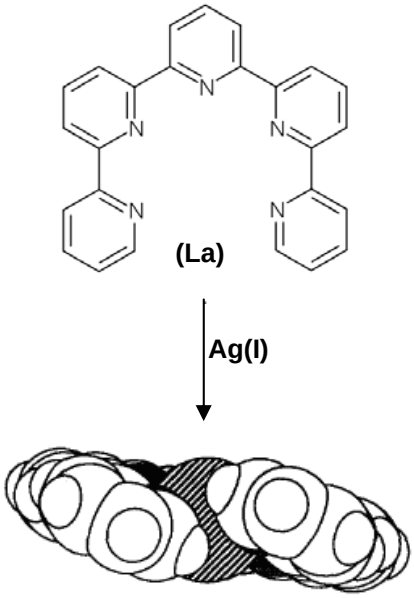

Figure 1.1. Constable’s single-stranded helicate.[11]

More recently, Zhang and co-workers have used a tetra-dentate ligand system (**Lb**) to generate a single-stranded copper(II) helicate. The metal centre is five-coordinate with the fifth position being occupied by a water molecule. Once again the ligand cavity is too large for the copper(II) centre resulting in the

formation of a helical structure (Figure 1.2). Zhang has also shown that a silver(I) double-stranded helicate can also be formed using this ligand.[12]

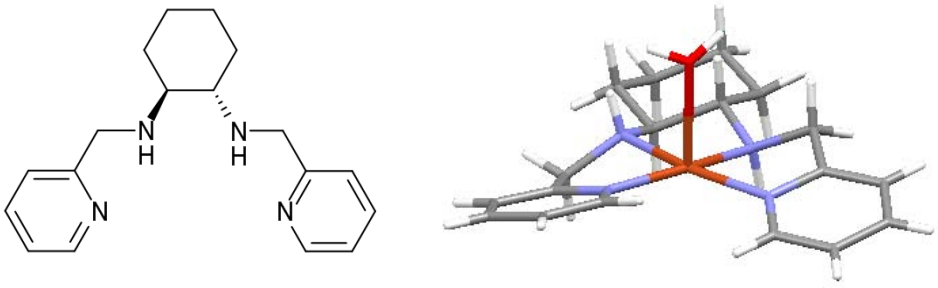

(a) **(b)**

Figure 1.2. Zhang's (a) Ligand **Lb** and (b) single-stranded copper(II) helicate.[12]

1.4.2 Double-Stranded Helicates

An abundant literature reports the formation of double-stranded helicates. Ligand **Lc** is one of the first ligands pre-designed to encourage the formation of a double helicate by virtue of steric interactions between the four methyl groups (Figure 1.3 (a)).[13]

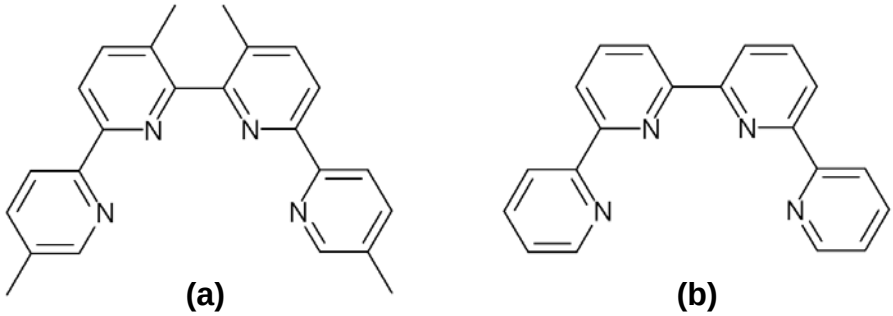

(a) **(b)**

Figure 1.3. (a) Ligand **Lc** and (b) Ligand **Ld**.

As anticipated, the reaction of **Lc** with copper(I) results in the formation of a double-stranded $[Cu_2L_2]^{2+}$ helicate. Interestingly, Constable *et al.* later discovered that the reaction of copper(I) with the less sterically hindered ligand **Ld** (Figure 1.3 (b)) also resulted in the formation of a double helicate.[14] This result shows that the tetrahedral coordination geometry of the metal centre was

enough to induce helicate formation. However, the Cu···Cu separation is larger in the methylated complex than in the nonmethylated one, indicating that the methyl groups do play an important role in controlling the pitch of the helical structure.

Most double-stranded helicates are formed from ligands consisting of bidentate binding sites and metal ions preferring four-coordinate geometry. However, a small number have also been prepared from ligands with terdentate binding sites and six-coordinate metal centres. One of the simplest examples involves the reaction of the poly-pyridyl ligand **La** with six-coordinate metal centres such as iron(II), nickel(II) and ruthenium(II) resulting in the formation of double-stranded helicates (Figure 1.4).[15] This is a prime example of how the self-assembly process can be controlled by the selection of the subunits.

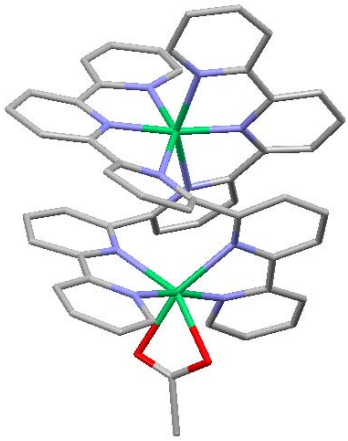

Figure 1.4. Constable's double-stranded nickel(II) helicate.[15]

Double helical architectures have also been synthesised using macrocyclic ligands. One of the first examples was provided by Fenton *et al.* who coordinated the Schiff base macrocycle **Le** to cobalt(II), nickel(II) and zinc(II). The X-ray crystal structure of the zinc(II) complex of **Le** is shown in

Figure 1.5 (b).[16] The large macrocyclic ring is compressed so that the metal ions, which occupy a distorted octahedral environment, can be accommodated.

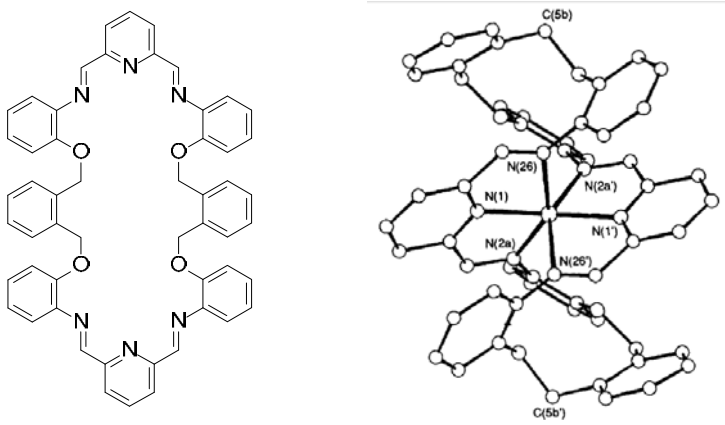

(a) **(b)**

Figure 1.5. (a) Ligand **Le** and (b) X-ray crystal structure of Fenton's zinc(II) helicate.[16]

1.4.3 Triple-Stranded Helicates

A multitude of triple-stranded helicates have been reported using three, six or nine-coordinate metal ions. The first structurally characterised triple helicate was reported by Williams *et al.* in 1991.[17] Williams incorporated a rigid spacer into the ligand (**Lf**) preventing it from acting as a tetra-dentate chelator. Therefore, the reaction of the ligand with six-coordinate cobalt(II) resulted in the formation of the triple-stranded helicate shown in Figure1.6.

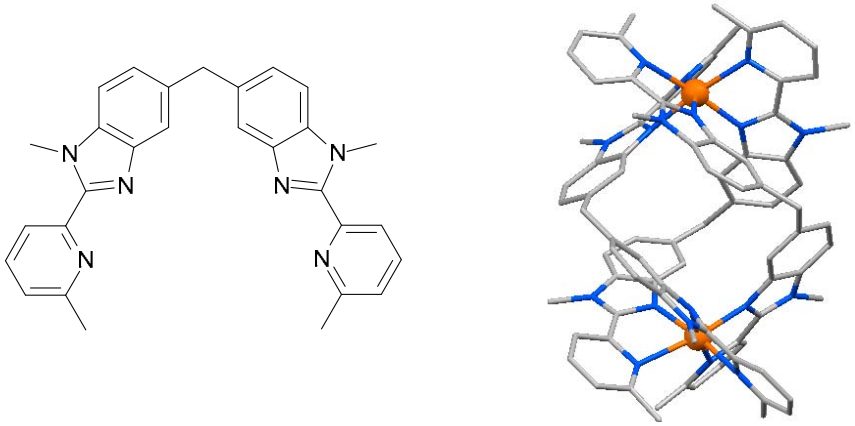

(a) **(b)**

Figure 1.6. (a) Ligand **Lf** and (b) William's triple-stranded helicate.[17]

The ligand has also been shown to form double-stranded helicates in the presence of four-coordinate metal centres such as copper(I).[18]

More recently, Hannon and co-workers have investigated the use of imine-based ligands such as **Lg** in the formation of an array of different helicates.[19] Figure 1.7 shows the formation of a triple-stranded helicate on coordination of **Lg** to iron(II).[20]

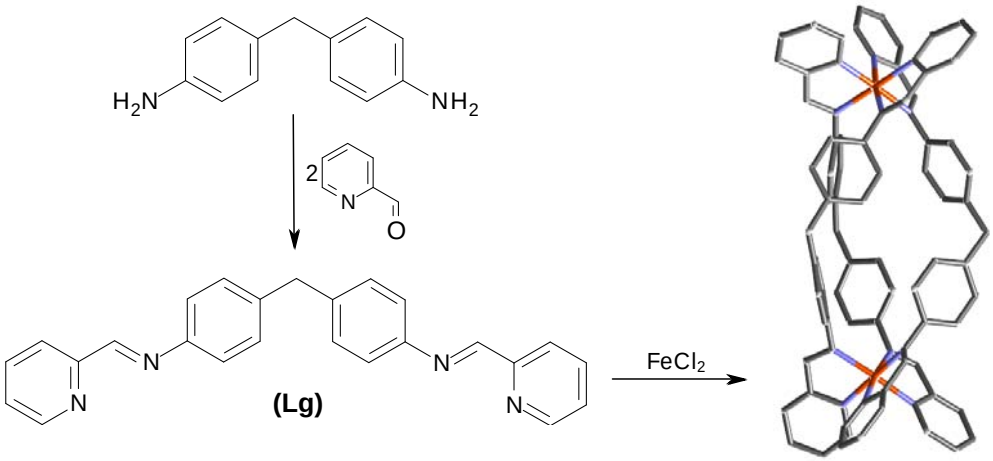

Figure 1.7. Hannon's triple-stranded helicate.[20]

The helicate formation is induced by the six-coordinate metal centres and the pre-designed structure of the ligand. The central methylene group incorporates flexibility into the ligand and the spacer groups sterically prevent the two bidentate binding sites from coordinating to the same metal ion. The ligand also has the advantages of being very inexpensive and easy to prepare.

During the last two decades hundreds of helicates have been reported, however, only a few heteronuclear metallo-helicates have been described. Piguet and co-workers have described the synthesis of heteronuclear helicates using ligand **Lh**. This heterotopic ligand consists of bi-dentate and tri-dentate binding sites separated by a rigid spacer unit. Therefore, the self-assembly of

Lh with ruthenium(II) and europium(III) metal ions results in the formation of the heteronuclear helicate shown in Figure 1.8.[21]

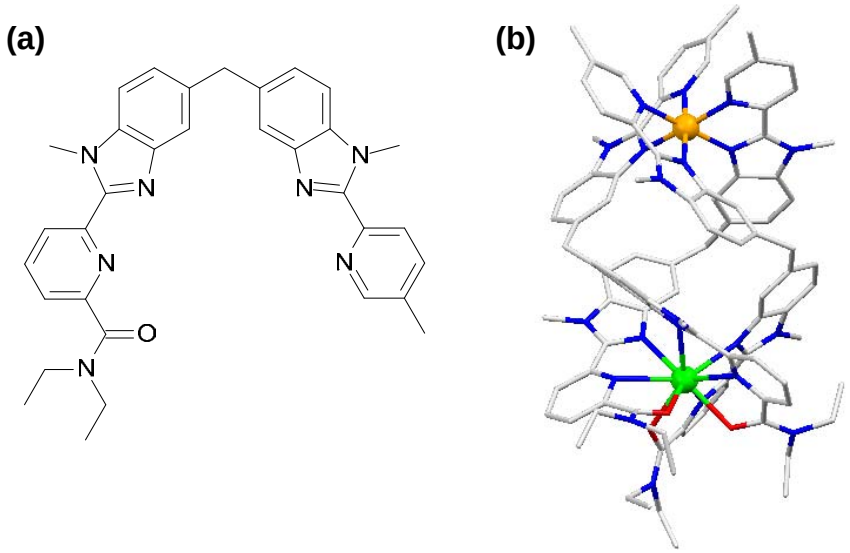

Figure 1.8. (a) Ligand **Lh** and (b) Piguet's heteronuclear helicate.[21]

1.4.4 Quadruply-Stranded Helicates

In 1998 Steel *et al.* were the first group to report the formation of a coordinatively saturated, quadruply-stranded helicate (Figure 1.9). This was achieved by employing a combination of four **Li** ligands and two square planar palladium(II) metal centres in a self-assembly process.[22]

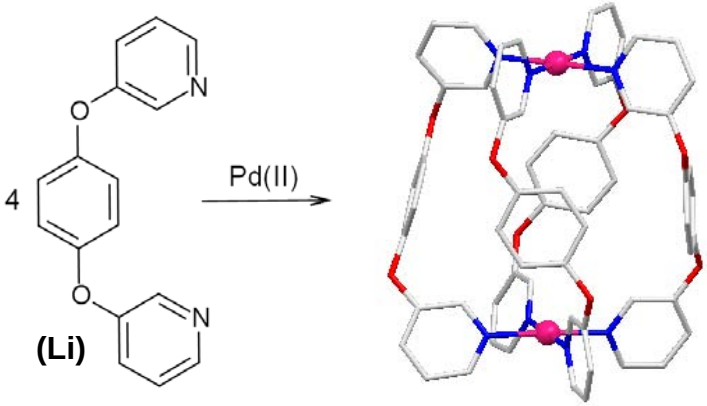

Figure 1.9. Steel's quadruply-stranded helicate.[22]

The X-ray crystal structure of the helicate revealed that a hexaflurophosphate ion is encapsulated within the central cavity. This is the first example in which a

polyatomic anion has been encapsulated within any helicate. Therefore the structure could prove useful in the potential use of helicates in host-guest recognition processes.

1.4.5 Applications of Helicates

Although the last two decades have seen the emergence of hundreds of beautiful helicates, much of this research has been aimed at enhancing our knowledge of the self-assembly processes and not on the potential applications of the end products. However, now that our understanding of this field has become more advanced a number of potential applications have slowly begun to emerge.

Many helicates are able to act as hosts in the binding and recognition of anionic guests: Rice and co-workers[23] have observed the binding of a nitrate anion by a cobalt(II) triple-stranded helicate and Janiak *et al.*[24] have reported anion binding within clefts formed by mononuclear $[FeL_3]^{2+}$ helicates. In 2006 Kruger *et al.* reported three triple-stranded helicates that have been specially designed to act as anion receptors. The helicates were formed from the ligands shown in Figure 1.10.[25]

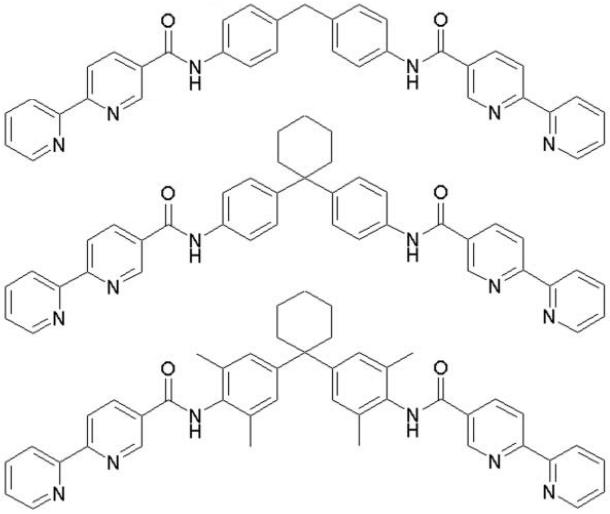

Figure 1.10. Kruger's helicating ligands.

^{1}H NMR titration experiments of the helicates with Bu_4NCl showed that they are capable of binding chloride anions within their intra-helical cavities in a host:guest ratio of 1:2. A molecular model for the proposed mode of binding is shown for one of the helicates in Figure 1.11.

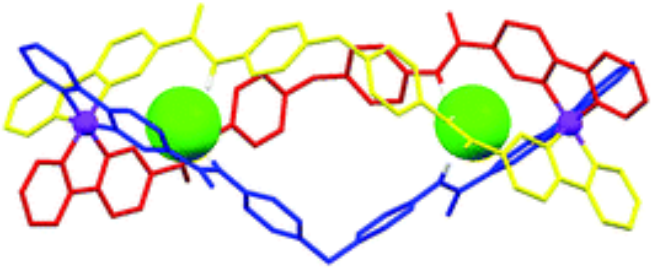

Figure 1.11. Molecular model of the triple helical $[Fe_2L_3]^{4+}$ complex showing the proposed mode of binding of two chloride ions (shown in space filling mode) within the intrahelical cavity.[25]

Another important application of supramolecular helicates lies in the pharmaceutical industry. Most important anti-cancer drugs involve molecules that interact directly with DNA. Lehn, Hannon, Sletten and Moreno have described supramolecular helicates which are capable of binding to and modifying the structure of DNA.[26] The DNA binding of helicates will be discussed in more detail in section 1.7.

1.5 Prismatic Supramolecular Architectures

1.5.1 Trigonal prismatic cages

Silver(I) ions are known to display a flexible coordination geometry varying from two-coordinate to six-coordinate. In 2001, Su and co-workers reported the synthesis of a trigonal prismatic cage from silver(I) ions and ligand **Lm**. The X-ray crystal structure shows that the two silver(I) centres occupy a trigonal planar geometry and are coordinated by three imino nitrogen atoms

(Figure 1.12). The central cavity of the cage is accommodated by a distorted triflate anion.[27]

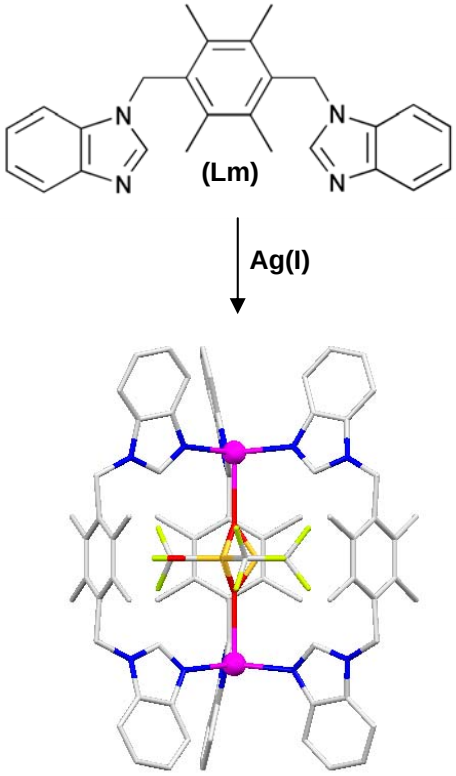

Figure 1.12. Su's trigonal prismatic cage.[27]

In 2005, Du *et al.* reported a trigonal cage formed by the reaction of tetrahedral copper(I) ions with ligand **Ln** (Figure 1.13). [28]

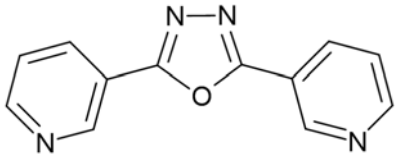

Figure 1.13. Ligand **Ln**.

In this case one of the metal coordination sites is occupied by an acetronitrile solvent molecule and the other three are coordinated to the nitrogenous ligands. The X-ray crystal structure reveals that each prismatic cage hosts a water molecule inside the central cavity (Figure 1.14).

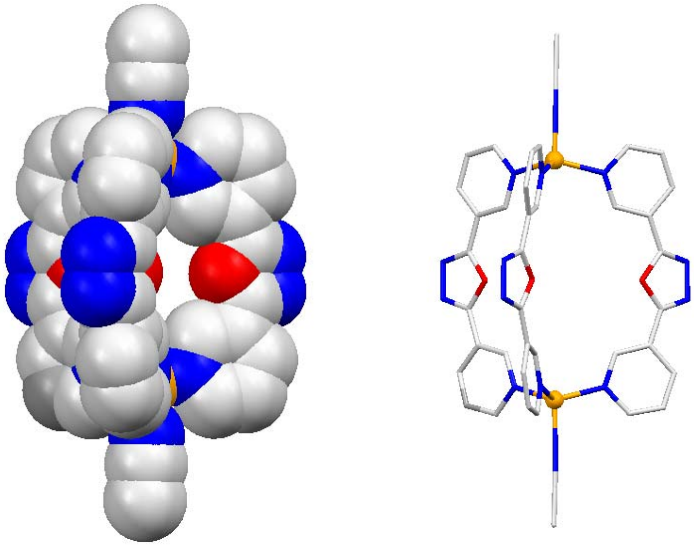

Figure 1.14. Du's copper(I) trigonal prismatic cage.[28]

1.5.2 Tetragonal prismatic cages

Metallo-supramolecular chemistry facilitates the formation of elaborate architectures that would be difficult, if not impossible to achieve using classical organic chemistry. In 1998, Atwood *et al.* were the first group to report the formation of a M_2L_4 cage, achieved by employing four bidentate ligands (**Lo**) bound to two octahedral copper(II) ions (Figure 1.15).[29]

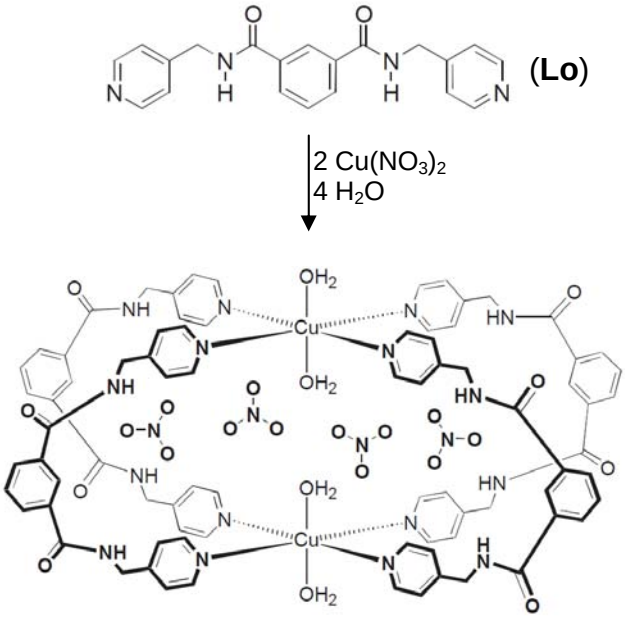

Figure 1.15. Atwood's tetragonal prismatic cage.[29]

This is an example of a tetragonal prismatic cage in which the axial positions are blocked by the use of water molecules. Similar examples incorporating cobalt(II) and zinc(II) have also been reported.[30]

Another tetragonal prismatic architecture was constructed by Su and co-workers using the previously described ligand **Lm** with copper(I) (Figure 1.16).[27] In this case each copper(I) metal centre adopts a square planar coordination environment and makes short contacts to an encapsulated perchlorate anion. A nickel(II) analogue of this complex has also been reported.[31]

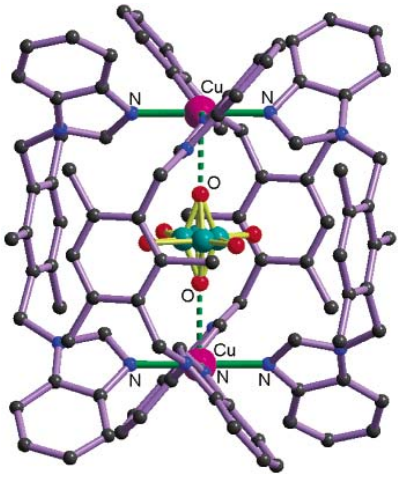

Figure 1.16. Su's copper(I) tetragonal prismatic cage.[27]

More recently, Su *et al.* have also presented the formation of another tetragonal cage using the bis-monodentate ligand **Lp** and copper(II) ions instead of copper(I) (Figure 1.17).[32] The six-coordinate metal centres bind four different pyridyl nitrogen atoms in the equatorial positions enabling the prismatic structure to be formed. The axial positions are occupied by anions.

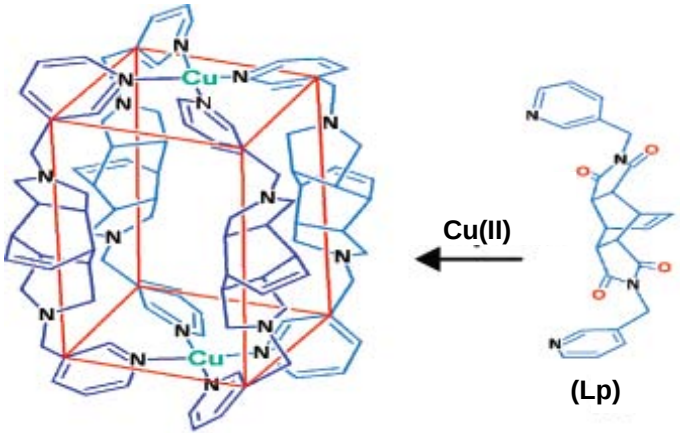

Figure 1.17. Su's copper(II) tetragonal prismatic cage (axial anions are not shown).[32]

Other examples utilizing square-planar metal ions also exist. Fujita and co-workers have prepared a rigid, bis-pyridyl ligand (**Lq**) which reacts with palladium(II) in a 1:2 ratio to yield a tetragonal prismatic cage. The X-ray crystal structure of the cage confirmed that a nitrate anion is encapsulated within the central cavity (Figure 1.18).[33]

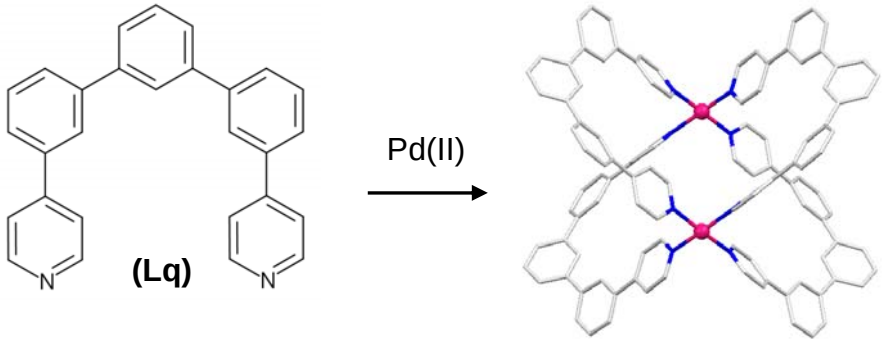

Figure 1.18. Fujita's tetragonal prismatic cage.[33]

Puddephatt *et al.* have also reported the formation of functional palladium(II) tetragonal prismatic cages from ligands **Lr** and **Ls** (Figure 1.19).[34]

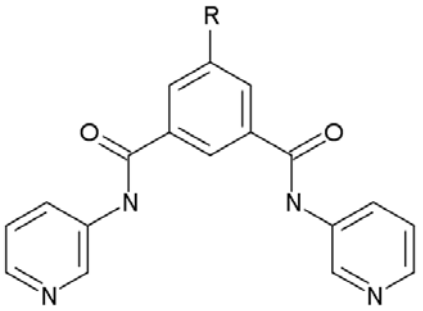

(Lr) R = H
(Ls) R = *t*-Bu

Figure 1.19. Ligands **Lr** and **Ls**.

The complexes exhibit interesting host-guest chemistry and have been shown to encapsulate cations, anions and water molecules (Figure 1.20).

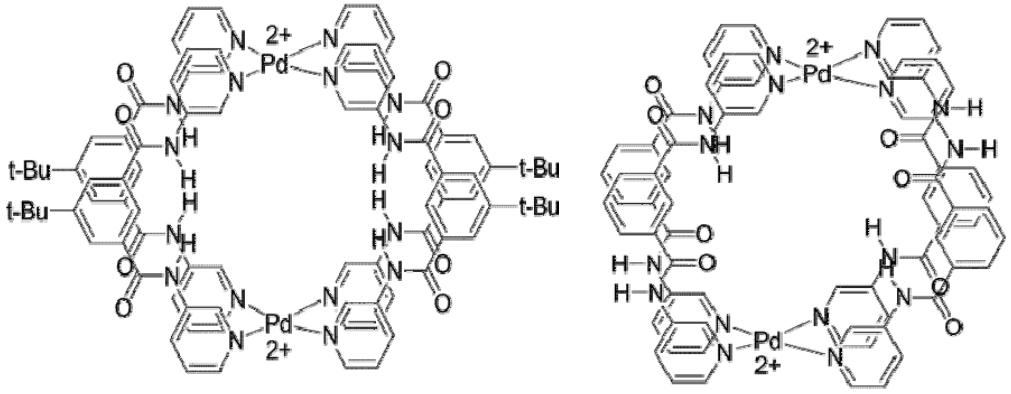

Figure 1.20. Puddephatt's tetragonal prismatic cages.[34]

1.6 Cyclic supramolecular architectures

1.6.1 Supramolecular Squares

A square is defined as having four distinct sides of equal length, four angles of 90º and a cavity running through the centre. Supramolecular squares are formed by self-assembly. In this section the use of metal ions that prefer a square planar coordination geometry, to access 90º and 180º angles, is discussed. The ligands used are also pre-selected to be complimentary in the formation of the square architecture.

In 1990, Fujita and co-workers reported the synthesis of a supramolecular square from (ethylenediamine)palladium(II) nitrate and 4,4'-bipyridine **(Lt)**. The leaving groups of (ethylenediamine)palladium(II) nitrate are *cis* to each other and coordinate to the rigid and highly directional ligand units resulting in the formation of the square shown in Figure 1.21.[35]

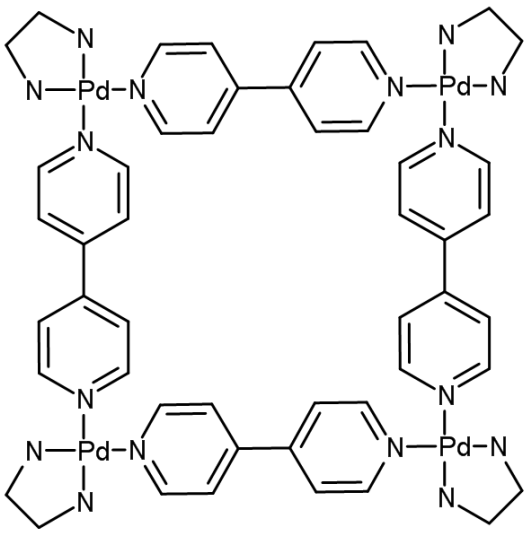

Figure 1.21. Fujita's square.

The central cavity within the square is π-electron deficient and has been shown to bind electron rich benzene derivatives, such as 1,4-dimethoxybenzene and 1,3,5-trimethoxybenzene, through hydrophobic and π-π stacking interactions.[4] When the reaction was repeated with longer analogues of 4,4'-bipyridine, such as bis(4-pyridyl)acetylene, a second minor product was formed in addition to the square. On the ^{1}H NMR spectrum of the minor product, the pyridyl protons are equivalent suggesting the formation of a highly symmetrical, macrocyclic product. It was proposed that the use of a more flexible ligand had allowed the formation of a molecular triangle that is in equilibrium with the more stable square architecture. Supramolecular triangles will be discussed in more detail in section 1.6.2.

A number of other techniques have been used to synthesise supramolecular squares. Figure 1.22 illustrates one such example reported by Lehn *et al.* In this instance the metal ions are blocked in a trans fashion and coordinated to right-angled ligands (**Lu**) which form the corners of the square.[36]

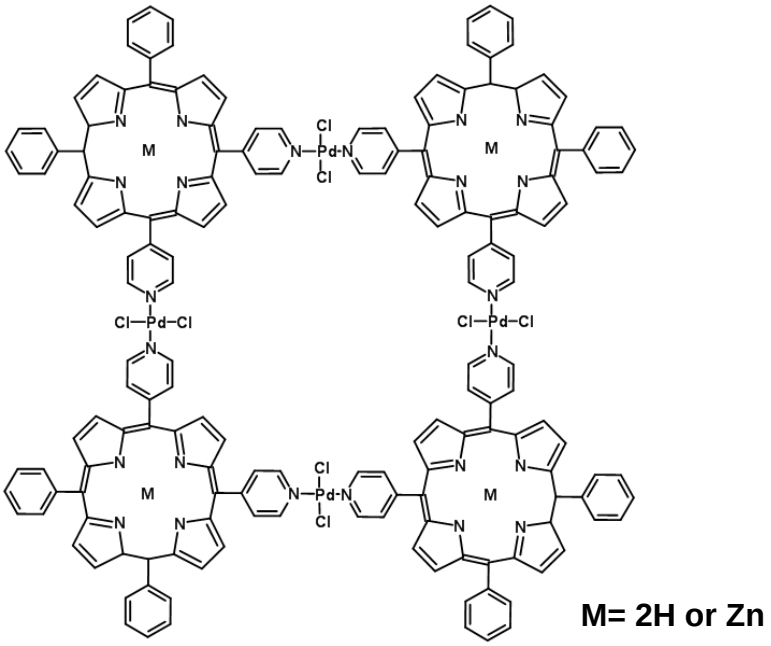

Figure 1.22. Lehn's supramolecular square structure.

More recently, Maverick *et al*. assembled supramolecular squares by the reaction of bis(β-diketone) ligands (**Lv**) with copper(II) ions. As with Lehn's square, the organic ligands form the corners of the square and the metal ions are located in the centre of the sides (Figure 1.23). Maverick's squares are able to function as hosts to guest molecules such as 4,4'-bipyridine and fullerenes.[37]

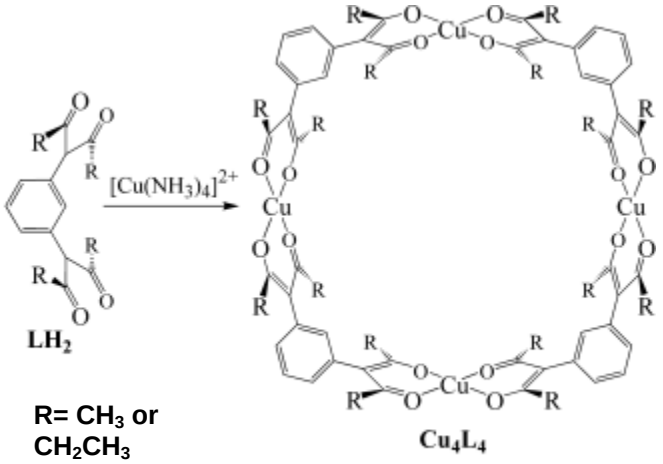

Figure 1.23. Maverick's supramolecular squares.[37]

1.6.2 Supramolecular Triangles

The equilibrium between a square and a triangle has already been discussed in the previous section. These structures involved relatively rigid ligands coordinating to square planar palladium(II).

Lippert *et al.* have reported the synthesis of a supramolecular triangle from [(en)Pd(2,2'-bpz-N^1,$N^{1'}$)]$^{2+}$ and *trans*-$(NH_3)_2$Pt(II). The palladium(II) ions form the three vertices of the triangle and the platinum(II) ions are located in the sides. The X-ray crystal structure reveals that the triangle encapsulates a perchlorate anion which is held in place by hydrogen bonding interactions (Figure 1.24).[38]

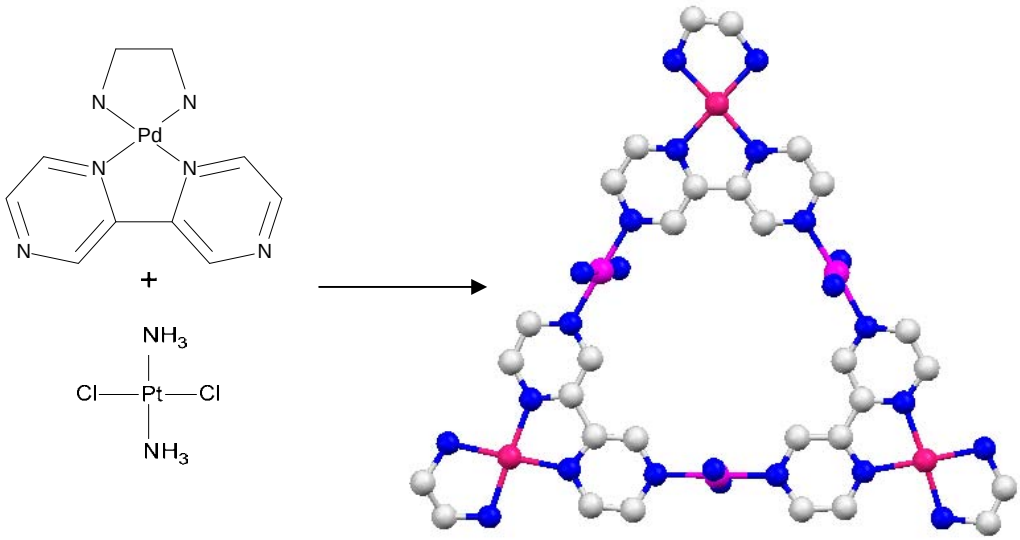

Figure 1.24. Lippert's supramolecular triangle.[38]

Hannon's ligand **Lw** is an analogue of the previously described ligand **Lg** (Figure 1.25). **Lg** reacts with tetrahedral metal ions to give a solution equilibrium of two dimeric isomers; a helicate and a box. **Lw** was designed with the goal of sterically disfavouring the formation of the box structure. While the methyl groups do indeed achieve this they also cause other dramatic effects too.[39]

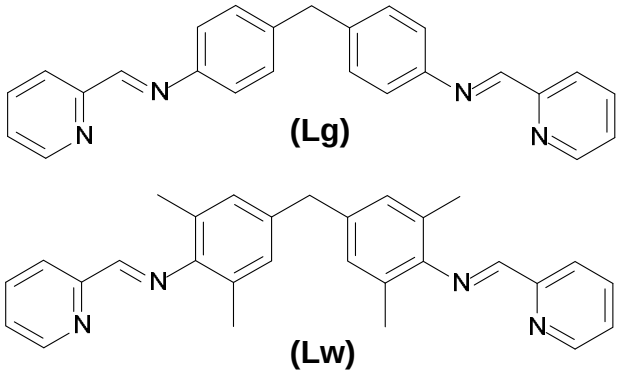

Figure 1.25. Hannon's ligands **Lg** and **Lw**.

The reaction of **Lw** with copper(I) ions formed a triangular helicate in which the ligand strands wrap over and under the plane formed by the three metal centres (Figure 1.26).

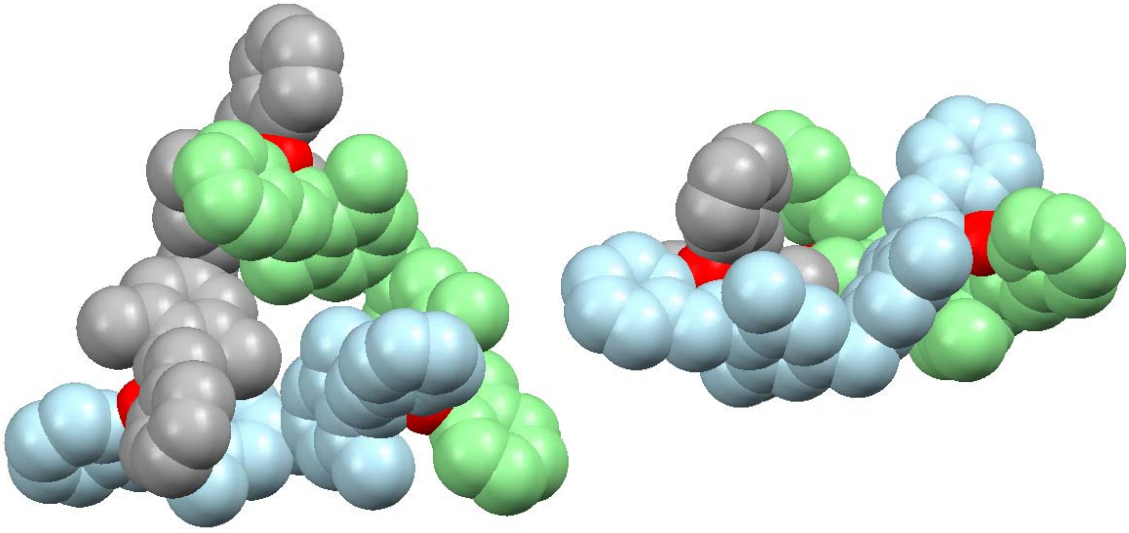

Figure 1.26. (a) Top view and (b) side view of the molecular structure of the $[Cu_3(\mathbf{Lw})_3]^{3+}$ ion. Each ligand is shown in a different colour to emphasise the helical nature of the triangle.[39]

These helical triangles have been shown to pack together to form tetrameric ball-shaped aggregates.

In 2007, Mukherjee and co-workers reported the self-assembly of a heterometallic triangle from the reaction of 1,1'-Bis(diphenylphosphino) ferrocene-palladium(II)ditriflate with sodium nicotinate (Figure 1.27).[40]

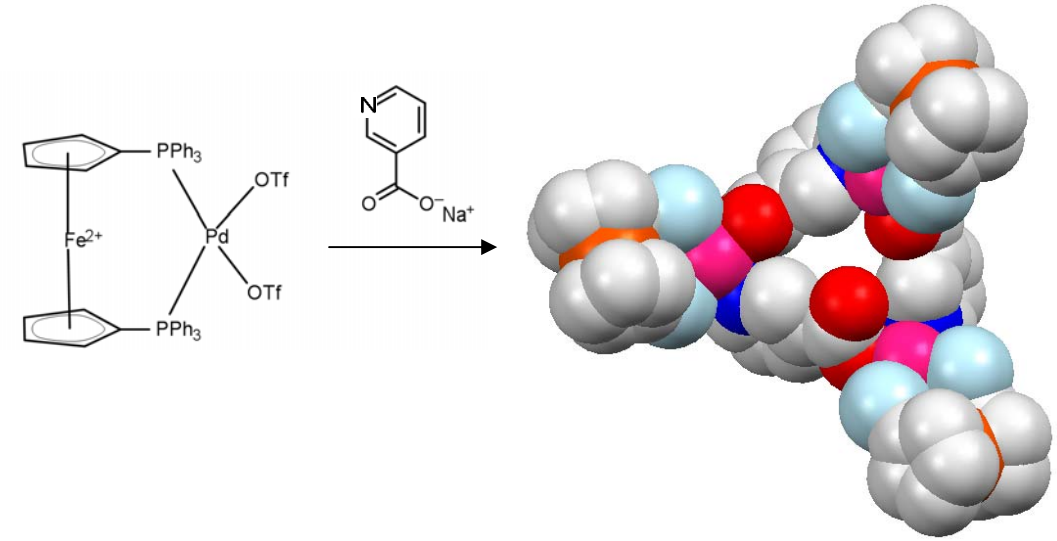

Figure 1.27. Mukherjee's supramolecular triangle. (Phenyl rings have been omitted for clarity). [40]

The bowing of the ligands along the sides of the triangle allow the O-Pd-N angles to approach close to their preferred 90º, minimising the angle strain at the metal centre.

The previous section focused on the principles of supramolecular chemistry and highlights the success of recent advances in this area. Our interest in this field stems from the potential for supramolecular complexes to be used as DNA recognition agents. Before introducing the modes of DNA recognition, the structure of DNA itself will be discussed.

1.7 Deoxyribonucleic Acid (DNA)

1.7.1 DNA Background

DNA is the nucleic acid which contains the genetic ‘blueprint’ of all cellular life forms and of many viruses. It is responsible for two major roles: conducting its own replication during cell division and directing the transcription of complementary molecules of RNA.

In 1869, whilst researching the structure of white blood cells, Miescher isolated the first crude sample of DNA. At the time the exact composition and function of the substance was unknown.[41] However, over the next century considerable research was carried out in this field. As a result of this research, in 1953, James D. Watson and Francis Crick were able to propose a structure for DNA.[42] The double helical structure elucidated by Watson and Crick was that of B-DNA. It is now known that several other forms of DNA also exist, however, B-DNA is considered to be the most prevalent form found in biological systems.

1.7.2 Structure of DNA

In groundbreaking research, Kossel and co-workers identified the purine (adenine and guanine) and pyrimidine (thymine and cytosine) bases that constitute the nitrogenous components of DNA (Figure 1.28 (a)).[43] Each base is connected to a 2'-deoxyribose sugar molecule which is in turn linked to a phosphate group to form a 'nucleotide'. DNA consists of four different nucleotides which link together to form polynucleotide chains (Figure 1.28 (b)).

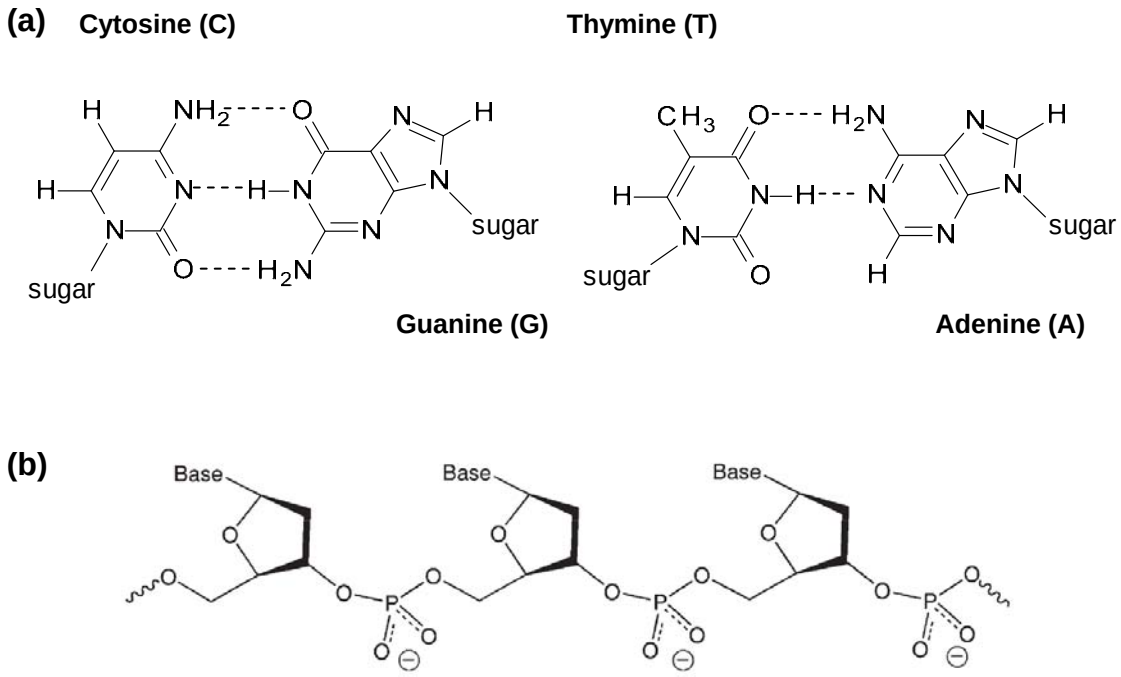

Figure 1.28. (a) The DNA bases and their Watson–Crick hydrogen-bond pattern and (b) the sugar-phosphate backbone.

B-DNA consists of two polynucleotide strands which intertwine to form a right-handed double helix (duplex). Figure 1.29 (a) shows the hydrogen bonding which occurs between the bases of a pair of polynucleotide chains. As illustrated in the diagram, adenine will always pair up with thymine and cytosine with guanine.

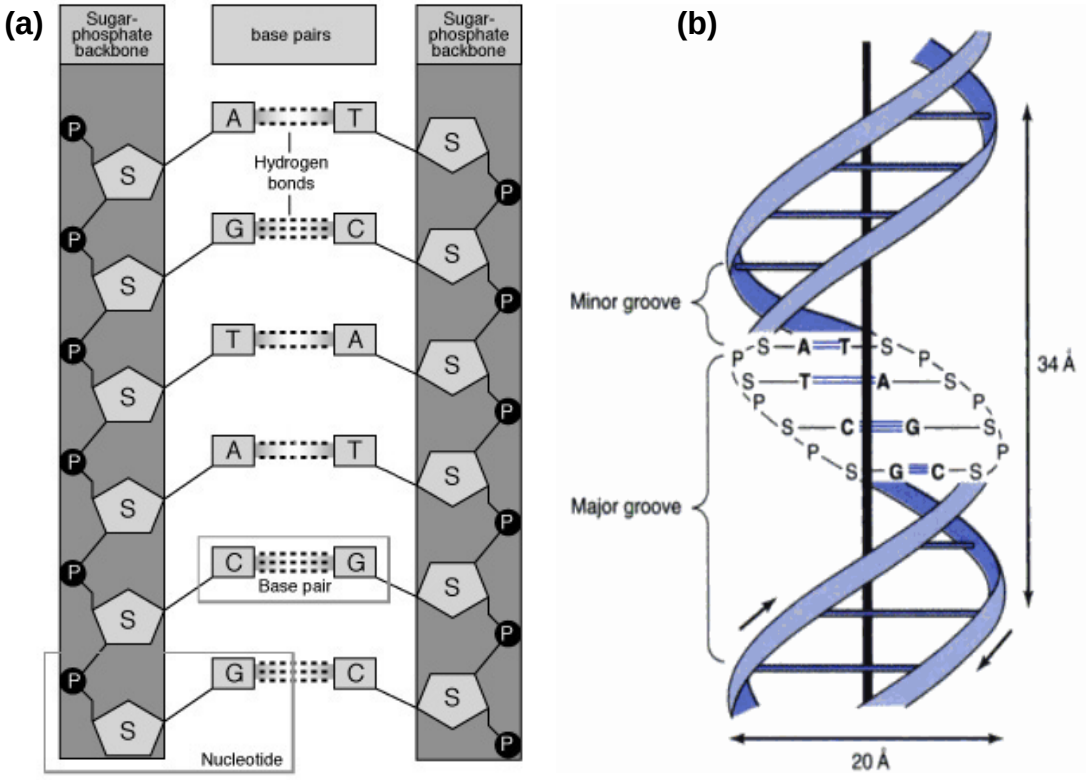

Figure 1.29. Schematic representations of B-DNA showing (a) DNA base pairing[44] and (b) minor and major grooves[45].

As the bases are hydrophobic they are located in the core of the DNA duplex while the hydrophilic sugar-phosphate units point out into solution. The aromatic bases are approximately perpendicular to the helical axis and are stacked on top of each other through π-π stacking interactions. The attachment points of the bases to the sugar-phosphate backbone are offset with respect to the hydrogen bonds between the bases. This leads to the occurrence of two distinct grooves in the double-helical structure. These are called the minor groove and the major groove (Figure 1.29 (b)).

In addition to the basic double helix, other forms of branched DNA structures called ‘junctions’ also exist. DNA junctions are formed when the polynucleotide chains of two or more double-helical fragments interconnect. David Lilley defines DNA junctions as ‘branch points where double-helical

segments intersect with axial discontinuities, such that strands are exchanged between the different helical sections'.[46] Researchers are interested in DNA junctions as they are often present as intermediates in genetic processes such as DNA replication and genetic recombination. Therefore, the ability to recognise and manipulate these junctions could prove invaluable. Figure 1.30 shows the crystal structures of a three- and four-way DNA junction.[46,47]

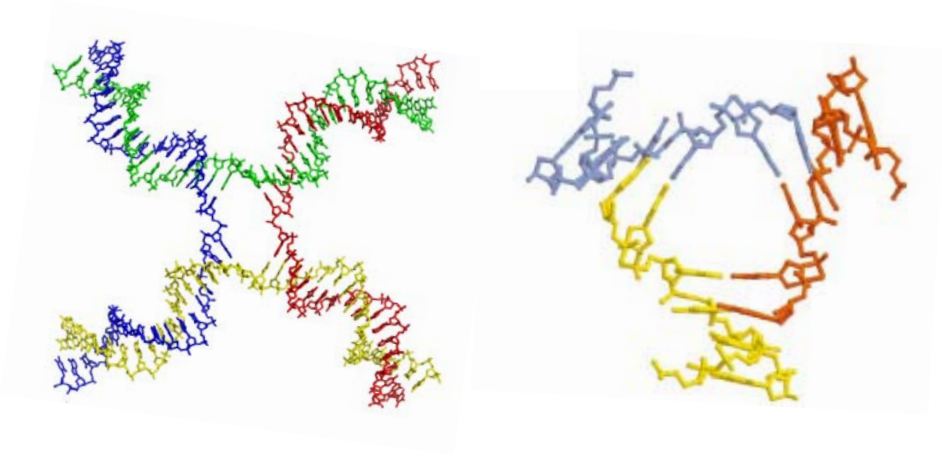

A DNA four-way junction

A DNA three-way junction

Figure 1.30. A DNA four-way[46] and three-way[47] junction bound by Cre.

Thus far we have touched upon some of the conformations that are adopted by duplex DNA. In addition to these, other structures of DNA have also been identified. One example is triple-stranded or triplex DNA. This is formed when duplex DNA associates with another polynucleotide strand. The additional strand lies in the major groove of the duplex and is held in place by hydrogen bonding interactions between the base pairs. A schematic representation of triplex DNA is depicted in Figure 1.31.[45]

Figure 1.31. A schematic representation of triplex DNA.[45]

Other DNA structures are also possible (Figure 1.32) but B-DNA is the principal form found in biological systems and is the focus of the study herein.

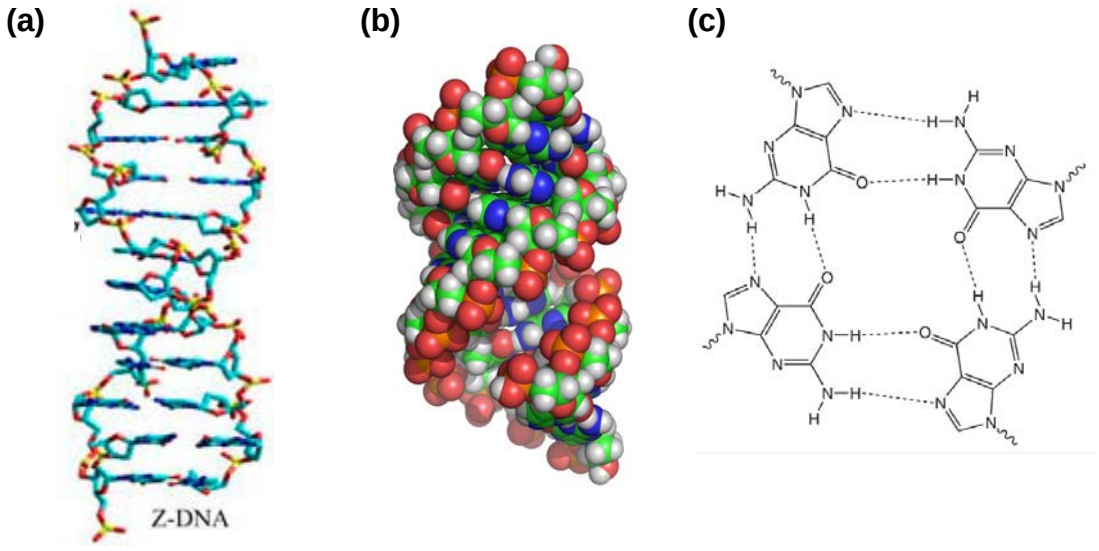

Figure 1.32. (a) Z-DNA,[48] (b) A-DNA[49] and (c) Guanine tetramers (the basis for quadruplex formation).

1.7.3 DNA Recognition

After Watson and Crick's discovery, scientists were quick to recognise the potential of DNA as a key drug target for the treatment of genetic diseases such as cancer. Six different methods of drug-DNA recognition have since been discovered: intercalation between the DNA bases, covalent binding or metal-coordination to the bases, sugar–phosphate backbone binding, minor groove recognition, major groove recognition and recognition of DNA junctions.[49,50] Well known examples of some of these modes of drug-DNA recognition are presented in the following section.

1.7.3.1 DNA Intercalation

Intercalation is the partial or full insertion of a planar aromatic molecule into the gap between two adjacent base pairs of DNA. While it does not disrupt the hydrogen bonding of the base pairs, the DNA helix lengthens slightly to accommodate the intercalated molecule. At the site of intercalation the helix is partially unwound, resulting in a localised distortion of the regular arrangement of the sugar-phosphate backbone. Addition of multiple intercalators has the effect of stiffening the DNA and causing the unwinding of supercoiled DNA. This causes the deactivation of the DNA, thus preventing replication and transcription from occurring.[51]

Intercalating molecules are typically electron deficient planar poly-aromatic molecules. A well known example is ethidium bromide which is used to stain DNA in gel electrophoresis experiments (Figure 1.33).[52]

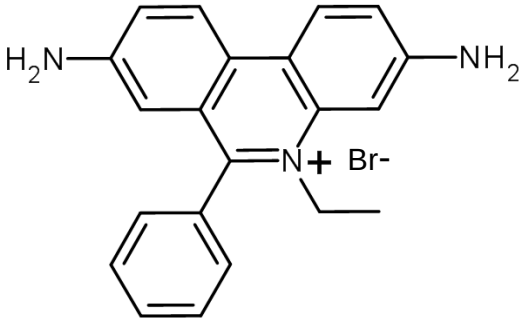

Figure 1.33.Ethidium bromide.

Another example is the anti-cancer drug doxorubicin which was discovered in the 1960s. Doxorubicin intercalates between DNA base pairs and works by inhibiting transcription and replication in rapidly growing cancer cells. The discovery of this drug was a milestone in the history of cancer chemotherapy as it has been found to be effective in the treatment of a vast range of different cancers.[53]

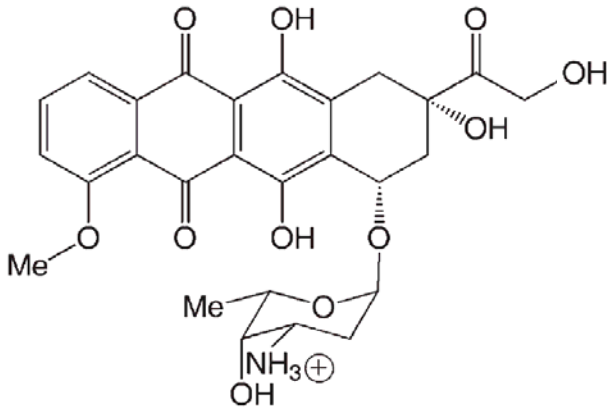

Figure. 1.34. Structure of doxorubicin.

In 1974, Lippard *et al*. reported the first metallo-intercalator constructed from a planar aromatic ligand bound to a square planar platinum(II) centre (Figure 1.35). The incorporation of metal ions into the design of intercalators is an attractive way of introducing a positive charge.[54]

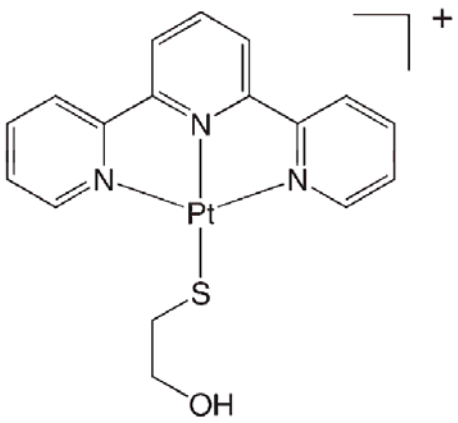

Figure 1.35. Structure of Lippard's intercalator.

More recently, the Barton group have created larger rhodium(II) and ruthenium(II) intercalators based on phzi and chrysi ligands (Figure 1.36).[55]

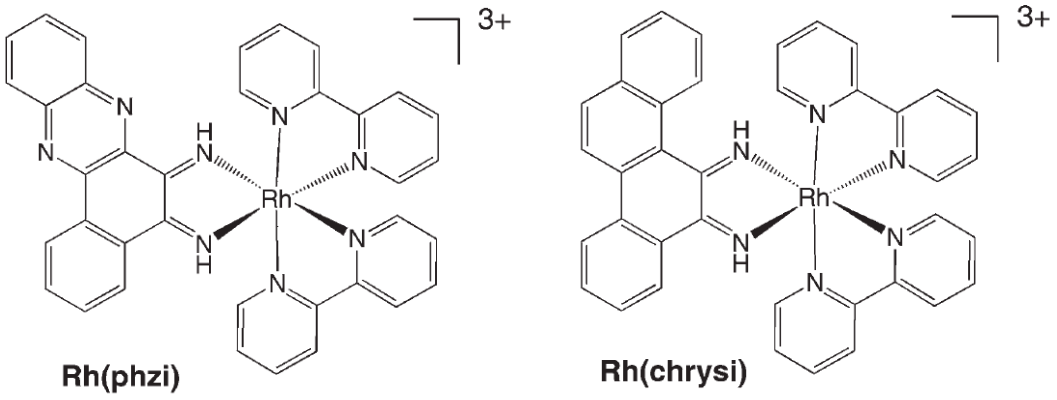

Figure 1.36. Barton's rhodium(II) intercalators.

The planar polycyclic aromatic ligands are too big to intercalate into normal DNA but show a strong preference for DNA mismatch sequences where the absence of Watson–Crick pairing will allow a larger intercalator to be accommodated. An application of the ruthenium(II) complexes is to detect DNA mismatches by fluorescence.

1.7.3.2 DNA alkylation

Another way in which drugs can interact with DNA is by binding directly to the DNA bases, usually to the N7 of guanine or adenine. Nitrogen mustards such as chlorambucil (Figure 1.37) bind to the DNA bases by alkylation of the nitrogen resulting in the formation of a covalent bond. This interaction causes the irreversible deactivation of the DNA.[56]

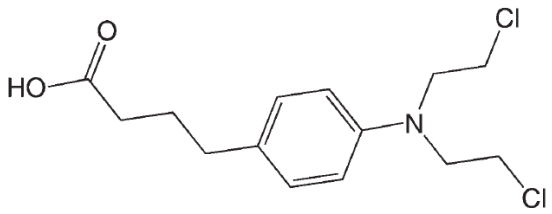

Figure 1.37. Structure of the Nitrogen Mustard, Chlorambucil.

Cis-platin is one of the most successful ‘alkylating’ drugs found in the clinic. It binds to DNA with displacement of the two chlorides and the formation of two metal-coordination bonds to N7 of two adjacent guanine residues on the same polynucleotide strand (Figure 1.38).[57]

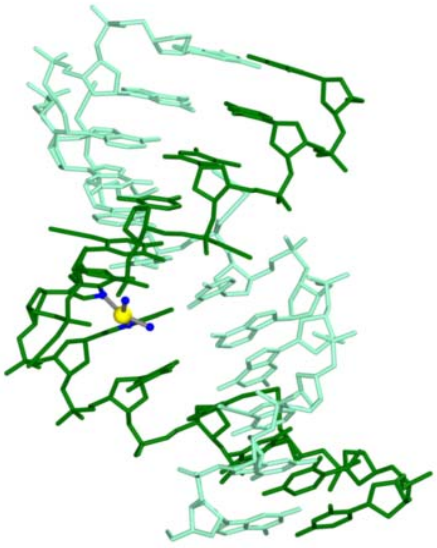

Figure 1.38. Cis-platin bound to two adjacent guanine residues of DNA[50]

1.7.3.3 Binding within a DNA groove

The intertwining of the two polynucleotide strands of DNA causes two distinct grooves to occur within its structure. Many drugs are the correct size and shape to fit into and bind within these grooves, often by hydrogen bonding and Van der Waals interactions.

In their analysis of DNA groove binders, Goodsell and Dickerson[58] identified that minor groove binders tend to contain between two and five aromatic rings and are flanked at each end by cationic groups. A typical example is berenil which is a drug used for treating sleeping sickness in veterinary medicine (Figure 1.39).[59]

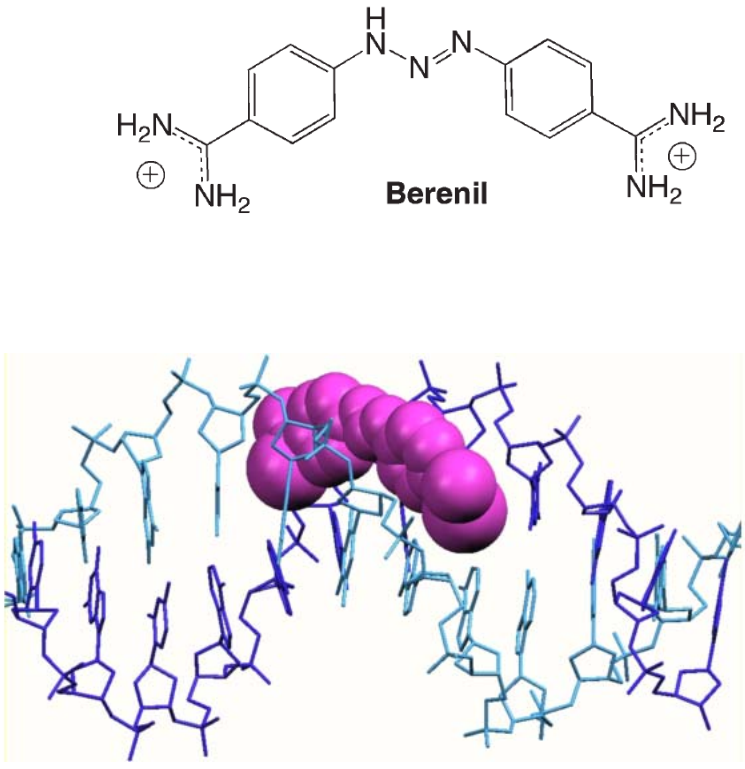

Figure 1.39. A berenil drug molecule and the binding of the molecule in the minor groove of DNA[50]

Numerous examples of DNA minor groove binders are known but synthetic agents that target the DNA major groove are rare.

Hannon and co-workers have developed a family of metallo-supramolecular cylinders which interact with the DNA major groove. One of these agents is the iron(II) triple-stranded helicate shown in Figure 1.40 (also described in section 1.4.3). At ~2 nm in length and ~1 nm in diameter, Hannon's iron(II) helicate is a similar size to the alpha-helical DNA recognition unit of zinc fingers.

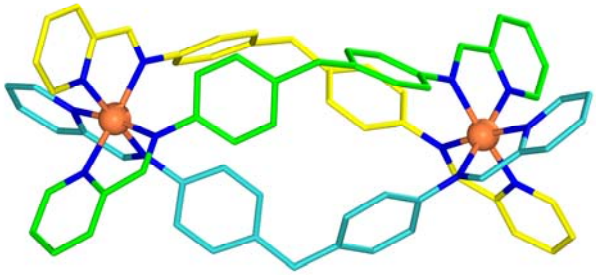

Figure 1.40. Hannon's triple-stranded iron(II) cylinder.

The helicate has been shown to bind in the DNA major groove and in addition causes the unexpected and dramatic intramolecular coiling of DNA (Figure 1.41). Experimental evidence shows that it is the specific size and shape of the cylinder that is important in producing this coiling effect.[60]

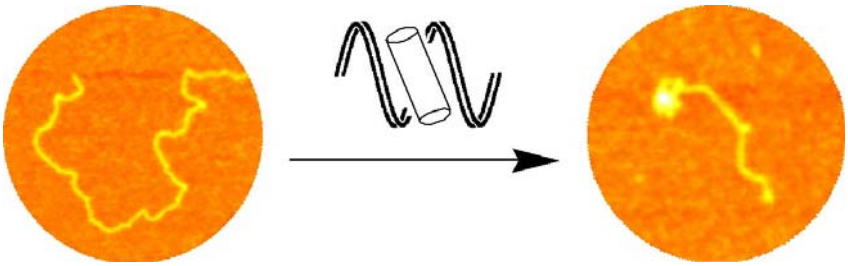

Figure. 1.41 Intramolecular DNA coiling induced by the supramolecular cylinder.[60]

1.7.3.4 DNA Junction Recognition

Further work carried out in collaboration with Miquel Coll led to the crystallisation of Hannon's iron(II) cylinder with a palindromic hexanucleotide. The results were remarkable and revealed the cylinder to be located at the heart of a three-way DNA junction. The crystal structure showed that the cylinder is the correct size and shape to fit perfectly into the cavity of the junction and is held in place by electrostatic and π-π stacking interactions (Figure 1.42).[61]

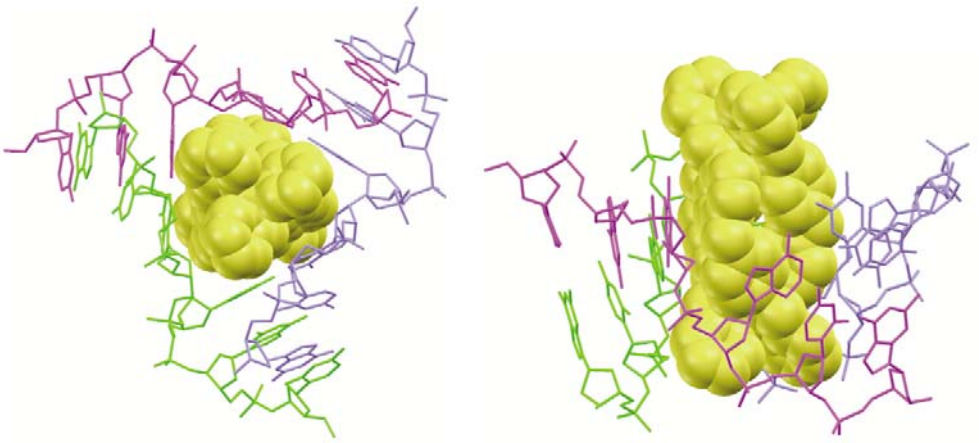

Figure 1.42. Binding within a DNA three-way junction. [61]

As has been described, a wide range of metallo-supramolecular architectures can be self assembled by the mixing and matching of metal ions and ligands.

In the following chapters the design, synthesis and characterisation of novel metallo-supramolecular complexes is presented. A number of these complexes have the potential to be used as DNA recognition agents. DNA binding studies and cytotoxic activities of these complexes are also reported in this work.

1.8 References

1. J. M. Lehn, *Proc. Natl. Acad. Sci.,* **2002**, 99, 4763-4768.
2. J. M Lehn, *Supramolecular Chemistry: Concepts and Perspectives*, **1995**, VCH, New York.
3. P.D. Beer, P.A. Gale, D.K. Smith, *Supramolecular Chemistry*, **1999**, Oxford University Press; J.W. Steed, J.L. Atwood, *Supramolecular Chemistry*, **2000**, John Wiley & Sons.
4. A. V. Davis, R. M. Yeh, K. N. Raymond, *Proc. Natl. Acad. Sci*., **2002**, 99, 4793-4796.
5. M. J. Hannon, C. L. Painting, W. Errington, *Chem. Commun.,* **1997**, 307-308; E. C. Constable, E. Schofield, *Chem. Commun.***, 1998**, 403-404.
6. M. Albrecht, *Chem. Rev.,* **2001,** 101, 3457-3497; C. Piguet, M. Borkovec, J. Hamacek, K. Zeckert, *Coord Chem. Rev.*, 249, **2005**, 705–726.
7. M. Fujita, O. Sasaki, T. Mitsuhashi, T. Fujita, J. Yazaki, K. Yamaguchi, K. Ogura, K. *Chem. Commun.,* **1996,** 1535-1536; M. Schweiger, S. R. Seidel, A. M. Arif, P. J. Stang, *Angew. Chem. Int. Ed.*, **2001**, 40, 3467-3469.
8. M. T. Youinou, N. Rahmouni, J. Fischer, J. A. Osborn, *Angew. Chem. Int. Ed.,* **1992**, 31, 733-735; L. Zhao, Z. Xu, L. K. Thompson, S. L. Heath, D. O. Miller, M. Ohba, *Angew. Chem. Int. Ed.,* **2000,** 39, 3114-3117; J. Michl, T. F. Magnera, *Proc. Nactl. Acad. Sci*., **2002**, 99, 4788-4792.
9. J. M. Lehn, A. Rigault, J. Siegel, J. Harrowfield, B. Chevrier, *Proc. Natl. Acad. Sci.,* **1987**, 84, 2565-2569;
10. C. Piguet, G. Bernardinelli, G. Hopfgartner, *Chem. Rev.*, **1997**, 97, 2005-2062.
11. E. C. Constable, M. G. B, Drew, G. Forsyth, M. D. Ward, *J. Chem. Soc., Chem. Commun.,* **1988**, 22, 1450-1451.
12. Y. Zhang, L. Xiang, Q. Wang, X. F Duan, G. Zi, *Inorg. Chim. Acta.,* **2008,** 361, 1246–1254.
13. J. M. Lehn, J. P. Sauvage, J. Simon, R. Ziessel, C. Piccini-Leopardi, G. Germain, J. P. Declerq, M. V. Meerssche, *Nouv. J. Chim.*, **1983**, 7, 413.

14. E. C. Constable, M. J. Hannon, A. Martin, P. R. Raithby, P. A. Tocher, *Polyhedron*, **1992**, 11, 2967-2971.
15. E. C. Constable, M. D. Ward, M. G. B. Drew, G. A. Forsyth, *Polyhedron,* **1989**, 8, 2551-2555.
16. D. E. Fenton, R. W. Matthews, M. McPartlin, B. P. Murphy, I. J. Scowen, P. A. Tasker, *J. Chem. Soc., Chem. Commun.*, **1994**, 1391-1392.
17. A. F. Williams, C. Piguet, G. Bernardinelli, *Angew. Chem. Int. Ed.,* **1991**, 30, 1490-1492.
18. C. Piguet, G. Bernardinelli, B. Bocquet, A. Quattropani, A. F. Williams, *J. Am. Chem. Soc.,* **1992**, 114, 7440-7451.
19. L. J. Childs, M. J. Hannon, *Supramolecular Chem.*, **2004**, 16, 7-22; L. J. Childs, J. Malina, M. Pascu, B. E. Rolfsnes, M. J. Prieto, M. J. Broome, P. M. Rodger, E. Sletten, V. Moreno, A. Rodger, M. J. Hannon, *Chem. Eur. J.,* **2006,** 12, 4919–4927; I. Meistermann, V. Moreno, M. J. Prieto, E. Molderheim, E. Sletten, S. Khalid, P. M. Rodger, J. Peberdy, C. J. Isaac, A. Rodger, M. J. Hannon, *Proc. Natl. Acad. Sci.,* **2002,** 99, 5069–5074; C. Uerpmann, J. Malina, M. Pascu, G. J. Clarkson, V. Moreno, A. Rodger, A. Grandas, M. J. Hannon, *Chem. Eur. J.*, **2005**, 11, 1750–1756.
20. M. J. Hannon, C. L. Painting, A. Jackson, J. Hamblin, W. Errington, *Chem. Commun.,* **1997**, 1807-1808.
21. S. Torelli, D. Imbert, M. Cantuel, G. Bernardinelli, S. Delahaye, A. Hauser, J. C. G. Bunzli, C. Piguet, *Chem. Eur. J.,* **2005**, 11, 3228-3242.
22. D. A. McMorran, P. Steel, *J. Angew. Chem. Int. Ed.,* **1998**, 37, 3295-3297.
23. L. P. Harding, J. C. Jeffery, T. Riis-Johannessen, C. R. Rice, Z. Zeng, *Dalton Trans*., **2004**, 2396-2397.
24. B. Wu, X. J. Yang, C. Janiak, P. G. Lassahn, *Chem. Commun.*, **2003**, 902–903.
25. S. Goetz, P. E. Kruger, *Dalton Trans.*, **2006**, 1277–1284.
26. B. Schoentjes, J. L. Lehn, *Helv. Chim. Acta.,* **1995**, 78, 1-12.
27. C. Y. Su, Y. P. Cai, C. L. Chen, H. X. Zhang, B. S. Kang, *J. Chem. Soc*., *Dalton Trans*., **2001**, 359–361.

28. M. Du, X. J. Zhao, J. H. Guo, *Inorg. Chem. Commun.,* **2005**, 8, 1–5.
29. L. J. Barbour, G. W. Orr, J. L. Atwood, *Nature,* **1998,** 393, 671-673.
30. L. J. Barbour, G. W. Orr, J. L. Atwood, *Chem. Commun.*, **2000**, 859–860; Y. B. Xie, J. R. Li, C. Zhang, X. H. Bu, *Crystal Growth Des.,* **2005**, 5, 1743-1749.
31. C. Y. Su, Y. P. Cai, C. L. Chen, M. D. Smith, W. Kaim, H. C. zur Loye, *J. Am. Chem. Soc.,* **2003,** 125, 8595-8613.
32. Z. M. Liu, Y. Liu, S. R. Zheng, Z. Q. Yu, M. Pan, C. Y. Su, *Inorg. Chem.,* **2007**, 46, 5814-5816.
33. D. K. Chand, K. Biradha, M. Fujita, *Chem. Commun.*, **2001**, 1652–1653.
34. N. L. S. Yue, D. J. Eisler, M. C. Jennings, R. J. Puddephatt, *Inorg. Chem.,* **2004**, 43, 7671-7681.
35. M. Fujita, J. Yazaki, K. Ogura, *J. Am. Chem. Soc.,* **1990**, 112, 5645-5647.
36. C. M. Drain, J. M. Lehn, *J. Chem. Soc., Chem. Commun.,* **1994**, 2313-2315.
37. C. Pariya, C. R. Sparrow, C. K. Back, G. Sandi, F. R. Fronczek, A. W. Maverick, *Angew. Chem. Int. Ed*., **2007**, 46, 6305-6308.
38. R. D. Schnebeck, E. Freisinger, B. Lippert, *Chem. Commun.*, **1999**, 675–676
39. L. J. Childs, N. W. Alcock, M.J. Hannon, *Angew. Chem., Intl. Ed.*, **2002**, 41, 4244-4247.
40. S. Ghosh, D. R. Turner, S. R. Batten, P. S. Mukherjee, *Dalton Trans.,* **2007**, 1869–1871.
41. R. Dahm, *Dev. Biol.*, **2005**, 278, 274–288.
42. J. D. Watson, F. Crick, *Nature*, **1953**, 171, 737-738.
43. F. H. Portugal, J. S. Cohen, *A century of DNA*, **1977**, MIT Press, Cambridge.
44. Source: National Human Genome Research Institute: www.genome.gov/Pages/Hyperion/DIR/VIP/Glossary/illustration/Pdf/nucleotide.pdf
45. A. D. Bates, A. Maxwell, *DNA Topology*, **2009**, Oxford University Press.
46. D. M. J. Lilley, *Quart. Rev. Biophy*., **2000**, 33, 109–159.

47. K. C. Woods, S. S. Martin, V. C. Chu, E. P. Baldwin, *J. Mol. Biol.*, **2001**, 313, 49-69.
48. H. Zhang, H. Yu, J. Ren, X. Qu, *Biophys. J*., **2006**, 90, 3203–3207.
49. F. R. Keene, J. A. Smith, J. G. Collins, *Coord. Chem. Rev.,* **2009**, 253, 2021-2035.
50. M. J. Hannon, *Chem. Soc. Rev*., **2007**, 36, 280–295.
51. L. S. Lerner, *J. Mol. Biol*., **1961**, 3,18-30.
52. C. G. Reinhardt, T. R. Krugh, *Biochem.*, **1978**, 17, 4845–4854.
53. R. Martınez, L. Chacon-Garcıa, *Curr. Med. Chem*., **2005**, 12, 127-151.
54. K. W. Jennette, S. J. Lippard, G. A. Vassiliades and W. R. Bauer, *Proc. Natl. Acad. Sci. U.S.A.*, **1974**, 71, 3839–3843.
55. J. R. Hart, M. D. Johnson, J. K. Barton, *Proc. Natl. Acad. Sci. U.S.A*., **2004**, 101, 14040–14044; E. Ruba, J. R. Hart, J. K. Barton, *Inorg. Chem.,* **2004**, 43, 4570–4578.
56. A. Masta, P. J. Gray, D. R. Phillips, *Nucl. Acids Res*., **1995**, 23, 3508–3515.
57. B. Lippert. *Cisplatin, Chemistry and Biochemistry of a Leading Anticancer Drug*, **1999**, Wiley-VCH, Weinheim; J. Reedijk. *Chem. Commun.,* **1996**, 801-806; J. D. Roberts, J. Peroutka, N. Farrell, *J. Inorg. Biochem.,* **1999***,* 77, 51-57; S. J. Lippard, J. M. Berg. *Principles of Bioinorganic Chemistry*, **1994**, University Science Books, Mill Valley, CA.
58. D. Goodsell, R. E. Dickerson, *J. Med. Chem.,* **1986,** 29, 727-733.
59. B. C. Baguley, *Mol. Cell. Biochem.,* **1982**, 43, 167-181.
60. M. J. Hannon, V. Moreno, M. J. Prieto, E. Moldrheim, E. Sletten, I. Meistermann, C. J. Isaac, K. J. Sanders, A. Rodger, *Angew. Chem. Int. Ed.*, **2001**, 40, 879-884.
61. A. Oleksi, A. G. Blanco, R. Boer, I. Usón, J. Aymami, A. Rodger, M. J. Hannon, M. Coll*. Angew. Chem., Int. Ed.,* **2006,** 45, 1227-1231.

Chapter 2

Tetra-Stranded, Dinuclear Palladium(II) and Platinum(II) Supramolecular Cylinders

2.1 Introduction

2.1.1 DNA Binding Complexes

Metal complexes that form coordination bonds to the DNA bases are at the forefront of clinical treatment of a variety of cancers, with three cis-platin like drugs having worldwide approval and three more used regionally.[1] Challenges remain including widening the spectrum of cancers that can be treated, circumventing acquired resistance and reducing side effects. A key design feature to address these issues is to develop drugs that have quite distinct molecular level actions from cis-platin. In this context, agents that bind non-covalently to DNA have attracted recent attention.[2]

In particular, the Hannon group have developed an array of metallo-supramolecular double and triple-stranded cylinders that bind non-covalently to DNA[3] and which also show activity against cancer cell lines.[4] A key feature for their activity is their large supramolecular size and shape. They are around 2 nm in length and 1 nm in diameter which distinguishes them from traditional small molecule drugs. The most studied of Hannon's complexes is the triple-stranded, dinuclear iron(II) cylinder shown in Figure 2.1 (also see chapter 1, section 1.4.3). This cylinder is helical in nature and is formed from three bis-pyridylimine ligands wrapped around two iron(II) metal centres.[5]

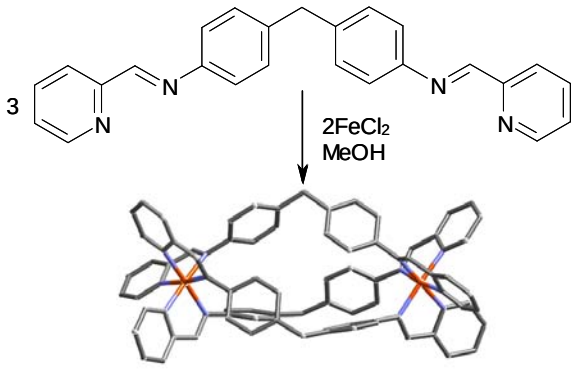

Figure 2.1. Hannon's triple-stranded, dinuclear Iron(II) cylinder.

As described in chapter 1, there are six ways in which drugs can bind to DNA. NMR experiments have confirmed that Hannon's iron(II) cylinder binds in the major groove of duplex DNA.[6] In addition, atomic force microscopy showed that it also causes dramatic intra-molecular coiling in linearised plasmid DNA; an effect that is unobserved among synthetic DNA binders.[7] More recently, X-ray crystallographic studies with a palindromic hexanucleotide presented a totally unexpected mode of drug-DNA recognition. The crystal structure revealed the iron(II) cylinder to be located within the central cavity of a 3 way DNA junction (Figure 2.2).[8] This represents a completely unprecedented, novel way in which drugs can bind to DNA. Many drugs target disease by interacting with DNA, however, they are non-specific in their approach which can result in a number of unwanted side effects. Targeting specific DNA structures, such as the 3 way junction, is a very attractive way of minimising the side effects caused by a drug.

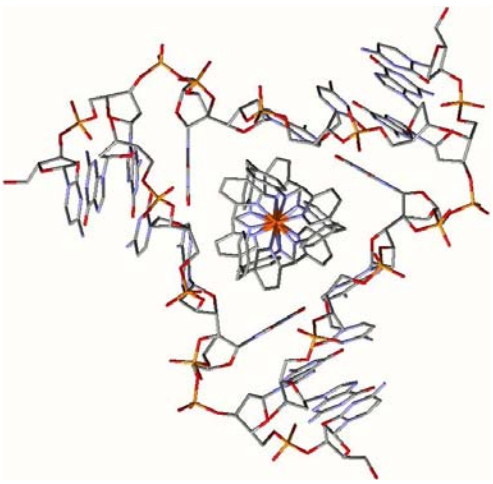

Figure 2.2. Hannon's triple-stranded, dinuclear Iron(II) cylinder bound in a three-way DNA junction.[8]

As discussed in chapter 1, DNA junctions occur when the polynucleotide chains of two or more double-helical fragments interconnect. Three way junctions are the simplest branched DNA structures and are involved in crucial biological

functions such as DNA replication. The most extensively researched junction is the four way junction (Holliday junction) which is generally accepted to be the central intermediate in homologous genetic recombination.

2.1.2 Research Aims

This study aims to extend the research in this area by designing and synthesising drug molecules which might be capable of recognising and binding within the central cavity of a Holliday junction (although as will be seen solubility issues have prevented Holliday junction binding studies). Therefore, the new drug needs to be the correct size and shape to target a junction with a square central cavity, rather than a triangular one. It is important to incorporate the key features of Hannon's iron(II) cylinder into the design of the new drug to ensure that it interacts with DNA in a similar way. The approach that is best suited to this application is to synthesise tetra-stranded analogues of Hannon's triple-stranded cylinder. A literature review of previously reported tetra-stranded supramolecular complexes has been discussed in chapter 1.

2.1.3 Molecular Design Approach

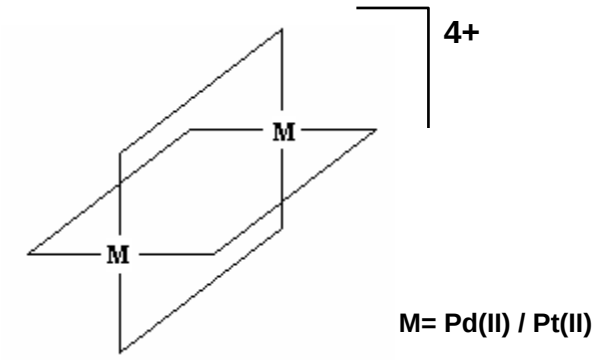

Figure 2.3. A schematic representation of our design approach, depicting two square planar metal centres linked by four ligand strands.

A schematic representation of the design approach is shown in Figure 2.3. Palladium(II) and platinum(II) metal centres were chosen to assemble the cylinders as they have the correct geometry to enable the formation of the required architectures. They also impart a positive charge to the cylinders which will allow for electrostatic interactions with the negatively charged DNA. The simplest of the ligands (**L**^{1}) used in this investigation is shown in Figure 2.4.

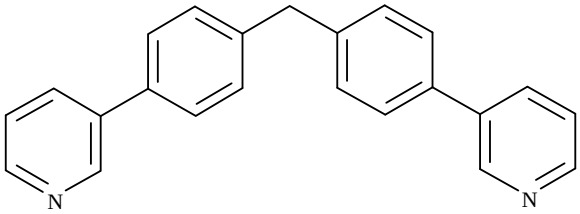

Figure 2.4 Ligand **L**^{1}.

The ligand design incorporates a central bis-phenyl spacer unit which is important in DNA recognition. The spacer separates two monodentate binding sites and prohibits them from coordinating to the same metal centre. The pyridyl binding units are connected to the spacer in the 3-position. This ensures that the nitrogen donor atoms are perfectly positioned to accommodate the square planar coordination requirements of the metal centres.

Four additional ligands with similar design features to ligand **L**^{1} have also been prepared (Figure 2.5). These ligands along with their resulting palladium(II) and platinum(II) complexes will be discussed in detail in the following section.

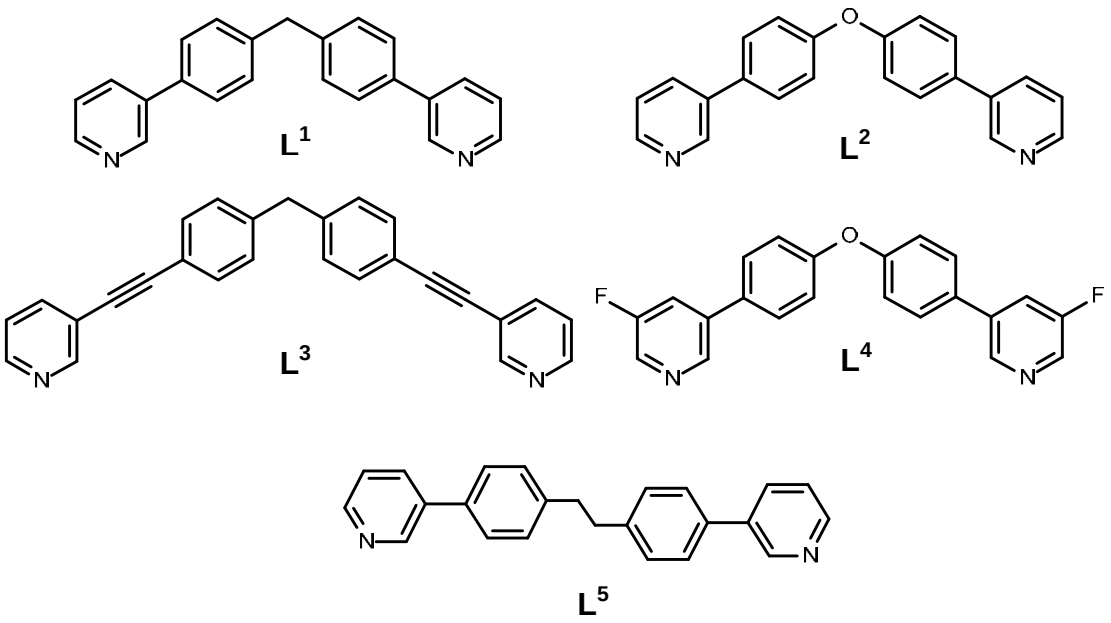

Figure 2.5. Bis-pyridyl Ligands.

2.2 Results and Discussion

2.2.1 Ligand L^1

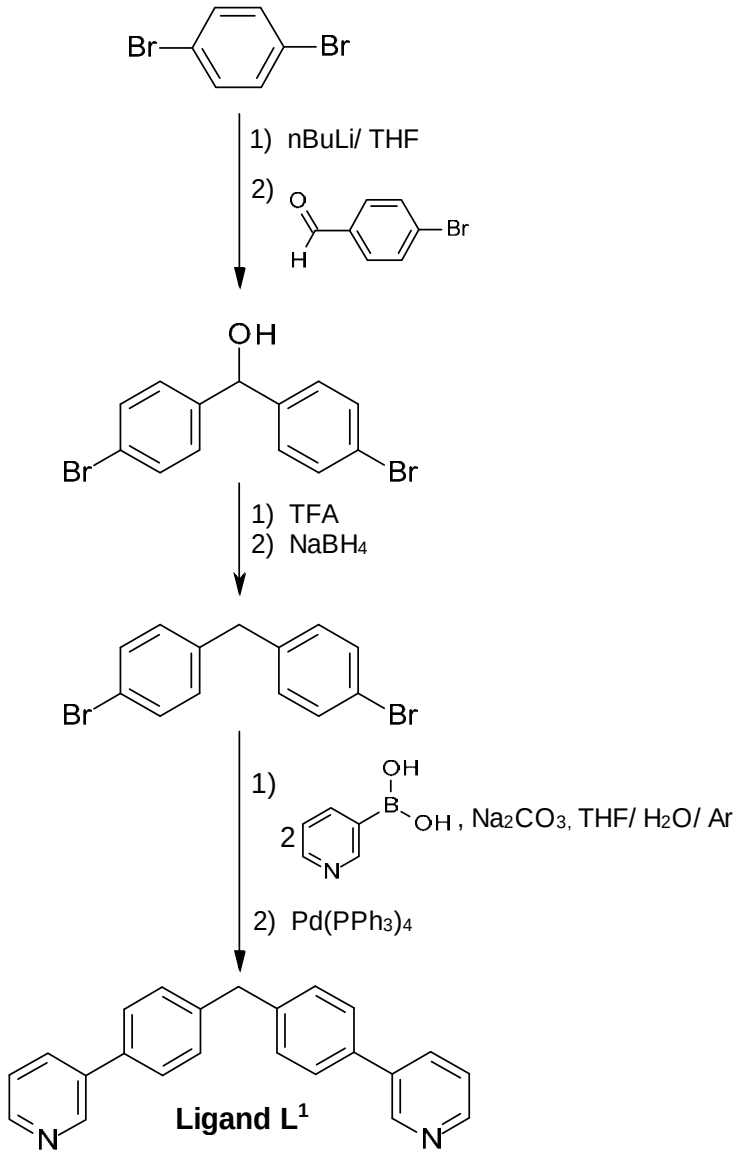

Scheme 2.1. Synthesis of Ligand **L^1**.

Ligand **L^1** was synthesized by a Suzuki coupling reaction between bis(4-bromophenyl)methane[9] and pyridine-3-yl-3-boronic acid using $Pd(PPh_3)_4$ as a catalyst and Na_2CO_3 as a base (Scheme 2.1).[10] As confirmed by ^1H NMR, ligand **L^1** was formed as the predominant product, however, the mono-substituted bromophenylmethane was also present as a side product. The

crude material was purified on a preparative RP-HPLC column using a linear gradient of 100 % water to 100 % methanol over 60 minutes. The product peak was collected at 50.15 minutes and the solvent removed under reduced pressure to yield the white product in 72 % yield.

The EI mass spectrum is dominated by a single peak corresponding to $\{\mathbf{L^1}\}^+$ at *m/z* 322 and partial microanalytical data are consistent with a $\{C_{23}H_{18}N_2\}$ formulation. The ^{1}H NMR spectrum in d_4-methanol reveals a single set of resonances and confirms the formation of the symmetrical ligand (Figure 2.6).

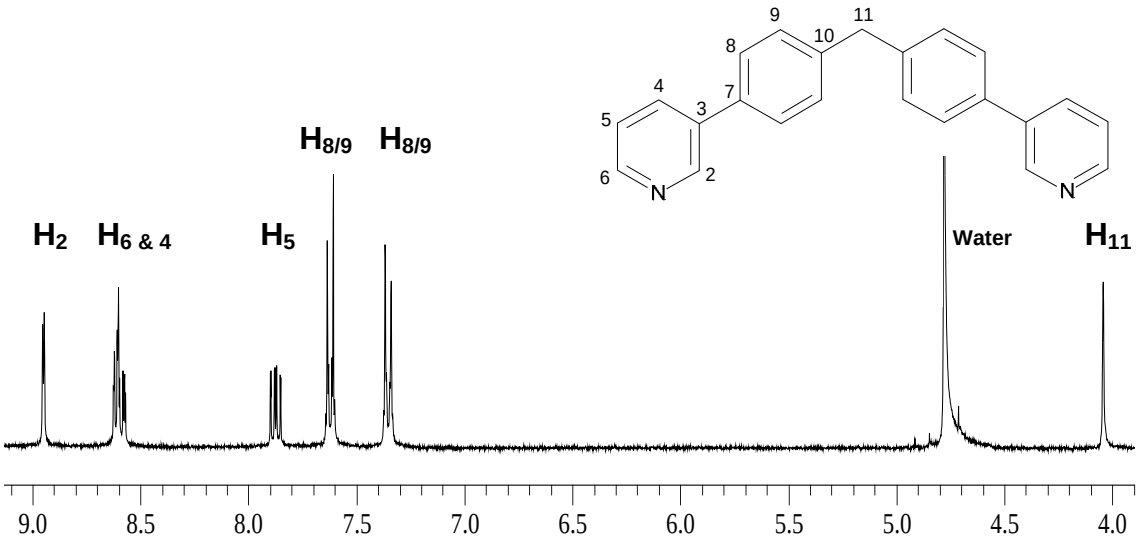

Figure 2.6. ^{1}H NMR spectrum of Ligand **L^1**
(300 MHz, d_4-methanol, 298 K).

2.2.2 Palladium(II) complexes of L^1

Ligand **L^1** was coordinated to palladium(II) by stirring a solution of the ligand with tetrakis(acetonitrile)palladium(II) tetrafluoroborate for 16 hours, under an argon atmosphere. The solution was filtered to remove a small amount of suspended material and the solvent removed under vacuum. The *crude* product was washed with chloroform, acetone and diethyl ether to yield a white solid in a high yield of 83 %.

The IR spectrum of the complex shows a strong, broad absorption at 1034 cm^{-1}; This is characteristic of non-coordinated tetrafluoroborate counter-ions. Elemental analysis data are consistent with an empirical formula of $\{Pd(C_{23}H_{18}N_2)_2(BF_4)_2\}_n$ and the ESI mass spectrum is dominated by peaks corresponding to $[Pd_2(\mathbf{L^1})_4(BF_4)(F)]^{2+}$ (*m/z* 804), $[Pd_2(\mathbf{L^1})_4(BF_4)]^{3+}$ (*m/z* 530) and $[Pd_2(\mathbf{L^1})_4]^{4+}$ (*m/z* 376), confirming the expected M_2L_4 formulation. The ^{1}H NMR spectra of ligand $\mathbf{L^1}$ and $[Pd_2(\mathbf{L^1})_4][BF_4]_4$ are shown in Figure 2.7.

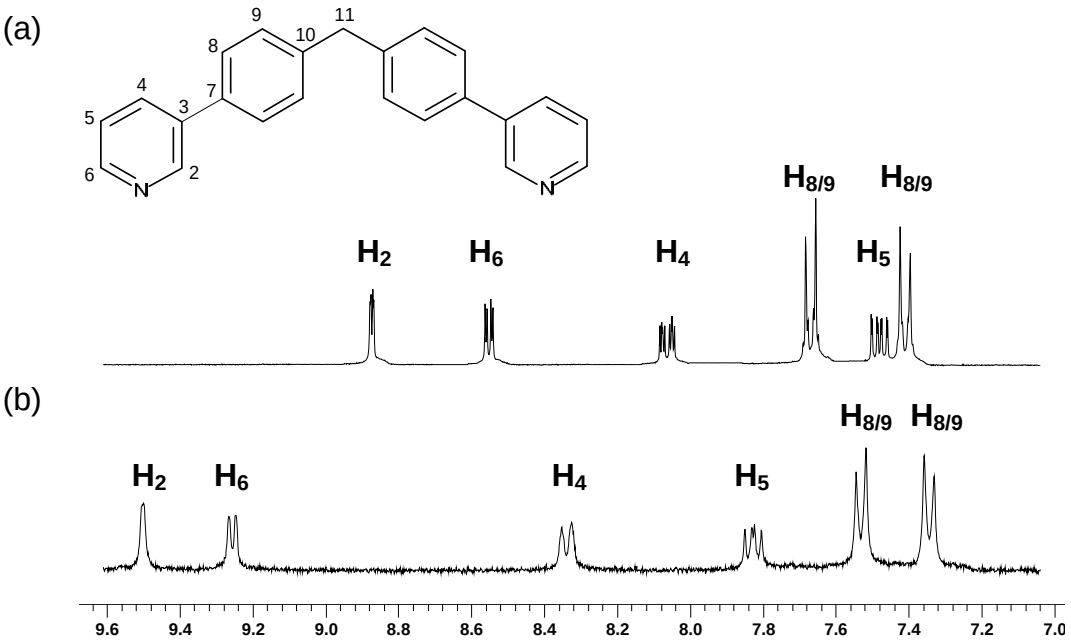

Figure 2.7. ^{1}H NMR spectra of the aromatic region of (a) Ligand $\mathbf{L^1}$ and (b) $[Pd_2(\mathbf{L^1})_4][BF_4]_4$ (300 MHz, d_6-DMSO, 298 K).

The ^{1}H NMR spectrum of the complex exhibits one aliphatic and six aromatic proton resonances, indicating the presence of a single, symmetrical species in solution. There is a considerable downfield shift of the pyridine signals relative to those in the free ligand due to the metal-ligand complexation.

The ^{19}F NMR spectrum of the cylinder displays a single peak at -147.7 ppm. This indicates that, at 298 K, the fluorine atoms of each counter-ion

are equivalent and that on the NMR timescale, all of the anions are in the same chemical environment.

Colourless crystals of this palladium(II) complex suitable for X-ray diffraction were obtained by the slow diffusion of benzene into a solution of the complex in DMSO.[11]

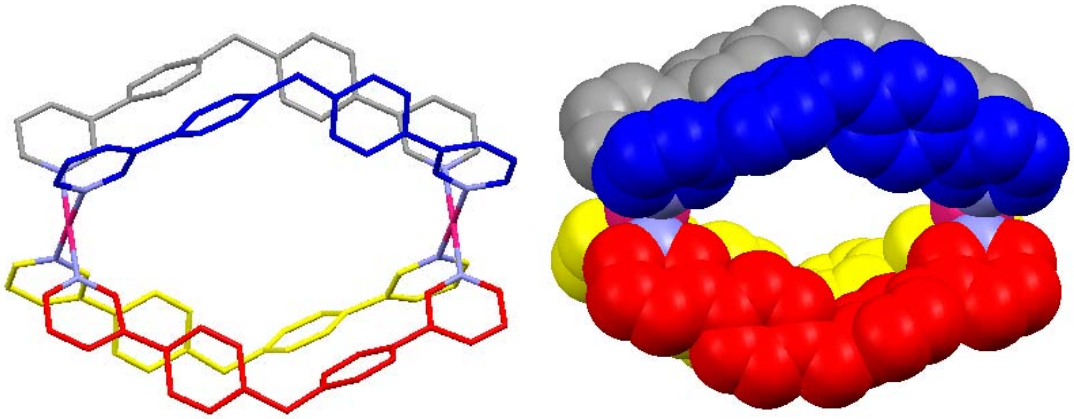

(a) (b)

Figure 2.8. (a) Perspective view and (b) space-filling representation of $[Pd_2(\mathbf{L}^1)_4]^{4+}$ cation. Hydrogen atoms, solvent molecules and anions are omitted for clarity.[11]

The X-ray crystal structure (Figure 2.8) confirms the formation of a tetra-stranded, dinuclear palladium(II) cylinder. Each metal centre occupies a four-coordinate, square planar environment with Pd-N bond distances of 1.983(4)-2.007(3) Å and N-Pd-N angles of 89.16(12)-90.74(12)º. The four ligands bridge the two palladium(II) centres resulting in a Pd···Pd separation of 12.7 Å. Within the ligands, the phenyl rings are twisted with respect to one another (71º, 74º) and with respect to the pyridine rings (27º, 35º, 40º, 46º). The cavity formed by the ligands is home to two DMSO molecules aligned along the Pd···Pd axis, however, the remaining solvent molecules and the counter-ions are highly disordered, prohibiting further discussions.

In contrast to Hannon's iron(II) cylinder which has a helical conformation, this palladium(II) cylinder crystallises with a plane of symmetry through the centre of the four ligands and is therefore achiral (Figure 2.9). The non-helical nature of this cylinder stems from the rigidity of $\mathbf{L^1}$ which also leads to an increase in the diameter of the cylinder (C···C 13.7 Å for Pd, 8.9 Å for Fe: H··H 14.9 Å for Pd, 10.8 Å for Fe). At 12.7 Å, the metal-metal separation is slightly larger than in the iron(II) cylinder (11.5 Å) and as the ligand is shorter, the overall length of the cylinder is smaller (C···C 15.0 Å for Pd, 17.3 Å for Fe: H··H 16.6 Å for Pd, 19.5 Å for Fe).

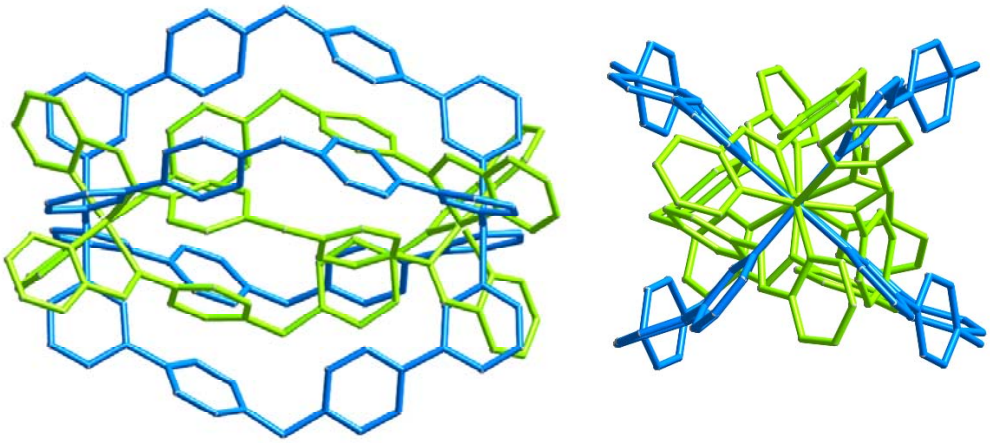

Figure 2.9. Overlay of the X-ray crystal structures of $[Pd_2(\mathbf{L^1})_4]^{4+}$ (blue) and $[Fe_2(\mathbf{L})_3]^{4+}$ (green). Hydrogen atoms are omitted for clarity.

The crystal packing of $[Pd_2(\mathbf{L^1})_4][BF_4]_4$ clearly shows that the cylinders are implicated in intermolecular π-π stacking interactions through the phenyl rings of the central spacer units with an inter-planar separation of 3.7 Å (Figure 2.10). This leads to the formation of chains of cylinders in which each cation is connected to its neighbour by two such interactions. Counter-ions and solvent molecules occupy the gaps between the cation chains.

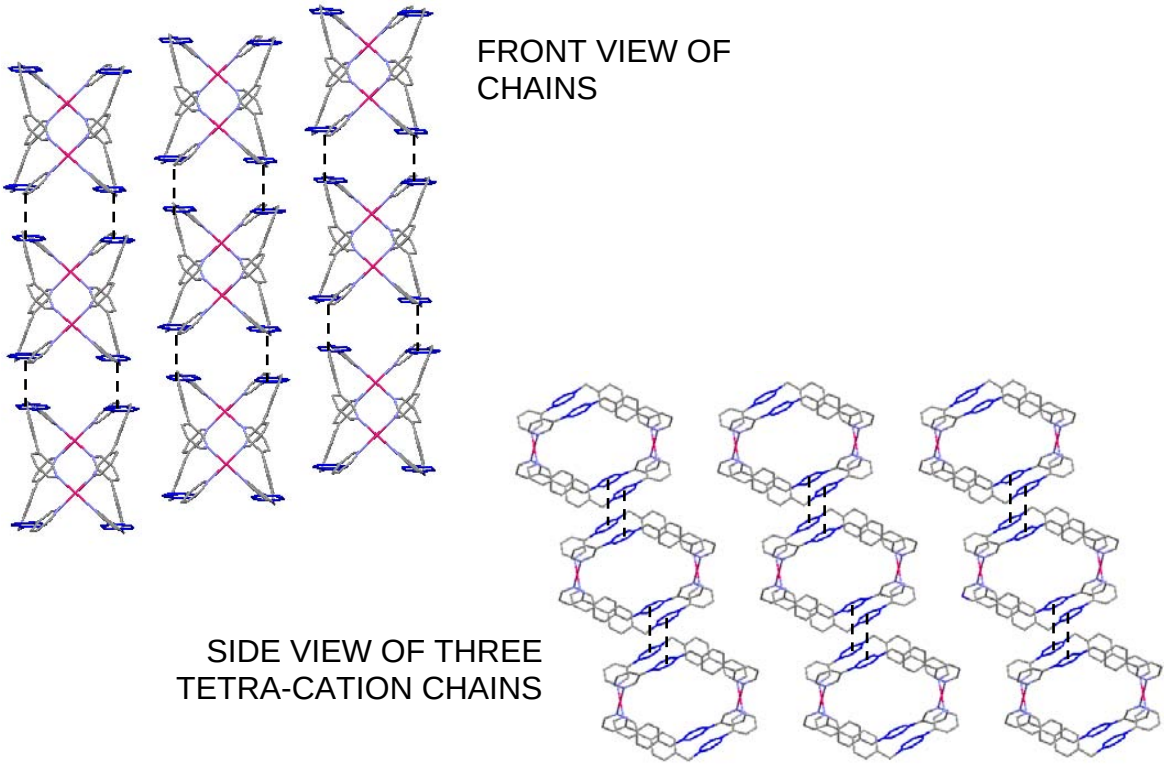

Figure 2.10. Packing diagrams for $[Pd_2(\mathbf{L}^{\mathbf{1}})_4]^{4+}$ cations showing the π-π stacking interactions between the phenyl rings. Hydrogen atoms, anions and solvent molecules have been removed for clarity.

Unfortunately, this palladium(II) cylinder did not prove to be water soluble, which is one of the preferred criteria for carrying out compound-DNA binding studies. However, changing the counter-ion of a complex often results in a variation in its aqueous solubility. Chloride ions are the most commonly used anions in commercial drugs.[12] Thus an attempt was made to exchange the tetrafluoroborate counter-ions of our complex with chloride ions. This was done by stirring a methanolic suspension of the complex with the chloride form of Dowex (a strongly basic exchange resin) for one hour and then filtering through a Dowex column. Disappointingly, on removal of the methanol, the resultant material was still insoluble in water. A ^{1}H NMR spectrum of the complex in

d$_6$-DMSO was very messy, indicating that some sort of degradation reaction had occurred.

In a second attempt the counter-ions in this cylinder were exchanged for nitrate ions which have also been shown to increase water solubility in several compounds. This was achieved by synthesising the complex in the normal way but precipitating the tetra-cation from the mother liqueur by the drop-wise addition of an acetonitrile solution of tetrabutylammonium nitrate. The resulting product was purified by washing with a range of organic solvents. Partial elemental analysis and ESI mass spectrometry confirm that the tetrafluoroborate counter-ions have been exchanged for nitrate anions. The microanalytical data support a {$Pd_2(\mathbf{L^1})_4(NO_3)_4$} formulation and the ESI mass spectrum reveals peaks with the correct isotope patterns and mass/charge ratios to correspond to $[Pd_2(\mathbf{L^1})_4(NO_3)_2]^{2+}$ (*m/z* 813), $[Pd_2(\mathbf{L^1})_4(NO_3)]^{3+}$ (*m/z* 521) and $[Pd_2(\mathbf{L^1})_4]^{4+}$ (*m/z* 376). The ^{1}H NMR spectrum in *d*$_6$-DMSO is analogous to that of $[Pd_2(\mathbf{L^1})_4][BF_4]_4$. A single set of signals is observed indicating the presence of a single solution species at 298 K. Recrystallisation of the nitrate salt from a DMSO solution by the slow diffusion of benzene afforded colourless crystals which proved suitable for investigation by X-ray diffraction. As expected, the crystal structure reveals a tetra-stranded, dinuclear cylinder. The X-ray crystal structures of the nitrate and tetrafluoroborate salts are both shown in Figure 2.11. The structures of the tetra-cations are indistinguishable and both pack into a crystal lattice in an analogous way.

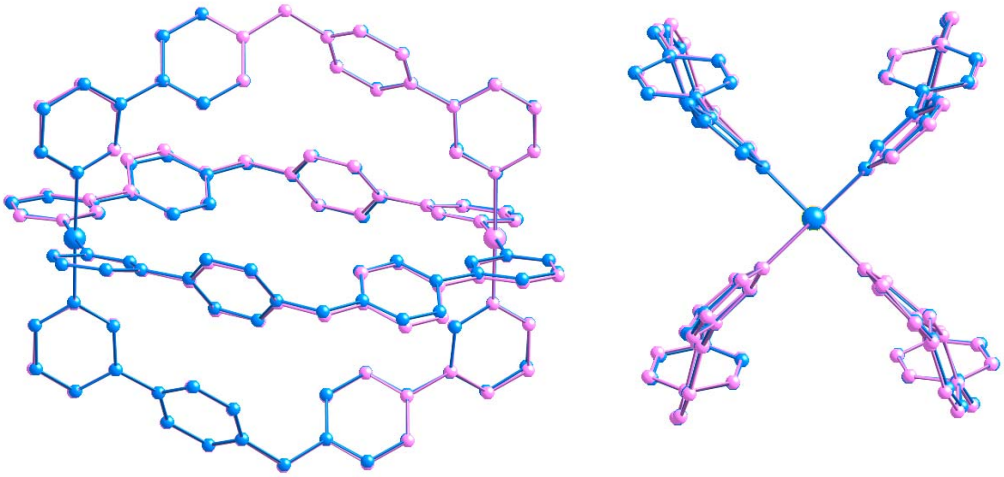

Figure 2.11. Overlays of the X-ray crystal structures of $[Pd_2(\mathbf{L^1})_4][NO_3]_4$ and $[Pd_2(\mathbf{L^1})_4][BF_4]_4$. Hydrogen atoms, solvent molecules and anions are omitted for clarity.

Unfortunately, solubility studies did not show any enhancement in the aqueous solubility of the nitrate cylinder compared to that of the tetrafluoroborate one. Therefore, in a final attempt the counter-ions of our tetra-cationic complex were exchanged for trifluoroacetate anions. This was done by synthesising the complex as previously described and precipitating it with a solution of sodium trifluoroacetate. The *crude* material was soluble in some of the organic solvents that had previously been used to purify the tetrafluoroborate and nitrate salts by simple washing. Therefore, purification of the trifluoroacetate salt was achieved by semi-preparative RP-HPLC using a solvent gradient of 100 % $H_20_{(0.05\ \%\ TFA)}$ to 100 % $methanol_{(0.05\ \%\ TFA)}$ over a 40 minute duration. The pure complex was observed and collected at 36.83 minutes.

The partial microanalytical data are consistent with a $[Pd_2(\mathbf{L^1})_4][CF_3CO_2]_4$ formulation. The ESI mass spectrum shows peaks (with the correct isotope distributions) corresponding to $[Pd_2(\mathbf{L^1})_4(TFA)_2]^{2+}$ (*m/z* 864) and $[Pd_2(\mathbf{L^1})_4(TFA)]^{3+}$ (*m/z* 539). A fragment ion corresponding to $[Pd_2(\mathbf{L^1})_3(TFA)_2]^{2+}$

is also observed at *m/z* 703. As with the tetrafluoroborate and nitrate salts, the ^{1}H NMR spectrum of $[Pd_2(\mathbf{L^1})_4][CF_3CO_2]_4$ only displays one set of resonances (Figure 2.12).

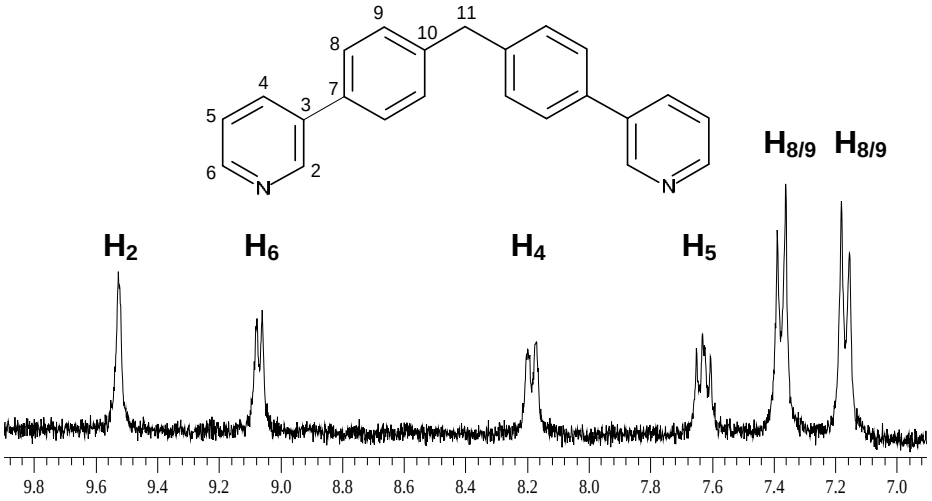

Figure 2.12. ^{1}H NMR spectrum of the aromatic region of $[Pd_2(\mathbf{L^1})_4][TFA]_4$ (300 MHz, d_4-methanol, 298 K).

Solubility studies proved the complex to be more soluble in organic solvents such as methanol compared to the tetrafluoroborate analogue, but it nevertheless remained insoluble in pure water.

Attempts to grow crystals from methanolic or DMSO solutions of this pure trifluoroacetate complex were unsuccessful. However, X-ray quality crystals were obtained by the slow diffusion of benzene into a DMSO solution of the *crude* product resulting in an unexpected outcome (Figure 2.13).[13]

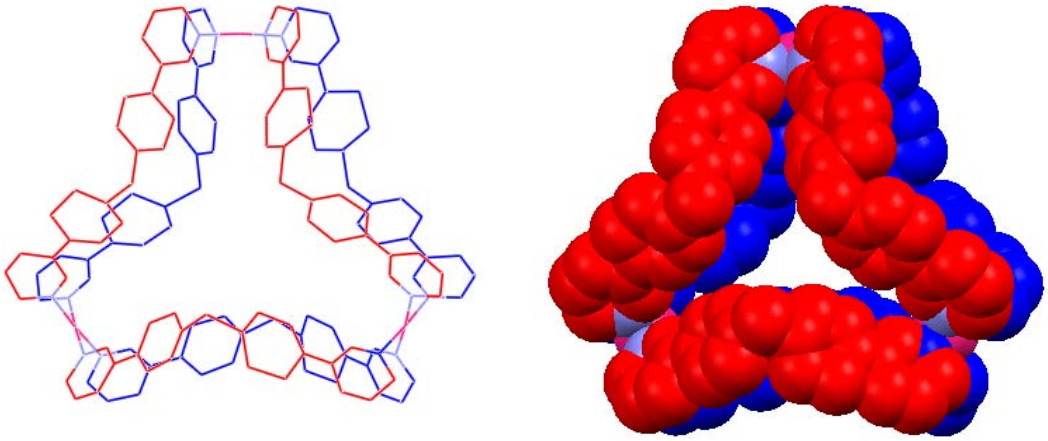

(a) **(b)**

Figure 2.13. (a) Perspective view and (b) space-filling representation of $[Pd_3(\mathbf{L^1})_6]^{6+}$ cation. Hydrogen atoms and anions are omitted for clarity.[13]

Intriguingly, the solid state structure did not display the $[Pd_2(\mathbf{L^1})_4]^{4+}$ tetra-cation that had been expected, but instead revealed a double-walled, hexa-cationic $[Pd_3(\mathbf{L^1})_6]^{6+}$ structure. The three square-planar Pd(II) atoms reside in a single plane and occupy the three corners of a triangle. Some examples of previously reported supramolecular triangles have already been discussed in chapter 1, section 1.6.2. In this triangle, each metal centre is linked to the next by two bridging ligands, one extending behind the plane of the Pd(II) centres (shown in blue) and the other protruding in front of it (shown in red). The size of the unit cell was measured for a number of crystals from the sample confirming that this was the only structure that had crystallised from the *crude* mixture. The HPLC trace of the *crude* material showed one major peak and several smaller ones. Fractions were collected from an analytical column and ESI mass spectrometry confirmed that the large peak corresponded to the required $[Pd_2(\mathbf{L^1})_4][CF_3CO_2]_4$ cylinder. Unfortunately the fractions of the other substituents did not contain enough material to give a mass spectrum. The HPLC trace showed that the tetra-stranded cylinder accounted for ~76 % of the *crude* mixture; therefore,

$[Pd_3(\mathbf{L^1})_6][CF_3CO_2]_6$ must only constitute a small percentage, but is evidently more inclined to crystallise out of solution in the conditions that were used.

2.2.3 Platinum(II) complex of L^1

The corresponding complex of platinum(II) was formed by the reaction of two equivalents of ligand $\mathbf{L^1}$ with bis(benzonitrile)dichloroplatinum(II) in the presence of silver(I) nitrate (for chloride abstraction). A ^{1}H NMR spectrum of the *crude* material shows the presence of one main product and several side products. Purification was achieved on two semi-preparative RP-HPLC columns; the first used a solvent gradient of 100 % water$_{(0.05\ \%\ TFA)}$ to 100 % methanol$_{(0.05\ \%\ TFA)}$ over 50 minutes and yielded the impure product after 34.00 minutes. The second column used a gradient of 100 % water to 100 % methanol over 40 minutes and presented the pure product after 26.56 minutes. The trifluoroacetic acid used on the first column resulted in an exchange of the nitrate counter-ions for trifluoroacetate anions. The ESI mass spectrum of this complex displays peaks corresponding to $[Pt_2(\mathbf{L^1})_4(CF_3CO_2)_2]^{2+}$ and $[Pt_2(\mathbf{L^1})_4(CF_3CO_2)]^{3+}$, confirming the change in counter-ion. The ^{1}H NMR spectrum of this complex is shown in Figure 2.14.

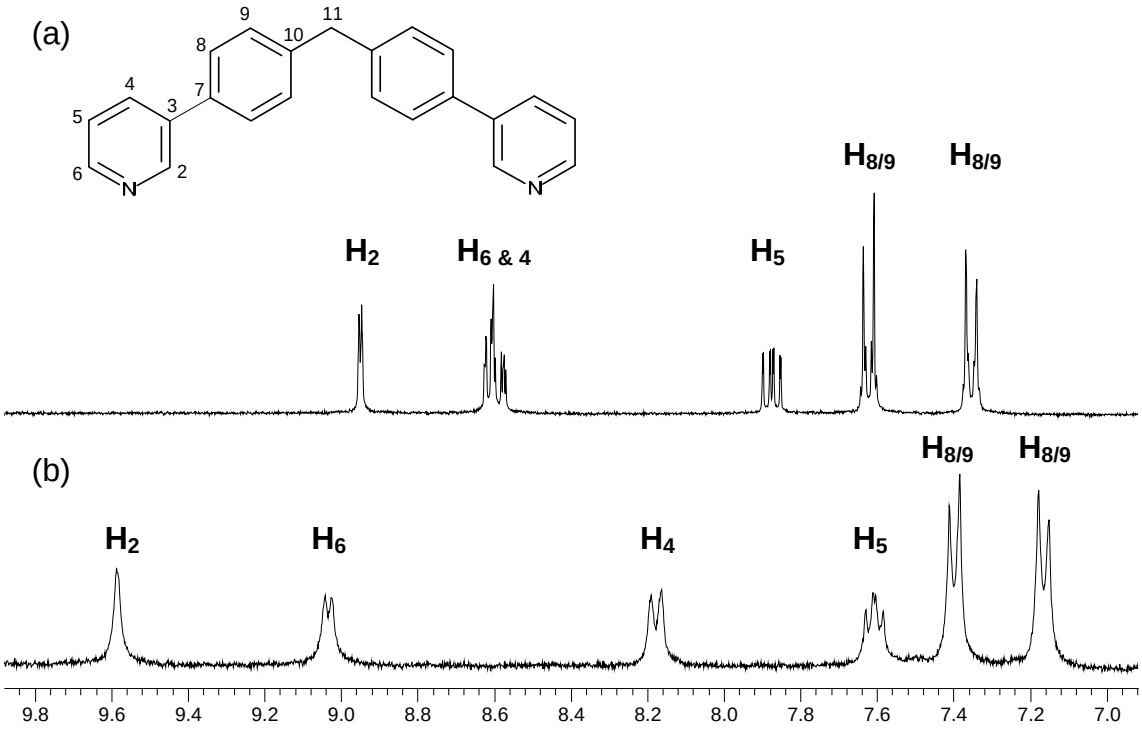

Figure 2.14. ^{1}H NMR spectrum of the aromatic region of (a) Ligand **L^{1}** and (b) $[Pt_2(\mathbf{L^1})_4][TFA]_4$ (300 MHz, *d*$_4$-methanol, 298 K).

The ^{1}H NMR spectrum in *d*$_4$-methanol reveals the presence of one set of signals which is consistent with a single solution species, symmetrically balanced through the central CH_2 substituent. As with the palladium(II) complex, there is a significant downfield shift of the **H$_2$** and **H$_6$** pyridine signals relative to those of the free ligand in the same solvent.

Unfortunately, attempts to crystallise the trifluoroacetate salt of this complex proved unsuccessful. However, colourless crystals were obtained by the slow diffusion of benzene into a solution of the *crude* nitrate salt in DMSO. The X-ray crystal structure unambiguously reveals a dimeric, tetra-stranded $[Pt_2(\mathbf{L^1})_4]^{4+}$ cation (Figure 2.15).[13]

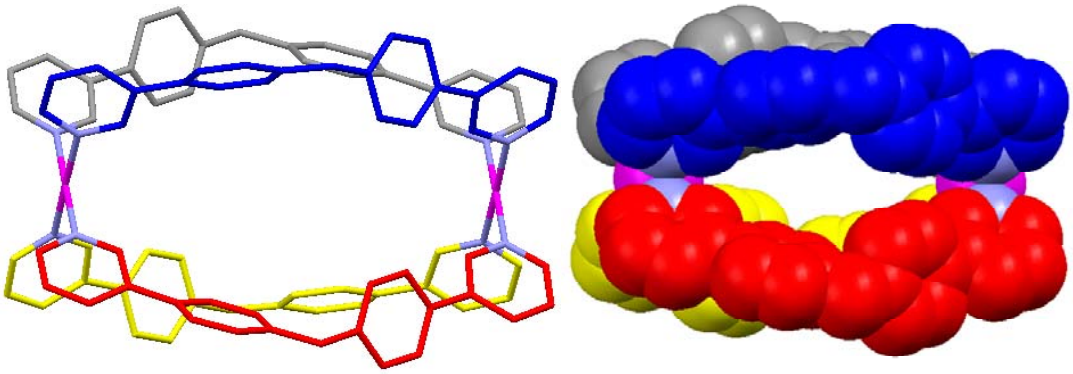

(a) (b)

Figure 2.15. (a) Perspective view and (b) space-filling representation of $[Pt_2(\mathbf{L^1})_4]^{4+}$ cation. Hydrogen atoms and anions are omitted for clarity.[13]

Each platinum(II) centre has square planar geometry with Pt-N bond distances ranging between 2.028(5)-2.036(5) Å and with N-Pt-N angles of 88.8(2)-91.7(2)º. In the ligands the phenyl rings are twisted about the central CH_2 by 74º and 75º. The phenyl rings are also twisted with respect to the pyridine rings (30º, 33º, 40º, 44º). The transannular Pt···Pt distance is 12.7 Å, which is the same as the Pd···Pd distance in the analogous $[Pd_2(\mathbf{L^1})_4][BF_4]_4$ complex. This platinum cylinder has a tetra-cationic charge but only two nitrate counter-ions have been found. The remaining anions could not be successfully identified among the residual electron density as they are highly disordered. Along with four benzene rings and two DMSO molecules, the detected counter-ions are located in the gaps between the cylinders and do not make any obvious contacts to them or to each other. A crystal packing diagram of $[Pt_2(\mathbf{L^1})_4]^{4+}$ is shown in Figure 2.16.

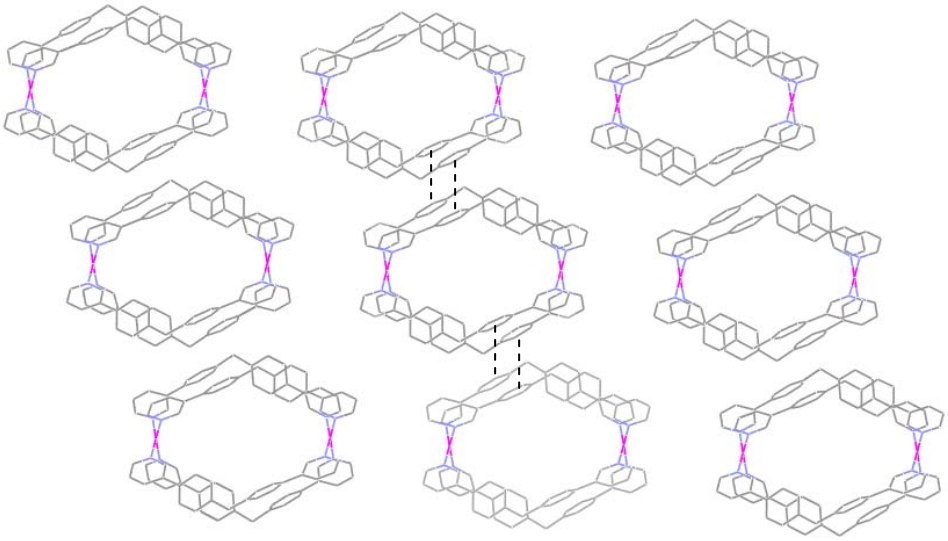

Figure 2.16. Packing diagram for $[Pt_2(\mathbf{L^1})_4]^{4+}$ cations showing the π-π stacking interactions between the phenyl rings. Hydrogen atoms, anions and solvent molecules have been removed for clarity.

Analysis of the crystal packing shows that the cylinders are packed in chains through π-π stacking interactions in the same way as for the analogous $[Pd_2(\mathbf{L^1})_4]^{4+}$. However, in this case the inter-planar distance between the phenyl rings is slightly smaller at 3.6 Å (compared to 3.7 Å in the palladium complex). Benzene, DMSO and nitrate counter-ions are found to occupy the gaps between the cationic chains.

It is pertinent to compare the crystal structure of this platinum(II) cylinder with that of the previously described $[Pd_2(\mathbf{L^1})_4][BF_4]_4$ complex. Therefore, an overlay of the structures is shown in Figure 2.17.

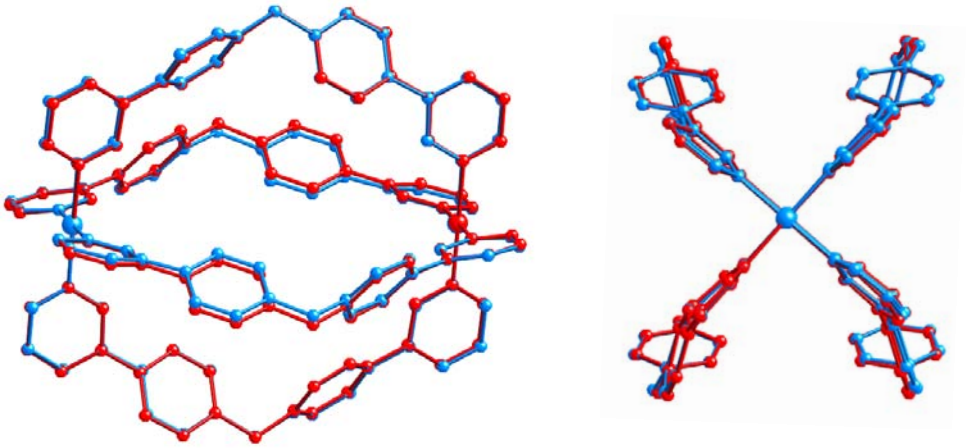

Figure 2.17. Overlays of the X-ray crystal structures of $[Pd_2(\mathbf{L}^1)_4]^{4+}$ and $[Pt_2(\mathbf{L}^1)_4]^{4+}$. Hydrogen atoms, solvent molecules and counter-ions are omitted for clarity.

Figure 2.17 shows that the cations are almost structurally identical. Clearly the replacement of the palladium(II) ions with platinum(II) has had very little effect on the arrangement of the ligands within the cylinder.

Solubility studies show that $[Pt_2(\mathbf{L}^1)_4][CF_3CO_2]_4$ is highly soluble in organic solvents such as DMF, DMSO and methanol but as with the palladium(II) complexes, it remains insoluble in pure water.

Thus far this study shows that counter-ion exchange alone has proved to be an ineffective way of increasing the aqueous solubility of $[Pd_2(\mathbf{L}^1)_4]^{4+}$ so another strategy needs to be employed. It is well known that ethers have the ability to act as hydrogen-bond acceptors. This trait enables them to engage in hydrogen bond interactions with water molecules resulting in an increase in the water solubility of the ether, relative to the same molecule without the hydrogen-bond acceptor. Therefore, the next approach was to functionalise the ligand with an ether group in the hope that it will enhance the aqueous solubility of the resulting complex.

2.2.4 Ligand L^2

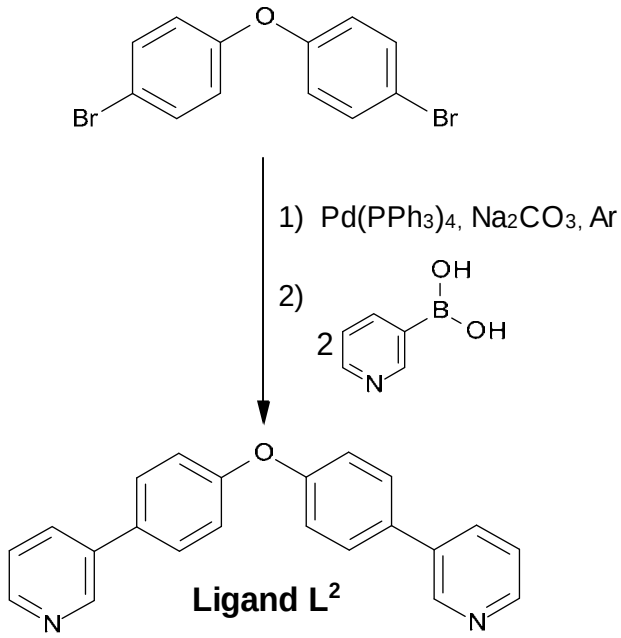

Scheme 2.2. Synthesis of Ligand **L^2**.

Ligand **L^2** is analogous to **L^1** except that the central CH_2 has been replaced by an oxygen atom. The ligand was prepared by a $Pd(PPh_3)_4$ catalyzed Suzuki coupling reaction between bis-4-bromophenylether and pyridine-3-yl-3-boronic acid (Scheme 2.2).[10] It was purified on a preparative RP-HPLC column using a linear gradient of 100 % water to 100 % methanol over 40 minutes and a 15 minute methanol wash. The product was collected at 49.58 minutes and the solvent removed to give the pure ligand in 64 % yield.

Partial microanalytical data are consistent with a $\{C_{22}H_{16}N_2O\}$ formulation and the EI positive ion mass spectrum shows an intense peak at *m/z* 324 which corresponds to $\{\mathbf{L^2}\}^+$. The ^{1}H NMR spectrum in d_1-chloroform reveals a single set of six aromatic resonances above 7 ppm confirming the formation of the symmetrical ligand (Figure 2.18).

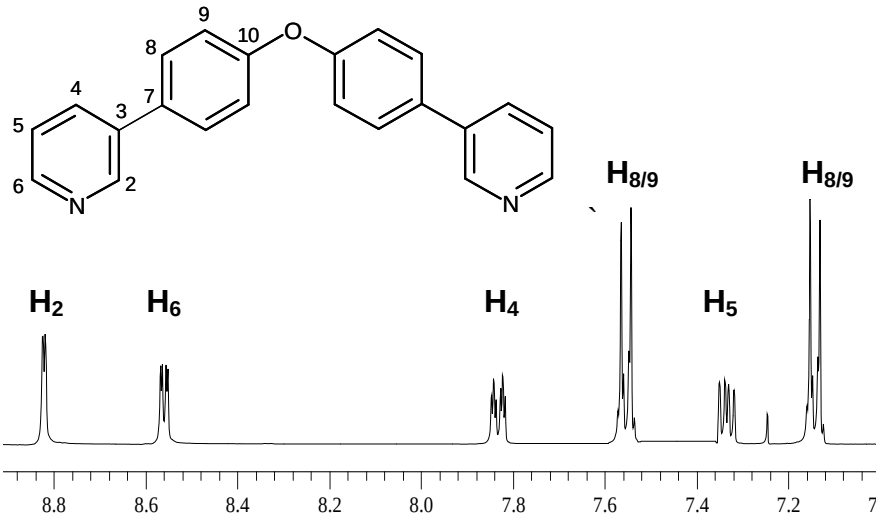

Figure 2.18. ^{1}H NMR spectrum of Ligand **L^{2}**
(400 MHz, *d$_{1}$*-chloroform, 298 K).

2.2.5 Palladium(II) complexes of L^{2}

Coordination of palladium(II) to ligand **L^{2}** was achieved by the reaction of tetrakis(acetonitrile)palladium(II) tetrafluoroborate with two equivalents of **L^{2}** in acetonitrile. The reaction took place over a 16 hour period under an inert argon atmosphere, presenting the white product in a near quantitative yield of 91 %.

FT-IR spectroscopy confirms the presence of a non-coordinated tetrafluoroborate anion by the occurrence of a strong absorption band at 1010 cm^{-1}. The partial elemental analysis data supports the formation of a tetra-stranded, dinuclear palladium(II) complex and the ESI mass spectrum is dominated by peaks corresponding to $[Pd_2L_4(BF_4)_2]^{2+}$, $[Pd_2L_4(BF_4)]^{3+}$ and $[Pd_2L_4]^{4+}$ species. The ^{1}H NMR spectrum of the complex was recorded in *d$_{6}$*-DMSO and is presented in Figure 2.19. The spectrum shows a single set of resonances indicating the formation of a distinct symmetrical species. The metal-ligand coordination is confirmed by the significant downfield shift of the pyridine signals of the complex relative to those in the free organic ligand. This

is especially apparent for **H_2** and **H_6** which are both downfield shifted by 0.8 ppm relative to the same signals in the free ligand.

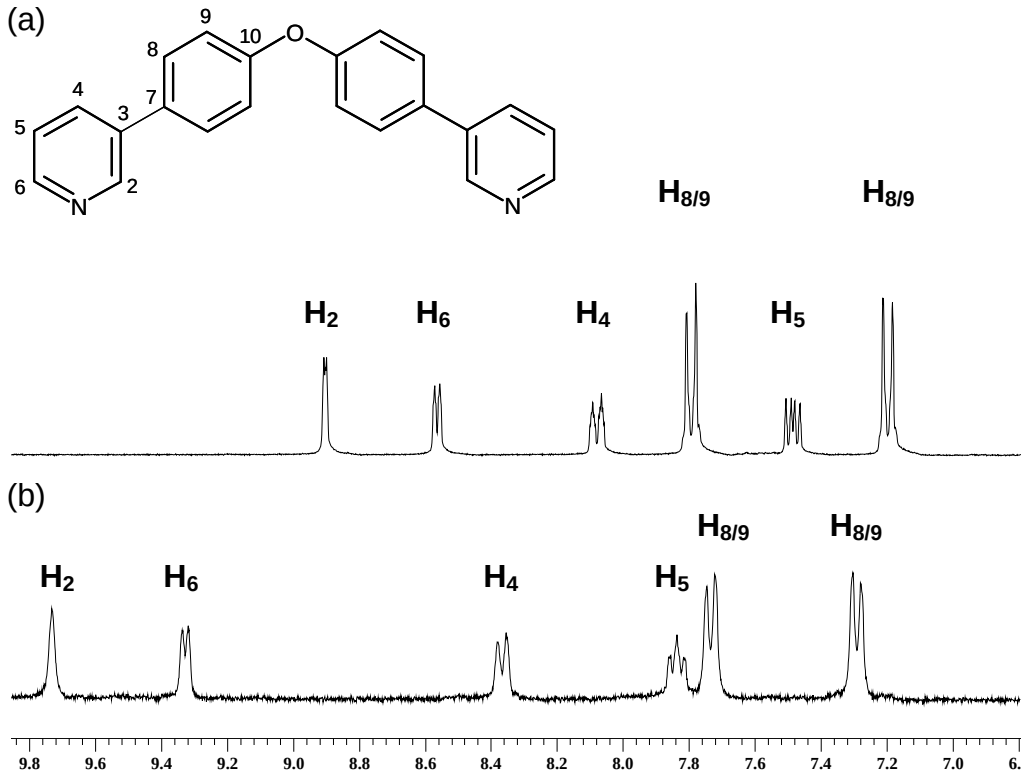

Figure 2.19. ^{1}H NMR spectra of (a) Ligand **L^2** and (b) $[Pd_2(\mathbf{L^2})_4][BF_4]_4$ (300 MHz, d_6-DMSO, 298 K).

On coordination to palladium(II) the phenyl signal that is furthest up-field becomes downfield shifted. In contrast, in the ^{1}H NMR of $[Pd_2(\mathbf{L^1})_4][BF_4]_4$ this phenyl signal is shifted up-field. The other main difference in the ^{1}H NMR spectra of these two complexes occurs for **H_2** which is considerably more downfield shifted in $[Pd_2(\mathbf{L^2})_4][BF_4]_4$ than in $[Pd_2(\mathbf{L^1})_4][BF_4]_4$. These differences might occur due to a change in the twist between the pyridine and phenyl rings.

Diffusion of benzene into a solution of the complex in DMSO gave single crystals suitable for X-ray diffraction studies. The crystal structure obtained from the studies is in agreement with that predicted from the spectroscopic evidence (Figure 2.20).[11]

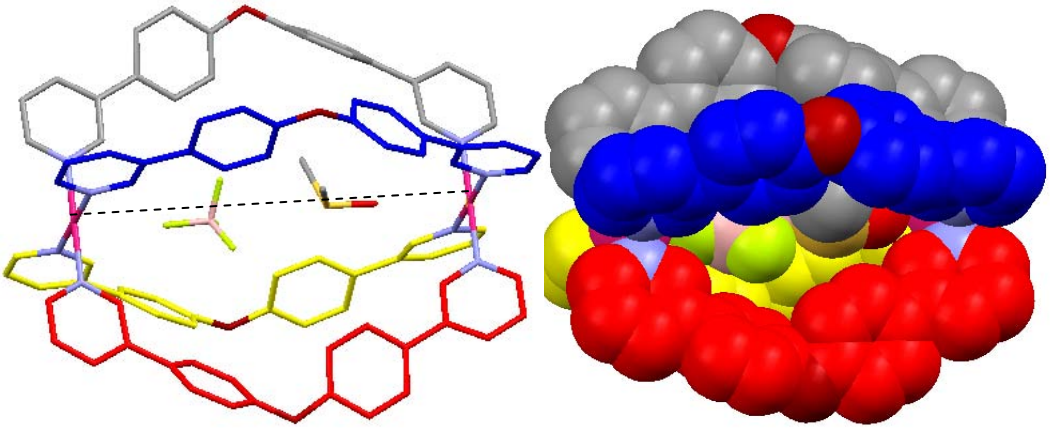

(a) (b)

Figure 2.20. (a) Perspective view and (b) space-filling representation of $[Pd_2(\mathbf{L^2})_4]^{4+}$ cation. Hydrogen atoms and anions are omitted for clarity.[11]

Each square-planar metal centre is bound to one pyridyl unit from each of the four ligands. The Pd-N bond distances (2.031(3)-2.036(3) Å) and the N-Pd-N bond angles (88.07(14)-92.63(18)º) are unremarkable and analogous to those found in the $[Pd_2(\mathbf{L^1})_4]^{4+}$ cation. Within each ligand the phenyl rings are twisted about the central oxygen spacer at angles to each other of 64º and 72º. The phenyl rings are also twisted with respect to the pyridyl binding units (16º, 32º, 39º, 50º). Encapsulated within the central cavity of the complex is a tetrafluoroborate counter-ion and a DMSO solvent molecule. These guest molecules are linearly located along the Pd···Pd axis as shown in Figure 2.20 (a). The shortest Pd-F distance for the encapsulated anion is 3.1 Å and the Pd-O distance for the DMSO molecule is 3.0 Å. This suggests that the guest molecules make weak ionic interactions with the palladium(II) centres.

The distance separating the two Pd(II)···Pd(II) centres is 12.4 Å which is slightly less (~2 %) than in the analogous $[Pd_2(\mathbf{L^1})_4][BF_4]_4$ complex due to shorter C_{phenyl}-O bond distances (1.39(5)-1.40(5) Å) compared to the C_{phenyl}-CH_2 ones (1.47(4)-1.60(4) Å). An overlay of $[Pd_2(\mathbf{L^1})_4]^{4+}$ and $[Pd_2(\mathbf{L^2})_4]^{4+}$ is shown in Figure 2.21.

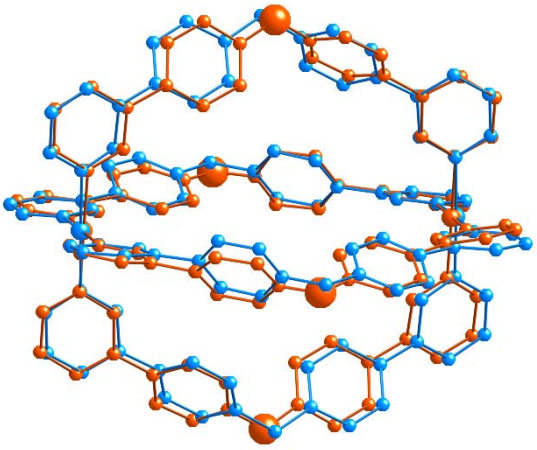

Figure. 2.21. An overlay of the X-ray structures of $[Pd_2(\mathbf{L}^1)_4]^{4+}$ and $[Pd_2(\mathbf{L}^2)_4]^{4+}$. Hydrogen atoms, solvent molecules & counter-ions are omitted for clarity.

The crystal packing diagram for $[Pd_2(\mathbf{L}^2)_4]^{4+}$ (Figure 2.22) is analogous to that of $[Pd_2(\mathbf{L}^1)_4]^{4+}$ and shows that the tetra-stranded cylinders are stacked into linear chains which are held together by face-to-face π-π stacking interactions.

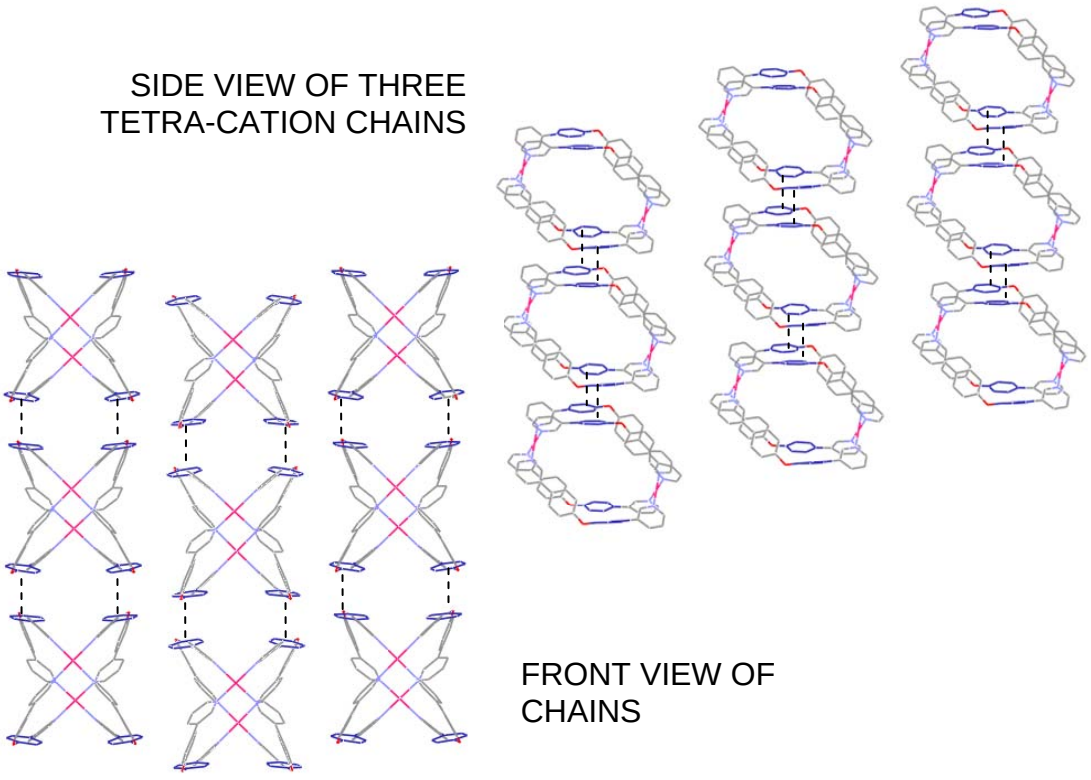

Figure 2.22. Packing diagrams for $[Pd_2(\mathbf{L}^2)_4]^{4+}$ cations showing the π-π stacking interactions between the phenyl rings. Hydrogen atoms, anions and solvent molecules have been removed for clarity.

The inter-planar distance between the stacked phenyl rings is 3.4 Å. The gaps between the cation chains are occupied by tetrafluoroborate counter-ions and the crystallising solvents, benzene and DMSO.

The complex is insoluble in 100 % water, however, there is an increase in the solubility of the complex in aqueous/organic solvent mixtures compared to the $[Pd_2(\mathbf{L^1})_4][BF_4]_4$ cylinder. The palladium(II) complex of $\mathbf{L^2}$ was also synthesised as a nitrate salt by precipitating the complex from acetonitrile with tetrabutylammonium nitrate. $[Pd_2(\mathbf{L^2})_4][NO_3]_4$ is still not soluble in water, however, there is a marked improvement in the solubility of the complex in high water component mixtures such as water:acetonitrile (2:1). In this solvent mixture the solubility was sufficient enough to obtain a weak ^{1}H NMR. However, when spectroscopic DNA binding studies were attempted using this solvent system, the complex precipitated on encountering the buffer and DNA solution.

2.2.6 Platinum(II) complex of $\mathbf{L^2}$

Complexation was achieved by heating two equivalents of ligand $\mathbf{L^2}$ and silver(I) tetrafluoroborate with one equivalent of bis(benzonitrile)dichloroplatinum(II) in acetonitrile for 48 hours. The silver salt is required to abstract the chloride ions and ensure that each metal centre has four accessible coordination sites. The *crude* product was purified on a semi-preparative RP-HPLC column using a linear gradient of 100 % water$_{(0.05\ \%\ TFA)}$ to 100 % methanol$_{(0.05\ \%\ TFA)}$ over 40 minutes and the pure product was observed and collected at 38.80 minutes. The use of TFA in the purification resulted in an exchange of the tetrafluoroborate counter-ions for trifluoroacetate anions.

The ESI mass spectrum exhibits two peaks which correspond to $[Pt_2(\mathbf{L^2})_4(CF_3CO_2)_2]^{2+}$ and $[Pt_2(\mathbf{L^2})_4(CF_3CO_2)]^{3+}$, these have the correct isotopic distribution patterns and confirm a change in counter-ion has taken place. The mono- and tetra-cationic species are not observed.

Although this platinum(II) complex does not prove to be soluble in pure water, it exhibits much better solubility in methanol and methanol/water solutions than its palladium(II) analogue. The ^{1}H NMR spectrum of this complex was recorded in *d*$_4$-methanol and is shown in Figure 2.23.

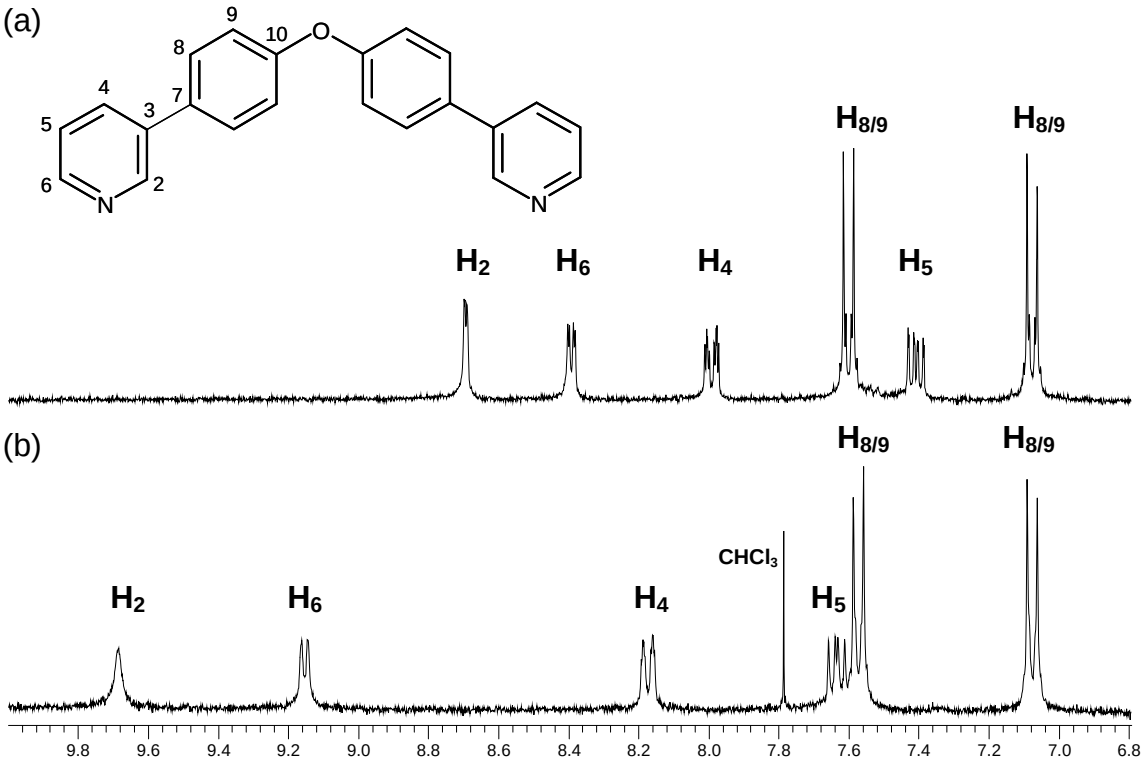

Figure 2.23. ^{1}H NMR spectra of (a) Ligand **L^2** and (b) $[Pt_2(\mathbf{L^2})_4][TFA]_4$ (300 MHz, *d*$_4$-methanol, 298 K).

The spectrum of this complex displays six aromatic signals indicating the presence of a single symmetrical species in solution. All of the pyridine proton signals are downfield shifted relative to those in the free ligand (in *d*$_4$-methanol), confirming that metal-ligand coordination has occurred. The multiplicity and

chemical shifts of the signals are similar to those observed in the ^{1}H NMR spectrum of the analogous $[Pt_2(\mathbf{L^1})_4][CF_3CO_2]_4$.

Several attempts were made to grow X-ray quality crystals of this complex, however, unfortunately all efforts proved to be unsuccessful.

2.2.7 Ligand L^3

The incorporation of the ether spacer led to a slight increase in the solubility of the resulting complexes, however, more progress is needed. Fluorine substituent's are known to participate in hydrogen bonding.[14] Fluorine is also a small functionalisation which would not affect the size and shape of the cylinder too much. Therefore fluorine was incorporated into ligand **L^3**.

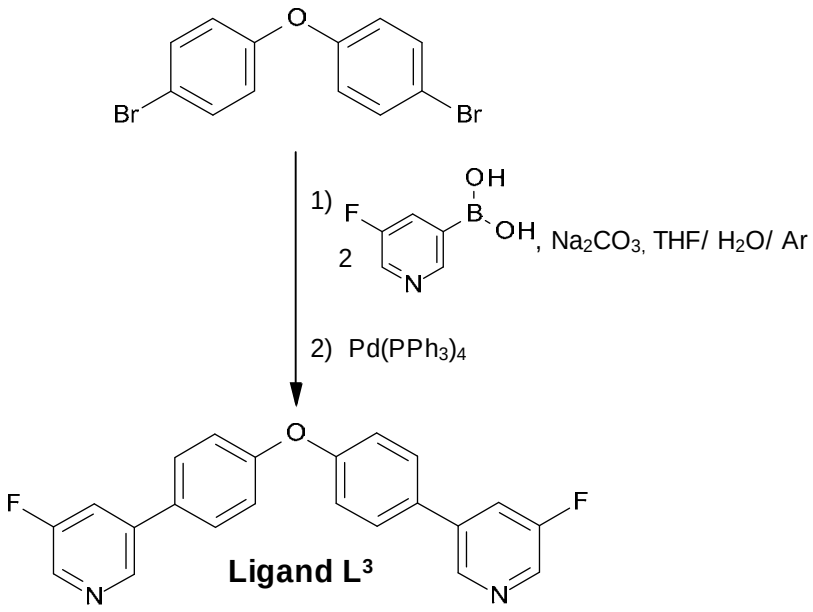

Scheme 2.3. Synthesis of Ligand **L^3**.

Ligand **L^3** is analogous to **L^2** except that fluorine has been incorporated into the 5 position of the pyridine rings. The ligand was synthesized via a Suzuki coupling reaction between bis-4-bromophenylether and two equivalents of

5-fluoropyridine-3-boronic acid. Na_2CO_3 was used to activate the boronic acid and the reaction was catalysed by $Pd(PPh_3)_4$ (Scheme 2.3).[10] The *crude* product was worked up and purified by preparative RP-HPLC using a hexane:ethyl acetate (6:4) solvent system. The pure product was observed and collected at 28.12 minutes in 50 % yield.

The EI mass spectrum of this ligand reveals an intense peak consistent with $\{\mathbf{L^3}\}^+$ at *m/z* 360 and partial elemental analysis data support a $\{C_{22}H_{14}N_2F_2O\}$ formulation. The ^{19}F NMR spectrum exhibits a single peak at -125.9 ppm and the ^1H NMR spectrum shows five resonances in the aromatic region which, as expected, indicates the formation of the required symmetrical ligand (Figure 2.24).

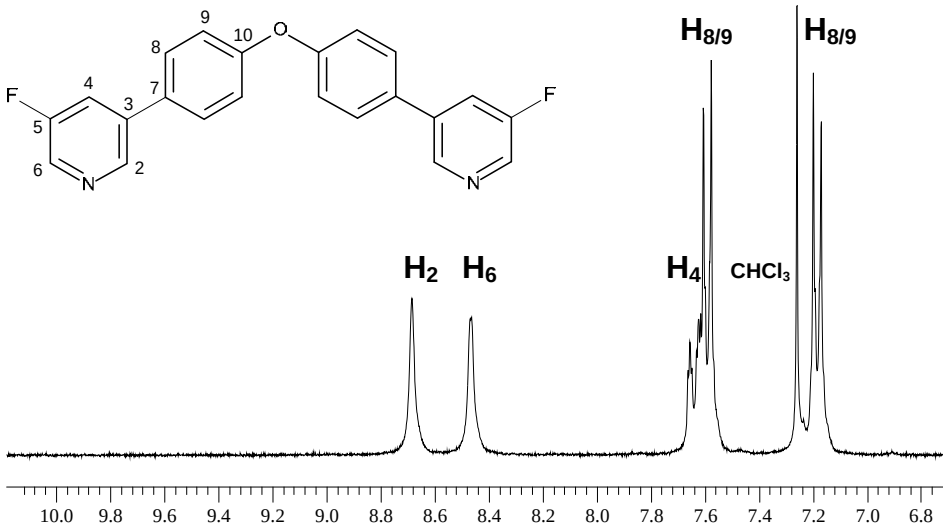

Figure 2.24. ^1H NMR spectrum of Ligand $\mathbf{L^3}$
(400 MHz, d_1-chloroform, 298 K).

From the ^1H NMR spectrum it is difficult to distinguish between $\mathbf{H_2}$ and $\mathbf{H_6}$ as they are both displayed as singlets. Therefore a ^1H-^{13}C HSQC experiment was carried out to aid in their assignment. The ^{13}C spectrum displays $\mathbf{C_2}$ as a singlet and $\mathbf{C_6}$ as a doublet (due to the coupling between ^{13}C and ^{19}F). The cross peaks

of the HSQC spectrum were used to correlate the carbon signals with the corresponding proton signals so that **H_2** and **H_6** could be assigned.

2.2.8 Palladium(II) complex of L^3

The palladium(II) complex of ligand **L^3** was formed by stirring two equivalents of ligand with one equivalent of tetrakis(acetonitrile)palladium(II) tetrafluoroborate under an argon atmosphere. After 16 hours the resulting solution was concentrated *in vacuo* and diethyl ether added drop-wise to precipitate the white product.

ESI mass spectrometry analysis of the product shows two peaks with the correct isotope pattern and charge to correspond to $[Pd_2(\mathbf{L^3})_4(BF_4)_2]^{2+}$ (*m/z* 914) and $[Pd_2(\mathbf{L^3})_4(BF_4)]^{3+}$ (*m/z* 580). The tetra- and mono-cationic peaks were not observed. The d_6-DMSO ^{1}H NMR spectra of ligand **L^3** and the corresponding palladium(II) complex are shown in Figure 2.25.

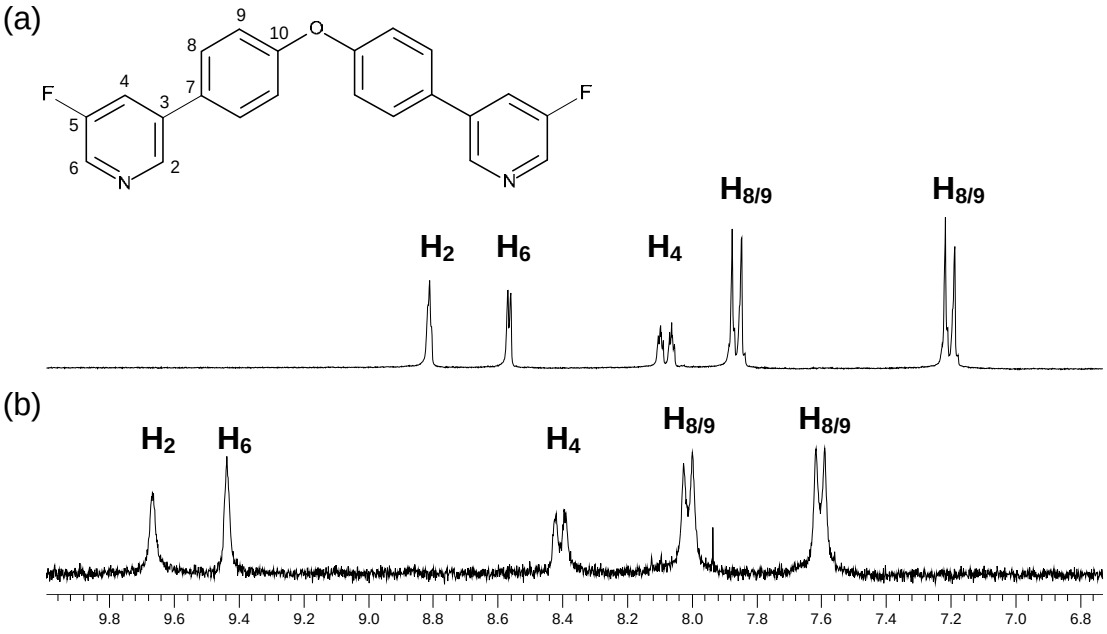

Figure 2.25. ^{1}H NMR spectra of (a) Ligand **L^3** and (b) $[Pd_2(\mathbf{L^3})_4][BF_4]_4$ (300 MHz, d_6-DMSO, 298 K).

The ^{1}H NMR spectrum of this complex reveals five aromatic signals indicating the formation of a single solution species with a symmetrical arrangement of ligands around the metal centres. There is a significant downfield shift of the proton signals in the complex relative to those in the free ligand. The greatest change is seen for $\mathbf{H_2}$ and $\mathbf{H_6}$ which are adjacent to the coordinating nitrogen atom and are both downfield shifted by 0.9 ppm.

Attempts to grow X-ray quality crystals of this complex were unfortunately unsuccessful. However, ligand $\mathbf{L^3}$ readily crystallised from a $CDCl_3$ solution of the ligand in an NMR tube (Figure 2.26).[13]

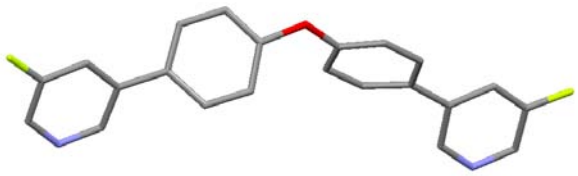

Figure 2.26. A perspective view of Ligand $\mathbf{L^3}$.[13]

As expected, the X-ray crystal structure depicts two fluorine atoms located on the 5 position of the pyridine rings and an oxygen atom as the central spacer. This data can be used as a means of visualising the structure of the $[Pd_2(\mathbf{L^3})_4]^{4+}$ tetra-cation. An illustration displaying the expected structure of the cylinder is shown in Figure 2.27.

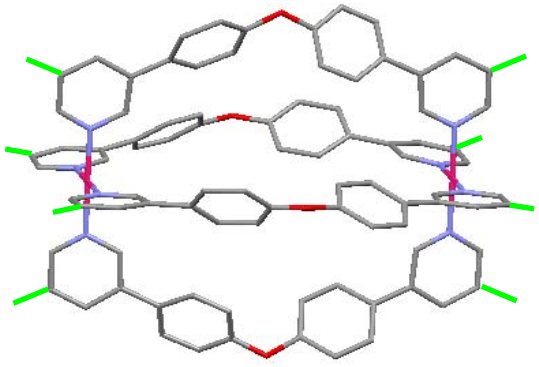

Figure 2.27. A representation of the proposed structure of $[Pd_2(\mathbf{L^3})_4]^{4+}$ cylinder based on the structures of $[Pd_2(\mathbf{L^2})_4]^{4+}$ and $\mathbf{L^3}$.

Unfortunately, the aqueous solubility of this complex has not been greatly enhanced by the fluorination of the ligand. The complex is soluble in water/organic solvent mixtures but remains insoluble in pure water.

2.2.9 Ligand L^4

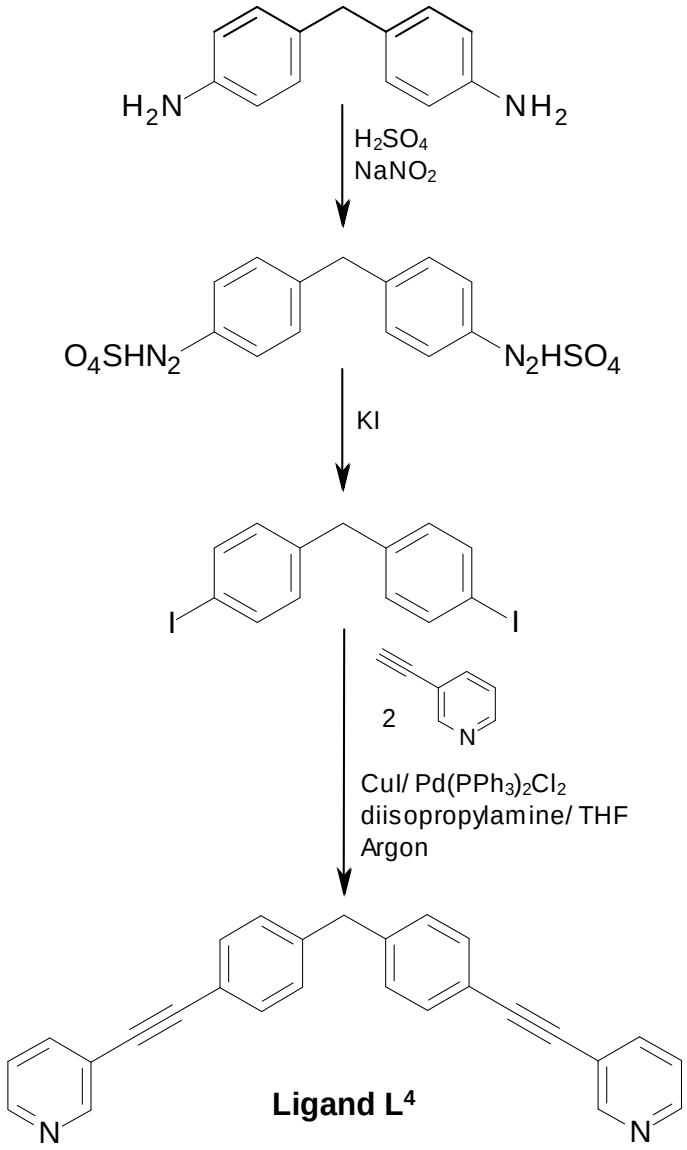

Scheme 2.4. Synthesis of Ligand **L^4**.

A fourth ligand was synthesized to investigate the effects of increasing the ligand length on the formation and behaviour of the resulting complexes. Ligand

L^4 was synthesized by a Sonogashira coupling reaction between bis(4-iodophenyl)methane[15] and 3-ethynylpyridine using $Pd(PPh_3)_2Cl_2$ as a catalyst and Cu(I) as a co-catalyst (Scheme 2.4).[16] The *crude* product consisted of a mixture between the desired ligand **L^4**, the half-ligand and a side product formed through the homocoupling of 3-ethynylpyridine. Purification was achieved by column chromatography on an alumina column using an ethyl acetate:hexane (1:1) eluent and gave the pure product in 72 % yield. The resulting ligand is longer than those previously described due to the incorporation of ethynyl bonds linking the central phenyl rings to the pyridyl binding units.

The EI mass spectrum of this ligand is dominated by a single peak corresponding to {**L^4**}$^+$ (*m/z* 370) and the partial microanalytical data support a $\{C_{27}H_{18}N_2\}$ formulation. The ^{1}H NMR spectrum of **L^4** in *d$_1$*-chloroform is shown in Figure 2.28.

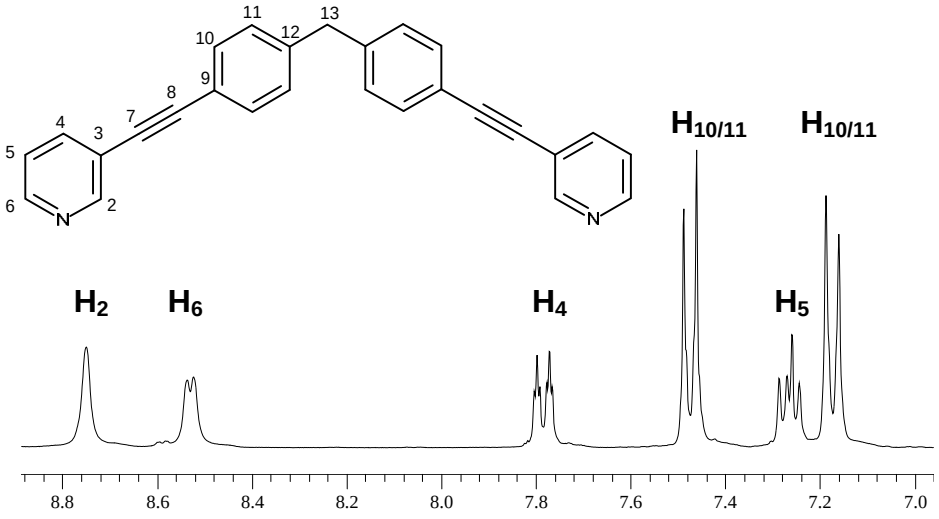

Figure 2.28. ^{1}H NMR spectrum of Ligand **L^4**
(300 MHz, *d$_1$*-chloroform, 298 K).

As expected, the spectrum shows six resonances in the aromatic section and one resonance in the aliphatic region indicating the formation of the symmetrical ligand.

2.2.10 Palladium(II) complex of L^4

The palladium(II) cylinder of ligand **L^4** was synthesized by stirring two equivalents of ligand with tetrakis(acetonitrile)palladium(II) tetrafluoroborate in acetonitrile overnight. The solvent was removed and the *crude* product washed to obtain the pure complex in a high yield of 95 %.

An IR spectrum of this complex shows a strong absorption at 1084 cm^{-1} which is characteristic of free tetrafluoroborate vibrations. Partial microanalytical data are consistent with an empirical formula of $\{Pd(C_{27}H_{18}N_2)_2(BF_4)_2\}_n$ and the ESI mass spectrum is dominated by a peak at *m/z* 424 corresponding to $[Pd_2(\mathbf{L^4})_4]^{4+}$. A small peak corresponding to $[Pd_2(\mathbf{L^4})_4(BF_4)_2]^{2+}$ is also observed but the mono- and tri-cationic species are not apparent. The ^{1}H NMR spectrum of the complex in d_6-DMSO indicates the presence of a single solution species with a symmetrical arrangement of the ligands around the two metal centres (Figure 2.29). There is a significant downfield shift of the pyridine proton signals relative to those in the free ligand. This is especially highlighted for **H_2** and **H_6** which are adjacent to the coordination site and are downfield shifted by 0.7 ppm.

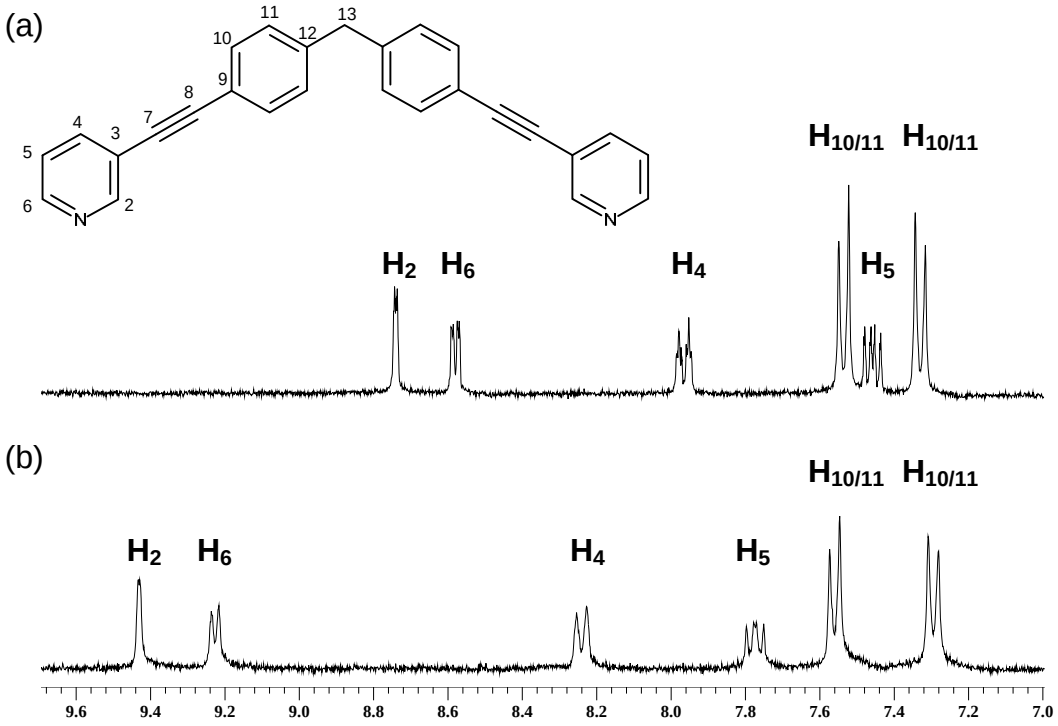

Figure 2.29. ^{1}H NMR spectra of the aromatic region of (a) Ligand **L^{4}** and (b) $[Pd_2(\mathbf{L}^{4})_4][BF_4]_4$ (300 MHz, d_6-DMSO, 298 K).

Crystals suitable for X-ray diffraction were grown over a two week period by the slow diffusion of benzene into a DMSO solution of the complex. The resulting X-ray crystal structure is shown in Figure 2.30.[11]

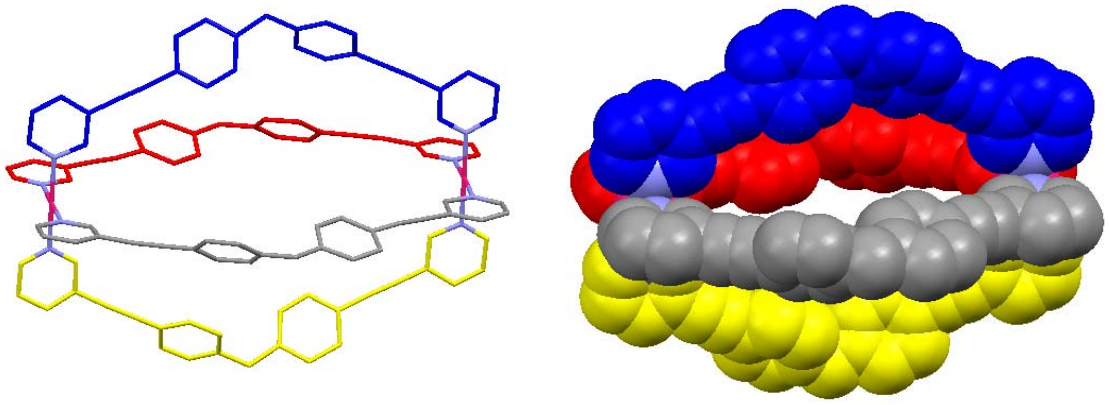

(a) (b)

Figure 2.30. (a) Perspective view and (b) space-filling representation of $[Pd_2(\mathbf{L}^{4})_4]^{4+}$ cation. Hydrogen atoms and anions are omitted for clarity.[11]

As predicted, the solid state structure of the cation reveals a tetra-stranded, dinuclear palladium(II) complex. The cylindrical structure is analogous to that of $[Pd_2(\mathbf{L^1})_4]^{4+}$ and $[Pd_2(\mathbf{L^2})_4]^{4+}$ except that it is significantly larger with a Pd···Pd separation of 17.5 Å. The Pd-N bond distances (2.004(1) Å and 2.007(8) Å) and N-Pd-N bond angles (89.7(2)º- 90.5(4)º) are typical and similar to those observed in the palladium(II) cylinders of $\mathbf{L^1}$ and $\mathbf{L^2}$. The two metal centers adopt a square planar geometry and are linked via the four ligands. In each ligand, one of the $C_{pyridine}$-CΞC links is almost planar with a bond angle of 178º, however at 175º, the other is slightly distorted to enable the formation of the tetra-stranded architecture. The phenyl rings of each ligand are twisted by 51º- 53º relative to one another and by 18º-33º relative to the adjacent pyridyl units. Intriguingly, in this cylinder the aromatic rings are twisted less than in the analogous $[Pd_2(\mathbf{L^1})_4][BF_4]_4$ and $[Pd_2(\mathbf{L^2})_4][BF_4]_4$. Two disordered tetrafluoroborate counter-ions and a disordered DMSO molecule are located within the central cavity of this palladium(II) cylinder. The remaining counter-ions, a DMSO molecule and three benzene molecules are situated around the cationic structure.

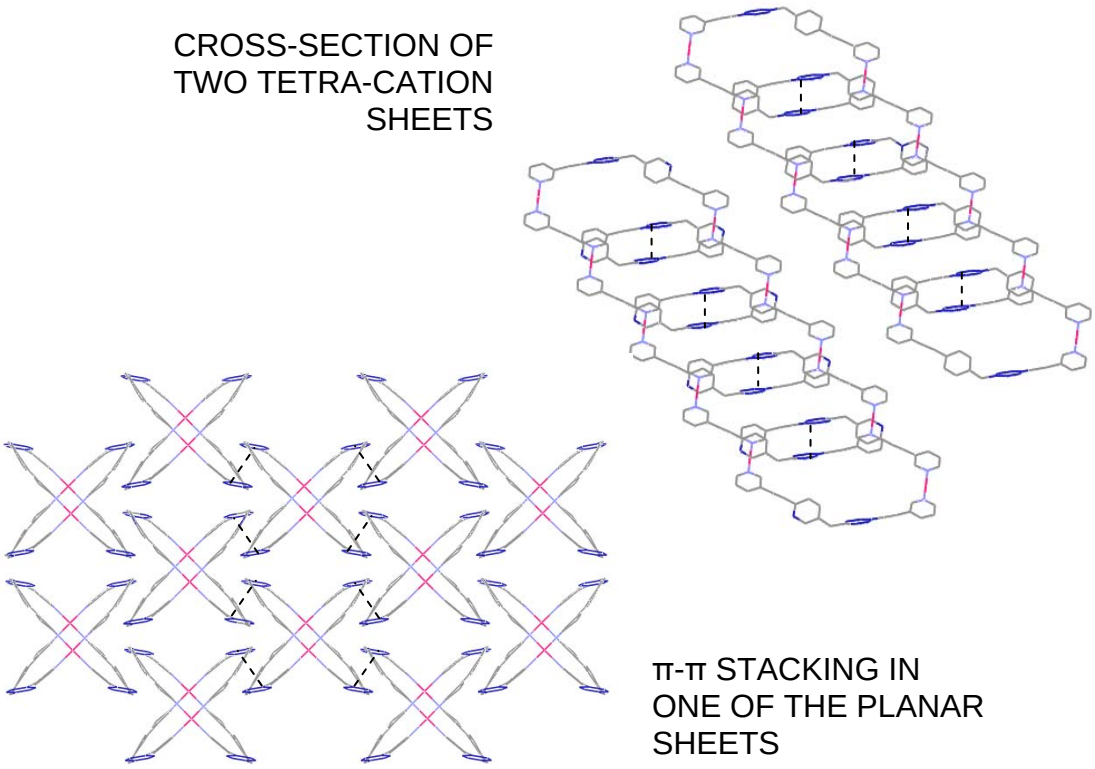

Figure 2.31. Packing diagrams for $[Pd_2(\mathbf{L^4})_4]^{4+}$ cations showing the π-π stacking interactions between the phenyl rings. Hydrogen atoms, anions and solvent molecules have been removed for clarity.

Figure 2.31 shows the crystal packing diagram for $[Pd_2(\mathbf{L^4})_4]^{4+}$. The tetra-cations are arranged into planar sheets held together by inter-molecular face-to-face π-π stacking interactions. Each cylinder is engaged in stacking interactions with four other cylinders enabling this large framework to be formed. Solvent molecules and anions fill the gaps formed between the cationic sheets.

As can be seen in Figure 2.32, $[Pd_2(\mathbf{L^4})_4]^{4+}$ packs differently from $[Pd_2(\mathbf{L^1})_4]^{4+}$ and $[Pd_2(\mathbf{L^2})_4]^{4+}$. In diagrams **A** and **B** the cylinders are packed into chains but in **C** they are packed into 3 dimensional sheets. This difference explains why the aromatic rings of $[Pd_2(\mathbf{L^4})_4]^{4+}$ are less twisted than in the analogous palladium(II) complexes.

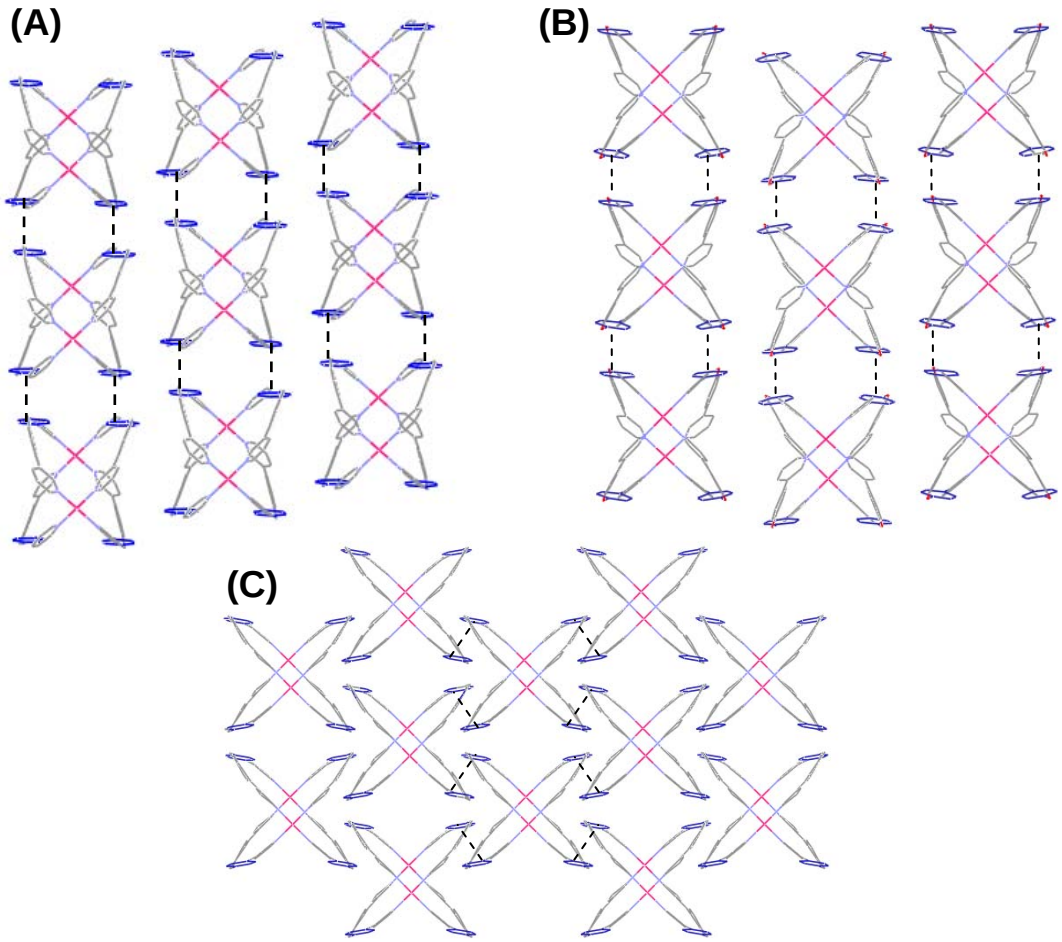

Figure 2.32. Packing diagrams for (**A**) $[Pd_2(\mathbf{L^1})_4]^{4+}$, (**B**) $[Pd_2(\mathbf{L^2})_4]^{4+}$ and (**C**) $[Pd_2(\mathbf{L^4})_4]^{4+}$. Hydrogen atoms, anions and solvent molecules have been removed for clarity.

Unfortunately, increasing the size of the cylinder did not effect the solubility as $[Pd_2(\mathbf{L^4})_4][BF_4]_4$ also proves to be insoluble in water.

2.2.11 Platinum(II) complex of L^4

The platinum(II) complex of ligand $\mathbf{L^4}$ was synthesized by heating an acetonitrile solution of bis(benzonitrile)dichloroplatinum(II) with two equivalents of $\mathbf{L^4}$ and silver(I) hexafluorophosphate for 48 hours. The solution was filtered to remove silver(I) chloride and the *crude* product washed with a range of solvents. A ^{1}H NMR spectrum of the resultant material showed a single set of resonances and

indicated that, unlike for the platinum(II) complexes of **L^1** and **L^2**, in this case no further purification was required. The 300 MHz ^{1}H NMR spectrum of $[Pt_2(\mathbf{L^4})_4][PF_6]_4$ in *d*$_6$-DMSO is shown in Figure 2.33. The spectrum displays one aliphatic signal and six aromatic signals, indicating that all four ligands are in an equivalent chemical environment. The spectrum is very similar to that of $[Pd_2(\mathbf{L^4})_4][BF_4]_4$ and on coordination to the platinum(II) centres, the pyridine signals have shifted downfield relative to those in the free ligand.

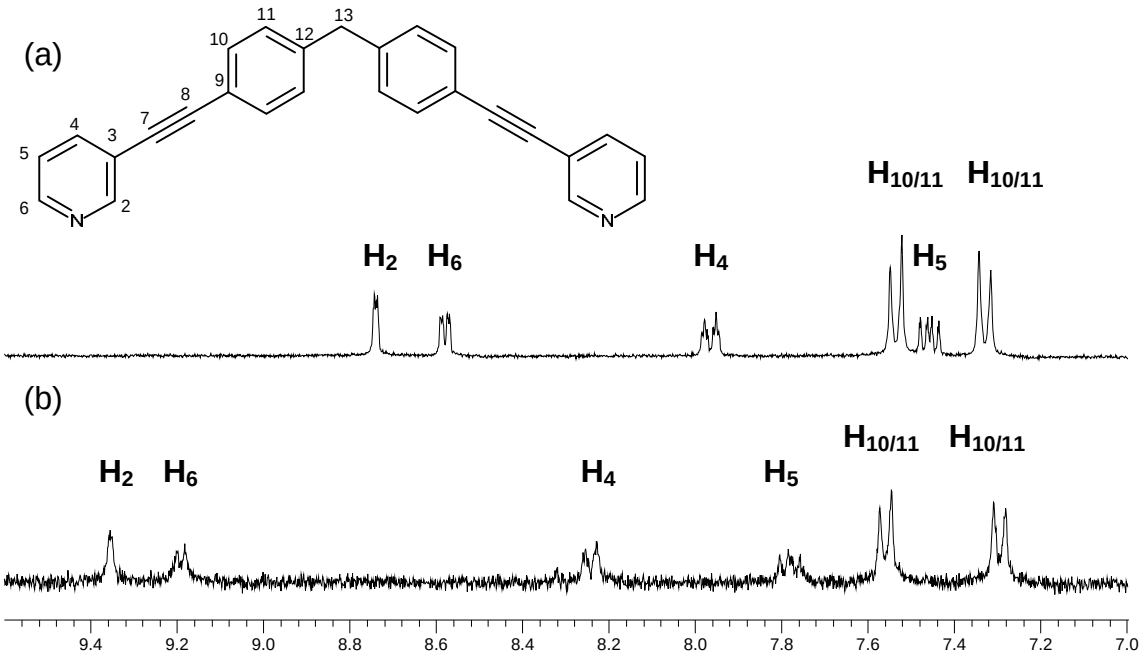

Figure 2.33. ^{1}H NMR spectra of the aromatic region of (a) Ligand **L^4** and (b) $[Pt_2(\mathbf{L^4})_4][PF_6]_4$ (300 MHz, *d*$_6$-DMSO, 298 K).

The elemental analysis data support a $\{Pt_2(C_{27}H_{18}N_2)_4(PF_6)_4\}$ formulation and the ESI mass spectrum is dominated by a peak at *m/z* 468 which corresponds to $[Pt_2(\mathbf{L^4})_4]^{4+}$. The tri-cationic species $[Pt_2(\mathbf{L^4})_4(PF_6)]^{3+}$ is also observed at *m/z* 672. The FT-IR spectrum shows absorption bands at 830 cm^{-1} and 2228 cm^{-1}, which can be attributed to the hexafluorophosphate and ethynyl

vibrations, respectively. These data are consistent with the formation of the desired tetra-stranded, dinuclear platinum(II) array.

Numerous attempts were made to grow X-ray quality crystals of the platinum complex, however, unfortunately these efforts were unsuccessful.

2.2.12 Ligand L^5

In keeping with the same theme of exploring variations in cylinder structure, a fifth ligand, ligand **L^5**, was synthesised. Ligand **L^5** is analogous to **L^1** except that the central methylene group has been replaced with an ethylene.

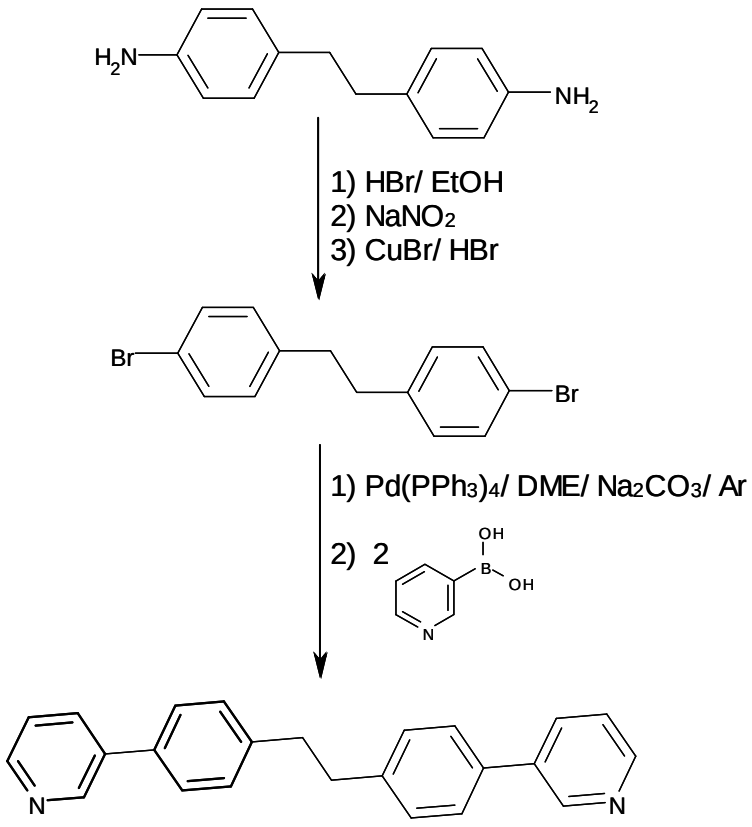

Ligand L^5

Scheme 2.5. Synthesis of Ligand **L^5**.

L^{5} was synthesized via a $Pd(PPh_3)_4$ catalysed Suzuki coupling reaction between bis(4-bromophenyl)ethane[17] and two equivalents of pyridine-3-yl-3-boronic acid (Scheme 2.5).[10] The *crude* ligand was purified on a silica column with a 2:1 mixture of petroleum ether:ethyl acetate as the eluent. The pure product was obtained as a white solid in 63 % yield.

Partial microanalytical data support a $\{C_{24}H_{20}N_2\}$ formulation and the results obtained from EI mass spectrometry show singly and doubly charged ions corresponding to $\{\mathbf{L}^{5}\}^{+}$ (*m/z* 336) and $\{\mathbf{L}^{5}\}^{2+}$ (*m/z* 168). Analysis of the ^{1}H NMR spectrum reveals a single set of resonances consisting of six aromatic signals and one aliphatic one (Figure 2.34). The spectrum is similar to the ^{1}H NMR spectrum of **L**^{1} except that the aliphatic signal has an integration of 4H instead of 2H.

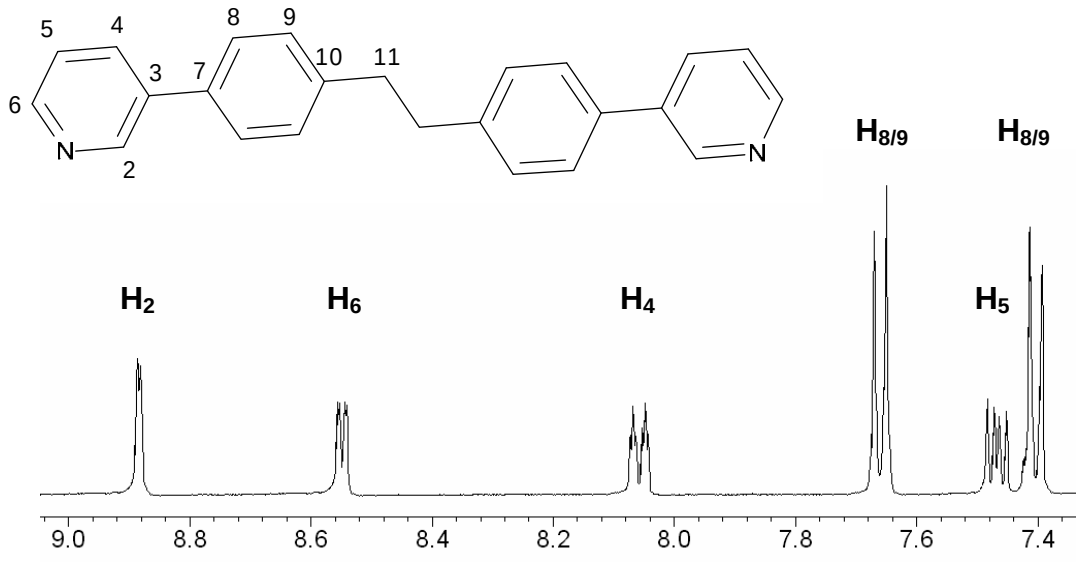

Figure 2.34. ^{1}H NMR spectrum of Ligand **L**^{5} (400 MHz, d_6-DMSO, 298 K).

2.2.13 Palladium(II) complexes of L^5

Ligand $\mathbf{L^5}$ was coordinated to naked palladium(II) by stirring two equivalents of ligand with tetrakis(acetonitrile)palladium(II) tetrafluoroborate under an argon atmosphere. The *crude* product was washed with a range of organic solvents and characterized.

The ESI mass spectrum of the product shows numerous positively charged peaks (Figure 2.35). Intriguingly, analysis of these peaks suggests that the reaction of palladium(II) with ligand $\mathbf{L^5}$ has not synthesised the expected tetra-stranded cylinder, but has instead led to the formation of the two distinct species $[Pd_3(\mathbf{L^5})_6][BF_4]_6$ and $[Pd_4(\mathbf{L^5})_8][BF_4]_8$.

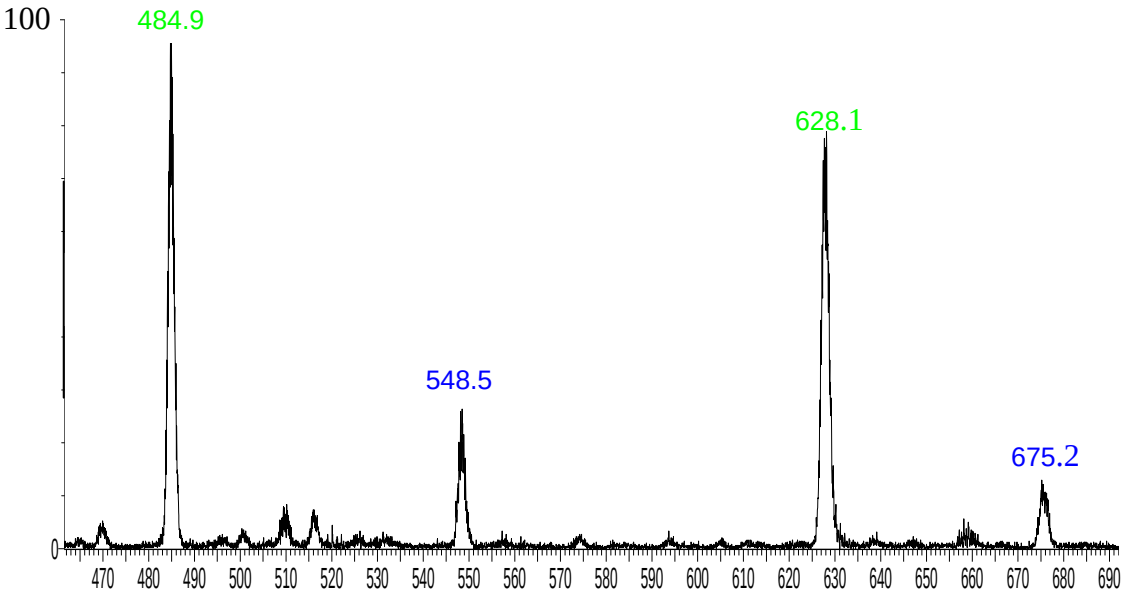

Figure 2.35. An expansion of part of the ESI mass spectrum of $[Pd_3(\mathbf{L^5})_6][BF_4]_6$ and $[Pd_4(\mathbf{L^5})_8][BF_4]_8$.

The ESI mass results cannot be confirmed by elemental analysis as both structures have the same empirical formula of $\{Pd(C_{24}H_{20}N_2)_2(BF_4)_2\}_n$.

The synthesis of $[Pd_3(\mathbf{L})_6][X]_6$ and $[Pd_4(\mathbf{L})_8][X]_8$ type structures has previously been reported by Fujita *et al.*.[18] In his paper, Fujita describes the

formation of two structures that are believed to be analogous to ours (Figure 2.36).

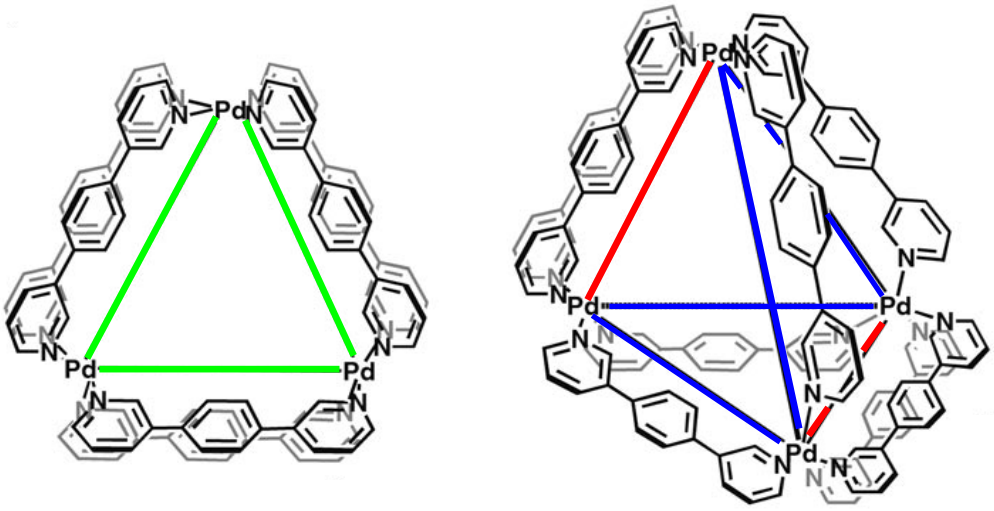

(A) **(B)**

Figure 2.36. Fujita's (A) $[Pd_3(\mathbf{L})_6][X]_6$ and (B) $[Pd_4(\mathbf{L})_8][X]_8$ complexes. Ligands in different chemical environments are shown along Pd···Pd axis of different colour.

Fujita's triangle **(A)** contains six equivalent ligands which all lie along the same Pd···Pd axis (green) and yield a ^{1}H NMR spectrum with one set of signals. The pyramid **(B)** contains eight ligands, equally split into two different chemical environments, one lying along the blue Pd···Pd axis and the other lying along the red. Therefore, the ^{1}H NMR spectrum of **(B)** displays two sets of signals of equal integration. The ^{1}H NMR spectrum of the palladium(II) complexes of $\mathbf{L^5}$ is shown in Figure 2.37. 2D COSY and NOESY experiments were used to aid in the assignment of the peaks.

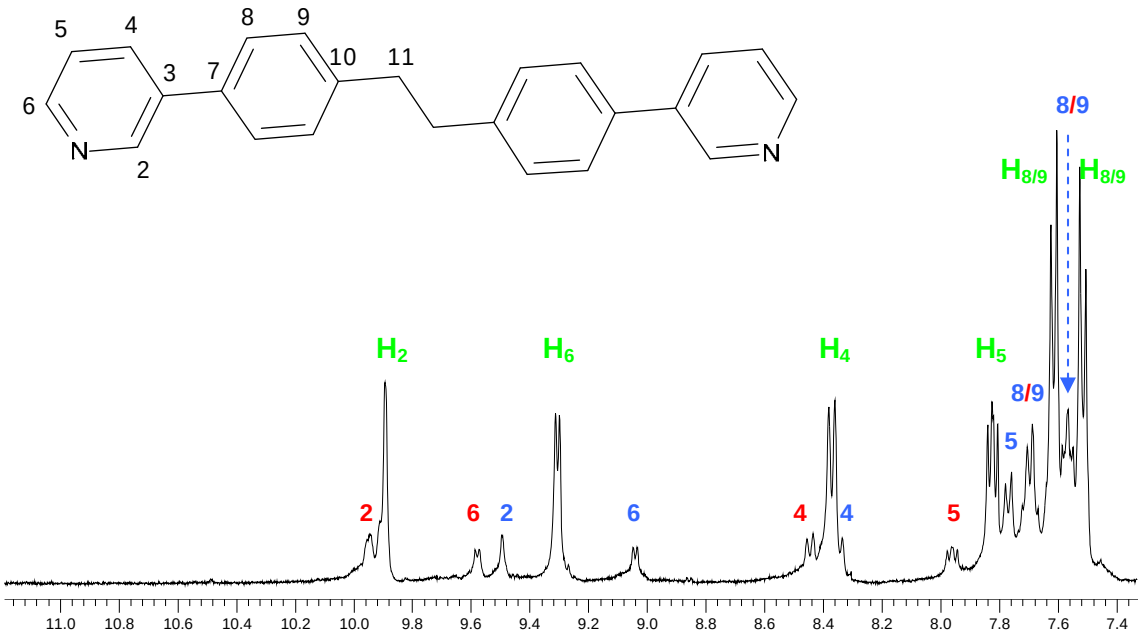

Figure 2.37. ^{1}H NMR spectrum of the aromatic region of $[Pd_3(\mathbf{L}^5)_6][BF_4]_6$ and $[Pd_4(\mathbf{L}^5)_8][BF_4]_8$ (300 MHz, d_6-DMSO, 298 K).

The spectrum shows two sets of signals, one contains protons in an equivalent chemical environment, corresponding to $[Pd_3(\mathbf{L}^5)_6][BF_4]_6$ and the other contains ligands in two chemical environments and corresponds to $[Pd_4(\mathbf{L}^5)_8][BF_4]_8$. This implies that a mixture of structures analogous to Fujita's triangle **(A)** and pyramid **(B)** are indeed present. The ratio of our triangle to pyramid is 1:0.3.

X-ray quality crystals were successfully grown by the slow diffusion of THF into a solution of the complexes in DMSO. ^{1}H NMR studies confirmed that the triangle structure is the most abundant species in our solution, therefore it is no surprise that this is the species that crystallised (Figure 2.38).

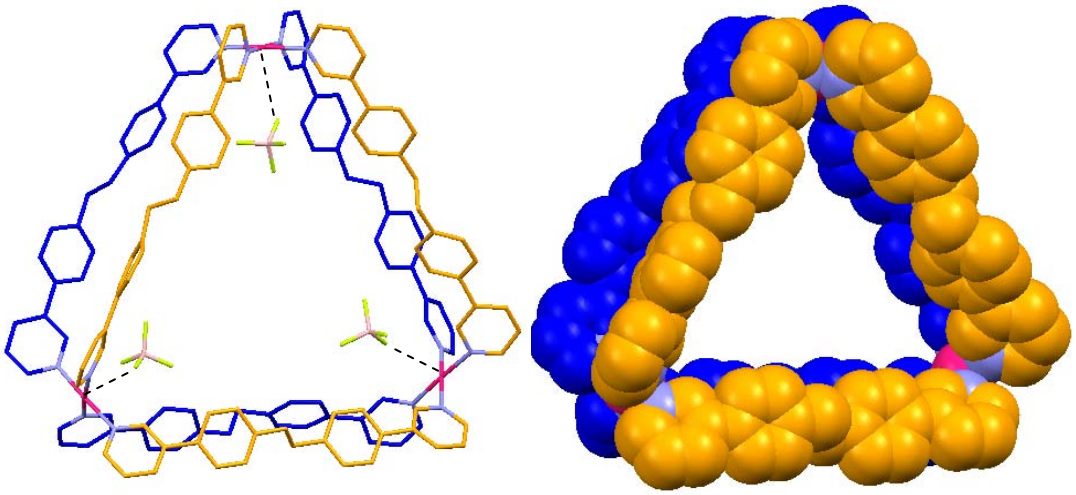

(a) (b)

Figure 2.38. (a) Perspective view and (b) space-filling representation of $[Pd_3(\mathbf{L^5})_6]^{6+}$ cation. Hydrogen atoms are omitted for clarity.[11]

As expected, each palladium(II) centre occupies a four coordinate square planar environment and is bound to pyridyl units from four different ligands. The metals occupy the corners of a triangle with Pd-Pd-Pd angles of ~60º and Pd···Pd separations of 17.7 Å, 17.8 Å and 18.0 Å. The Pd-N bond distances (1.948(12)-2.054(12) Å) and N-Pd-N angles (88.4(5)-92.9(8)º) are unremarkable and similar to those found in the other palladium(II) complexes that have been described in this chapter. The side view shows that three ligands rise above the plane of the metals and three sit below it (Figure 2.39).

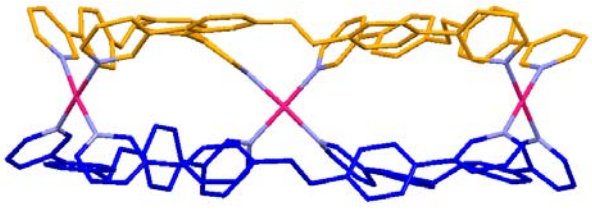

Figure 2.39. The side view of $[Pd_3(\mathbf{L^5})_6]^{6+}$.

Encapsulated within the cavity of the complex are three of the tetrafluoroborate counter-ions, one in each corner of the triangle (Figure 2.38a). The Pd-F

distances for the encapsulated anions are 2.7 Å, 3.2 Å and 3.4 Å, suggesting that the counter-ions make weak ionic interactions with the metal centres. The remaining counter-ions and solvent molecules occupy the spaces between the hexa-cationic triangles.

A crystal packing diagram of the complex is shown in Figure 2.40. The structures pack together in a head to tail fashion, however there are no obvious inter-molecular forces holding them together.

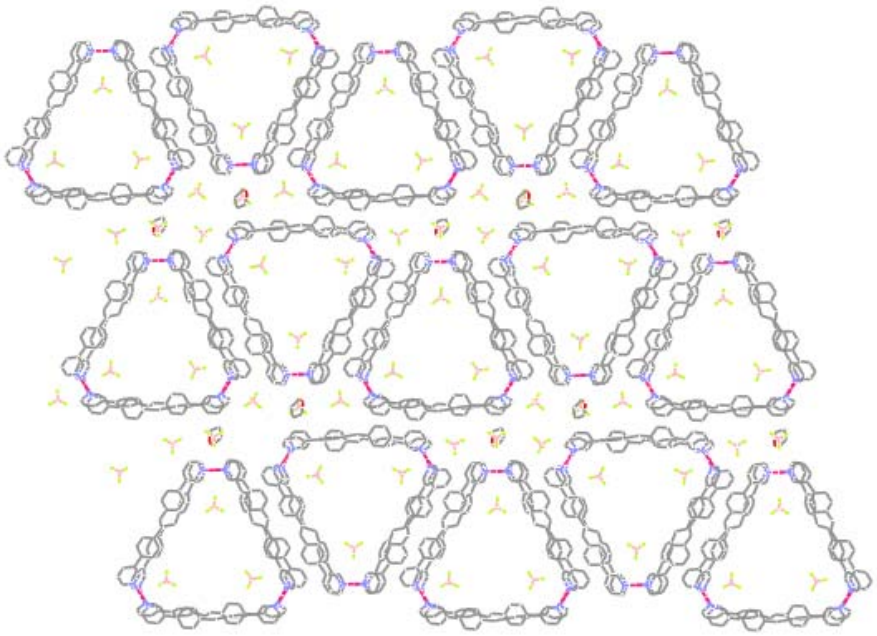

Figure 2.40. Crystal packing diagram of $[Pd_3(\mathbf{L^5})_6][BF_4]_6$.

2.3 Conclusions

In this chapter the synthesis and characterisation of five new ligands has been described. The ligands were successfully utilised in the synthesis of four novel tetra-stranded, dinuclear palladium(II) cylinders, three tetra-stranded, dinuclear platinum(II) cylinders, two Pd_3L_6 triangles and a Pd_4L_8 pyramid.

The aim of this chapter was to synthesise tetra-stranded, dinuclear cylinders which have a potential to be biologically active. Therefore, chapter 3 reports the cytotoxicity and DNA binding studies of four of these new complexes.

2.4 Experimental

2.4.1 General

All solvents and reagents were purchased from Aldrich, Fisher and Fluorochem and were used without further purification. ^{1}H NMR spectra were recorded on AC300, AV300 and AV400 Brüker spectrometers and processed using standard Brüker software. Infrared spectra were recorded from KBr pellets on a Perkin Elmer Paragon 1000 FT-IR spectrometer. Electrospray Ionisation (ESI) spectra were recorded on a Micromass LCT Time of flight mass spectrometer in positive ionization mode**.** Microanalyses data were obtained using a CE Instruments EA1110 elemental analyser. HPLC was performed using a Dionex HPLC system with a reverse phase preparative or semi-preparative column.

X-ray crystal analyses were performed by Dr Benson Kariuki and Dr Louise Male using a Bruker Smart 6000 CCD diffractometer equipped with an Oxford Cryosystem Cooler and structural refinements used SHELXTL.

2.4.2.1 Synthesis of Bis(4-bromophenyl)methanol intermediate[9]

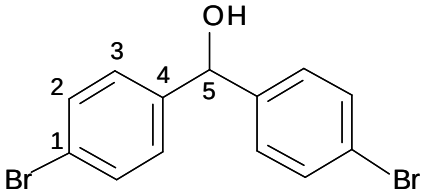

$C_{13}H_{10}Br_2O$
FW: 339.91

n-Butyl lithium (14.6 ml, 22.0 mmol, 1.51 M in hexane) was added dropwise to a nitrogen purged flask containing a THF (50 ml) solution of 1,4-dibromobenzene (5.66 g, 24.0 mmol) cooled to -78 ºC. The cream slurry was stirred under a nitrogen atmosphere for 40 minutes before adding to a solution of 4-bromobenzylaldehyde (3.70 g, 20.0 mmol) in THF (40 ml) which had also been cooled to -78 ºC. The resulting solution was allowed to warm to

room temperature and was stirred for 2 hours before pouring into water (250 ml). The suspension was extracted with ethyl acetate (3 X 20 ml), washed with water (2 X 20 ml) and dried over magnesium sulphate. The solvent was removed *in vacuo* and the *crude* material washed with hexane to yield the required product (5.55 g, 82 % yield).

^{1}H NMR (300 MHz, $CDCl_3$, 298 K): δ 7.45 (4H, d, *J* = 8.3 Hz, $H_{2/3}$), 7.21 (4H, d, *J* = 8.3 Hz, $H_{2/3}$), 5.73 (1H, s, H_5), 2.27 (1H, s, H_{OH}).

2.4.2.2 Synthesis of Bis(4-bromophenyl)methane intermediate[9]

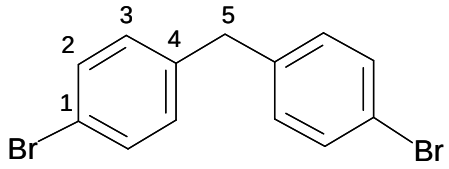

$C_{13}H_{10}Br_2$
FW: 323.91

Over a 10 minute duration, sodium borohydride (1.89 g, 50.0 mmol) was added to a solution of bis(4-bromophenyl)methanol (1.71 g, 5.0 mmol) in TFA (40 ml). The solution was stirred for 40 minutes at room temperature and then poured into water (250 ml). Aqueous sodium hydroxide was added slowly in order to make the suspension alkaline. The mixture was extracted with diethyl ether (3 X 20 ml) and the combined fractions washed with water (2 X 30 ml) and brine (1 X 30 ml) and dried over magnesium sulphate. The diethyl ether was removed *in vacuo* and the material dissolved in hexane and filtered through a short silica column to yield the required white product (1.18 g, 73 % yield).

^{1}H NMR (300 MHz, $CDCl_3$, 298 K): δ 7.40 (4H, d, *J* = 8.1 Hz, $H_{2/3}$), 7.02 (4H, d, *J* = 8.1 Hz, $H_{2/3}$), 3.87 (2H, s, H_5).

2.4.2.3 Synthesis of Ligand (L^1)[10]

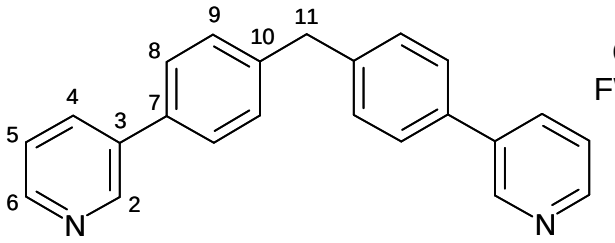

$C_{23}H_{18}N_2$
FW: 322.15

Method adapted from procedure of postdoctoral researcher Ekaterina Ryabova: Argon was bubbled through a mixture of bis(4-bromophenyl)methane (0.50 g, 1.53 mmol), pyridine-3-yl-3-boronic acid (0.56 g, 4.59 mmol), sodium carbonate (6.12 mmol), water (12 ml) and THF (12 ml) prior to the addition of the catalyst, tetrakis(triphenylphosphine)palladium(0) (0.18 g, 0.15 mmol). The slurry was heated at 80 °C for 48 hours. On conclusion of the reaction the mixture was diluted with water (30 ml) and extracted with ethyl acetate (3 X 20 ml). The combined organic fractions were washed with water (2 X 30 ml) and brine (1 X 30 ml) and dried over anhydrous magnesium sulphate. The solvent was evaporated to give the *crude* product which was purified by preparative RP-HPLC using a linear gradient of 100 % water to 100 % methanol over 60 minutes with a 10 minute methanol wash. The product peak was observed and collected at 50.15 minutes (355 mg, 72 % yield).

^{1}H NMR (300 MHz, $(CD_3)_2SO$, 298 K): δ 8.88 (2H, d, *J*= 2.3 Hz, H_2), 8.56 (2H, dd, *J*= 4.8, 1.6 Hz, H_6), 8.07 (2H, ddd, *J*= 8.1, 2.3, 1.6 Hz, H_4), 7.67 (4H, d, *J*= 8.4 Hz, $H_{8/9}$), 7.48 (2H, dd, *J*= 8.1, 4.8 Hz, H_5), 7.41 (4H, d, *J*= 8.4 Hz, $H_{8/9}$), 4.06 (2H, s, H_{11}).

^{13}C NMR (400 MHz, CD_2Cl_2, 300 K): δ 146.4 $C_{2/6}$, 146.2 $C_{2/6}$, 139.5 $C_{3/7/10}$, 134.6 $C_{3/7/10}$, 134.0 $C_{3/7/10}$, 132.5 C_4, 127.9 $C_{5/8/9}$, 125.5 $C_{8/9}$, 121.9 $C_{5/8/9,}$ 39.5 C_{11}.

Mass Spectrum (EI): *m/z* 322 $\{Ligand\}^+$.

Elemental analysis (%) calculated for $C_{23}H_{18}N_2 \cdot 0.5CH_3CN$: C: 84.1; H: 5.7; N: 10.2; Found: C: 84.2; H: 5.8; N: 10.31.

IR (KBr): ν= 1473(s), 1440(w), 1426 (m), 1395(m), 1023(m), 1001(s), 865(s), 798(s), 787(s), 758(s), 712(s), 611(s), 551(m) cm^{-1}.

2.4.2.4 Synthesis of $[Pd_2(L^1)_4][BF_4]_4$

Tetrakis(acetonitrile)palladium(II) tetrafluoroborate (0.017 g, 0.038 mmol) was added to a degassed solution of ligand **L^1** (0.024 g, 0.076 mmol) in acetonitrile (5 ml). The yellow solution was stirred overnight under an argon atmosphere. The solution was then filtered and the solvent removed under reduced pressure to yield an off white solid. The *crude* product was washed with chloroform (5 ml), acetone (5 ml) and diethyl ether (5 ml) and dried *in vacuo* (29.0 mg, 83 % yield).

^{1}H NMR (300 MHz, $(CD_3)_2SO$, 298 K): δ 9.51 (2H, s, H_2), 9.27 (2H, d, *J*= 6.0 Hz, H_6), 8.34 (2H, d, *J*= 8.1 Hz, H_4), 7.83 (2H, dd, *J*= 8.1, 6.0 Hz, H_5), 7.53 (4H, d, *J*= 8.0 Hz, $H_{8/9}$), 7.35 (4H, d, *J*= 8.0 Hz, $H_{8/9}$), 4.17 (2H, s, H_{11}).

^{19}F NMR (300 MHz, $(CD_3)_2SO$, 298 K): δ -147.7 (s, F_{BF4}).

Mass Spectrum (E.S.I): *m/z* 837.8 $\{Pd_2L_4 + 2BF_4\}^{2+}$, 804.4 $\{Pd_2L_4 + F + BF_4\}^{2+}$, 529.9 $\{Pd_2L_4 + BF_4\}^{3+}$, 375.6 $\{Pd_2L_4\}^{4+}$, 323.2 $\{L + H\}^+$.

Elemental analysis (%) calculated for $[Pd_2(C_{23}H_{18}N_2)_4][BF_4]_4 \cdot 6H_2O$: C: 56.4; H: 4.3; N: 5.7; Found: C: 56.4; H: 4.3; N: 5.6.

IR (Neat): ν= 3092(br), 1602(m), 1510(w), 1480(m), 1438(m), 1401(w), 1284(w), 1243(m), 1194(w), 1034(br,s), 799(s), 763(m), 701(s), 665(m) cm^{-1}.

2.4.2.5 Synthesis of $[Pd_2(L^1)_4][NO_3]_4$

Tetrakis(acetonitrile)palladium(II) tetrafluoroborate (0.017 g, 0.038 mmol) was added to a degassed solution of ligand **L^1** (0.024 g, 0.076 mmol) in acetonitrile (5 ml). The solution was stirred overnight under an argon atmosphere. Excess tetrabutylammonium nitrate was dissolved in acetonitrile and added dropwise to the reaction mixture until a white precipitate appeared. The *crude* product was filtered off, washed with chloroform (5 ml), acetone (5 ml) and diethyl ether (5 ml) and dried *in vacuo* (21.5 mg, 65 % yield).

^{1}H NMR (300 MHz, $(CD_3)_2SO$, 298 K): δ 9.67 (2H, s, H_2), 9.27 (2H, d, *J*= 5.9 Hz, H_6), 8.33 (2H, d, *J*= 7.9 Hz, H_4), 7.81 (2H, dd, *J*= 7.9, 5.9 Hz, H_5), 7.60 (4H, d, *J*= 8.1 Hz, $H_{8/9}$), 7.34 (4H, d, *J*= 8.1 Hz, $H_{8/9}$), 4.14 (2H, s, H_{11}).

Mass Spectrum (E.S.I): *m/z* 813.2 $\{Pd_2L_4 + NO_3\}^{2+}$, 547.4 $\{Pd_2L_4 + NO_3 + (CH_3)_2SO\}^{3+}$, 521.5 $\{Pd_2L_4 + NO_3\}^{3+}$, 375.4 $\{Pd_2L_4\}^{4+}$.

Elemental analysis (%) calculated for $[Pd_2(C_{23}H_{18}N_2)_4][NO_3]_4 \cdot 5.5H_2O$: C: 59.7; H: 4.5; N: 9.1; Found: C: 59.1; H: 4.7; N: 9.5.

2.4.2.6 Synthesis of $[Pd_2(L^1)_4][TFA]_4$

Tetrakis(acetonitrile)palladium(II) tetrafluoroborate (0.017 g, 0.038 mmol) was added to a degassed solution of ligand **L^1** (0.024 g, 0.076 mmol) in acetonitrile (5 ml). The solution was stirred overnight under an argon atmosphere and then treated with an acetonitrile solution of sodium trifluoroacetate. The *crude* material was purified on a semi-preparative RP-HPLC column using a gradient of 100 % $H_20_{(0.05\ \%\ TFA)}$ to 100 % $methanol_{(0.05\ \%\ TFA)}$ over 40 minutes followed by a 10 minute $methanol_{(0.05\ \%\ TFA)}$ wash. The pure complex was observed and collected at 36.83 minutes (15.3 mg, 41 % yield).

^{1}H NMR (300 MHz, CD_3OD, 298 K): δ 9.53 (2H, s, H_2), 9.07 (2H, d, *J*= 5.4 Hz, H_6), 8.18 (2H, d, *J*= 8.3 Hz, H_4), 7.63 (2H, dd, *J*= 8.3, 5.4 Hz, H_5), 7.37 (4H, d, *J*= 8.0 Hz, $H_{8/9}$), 7.17 (4H, d, *J*= 8.0 Hz, $H_{8/9}$), 4.02 (2H, s, H_{11}).

Mass Spectrum (E.S.I): *m/z* 864.3 $\{Pd_2L_4 + 2TFA\}^{2+}$, 703.2 $\{Pd_2L_3 + 2TFA\}^{2+}$, 538.5 $\{Pd_2L_4 + TFA\}^{3+}$.

Elemental analysis (%) calculated for $[Pd_2(C_{23}H_{18}N_2)_4][C F_3CO_2]_4 \cdot 2.25NaF_3C_2O_2$ C: 55.5; H: 3.2; N: 5.0; Found: C: 55.1; H: 3.5; N: 5.1.

2.4.2.7 Synthesis of $[Pt_2(L^1)_4][TFA]_4$

Bis(benzonitrile)dichloroplatinum(II) (0.018 g, 0.038 mmol), ligand **L^1** (0.024 g, 0.076 mmol) and silver(I) nitrate (0.013 g, 0.076 mmol) were heated under reflux for 48 hours in acetonitrile (6 ml). The reaction mixture was filtered to remove the silver(I) chloride and the solvent evaporated to give the *crude* product. The material was purified by semi-preparative RP-HPLC using a gradient of 100 % water$_{(0.05\ \%\ TFA)}$ to 100 % methanol$_{(0.05\ \%\ TFA)}$ over 50 minutes. The impure product peak was observed and collected at 34.00 minutes. The obtained solid was further purified on another semi-preparative RP-HPLC column using a gradient of 100 % water to 100 % methanol over 40 minutes. The pure product was collected at 26.56 minutes, the solvent removed and the white product dried *in vacuo* (10.9 mg, 27 % yield).

^{1}H NMR (300 MHz, CD_3OD, 298 K): δ 9.59 (2H, s, H_2), 9.03 (2H, d, *J*= 5.3 Hz, H_6), 8.18 (2H, d, *J*= 8.0 Hz, H_4), 7.60 (2H, dd, *J*= 8.0, 5.3 Hz, H_5), 7.40 (4H, d, *J*= 8.3 Hz, $H_{8/9}$), 7.16 (4H, d, *J*= 8.3 Hz, $H_{8/9}$), 4.01 (2H, s, H_{11}).

Mass Spectrum (E.S.I): *m/z* 952.3 $\{Pt_2L_4 + 2TFA\}^{2+}$, 597.5 $\{Pt_2L_4 + TFA\}^{3+}$.

2.4.3.1 Synthesis of Ligand $(L^2)^{10}$

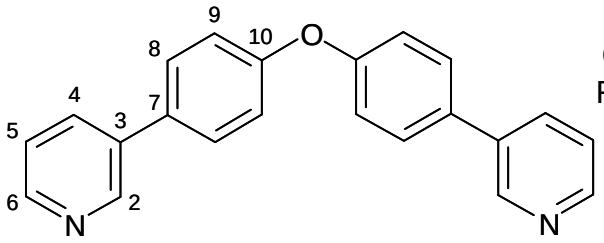

$C_{22}H_{16}N_2O$
FW: 324.13

Method adapted from procedure of postdoctoral researcher Ekaterina Ryabova:

A solution of tetrakis(triphenylphosphine)palladium(0) (0.051 g, 0.044 mmol) in dimethoxyethane (2 ml) and aqueous sodium carbonate (1 M, 3.52 ml) was added to an argon filled glass vial containing bis-4-bromophenylether (0.289 g, 0.88 mmol). A slurry of pyridine-3-yl-3-boronic acid (0.324 g, 2.33 mmol) in ethanol (2 ml) was added, the vial purged with argon once again and the mixture heated at 90 °C for 1 hour. The solution was cooled to room temperature and left stirring overnight. On conclusion of the reaction, the mixture was diluted with water (30 ml) and extracted with ethyl acetate (3 X 20 ml). The combined organic fractions were washed with water (2 X 30 ml) and brine (1 X 30 ml) and dried over anhydrous magnesium sulphate. The solvent was evaporated to give the *crude* product which was purified by preparative RP-HPLC using a linear gradient of 100 % water to 100 % methanol over 40 minutes with a 15 minute methanol wash. The product peak was observed and collected at 49.58 minutes.

^{1}H NMR (300 MHz, $(CD_3)_2SO$, 298 K): δ 8.90 (2H, d, *J*= 2.7 Hz, H_2), 8.56 (2H, d, *J*= 4.6 Hz, H_6), 8.08 (2H, d, *J*= 8.1 Hz, H_4), 7.78 (4H, d, *J*= 8.4 Hz, $H_{8/9}$), 7.48 (2H, dd, *J*= 8.1, 4.6 Hz, H_5), 7.20 (4H, d, *J*= 8.4 Hz, $H_{8/9}$).

^{13}C NMR (400 MHz, $CDCl_3$, 300 K): δ 159.9 $C_{3/7/10}$, 151.0 $C_{2/6}$, 150.8 $C_{2/6}$, 138.6 $C_{3/7/10}$, 136.8 C_4, 135.9 $C_{3/7/10}$, 131.3 $C_{8/9}$, 126.2 C_5, 122.2 $C_{8/9}$.

Mass Spectrum (EI): *m/z* 324 $\{Ligand\}^+$.

Elemental analysis (%) calculated for $C_{22}H_{16}N_2O$: C: 81.5; H: 5.0; N: 8.6; Found; C: 81.3; H: 4.8; N: 8.4.

IR (KBr): ν= 1596(m), 1565(w), 1519(s), 1478(s), 1432(m), 1396(w), 1339(w), 1278(s), 1170(s), 1134(w), 1108(w), 1016(m), 836(s), 795(s), 697(s), 543(m) cm^{-1}.

2.4.3.2 Synthesis of $[Pd_2(L^2)_4][BF_4]_4$

Tetrakis(acetonitrile)palladium(II) tetrafluoroborate (0.017 g, 0.038 mmol) was added to a degassed solution of ligand **L^2** (0.025 g, 0.076 mmol) in acetonitrile (5 ml). The solution was stirred overnight under an argon atmosphere. The solution was filtered and treated with diethyl ether resulting in the precipitation of an off white solid. The *crude* product was washed with chloroform (5 ml), acetone (5 ml), ethanol (5 ml) and diethyl ether (5 ml) and dried *in vacuo* (31.8 mg, 90 % yield).

^{1}H NMR (300 MHz, $(CD_3)_2SO$, 298 K): δ 9.73 (2H, s, H_2), 9.32 (2H, d, *J*= 5.7 Hz, H_6), 8.36 (2H, d, *J*= 8.1 Hz, H_4), 7.83 (2H, dd, *J*= 8.1, 5.7 Hz, H_5), 7.72 (4H, d, *J*= 7.5 Hz, $H_{8/9}$), 7.29 (4H, d, *J*= 7.5 Hz, $H_{8/9}$).

Mass Spectrum (E.S.I): *m/z* 841.8 $\{Pd_2L_4 + 2BF_4\}^{2+}$, 532.5 $\{Pd_2L_4 + BF_4\}^{3+}$, 377.6 $\{Pd_2L_4\}^{4+}$.

Elemental analysis (%) calculated for $[Pd_2(C_{22}H_{16}N_2O)_4][BF_4]_4 \cdot 0.5CH_3CN \cdot 4CHCl_3$: C: 47.4; H: 3.0; N: 5.1; Found: C: 47.4; H: 3.1; N: 5.3.

IR (Neat): ν= 3087(br), 1599(m), 1509(m), 1480(s), 1440(m), 1281(w), 1244(s), 1179(m), 1010(br,s), 875(m), 804(s), 700(s), 666(m) cm^{-1}.

2.4.3.3 Synthesis of $[Pd_2(L^2)_4][NO_3]_4$

Under an argon atmosphere, tetrakis(acetonitrile)palladium(II) tetrafluoroborate (0.017 g, 0.038 mmol) was stirred overnight with ligand **L^2** (0.025 g, 0.076 mmol) in acetonitrile (5 ml). Excess tetrabutylammonium nitrate was dissolved in acetonitrile and added drop wise to the reaction mixture until a white solid precipitated. The *crude* product was filtered off, washed with chloroform (5 ml), acetone (5 ml) and diethyl ether (5 ml) and dried *in vacuo*.

^{1}H NMR (300 MHz, $(CD_3)_2SO$, 298 K): δ 9.87 (2H, s, H_2), 9.36 (2H, d, *J*= 5.7 Hz, H_6), 8.36 (2H, d, *J*= 7.8 Hz, H_4), 7.83 (2H, dd, *J*= 7.8, 5.7 Hz, H_5), 7.78 (4H, d, *J*= 8.1 Hz, $H_{8/9}$), 7.31 (4H, d, *J*= 8.1 Hz, $H_{8/9}$).

Mass Spectrum (E.S.I): *m/z* 817.3 $\{Pd_2L_4 + 2NO_3\}^{2+}$, 576.2 $\{Pd_2L_4 + NO_3 + 2(CH_3)_2SO\}^{3+}$, 550.2 $\{Pd_2L_4 + NO_3 + (CH_3)_2SO\}^{3+}$, 524.2 $\{Pd_2L_4 + NO_3\}^{3+}$.

Elemental analysis (%) calculated for $[Pd_2(C_{22}H_{16}N_2O)_4][NO_3]_4 \cdot 6H_2O \cdot CH_3CN$: C: 56.7; H: 4.2; N: 9.5; Found: C: 56.7; H: 4.2; N: 9.6.

2.4.3.4 Synthesis of $[Pt_2(L^2)_4][TFA]_4$

Bis(benzonitrile)dichloroplatinum(II) (0.018 g, 0.038 mmol), ligand **L^2** (0.024 g, 0.076 mmol) and silver(I) tetrafluoroborate (0.015 g, 0.076 mmol) were heated under reflux for 48 hours in acetonitrile (6 ml). The reaction mixture was filtered to remove the silver(I) chloride. The solvent was evaporated to give the *crude* product which was purified by semi-preparative RP-HPLC using a gradient of 100 % water$_{(0.05\ \%\ TFA)}$ to 100 % methanol$_{(0.05\ \%\ TFA)}$ over 40 minutes and the pure product was observed and collected at 38.80 minutes. The solvent was removed under reduced pressure and the white product dried *in vacuo.*

^{1}H NMR (300 MHz, CD_3OD, 298 K): δ 9.81 (2H, s, H_2), 9.28 (2H, d, *J*= 5.4 Hz, H_6), 8.30 (2H, d, *J*= 8.1 Hz, H_4), 7.76 (2H, dd, *J*= 8.1, 5.4 Hz, H_5), 7.70 (4H, d, *J*= 8.8 Hz, $H_{8/9}$), 7.20 (4H, d, *J*= 8.8 Hz, $H_{8/9}$).

Mass Spectrum (E.S.I): *m/z* 956.2 $\{Pt_2L_4 + 2TFA\}^{2+}$, 917.8 $\{Pt_2L_4 + TFA + Cl\}^{2+}$, 599.8 $\{Pt_2L_4 + TFA\}^{3+}$, 574.2 $\{Pt_2L_4 + Cl\}^{3+}$.

2.4.4.1 Synthesis of Ligand (L^3)[10]

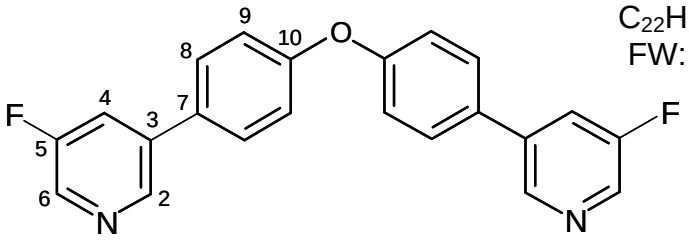

$C_{22}H_{14}N_2F_2O$
FW: 360.11

Argon was bubbled through a mixture of bis-4-bromophenylether (0.310 g, 0.946 mmol), 5-fluoropyridine-3-boronic acid (0.400 g, 2.839 mmol), sodium carbonate (3.785 mmol), water (12 ml) and THF (12 ml) prior to the addition of the catalyst, tetrakis(triphenylphosphine)palladium(0) (0.109 g, 0.095 mmol). The slurry was heated at 80 °C for 48 hours. On conclusion of the reaction, the mixture was diluted with water and extracted with ethyl acetate (3 X 20 ml). The combined organic fractions were washed with water (2 X 30 ml) and brine (1 X 30 ml) and dried over anhydrous magnesium sulfate. The solvent was evaporated to give the *crude* product which was purified by preparative RP-HPLC using a hexane:ethyl acetate (6:4) solvent system for 44.00 minutes. The product peak was observed and collected at 28.12 minutes (0.162 g, 48 % yield).

^{1}H NMR (400 MHz, $CDCl_3$, 298 K): δ 8.65 (2H, s, H_2), 8.43 (2H, s, H_6), 7.54-7.57 (2H, m, H_4), 7.56 (4H, d, *J*= 8.8 Hz, $H_{8/9}$), 7.16 (4H, d, *J*= 8.8 Hz, $H_{8/9}$).

^{13}C NMR (400 MHz, $(CD_3)_2SO$, 300 K): δ 159.9 $C_{10,}$ 155.7 $C_{7,}$ 142.5 C_2, 135.4 $C_{3/5,}$ 134.8 C_6, 129.8 $C_{3/5,}$ 127.8 $C_{8/4}$, 119.4 $C_{8/4}$, 118.1 C_9.

^{19}F NMR (300 MHz, $CDCl_3$, 298 K): δ -125.9 (s, F_5).

Mass Spectrum (EI): *m/z* 360 $\{Ligand\}^+$.

Elemental analysis (%) calculated for $C_{22}H_{14}N_2F_2O$: C: 73.3; H: 3.9; N: 7.8; Found: C: 73.1; H: 3.7; N: 7.6.

IR (Neat): ν= 3019(br), 1599(m), 1568(w), 1509(s), 1434(s), 1300(w), 1395(s), 1275(m), 1260(s), 1230(s), 1199(s), 1150(s), 1110(m), 1023(m), 1015(m), 936(w), 885(s), 874(m), 827(s), 838(s), 704(s), 689(s), 642(m) cm^{-1}.

2.4.4.2 Synthesis of $[Pd_2(L^3)_4][BF_4]_4$

Tetrakis(acetonitrile)palladium(II) tetrafluoroborate (0.017 g, 0.038 mmol) was added to a degassed solution of ligand **L^3** (0.027 g, 0.076 mmol) in acetonitrile (5 ml) and the clear solution stirred under argon. After 16 hours the solution was filtered, concentrated *in vacuo* and treated with diethyl ether resulting in the precipitation of a white solid. The *crude* product was washed with chloroform (5 ml) and diethyl ether (5 ml) and dried *in vacuo* (29.0 mg, 76 % yield).

^{1}H NMR (300 MHz, $(CD_3)_2SO$, 298 K): δ 9.87 (2H, s, H_2), 9.65 (2H, s, H_6), 8.61 (2H, d, *J*= 9.0 Hz, H_4), 8.22 (4H, d, *J*= 8.4 Hz, $H_{8/9}$), 7.81 (4H, d, *J*= 8.4 Hz, $H_{8/9}$).

Mass Spectrum (E.S.I): *m/z* 914.3 $\{Pd_2L_4 + 2BF_4\}^{2+}$, 580.5 $\{Pd_2L_4 + BF_4\}^{3+}$.

2.4.5.1 Synthesis of 4,4'-diiododiphenylmethane intermediate[15]

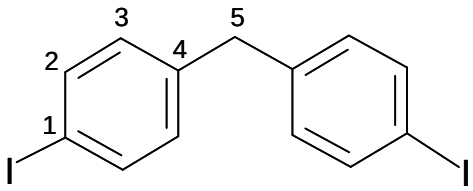

$C_{13}H_{10}I_2$
FW: 419.89

4,4'-diaminodiphenylmethane (17.0 g, 85.9 mmol) was dissolved in conc sulphuric acid (300 ml) and cooled to 0 ºC. The temperature was maintained below 5 ºC during the drop wise addition of aqueous sodium nitrite solution (17.0 g 0.239 mol, 30 ml). The slurry was stirred at 5 ºC for 30 minutes and then poured into an aqueous solution of potassium(I) iodide (100 g, 1 L) heated to 55 ºC. Stirring was continued at this temperature for 1 hour after which the mixture was allowed to cool to room temperature. After the addition of dichloromethane (1 L), the mixture was neutralized by the addition of aqueous sodium hydroxide and then decolorized with a saturated solution of aqueous sodium bisulfite solution. The organic phase was washed with 10 % aqueous hydrochloric acid (500 ml), distilled water (2 X 100 ml), saturated aqueous sodium bicarbonate (2 X 50 ml), water (2 X 50 ml) again and dried over magnesium sulphate. The solvent was removed *in vacuo* to afford a yellow oil which was purified on a silica column using hexane as the eluant. Removal of the hexane afforded the desired product as a white solid (13.34 g, 37 % yield).

^{1}H NMR (300 MHz, $CDCl_3$, 298 K): δ 7.60 (4H, d, *J*= 8.6 Hz, $H_{2/3}$), 6.90 (4H, d, *J*= 8.6 Hz, $H_{2/3}$), 3.85 (2H, s, H_5).

Mass Spectrum (EI): *m/z* 420 $\{Spacer\}^+$.

2.4.5.2 Synthesis of Ligand (L^4)[16]

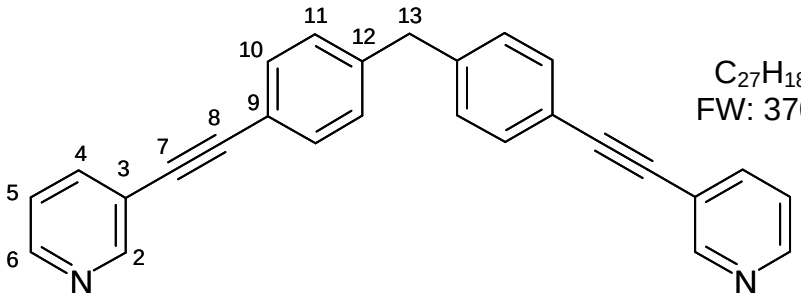

$C_{27}H_{18}N_2$
FW: 370.15

3-Ethynylpyridine (0.184 g, 1.79 mmol) was added to a degassed mixture of bis(4-iodophenyl)methane (0.300 mg, 0.71 mmol), copper (I) iodide (0.009 g, 0.04 mmol) and bis(triphenylphospine)dichloropalladium(II) (0.030 mg, 0.04 mmol) dissolved in diisopropylamine (7 ml) and dry THF (3 ml). The suspension was stirred under an argon atmosphere at 50 ^{o}C for 48 hours. The solvents were then removed under reduced pressure and the *crude* product dissolved in diethyl ether (20 ml). The organic layer was then washed with saturated sodium hydrogen carbonate (20 ml) solution and water (20 ml) and the combined washings extracted with diethyl ether (3 X 20 ml). The combined organic portion was dried under anhydrous magnesium sulphate and the solvent evaporated under reduced pressure. The *crude* product was purified by column chromatography on an alumina column (ethyl acetate:hexane 1:1) to yield a white solid (0.189 g , 72 % yield).

^{1}H NMR (300 MHz, $(CD_3)_2SO$, 298 K): δ 8.74 (2H, d, *J*= 1.9 Hz, H_2), 8.58 (2H, dd, *J*= 5.0, 1.9 Hz, H_6), 7.96 (2H, d, *J*= 8.1 Hz, H_4), 7.53 (4H, d, *J*= 8.1 Hz, $H_{10/11}$), 7.46 (2H, dd, *J*= 8.1, 5.0 Hz, H_5), 7.33 (4H, d, *J*= 8.1 Hz, $H_{10/11}$), 4.05 (2H, s, H_{13}).

^{13}C NMR (400 MHz, $CDCl_3$, 300 K): δ 152.0 C_2, 148.2 C_6, 141.1 $C_{3/9/12}$, 138.1 C_4, 131.6 $C_{10/11}$, 128.8 $C_{10/11}$, 122.7 C_5, 120.2 $C_{3/9/12}$, 92.3 $C_{7/8}$, 85.6 $C_{7/8,}$ 41.5 C_{13}.

Mass Spectrum (EI): *m/z* 370 $\{Ligand\}^+$.

Elemental analysis (%) calculated for $C_{27}H_{18}N_2$: C: 87.5; H: 4.9; N: 7.6; Found: C: 87.8; H: 4.8; N: 7.5.

IR (Neat): ν= 3029(br), 2218(m), 1581(w), 1560(m), 1505(m), 1475(m), 1405(s), 1188(m), 1123(m), 1100(m), 1038(w), 1021(s), 950(m), 923(w), 824(m), 801(s), 785(s), 701(s), 624(s) cm^{-1}.

2.4.5.3 Synthesis of $[Pd_2(L^4)_4][BF_4]_4$

Tetrakis(acetonitrile)palladium(II) tetrafluoroborate (0.017 g, 0.038 mmol) was added to a degassed solution of ligand **L^4** (0.028 g, 0.076 mmol) in acetonitrile (5 ml). The light yellow solution was stirred overnight under an argon atmosphere. The solution was filtered and the solvent removed under reduced pressure to yield a cream solid. The *crude* product was washed with chloroform (5 ml) and diethyl ether (5 ml) and dried *in vacuo* (0.037 g, 95 % yield).

^{1}H NMR (300 MHz, $(CD_3)_2SO$, 298 K): δ 9.43 (2H, s, H_2), 9.23 (2H, d, *J*= 6.0 Hz, H_6), 8.24 (2H, d, *J*= 8.1 Hz, H_4), 7.78 (2H, dd, *J*= 8.1, 6.0 Hz, H_5), 7.55 (4H, d, *J*= 8.3 Hz, $H_{10/11}$), 7.25 (4H, d, *J*= 8.3 Hz, $H_{10/11}$), 4.12 (2H, s, H_{13}).

Mass Spectrum (E.S.I): *m/z* 934.9 $\{Pd_2L_4 + 2BF_4\}^{2+}$, 900.9 $\{Pd_2L_4 + BF_4 + F\}^{2+}$, 594.2 $\{Pd_2L_4 + BF_4\}^{3+}$, 571.6 $\{Pd_2L_4 + F\}^{3+}$, 463.2 $\{Pd_2L_4 + 2(CH_3)_2SO\}^{4+}$, 423.9 $\{Pd_2L_4\}^{4+}$, 371.4 $\{Ligand + H\}^+$.

Elemental analysis (%) calculated for $[Pd_2(C_{27}H_{18}N_2)_4][BF_4]_4.9H_2O$: C: 58.9; H: 4.1; N: 5.1; Found: C: 58.9; H: 3.9; N: 5.1.

IR (Neat): ν= 3441(br), 3389(br), 3081(br), 2227(m), 1598(w), 1572(w), 1509(m), 1479(w), 1420(w), 1196(w), 1084(s), 813(m), 790(w), 695(m), 666(w), 520(w) cm^{-1}.

2.4.5.4 Synthesis of $[Pt_2(L^4)_4][PF_6]_4$

Ligand $\mathbf{L^4}$ (0.028 g, 0.076 mmol), bis(benzonitrile)dichloroplatinum(II) (0.018 g, 0.038 mmol) and silver(I) hexafluorophosphate (0.019 g, 0.076 mmol) were heated under reflux in acetonitrile (10 ml) for 48 hours. The solution was filtered and the solvent removed under reduced pressure to yield an off white solid. The *crude* product was washed with chloroform (5 ml), acetone (5 ml) and diethyl ether (5 ml) and dried *in vacuo* (0.016 g, 35 % yield).

^{1}H NMR (300 MHz, $(CD_3)_2SO$, 298 K): δ 9.36 (2H, s, H_2), 9.19 (2H, d, *J*= 5.9 Hz, H_6), 8.24 (2H, d, *J*= 8.0 Hz, H_4), 7.78 (2H, dd, *J*= 8.0, 5.9 Hz, H_5), 7.56 (4H, d, *J*= 8.3 Hz, $H_{10/11}$), 7.29 (4H, d, *J*= 8.3 Hz, $H_{10/11}$), 4.12 (2H, s, H_{13}).

Mass Spectrum (E.S.I): *m/z* 672.4 $\{Pt_2L_4 + PF_6\}^{3+}$, 662.2 $\{Pt_2L_4 + Cl + (CH_3)_2SO\}^{3+}$, 635.8 $\{Pt_2L_4 + Cl\}^{3+}$, 507.1 $\{Pt_2L_4 + 2(CH_3)_2SO\}^{4+}$, 487.4 $\{Pt_2L_4 + (CH_3)_2SO\}^{4+}$, 467.9 $\{Pt_2L_4\}^{4+}$.

Elemental analysis (%) calculated for $[Pt_2(C_{27}H_{18}N_2)_4][PF_6]_4.7H_2O$: C: 50.3; H: 3.4; N: 4.3; Found: C: 50.2; H: 3.3; N: 4.3.

IR (Neat): ν= 3087(br), 2228(m), 1650(br), 1600(w), 1573(w), 1509(w), 1478(w), 1416(m), 1194(w), 1019(w), 829(br,s), 739(m), 694(s) cm^{-1}.

2.4.6.1 Synthesis of Bis(4-bromophenyl)ethane intermediate[17]

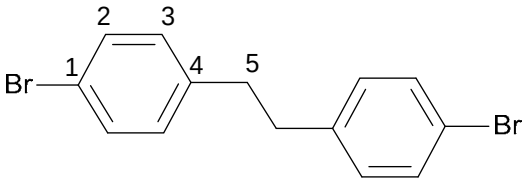

$C_{14}H_{12}Br_2$
FW: 337.93

A solution of Bis(4-aminophenyl)ethane (1 g, 4.7 mmol) was dissolved in HBr (48 %, 2.8 ml) and ethanol (11 ml) and cooled to 0 ºC prior to the addition of aqueous sodium nitrite (0.86 g, 12,05 mmol in 1.5 ml of H_2O). After stirring for 15 minutes the solution was added to a solution of copper(I) bromide (0.746 g, 4.98 mmol) in HBr (14 ml) at 95 °C. After stirring at 95 °C for 15 minutes, the solution was cooled to room temperature and diluted with water (50 ml). The mixture was extracted with ethyl acetate (3 X 20 ml), washed with a saturated solution of sodium hydrogen carbonate and dried over magnesium sulphate. The *crude* material was purified on a silica column with petroleum ether:ethyl acetate (1:1) eluent. The solvent was removed *in vacuo* and bis(4-bromophenyl)ethane isolated as a white solid (0.901 g, 57 % yield).

^{1}H NMR (300 MHz, $CDCl_3$, 298 K): δ 7.37 (4H, d, *J*= 9.0 Hz, $H_{2/3}$), 6.98 (4H, d, *J*= 9.0 Hz, $H_{2/3}$), 2.82 (4H, s, H_5).

2.4.6.2 Synthesis of Ligand (L^5)[10]

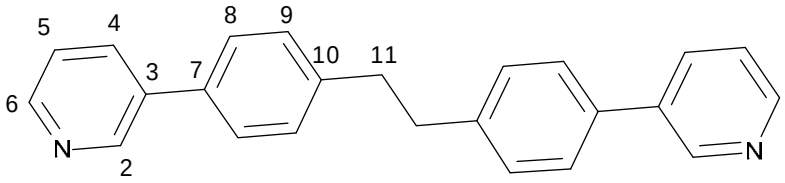

$C_{24}H_{20}N_2$
FW: 336.43

Method adapted from procedure of postdoctoral researcher Ekaterina Ryabova:

A solution of tetrakis(triphenylphosphine)palladium(0) (5 mol %, 51 mg, 0.044 mmol) in dimethoxyethane (2 ml) and aqueous sodium carbonate (1 M, 3.52 ml, 3.52 mmol) were added to an argon purged Schlenk flask containing bis(4-bromophenyl)ethane (0.3 g, 0.88 mmol). The flask was purged with argon once again and the resultant solution stirred at room temperature for 15 minutes. An ethanolic (2 ml) solution of pyridine-3-yl-3-boronic acid (0.324 g, 2.33 mmol) was added to the Schlenk and the mixture heated at 90 °C under an argon atmosphere. After 1 hour, the solution was cooled to room temperature and left stirring overnight. On completion of the reaction the mixture was filtered, the solvent removed and the solid residue dissolved in ethyl acetate (50 ml). The solution was dried over magnesium sulfate, filtered and the solvent removed under vacuum to afford the *crude* product. The ligand was purified on silica gel using petroleum ether:ethyl acetate (2:1) as the eluent.

^{1}H NMR (300 MHz, $(CD_3)_2SO$, 298 K): δ 8.88 (2H, d, *J*= 2.0 Hz, H_2), 8.55 (2H, dd, *J*= 4.6, 2.0 Hz, H_6), 8.06 (2H, dt, *J*= 8.1, 2.0 Hz, H_4), 7.66 (4H, d, *J*= 8.4 Hz, $H_{8/9}$), 7.47 (2H, dd, *J*= 8.1, 4.6 Hz, H_5), 7.40 (4H, d, *J*= 8.4 Hz, $H_{8/9}$), 2.99 (4H, s, H_{11}).

Mass Spectrum (EI): *m/z* 336 $\{Ligand\}^+$, 168 $\{Ligand\}^{2+}$.

Elemental analysis (%) calculated for $C_{24}H_{20}N_2$: C: 85.7; H: 6.0; N: 8.3; Found: C: 85.6; H: 6.0; N: 8.2.

IR (KBr): ν= 1607(w), 1475(s), 1449(w), 1433(m), 139.6(m), 1340(w), 1186(m), 1021(m), 999(m), 840(s), 802(vs), 758(w), 706(s), 621(w), 555(m) cm^{-1}.

2.4.6.3 Synthesis of $[Pd_3(L^5)_6][BF_4]_6$ and $[Pd_4(L^5)_8][BF_4]_8$

Tetrakis(acetonitrile)palladium(II) tetrafluoroborate (0.017 g, 0.038 mmol) was added to a degassed solution of ligand **L^5** (0.025 g, 0.076 mmol) in acetonitrile (5 ml). The solution was stirred overnight under an argon atmosphere, filtered and treated with diethyl ether resulting in the precipitation of a yellow solid. The *crude* product was washed with chloroform (5 ml), acetone (5 ml), ethanol (5 ml) and diethyl ether (5 ml) and dried *in vacuo*.

Triangle NMR

^{1}H NMR (300 MHz, $(CD_3)_2SO$, 298 K): δ 9.89 (2H, s, H_2), 9.31 (2H, d, *J*= 5.4 Hz, H_6), 8.37 (2H, d, *J*= 8.3 Hz, H_4), 7.82 (2H, dd, *J*= 8.3, 5.4 Hz, H_5), 7.62 (4H, d, *J*= 8.0 Hz, $H_{8/9}$), 7.51 (4H, d, *J*= 8.0 Hz, $H_{8/9}$), 3.00 (4H, s, H_{11}).

Pyramid NMR

^{1}H NMR (300 MHz, $(CD_3)_2SO$, 298 K): δ 9.95 (2H, s, $H_{2'}$), 9.58 (2H, d, *J*= 5.7 Hz, $H_{6'}$), 9.50 (2H, s, H_2), 9.04 (2H, d, *J*= 5.4 Hz, H_6), 8.37 (2H, d, *J*= 8.1 Hz, $H_{4'}$), 8.34 (2H, m, H_4), 7.96 (2H, dd, *J*= 8.1, 5.7 Hz, $H_{5'}$), 7.76-7.78 (2H, m, H_5), 7.55-7.72 (8H, m, $H_{8/9\ \&\ 8'/9'}$), 3.00 (8H, s, $H_{11\ \&\ 11'}$).

Mass Spectrum (E.S.I): *m/z* 1342.5 $\{Pd_3L_6 + 4BF_4\}^{2+}$, 1184.2 $\{Pd_4L_8 + 5BF_4\}^{3+}$, 675.2 $\{Pd_4L_8 + 3BF_4\}^{5+}$, 628.2 $\{Pd_3L_6 + 2BF_4\}^{4+}$, 548.5 $\{Pd_4L_8 + 2BF_4\}^{6+}$, 484.9 $\{Pd_3L_6 + BF_4\}^{5+}$.

2.5 References

1. M. J. Hannon, *Pure Appl. Chem.,* **2007**, 79, 2243-2261.
2. M. J. Hannon*, Chem. Soc. Rev.,* **2007**, 36, 280-295.
3. L. J. Childs, J. Malina, M. Pascu, B. E. Rolfsnes, M. J. Prieto, M. J. Broome, P. M. Rodger, E. Sletten, V. Moreno, A. Rodger, M. J. Hannon, *Chem. Eur. J.,* **2006,** 12, 4919-4927; C. Uerpmann, J. Malina, M. Pascu, G. J. Clarkson, V. Moreno, A. Rodger, A. Grandas, M. J. Hannon, *Chem. Eur. J.*, **2005**, 11, 1750-1756; L. Cardo, M. J. Hannon, *Inorg. Chim. Acta*., **2009**, 362, 784–792.
4. A. C. G. Hotze, B. M. Kariuki, M. J. Hannon, *Angew. Chem.,* **2006,** 118, 4957-4960.
5. M. J. Hannon, C. L. Painting, A. Jackson, J. Hamblin, W. Errington, *Chem. Commun.,* **1997**, 1807-1808.
6. E. Moldrheim, M. J. Hannon, I. Meistermann, A. Rodger, E. Sletten, *J. Biol. Inorg. Chem.,* **2002**, 7, 770-780.
7. M. J. Hannon, V. Moreno, M. J. Prieto, E. Moldrheim, E. Sletten, I. Meistermann, C. J. Isaac, K. J. Sanders, A. Rodger, *Angew. Chem. Int. Ed. Engl.,* **2001,** 40, 879-884; I. Meistermann, V. Moreno, M. J. Prieto, E. Molderheim, E. Sletten, S. Khalid, P. M. Rodger, J. Peberdy, C. J. Isaac, A. Rodger, M. J. Hannon, *Proc. Natl. Acad. Sci.,* **2002,** 99, 5069-5074.
8. A. Oleksi, A. G. Blanco, R. Boer, I. Uson, J. Aymami, A. Rodger, M. J. Hannon, M. Coll, *Angew. Chem. Int. Ed.,* **2006,** 45, 1227-1231.
9. J. M. Tour, A. M. Rawlett, M. Kozaki, Y. Yao, R. C. Jagessar, S. M. Dirk, D. W. Price, M. A. Reed, C. W. Zhou, J. Chen, W. Wang, I. Campbell, *Chem. Eur. J.,* **2001,** 7, 5118-5134.
10. S. Kotha, K. Mandal, K. K. Arora, V. R. Pedireddi, *Adv. Synth. Catal.,* **2005,** 347, 1215-1218.
11. X-ray crystal data were collected and solved by Dr. Benson M. Kariuki at the University of Birmingham.
12. E. Kerns, L. Di, *Drug-Like Properties: Concepts, structure design and methods: From ADME to Toxcity Optimization,* **2008,** Academic Press.

13. X-ray crystal data were collected and solved by Dr. Louise Male at the University of Birmingham.
14. F. M. D. Ismail, *J. Fluorine Chem.,* **2002,** 118, 27–33.
15. W. B. Austin, N. Bilow, W. J. Kelleghan, K. S. Y. Lau, *J. Org. Chem.,* **1981,** 46, 2280-2286.
16. Procedure given by Professor Arne Lutzen.
17. P. Nguyen, E. Corpuz, T. M. Heidelbaugh, K. Chow, M. E. Garst, *J. Org. Chem.,* **2003,** 68, 10195-10198.
18. D. K. Chand, K. Biradha, M. Kawano, S. Sakamoto, K. Yamaguchi, M. Fujita, *Chem. Asian. J.*, **2006**, 1, 82–90.

Chapter 3

Tetra-Stranded, Dinuclear Cylinders and their Biological Activities

3.1 Introduction

Metal ion directed self assembly has proved to be a useful tool in the construction of a vast array of discrete molecular architectures.[1] As described in chapter 1, scientists have taken advantage of this method for the synthesis of a library of structures including helicates,[2] boxes,[3] grids[4] and cages.[5] The resulting metallo-structures have a general formula of M_xL_y, with varying numbers of metal ions and ligands employed. They are of particular interest due to their uses in applications such as storage,[6] recognition[7] and catalysis.[8] However, our interest in these types of complexes is different and stems from their potential to be used as metallo-drugs in the treatment of genetic diseases.

In chapter 2, the synthesis and characterisation of a collection of novel, tetra-stranded, dinuclear cylinders of formula $[M_2L_4][X_4]$ has been discussed. In this chapter, the biological activity of four of these cylinders (Figure 3.1) is investigated.

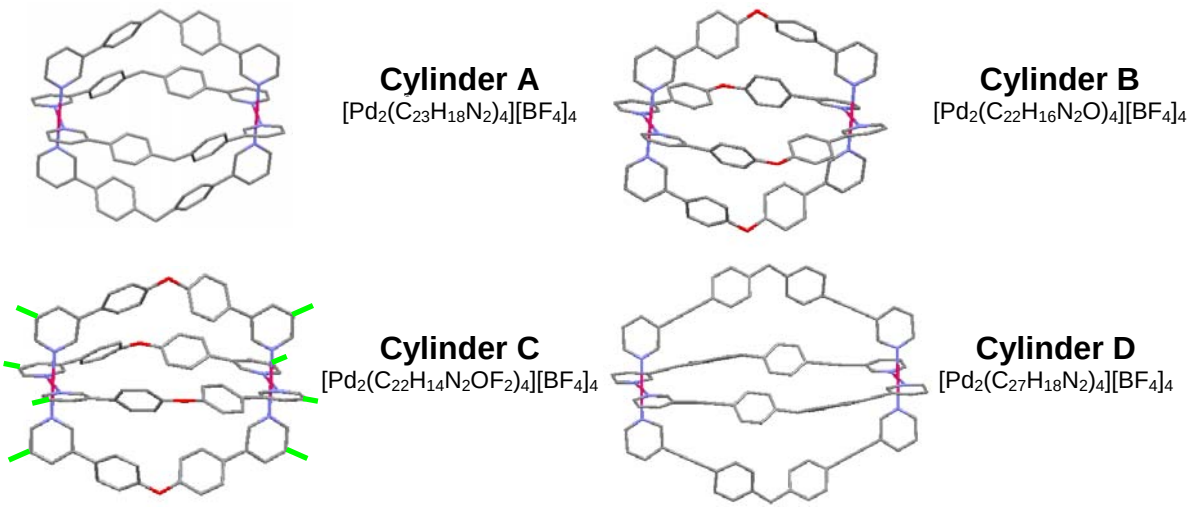

Figure 3.1. Tetra-stranded, dinuclear palladium(II) cylinders

In the following sections the DNA binding studies of cylinders **A**, **B**, **C** and **D** are described. In addition, the cytotoxic activities of these cylinders against human ovarian (A2780/ A7280cr) and breast (T47D) cancer cell lines is discussed and the genotoxicity and mutagenicity of the more active of the complexes presented.

3.2 Results and Discussion

3.2.1 DNA Binding Studies

In order to investigate DNA binding via circular dichroism (CD) and linear dichroism (LD), compounds must be added to an aqueous solution of DNA. However, as discussed in chapter 2, the cylinders are insoluble in pure water and only sparingly soluble in some water/solvent mixtures. This prevents detailed spectroscopic DNA binding studies from being carried out. Therefore, confirmation of their ability to bind to DNA comes from gel electrophoresis and atomic force microscopy (AFM) studies.

3.2.1.1 Agarose gel electrophoresis

Agarose gel electrophoresis is a technique which can be used to separate DNA molecules according to their size or conformation.[9] The DNA used in this work is the circular plasmid pBR322. In solution, the plasmid exists in two interchangeable forms, an open circular (OC) form and a negatively-supercoiled (NS) form (Figure 3.2).[10] If the OC form is twisted about the helical axis, these twists are accommodated for by the coiling of the DNA and results in the formation of the supercoiled form and vice versa.

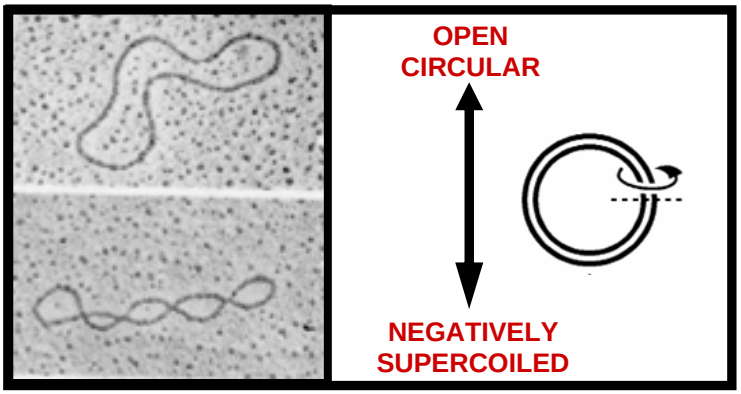

Figure 3.2. Microscope images of the two solution forms of pBR322.[10]

Agarose gel electrophoresis was used to detect the binding of the cylinders to the DNA plasmid. To overcome the issues with solubility the cylinders were dissolved in 2 % DMSO/water solutions. Different concentrations of the cylinders were then incubated with aqueous solutions of the plasmid for 1 hour (Table 1).

WELL	**1**	**2**	**3**	**4**	**5**	**6**	**7**	**8**	**9**	**10**
Base pairs: Cylinder	Control (2 % DMSO)	15/1	10/1	8/1	6/1	5/1	4/1	3/1	2/1	Control (no DMSO)

Table 1. Ratios of plasmid and cylinder used in gel electrophoresis studies.

After incubation, the plasmid-cylinder aliquots were injected into the wells of the agarose gel and an electrical current (5 Vcm^{-1}) applied for 3 hours. During electrophoresis the negatively charged plasmid molecules migrate towards the positively charged anode. The rate of migration is dependent on the size and conformation of the DNA. The gel was subsequently stained with ethidium bromide and the positions of the plasmid detected using a UVIPro Platinum 2.0 system at 312 nm.

3.2.1.2 Results and Discussion

Figure. 3.3 shows the electrophoretic mobility of the plasmid-cylinder structures.

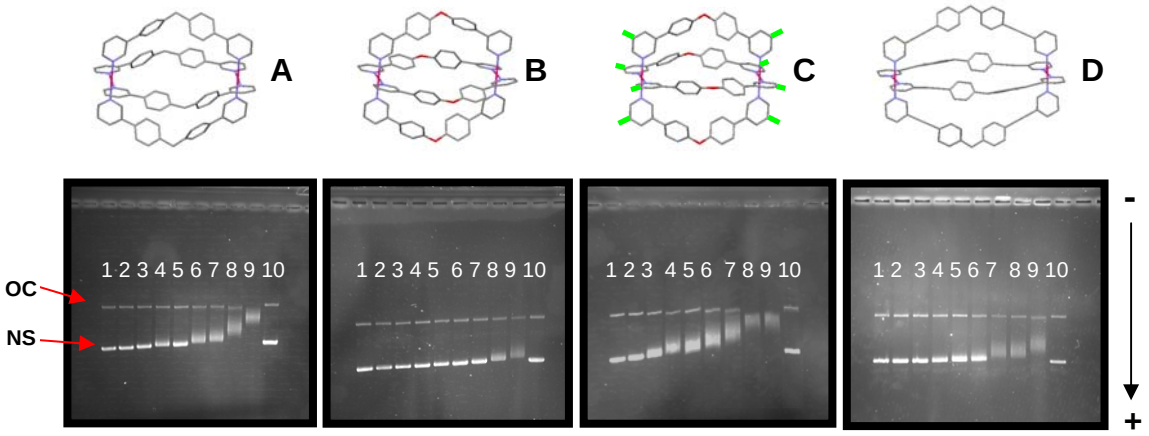

Figure 3.3. Agarose gel electrophoresis of pBR322 treated with cylinders **A-D**.

At low cylinder concentrations, distinct OC and NS bands can be seen. As the concentration of the cylinder is increased, the mobility of the NS band decreases. In the case of cylinders **A** and **C**, at high concentrations the mobility of the OC band is also accelerated. These results show that all four cylinders bind to and lengthen and/or stiffen the structure of the DNA. It is also apparent that an increase in the concentration of cylinder results in an increase in DNA binding.

Some agents, for example intercalators, unwind the DNA double helix on binding. Therefore, as the concentration of the drug is increased, an increase in the unwinding of the helix is observed. Further binding will result in the positive-supercoiling of the OC form of the plasmid (Figure 3.4), explaining any increase in the mobility of this band at high compound concentrations.[10]

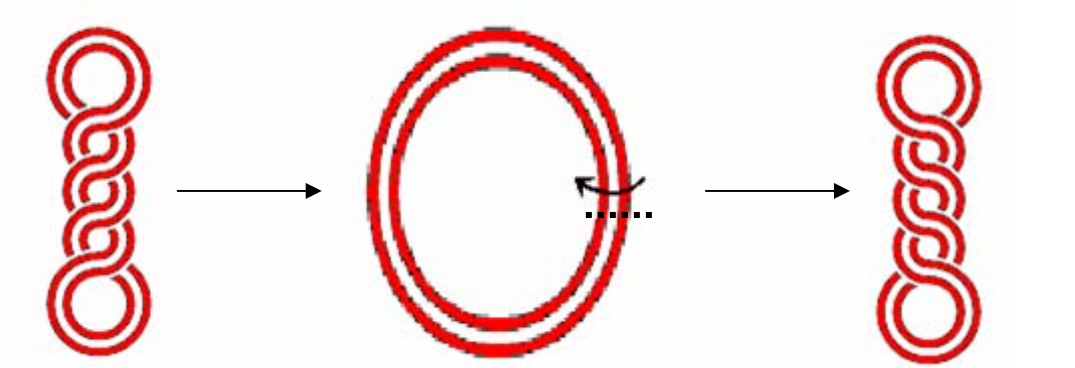

Figure 3.4. The positive supercoiling of the plasmid resulting from drug intercalation

If enough complex is added to the DNA the OC and NS bands will co-migrate and the DNA unwinding angle (ϕ)[11] can be calculated using the following formula:

$$\phi = -18\sigma / r_{(c)}$$

$r_{(c)}$ is the ratio of cylinders bound per plasmid when the NS and OC bands co-migrate. The number of cylinders bound is taken to be equal to the mixing ratios based on the assumption that all cylinders present in the sample are completely bound to the DNA. $r_{(c)}$ can be easily determined by experiment. It is well known that cis-platin has a DNA unwinding angle of 13°, this along with the experimentally determined $r_{(c)}$ can be used to calculate the value of the superhelicity constant (σ = -0.059).[12]

The DNA unwinding angles have been calculated for cylinders **A**-**D** and are compared with a racemic mixture of Hannon's triple-stranded, dinuclear iron(II) cylinder (see chapter 2, section 2.1.1) and its ruthenium(II) analogue[13] in Table 2.

	Unwinding Angle (ϕ)
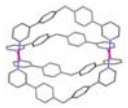 **A**	4º
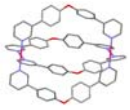 **B**	< 4º
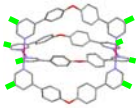 **C**	6º
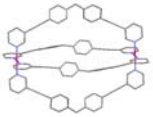 **D**	< 4º
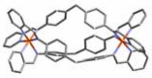 **Fe(II) cylinder**	27º [13]
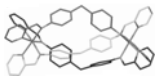 **Ru(II) cylinder**	13º [13]

Table 2. Angle of unwinding of pBR322 caused by cylinders **A**-**D** and Hannon's iron(II) and ruthenium(II) cylinders.

The results show that Hannon's iron(II) cylinder is the most effective at unwinding the plasmid DNA. Intriguingly, the analogous ruthenium(II) cylinder has an unwinding angle that is about half that of the iron(II) cylinder. Of the tetra-stranded cylinders, **C** has the highest unwinding angle followed by cylinder **A**. An unwinding angle could not be calculated for cylinders **B** and **D** as the OC and NS bands did not co-migrate at the concentrations used in these experiments. All four tetra-stranded cylinders show less unwinding than both of the triple-stranded agents. The iron(II) cylinder unwinds the DNA duplex by binding non-covalently to the major groove of DNA. It is possible that cylinders **A**-**D** also have a similar mode of action, but due to their bulkier sizes they only

partially insert and bind within the groove, resulting in a smaller amount of unwinding.

3.2.1.3 Atomic Force Microscopy

The next step was to get some molecular-level images of the cylinders with DNA, this was done using an atomic force microscope (AFM). An AFM is a mechanical imaging instrument that measures the 3D topography of a surface using a sharpened tip. A sample is added to a substrate such as mica or graphite and a magnified image is generated by monitoring the motion of the tip as it is scanned back and forth over the surface. AFMs are capable of measuring images at nanoscale (even individual atoms) and therefore have a vast number of applications in many areas of science and technology.[14] Of particular interest is the ability of AFMs to image DNA molecules and DNA-compound adducts that are attached to the surface of a substrate.[15]

The AFM studies were conducted during a visit to the Universidad Autónoma de Madrid. The experiments were carried out in the laboratory of Dr Felix Zamora and under the guidance of Dr Lorena Weltze. Unfortunately a sample of cylinder **C** was not available when the work was carried out. Therefore, only the studies with cylinders **A**, **B** and **D** will be reported in this work. All experiments were carried out on muscovite mica which is commonly used to immobilize DNA molecules onto a flat surface.

DNA samples were prepared by depositing a drop of ct-DNA solution and nickel chloride (10 μM) solution onto a freshly cleaved mica surface. After adsorption for 2 minutes, the surface was rinsed in a jet of ultra-pure water and blow dried with compressed argon. The nickel(II) cations act as a bridge in the immobilisation of the negatively charged DNA onto the negatively charged mica

surface.[16] DNA-cylinder adducts were prepared by mixing the DNA with different concentrations of the cylinders. The freshly prepared DNA-cylinder solutions and nickel chloride were adsorbed onto the mica surface and washed and dried as previously described. The AFM images were obtained in tapping mode using a Nanotec Electrónica AFM and analysed using WSxM software.[17]

3.2.1.4 Results and Discussion

Figure 3.5 shows an AFM image of two ct-DNA molecules adsorbed onto a mica surface using nickel(II) chloride. Without cylinders, the free DNA exists as long fibres with little twisting or coiling of the DNA strands. At 1 nm, the molecular height is typical for AFM measurements.[15] However, as depicted in Figure 3.5, the lengths of the molecules vary considerably.

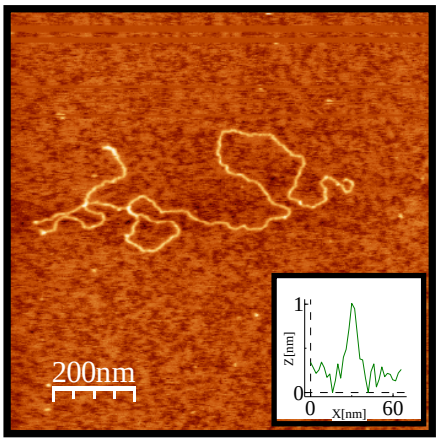

Figure 3.5. AFM topographic image showing ct-DNA adsorbed onto a mica substrate.

Upon interaction with cylinder **A** (0.03 μM) the ct-DNA started to bend and coil (Figure 3.6(a)) and the long fibres of the free DNA are no longer obvious. On increasing the concentration of the cylinder to 0.075 μM, the coiling of the DNA fibres is even more apparent and the DNA molecules appear to cluster together to form large aggregates (Figure 3.6(b)). A further increase in the cylinder concentration (10 μM) results in the condensation of several DNA molecules

into small, compact nano-structures (Figure 3.6(c)). However, due to the high concentration of the cylinder, it is possible that these structures may also contain nano-particles of the crystallised cylinders.

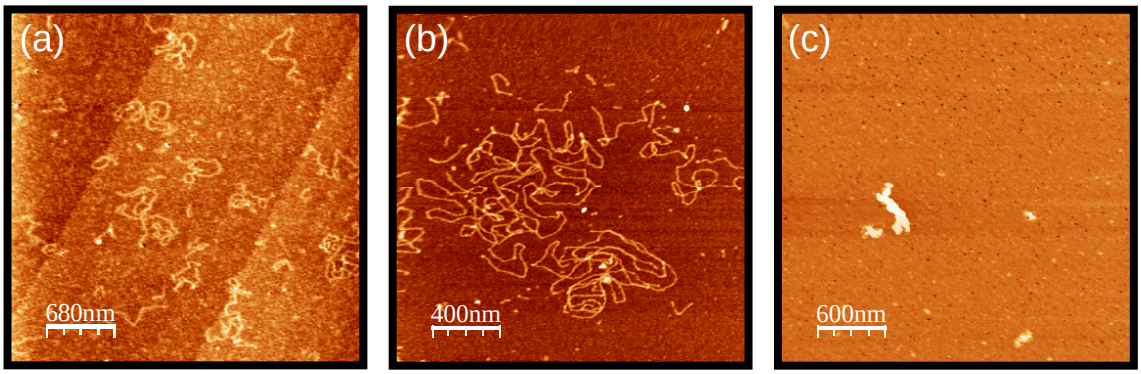

Figure 3.6. AFM topographic images of ct-DNA with (a) 0.03 μM (b) 0.075 μM and (c) 10 μM of cylinder **A**.

Cationic condensing agents are believed to work by neutralizing the negative charge of the DNA sugar-phosphate backbone. This decreases the electrostatic repulsions between the DNA fibres, allowing them to tightly pack together.[18] A well-studied example is the inorganic cation cobalt(III) hexamine which condenses and aggregates DNA into intermolecular clusters. An AFM image of cobalt(III) hexamine with the linearised DNA plasmid pBR322 is shown in Figure 3.7.[19] The result obtained with the cobalt(III) complex is similar to that seen for the highest concentration of cylinder **A**.

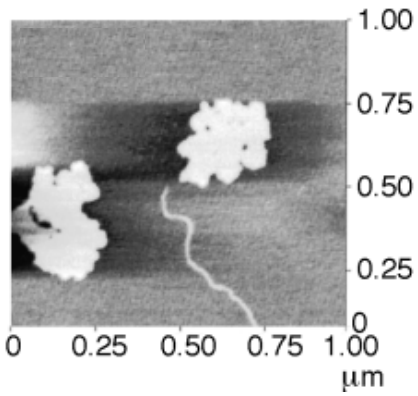

Figure 3.7. AFM images of linear plasmid pBR322 with cobalt(III) hexamine (Taken from reference 19).

Spermine is another well known DNA condensation agent. Drew and Dickerson's crystal structure of DNA with spermine showed that the tetra-cation is located in the DNA major groove and results in the kinking of the double helix.[20] Figure 3.8 shows AFM images of spermine with the DNA plasmid pCmV luciferase.[21] The effects are similar to those observed at low and high concentrations of cylinder **A** (Figure 3.6(a) and (b)) except that much higher concentrations of spermine are required.

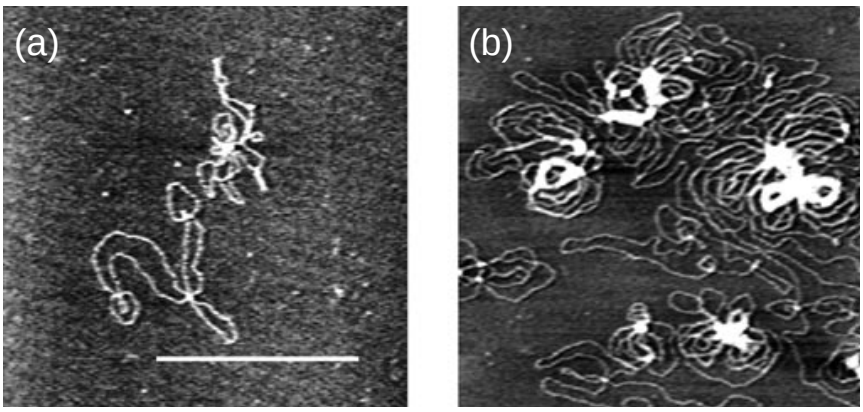

Figure 3.8. AFM images of DNA with (a) 10 mM and (b) 500 mM of spermine (Taken from reference 21).

Similar trends were also seen in the AFM experiments of ct-DNA with cylinder **B**. Figure 3.9 shows the AFM topographic images of ct-DNA with cylinder **B**, adsorbed onto muscovite mica.

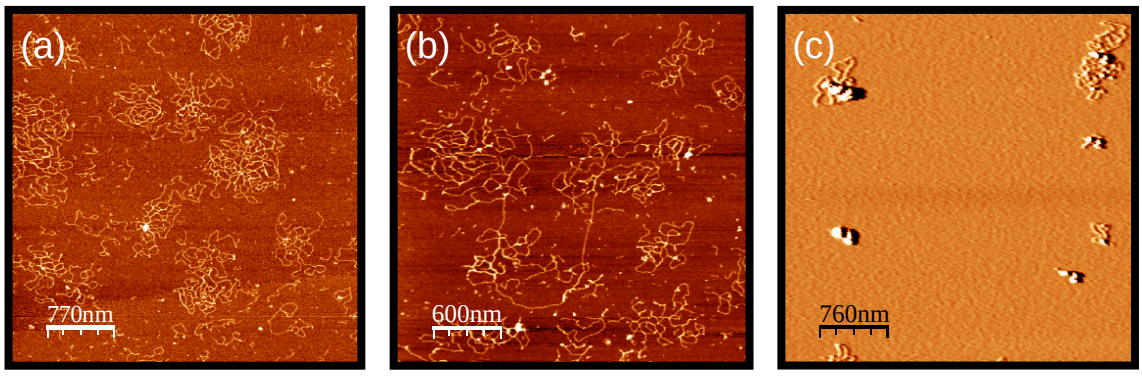

Figure 3.9. AFM topographic images of ct-DNA with (a) 0.03 μM (b) 0.075 μM and (c) 10 μM of cylinder **B**.

This cylinder clearly binds to the DNA and an increase in the concentration of **B** results in an increase in the aggregation of the DNA. Figure 3.9(c) shows the condensation of the DNA at high cylinder concentrations (10 μM). A close look shows that some of the nano-structures appear to be in the process of being formed as they are surrounded by DNA fibres.

As with cylinders **A** and **B**, on mixing with ct-DNA, an increase in the concentration of cylinder **D** results in an increase in the aggregation of the DNA (Figure 3.10).

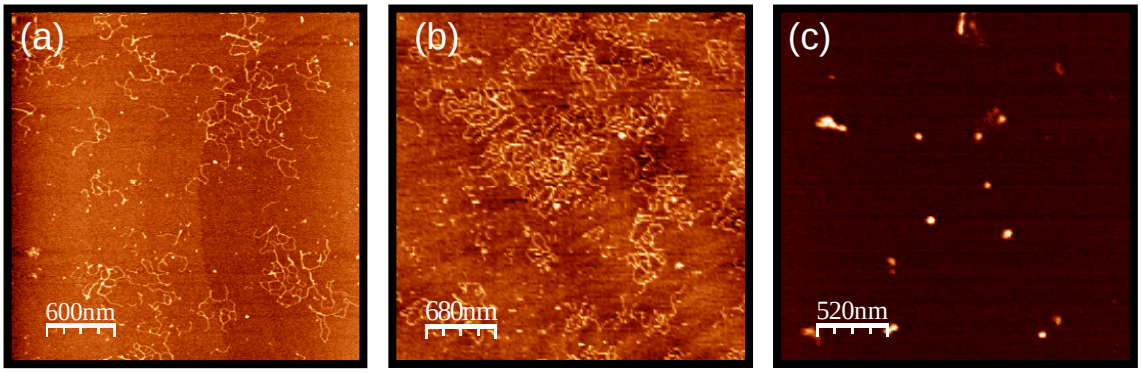

Figure 3.10. AFM topographic images of ct-DNA with (a) 0.03 μM (b) 0.075 μM and (c) 10 μM of cylinder **D**.

Interestingly, the AFM images of DNA with cylinders **A**, **B** and **D** differ from those reported for Hannon's iron(II) cylinder which causes intramolecular DNA coiling.[19] The coiling process is cooperative and at some concentrations uncoiled, bent DNA strands are observed in the presence of other fully coiled ones (Figure 3.11(a)). At higher concentrations all of the DNA strands are coiled (Figure 3.11(b)).

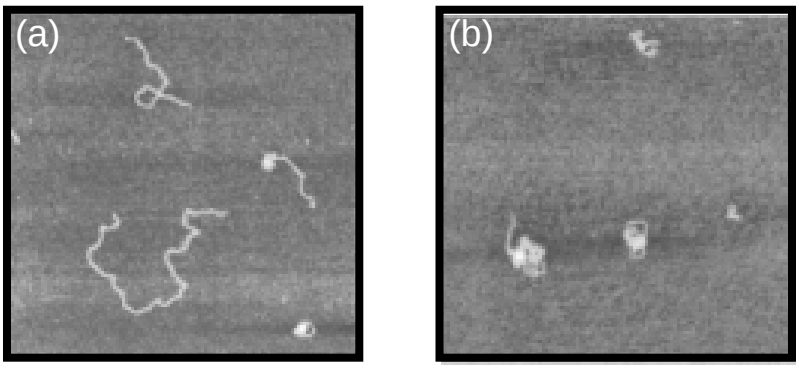

Figure 3.11. AFM images of linear plasmid DNA with Hannon's iron(II) cylinder in base pair to metal complex ratios of (a) 10:3 and (b)10:5 (Taken from reference 19).

The difference in the results might be because the iron(II) cylinder acts by binding in the DNA major groove whereas the tetra-stranded cylinders are too large to fully insert into this binding site.

3.2.2 Cytotoxicity Tests

3.2.2.1 The MTT Assay

To explore the anti-cancer activity of the cylinders their cytotoxicity was determined using the 3-[4,5-Dimethylthiazol-2-yl]-2,5-diphenyl tetrazolium bromide (MTT) assay.[22] Cultured cancer cells were grown in 96 well plates in the presence of different concentrations of the cylinders (25 μM – 1.5 μM). After 72 hours the amount of living cells present were determined by the addition of MTT. In viable (living) cells the mitochondrial enzyme succinate dehydrogenase converts the yellow water soluble MTT (a tetrazole) into blue formazan crystals (Figure 3.12).

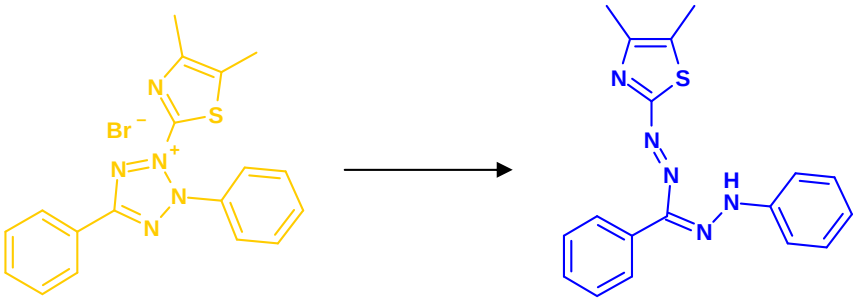

Figure 3.12. Reduction of MTT to Formazan crystals.

These blue crystals were then dissolved in DMSO to give a pink/purple solution & the UV absorbance measured at 590 nm. A dose response curve was plotted from which the IC_{50} values were determined. The IC_{50} is the concentration of complex required to inhibit 50 % cell growth. In other words, it is the concentration of the cylinder in wells that contain half the number of cells that are present in the control wells.[23]

In the studies herein, the MTT assay was carried out using the ovarian cancer line A2780 and its cis-platin resistant subline A2780cr and the breast cancer cell line T47D.

3.2.2.2 Results and Discussion

The IC_{50} values of cylinders **A**-**D** were determined by the MTT assay and are compared to those of cis-platin and Hannon's iron(II) cylinder in Table 3.

	A2780	A2780cr	T47D
Cylinder A	8.1 ± 1.3	10.3 ± 1.2	5.6 ± 0.5*
Cylinder B	5.1 ± 1.1	9.0 ± 0.9	4.8 ± 1.1*
Cylinder C	>100	>100	>100
Cylinder D	>100	>100	>100*
Iron(II) Cylinder	8.7 ± 1.1 [24]	13.1 ± 2.3 [24]	52.0 ± 10 [25]
Cis-platin	4.5 ± 0.8	16.0 ± 1.8	28.3 ± 1.7*

Table 3. IC_{50} values (μM) of cylinders **A-D**, Hannon's iron(II) cylinder and cis-platin in cancer cell lines. The results represent the mean of 4 separate experiments ± SD (n=4)
*experiments performed by Carlos Sanchez-Cano

Cylinders **A** and **B** show good activity in all of the cell lines that were tested and the IC_{50} data are comparable to or better than those of cis-platin. The cylinders are also active in the cis-platin resistant cell line, consistent with their expected different mode of action. The mechanism by which the cylinders enter the cells is unknown and has not yet been investigated. However, it is unlikely that they enter the cells in the same was as cis-platin because they are much bigger and exhibit different solubility. Intriguingly the fluorinated cylinder (**C**) and the large ethynyl cylinder (**D**) are inactive giving IC_{50} values >100 μM. As the structures of **A** and **B** are very similar, this could indicate that it is their precise size and shape that is important in their activity. It is not possible to compare these results with those of the other literature Pd_2L_4 complexes as their cytotoxic activities have not been reported. However, comparison with Hannon's triple-stranded iron(II) cylinder is particularly interesting with cylinders **A** and **B**

showing comparable activity in the ovarian carcinoma cell lines but much higher activity in the T47D breast cancer cell line.

These results demonstrate that metallo-supramolecular structures may be very powerful for the design of new types of anti-tumour agent. However, in the development of new drug candidates the potential risks of the drugs need to be carefully evaluated. Numerous tests need to be carried out to confirm that the drug is safe to use in humans.[26] With this in mind, additional biological studies were carried out to further probe the suitability of the two more cytotoxic cylinders (**A** and **B**) as potential anti-cancer drugs.

3.2.3 Toxicological Studies

3.2.3.1 Bacterial Mutagenicity (Ames) Test

A Mutagen is a chemical that causes changes to DNA, for example insertions or deletions of one or more of the nucleotide bases. Mutagenic substances are also typically carcinogenic. The Ames test is a biological assay which is used to assess the mutagenic potential of new drug candidates.[27] A negative result in the Ames test indicates that the tested drug is also non-carcinogenic.

The test utilises strains of *Salmonella typhimurium* (HIS-) that carry mutations in the genes used to synthesise histidine. Therefore, the bacteria require an external supply of histidine in order to grow. Addition of a mutagenic compound to these bacteria leads to a genetic reversion in some of the bacteria, resulting in a resumption in their ability to synthesise histidine. The *Salmonella typhimurium* strains used in these experiments are the TA98 strain and the TA100 strain which carry frameshift and base pair substitution mutations, respectively.[28]

Promutagens are non-mutagenic compounds that must be activated via a chemical modification (e.g. oxidation) in order to become mutagenic. In vivo, this activation process is carried out by the metabolizing enzymes of the liver. Bacteria do not produce the enzymes required to activate promutagens and are therefore treated with a mixture of rat liver enzymes (S9) in order to mimic *in vivo* metabolic activation.[29]

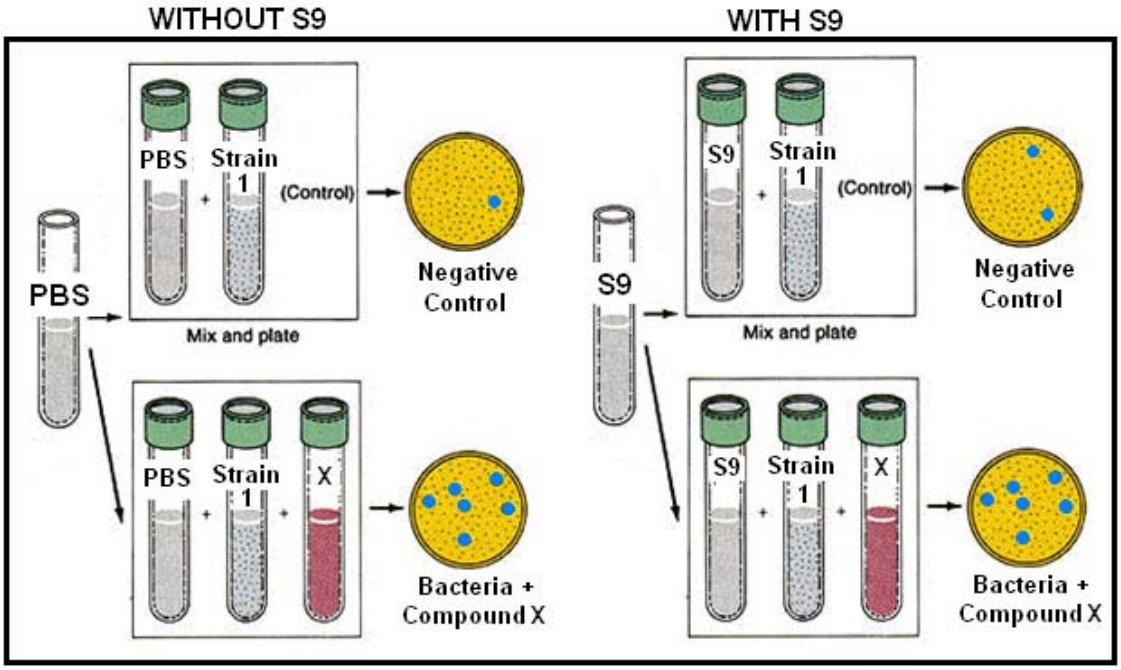

Figure 3.13. A schematic representation of the Ames Test.[30]

Figure 3.13 shows a schematic representation of the Ames test which has been adapted from reference 30. The bacteria and test compound were spread onto a minimal-agar plate (both with and without S9) and molten top-agar poured on top. A small amount of histidine was added to allow the bacteria to grow for a short period of time. When the histidine is exhausted only bacteria that have undergone a reverse mutation and regained their ability to synthesise histidine will survive. Some of the bacteria are also able to revert spontaneously so the results are compared with a negative control (without test compound). Positive

controls (consisting of a known mutagen or promutagen) were also used to demonstrate that the test is working and reagent controls confirm that the reagents used were uncontaminated. The plates were prepared in triplicate and incubated in the dark at 37 °C. After 48 hours the number of colonies on each plate was counted. As a rule of thumb: *the number of revertant colonies present after exposure to a compound should be more than double those found in the negative control if the substance is to be classed as a mutagen*.[31]

3.2.3.2 Results and Discussion

The Ames bacterial mutagenicity test was carried out on the cytotoxic cylinders, **A** and **B**. A range of cylinder concentrations were tested with the highest concentration being well over the IC_{50} value for each cylinder. Figure 3.14 shows the results from the tests with the TA98 strain of *Salmonella typhimurium*.

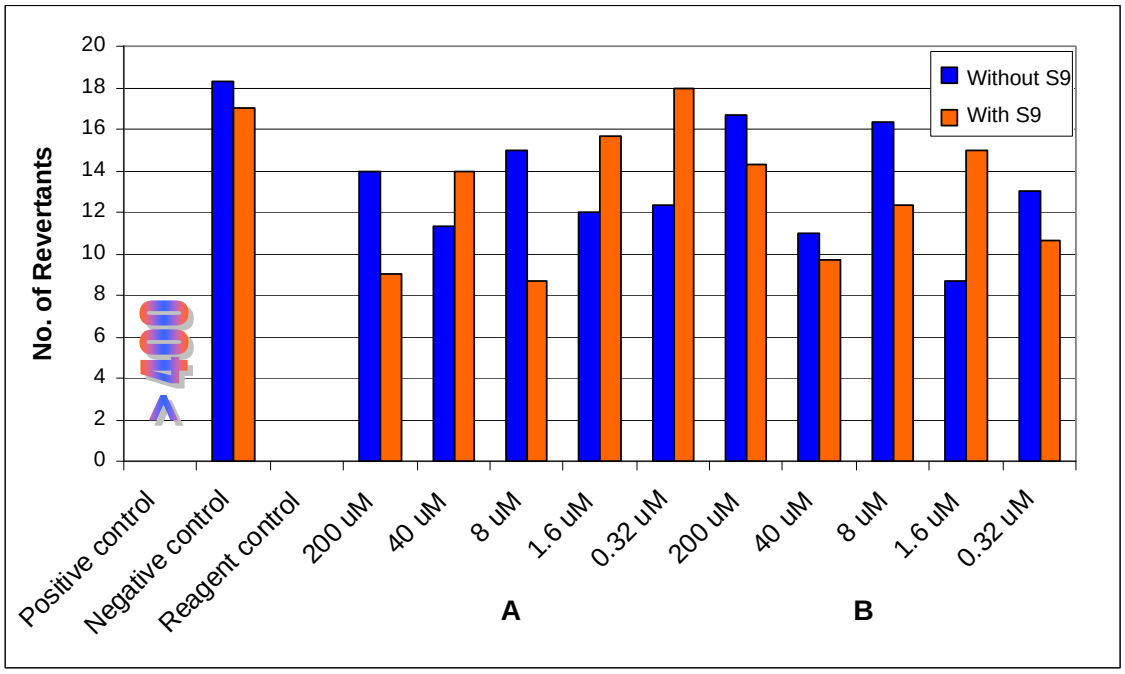

Figure 3.14. Ames Test Results for cylinders **A** and **B** with *Salmonella Typhimurium* TA98
(Positive Controls: Promutagen- chrysoidine Y & Mutagen- 4-nitroquinoline-N-oxide)

The graph clearly shows that there is no dose-dependent response across the range of concentrations tested, both with and without S9. Even at high concentrations there is no significant difference in the number of colonies present in the negative control and in the plates containing the cylinders. Therefore, the result of the test is negative and cylinders **A** and **B** do not cause frame-shift mutations in DNA.

Figure 3.15 shows the results obtained for the tests carried out with the TA100 strain of *Salmonella Typhimurium*.

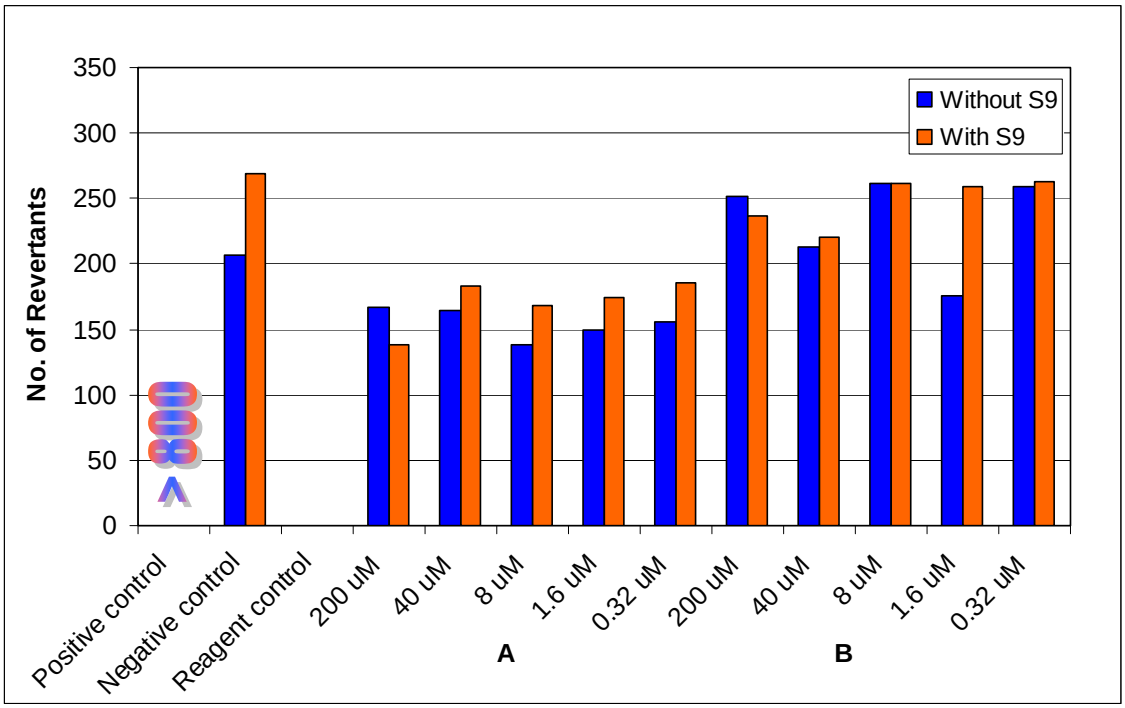

Figure 3.15. Ames Test Results for cylinders **A** and **B**
With *Salmonella Typhimurium* TA100
(Positive Controls: Promutagen- chrysoidine Y & Mutagen- sodium azide)

It is well known that *Salmonella Typhimurium* TA100 has a naturally higher reversion rate than the TA98 strain and this is confirmed by these results.[28] As with the TA98 strain, the experiments with TA100 demonstrate that there is no significant difference in the number of colonies present with or without the

cylinders. This is also the case for the experiments carried out with the S9 enzymes. Therefore, the result of the test is negative and reveals that **A** and **B** do not cause base pair substitution mutations in DNA.

The Ames test results confirm that cylinders **A** and **B** have no promutagenic or mutagenic effects on the *Salmonella typhimurium* strains tested. Therefore, neither of the cylinders causes base-pair substitution or frameshift mutations under the conditions that were used. A negative result at this point is invaluable as it takes the cylinders one step closer to clinical trials.

3.2.3.3 Single Cell Gel Electrophoresis (Comet) assay

Besides the Ames test, pharmaceutical companies also routinely screen for the genotoxicity of drug candidates by way of the comet assay.[32] Originally described in 1984 by Ostling and Johannson, the comet assay is a simple, well established method used for the measurement of DNA strand breaks in eukaryotic cells.[33] Over the years, many variations of the assay have been reported, each employing subtle changes to make it more suited for the measurement of different types of DNA damage. The procedure described here is the alkaline version of the comet assay reported by Singh *et al.* in 1988.[34] Figure 3.16 shows a schematic representation of the alkaline comet assay adapted from reference 35.

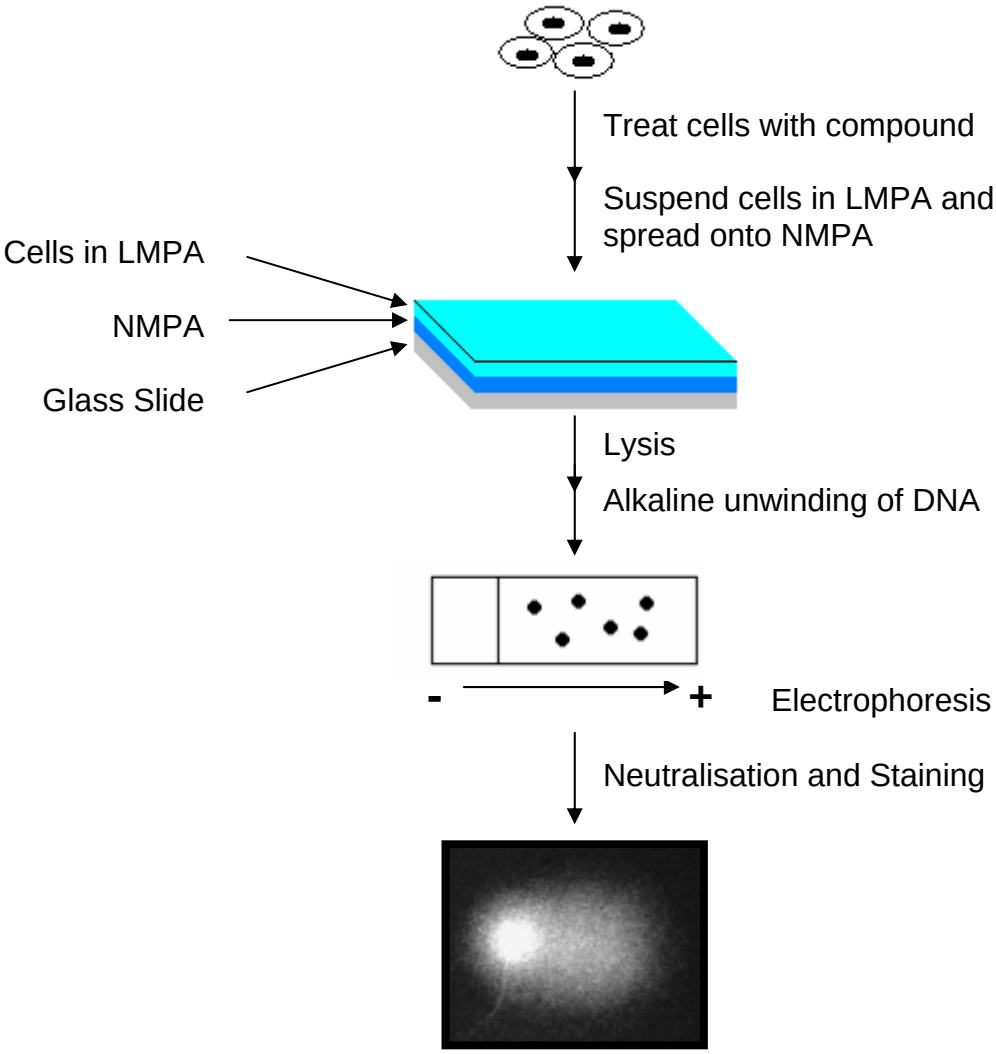

Figure 3.16. A schematic representation of the alkaline comet assay.[35]

A2780 (ovarian) carcinoma cells were seeded in 6-well plates and treated with cylinders **A** (9 μM) and **B** (6 μM). Following a 24 hour treatment the cells were detached from the wells by gentle scrapping and suspended into low melting point agarose (LMPA). The suspension was spread onto a glass microscope slide which had been pre-coated with normal melting point agarose (NMPA). The LMPA was allowed to set and the slides incubated in lysis buffer for 1 hour. The role of the lysis buffer is to remove all of the proteins, RNA, membranes and cytoplasmic constituents of the cell, leaving only the supercoiled DNA or 'nucleoid' behind. Following lysis, the slides were incubated in the alkaline

electrophoresis buffer to allow the DNA duplex to unwind. Electrophoresis was then carried out for 20 minutes. During electrophoresis, the intact DNA remains tightly wound in the nucleoid, or comet 'head', but the loops of DNA around any strand breaks migrate out towards the positively charged anode and result in the formation of the comet 'tail'. Finally, the slides were stained with a solution of sybr gold and examined under a fluorescence microscope (Zeiss Axiovery 10, Germany). Figure 3.17 shows fluorescence microscope images of undamaged and damaged A2780 nuclei.

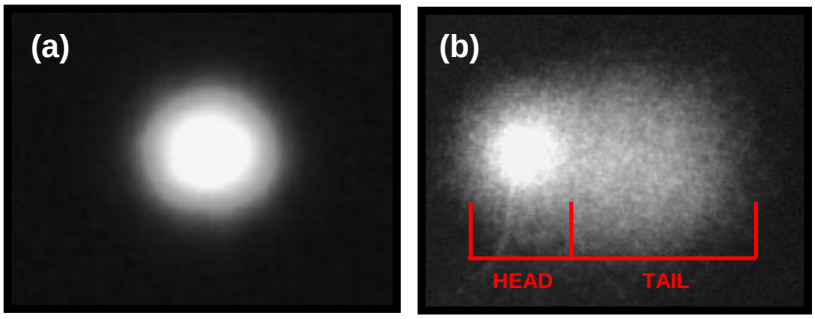

Figure 3.17. Fluorescence microscope images of carcinoma cells (**a**) without and (**b**) with DNA damage.

The intensity and length of the comet tail was quantified for 100 comets per slide and is directly proportional to the extent of DNA damage that has occurred.

3.2.3.4 Results and Discussion

The alkaline comet assay was used to ascertain whether the formation of DNA strand breaks might be involved in the mechanism of action of cylinders **A** and **B**. The results of the assay are shown in Figure 3.18.

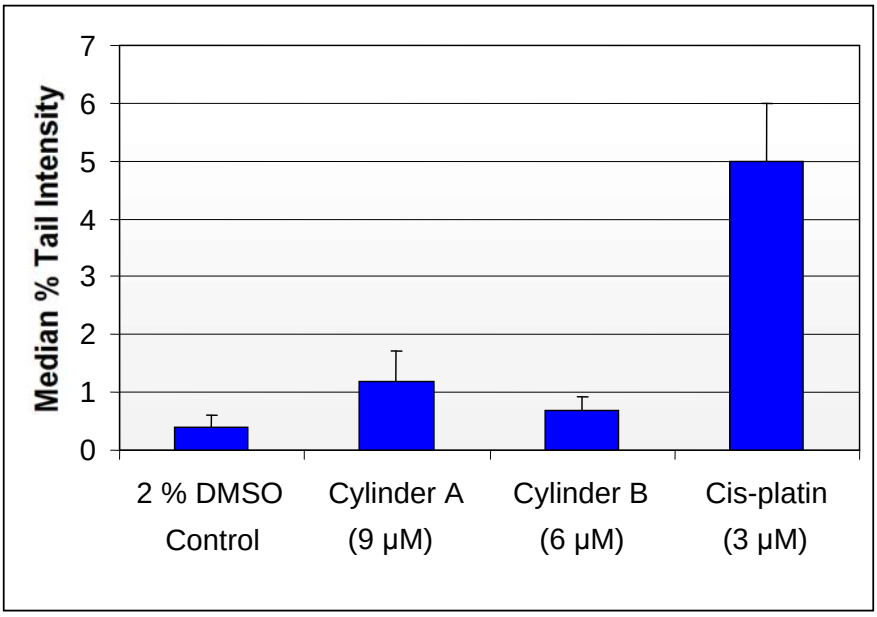

Figure 3.18. Results of comet assay expressed in terms of the % of DNA in the comet tail in A2780 cells exposed to cylinders **A** and **B** and cis-platin.

The results demonstrate that for cylinders **A** and **B**, the % tail intensity is not significantly higher than that observed in the DMSO control. Also, parallel experiments carried out with cis-platin showed that just 3 µM of the drug produced a median % tail intensity of over 5 %, much greater than is seen with **A** and **B**. This is a significant result as the genotoxicity of some currently available drugs, such as cis-platin, are responsible for the formation of secondary cancers (especially leukemias) in patients that are undergoing treatment with them.[36] Therefore, the design and synthesis of drug candidates which are cytotoxic but not genotoxic is very important.

3.3 Conclusions

Agarose gel electrophoresis experiments show that on incubation with the plasmid pBR322, cylinders **A**, **B**, **C** and **D** bind to and cause the unwinding of supercoiled DNA (**C** > **A** > **D** > **B**). AFM imaging has illustrated that **A**, **B** and **D** also cause the aggregation of ct-DNA. The MTT assay has demonstrated that **A** and **B** show considerable cytotoxic activity against ovarian (A2780 and A2780cr) & breast cancer (T47D) cell lines but cylinders **C** and **D** are inactive. Preliminary toxicological studies show that **A** and **B** are also non-mutagenic and non-genotoxic. These results are very exciting as drug candidates that possess cytotoxic activities against cancer cells without being mutagenic and genotoxic, present a considerable advancement in this research field.

3.4 Experimental

3.4.1 Gel Electrophoresis

Gel electrophoresis experiments were carried out using an Amersham Biosciences HE99X Max submarine kit. The agarose (Fisher) gel was prepared by heating 2 g of agarose (1 %) in 200 ml of TAE (1X) buffer and allowing the gel to cool and set. The plasmid pBR322 (New England Biolabs) was dissolved in ultra-pure water (1 μg/μl) and the cylinders dissolved in 2 % dmso/water solutions. Aliquots of the plasmid and varying amounts of complex were mixed together and incubated at 37 ºC for 1 hour. 4 μl of loading buffer (30 % glycerol, 0.05% bromophenol blue and 0.025 % cyanol xylene) was added to each mixture and 16 μl loaded onto the agarose gel. The gel was run in TAE (1X) electrophoresis buffer at 5 Vcm^{-1} for 180 minutes. Gel staining was performed in the same buffer containing ethidium bromide (0.5 $mgml^{-1}$). The gel was visualized using a UVIPro Platinum 2.0 system (UViDoc, Cambridge, UK) at 312 nm.

3.4.2 Atomic Force Microscopy

The AFM images were obtained in dynamic mode using a Nanotec Electrónica AFM. Olympus cantilevers (RC800PSA (ORC8)) were used with a nominal force constant of 0.75 Nm^{-1} and < 20 nm nominal radius tip. The samples were measured in air at a scan rate of 1 Hz. Data was acquired at room temperature and analysed using WSxM software, which is freely distributed by Nanotec Electrónica (www.nanotec.es).

Highly polarised, ct-DNA (Sigma-Aldrich) was dissolved in ultra-pure water and kept frozen until the day of the experiment. Stock solutions of cylinders

A (541 μM), **B** (538 μM) and **D** (490 μM) were made up in 5 % dmso/water on the day of use. Muscovite mica was purchased from Electron Microscopy Sciences and a flat, freshly cleaved surface prepared by lifting off the top layers of the mica with adhesive tape. DNA samples were prepared by depositing 8 μl of ct-DNA (0.002 $\mu g \mu l^{-1}$) solution and 2 μl of nickel chloride (10 μM) solution onto the cleaved mica surface. After adsorption for 2 minutes, the surface was rinsed for 10 seconds in a jet of ultra-pure water and blow dried with compressed argon. DNA-cylinder samples were made by mixing 5 μl of ct-DNA with 5 μl of the required concentration of cylinder and adding 8 μl of this final solution to a 2 μl drop of nickel chloride (10 μM) on the mica surface. The solution was allowed to adhere for 2 minutes and was then washed and dried as previously described.

3.4.3 Cell Culture

Materials: The media were obtained from Invitrogen and the supplements were purchased from Sigma-Aldrich unless otherwise stated.

The A2780 (human ovarian carcinoma) and A2780cr (cis-platin-resistant) cell lines were cultured in Dulbecco's Modified Eagle's Medium (DMEM) and the T47D (human breast carcinoma) cell line was maintained in Roswell Park Memorial Institute (RPMI-1640) medium. Both media were supplemented with 10 % FBS (Invitrogen), 1 % L-glutamine, 1 % hepes buffer, 1 % sodium pyruvate and an antibiotics-antimycotic solution (1X). All three cell lines were cultured in T_{25} flasks (Nunc) and kept in a humid, 5 % CO_2 atmosphere at 37 ºC. Cells were removed from confluent monolayers by trypsinisation with

1 % trypsin-EDTA in PBS. The trypan blue dye exclusion test was used to determine the cell viability.

3.4.4 Cytotoxicity Assay

Cells were seeded in 100 μl of complete medium in 96-well microtitre plates (Corning Costar®). 4,000 cells/well were seeded for A2780 and A2780cr and 25,000 cells/well were seeded for T47D. Before treating, the cells were allowed to adhere to the bottom of the wells by incubating the plates at 37 ºC for 24 hours. Due to the poor aqueous solubility of the complexes, the stock solutions of **A**, **B**, **C** and **D** (100 μM) were freshly prepared in solutions of 2 % DMSO and 98 % complete medium. Cis-platin was dissolved directly in complete medium. For each concentration (50 μM, 25 μM, 12.5 μM, 6.3 μM, 3.1 μM), 100 μl of compound was added to the 100 μl of medium and cells in each well. In the control groups only complete medium or complete medium with 2 % DMSO was added. Each experiment was performed in quadruplicate and independently repeated at least four times. The plates were incubated under standard cell culture conditions (5 % CO_2 atmosphere, 37 ºC) for 72 hours. Cell proliferation was evaluated by the addition of 50 μl MTT (3-(4,5-dimethylthiazol-2-yl)-2,5-diphenyl-2H-tetrazolium bromide) solution (5 mg/ml in PBS) to each well and incubating the plates at 37 ºC for a further 2 hours. The medium was subsequently removed from the wells and the purple formazan crystals dissolved in 100 μl DMSO. The absorbance was measured at 590 nm using a microplate reader (Bio-Rad). IC_{50} values were obtained by GraphPad Prism software, version 3.05, 2000.

3.4.5 Bacterial Mutagenicity Assay

The procedure used was based on the protocol of Maron and Ames.[31] All reagents and equipment were sterilised in advance and only one strain of bacteria was assayed on any one day to avoid cross contamination.

Controls: Chrysoidine Y (20 µg/plate) and sodium azide (3 µg/plate) were used as positive controls, DMSO was used as a reagent control and PBS was employed as the negative control.

Minimal agar (11.5 g Agar, 700 ml water, 15 ml Vogel-Bonner salts ($MgSO_4.7H_2O$, citric acid monohydrate, K_2HPO_4, $NaNH_4PO_4.4H_2O$), 38 ml 40 % glucose) plates were prepared a week in advance to allow the agar to dry thoroughly. 16 hours prior to the experiment, 10 ml of nutrient broth was inoculated with a loopful (10 µl) of the required bacterial strain. Light was excluded and the bacteria were incubated on a rotary shaker at 37 °C. On the day of the assay the master culture was kept on ice. The top agar (0.6 g agar bacteriological, 0.5 g NaCl in 100 ml H_20) was supplemented with 0.05 mM histodine and biotin (1 ml per 9 ml agar) and poured into top-agar tubes in a heating block set to 42 °C. The rat liver S9-mixture was freshly prepared and kept on ice until needed. The stock solutions and the dilutions of the test compounds were also freshly prepared in 100 % dmso. Compounds and controls were incubated with bacteria (both with and without S9) for 20 mins at 37 ºC. The mixtures were subsequently poured onto the minimal agar plates with the molten top agar and incubated in the dark in an oven set to 37 °C. After 24 hours the background bacterial lawn was checked under a microscope. After

a further 24 hours the plates were placed on a light-box and the bacterial colonies were counted. Each experiment was performed in triplicate.

3.4.6 Comet Assay

This method is based on that of Singh *et al*.[34] 1.25 X 10^6 A2780 carcinoma cells were seeded per well in 6 well plates. The plates were incubated at 37 °C, under standard cell culture conditions (37 ºC, 5 % CO_2) for 24 hours prior to cell treatment. The stock solutions of the complexes were freshly prepared in 2 % DMSO and 98 % complete medium and directly used for dilutions. Cells were treated with 3 different concentrations of compound and a 2 % DMSO control. Cis-platin was directly dissolved in complete medium and further diluted. The compounds were tested up to a top concentration just above the calculated IC_{50}. Following treatment the cells were incubated for 24 hours at 37 ºC. Subsequently, cells were washed with cold PBS and gently scraped into fresh PBS (1 ml). The cell suspension was centrifuged (8000 x g, 5 min) and the resulting pellets re-suspended in fresh PBS (100 µl). 5 µl of the re-suspended cells were added to a sterile eppendorf containing 300 µl low melting point agarose pre-warmed to 37 °C. The suspension was mixed and transferred onto a glass microscope slide (150 µl per slide, VWR International) which had been pre-coated with 0.5 % normal melting point agarose. The cell suspension was spread over the slide and covered using a glass coverslip (VWR International). The slides were put on a metal tray over ice to allow the agarose to solidify. After 10 minutes, the coverslips were removed and the samples incubated at 4 ºC in cold lysis buffer (2.5 M NaCl, 0.1 M Na_2EDTA, 10 mM Tris base, 1 % sodium N-lauryl sarcosinate, 10 % DMSO and 1 % Triton X-100) for 1 hour.

Following lysis, the slides were positioned in a horizontal electrophoresis tank containing electrophoresis buffer (300 mM NaOH and 1 mM Na_2EDTA) which had been prepared 16 hours earlier and kept at 4 ºC. The slides were left in the dark for 20 minutes to allow the unwinding of DNA before electrophoresis. Electrophoresis was performed in the same buffer (25 V, 0.8 Vcm^{-1}) for 20 minutes. Slides were washed three times (5 minutes) with cold neutralising buffer (0.4 M Tris, adjusted to pH 7.5), stained with 50 µl Sybr gold solution (Invitrogen, 1X solution) and covered with coverslips. The samples were left in the dark at 4 °C prior to examination.

The slides were analysed at 320X magnification using a fluorescence microscope (Zeiss Axiovert 10, Germany), fitted with a 515 - 560 nm excitation filter and a barrier filter of 590 nm. A USB digital camera (Merlin, Allied Vision Technologies) received the images, which were analysed using a personal computer-based image analysis system, Comet assay IV (Perceptive instruments). For each slide, one hundred randomly selected comets were examined and each experiment was performed in triplicate.

Measurement of median percent tail DNA was chosen to assess the extent of DNA damage as this has been shown to experience much less inter-run variation than other comet parameters due to being independent of electrophoresis run time and voltage.

3.5 References

1. J. M. Lehn, *Supramolecular Chemistry: Concepts and Perspectives*., VCH, Weinheim, **1995**.
2. U. Koert, M. M. Harding, J. M. Lehn, *Nature,* **1990**, 346, 339-342; C. R. K. Glasson, L. F. Lindoy, G. V. Meehan, *Coord. Chem. Rev.,* **2008***,* 252, 940–963.
3. M. Fujita, J. Yazaki, K. Ogura, *J. Am. Chem. Soc.,* **1990,** 112, 14, 5645-5647; M. J. Hannon, C. L. Painting, W. Errington, *Chem. Commun.,* **1997**, 307-308.
4. J. Michl, T.F. Magnera, *Proc. Nactl. Acad. Sci*., **2002**, 99, 8, 4788-4792; L. Zhao, Z. Xu, L. K. Thompson, S. L. Heath, D. O. Miller, M. Ohba, *Angew. Chem. Int. Ed*., **2000**, 39, 3114-3117.
5. B. Olenyuk, J. A. Whiteford, A. Fechtenkotter, P. J. Stang, *Nature*, **1999,** 398, 796-799; D. Moon, S. Kang, J. Park, K. Lee, R. P. John, H. Won, G. H. Seong, Y. S. Kim, G. H. Kim, H. Rhee, M. S. Lah, *J. Am. Chem. Soc.,* **2006,** 128, 3530-3531; C. L. Chen, J. Y. Zhang, C. Y. Su, *Eur. J. Inorg. Chem*., **2007**, 2997-3010.
6. A. V. Davis, K. N. Raymond, *J. Am. Chem. Soc.,* **2005,** 127, 7912-7919; T. Kusukawa, M. Fujita, *J. Am. Chem. Soc.,* **2002,** 124, 13576-13582; K. Umemoto, H. Tsuksi, T. Kusukawa, K. Biradha, M. Fujita, *Angew. Chem. Int. Ed.,* **2001**, 40, 2620-2622.
7. J. M. C. A. Kerckhoffs, F. W. B. van Leeuwen, A. L. Spek, H. Kooijman, M. Crego-Calama, D. N. Reinhoudt, *Angew. Chem. Int. Ed.,* **2003**, 42, 5717-5722.
8. M. Yoshizawa, Y. Takeyama, T. Okano, M. Fujita, *J. Am. Chem. Soc.,* **2003,** 125, 3243-3247.
9. A. M. Guilliatt, *PCR Mutation Detection Protocols: Agarose and Polyacrylamide Gel Electrophoresis,* **2002,** Humana Press.
10. http://www.bx.psu.edu/~ross/workmg/Struc_Nucleic_Acids
11. W. R. Bauer, *Annu. Rev. Biophys. Bioeng.,* **1978**, 7, 287-313.
12. S. F. Bellon, J. H. Colleman, S. J. Lippard, *Biochem.,* **1991**, 30, 8026-8035.
13. J. Malina, M. J. Hannon, V. Brabec, *Chem. Eur. J.*, **2008**, 14, 10408-10414.

14. P. E. West, *Introduction to Atomic Force Microscopy Theory Practice Applications*, **2007** (available free at www.afmuniversity.org/download.html).
15. M. Mounir, J. Lorenzo, M. Ferrer, M. J. Prieto, O. Rossell, F. X. Aviles, V. Moreno, *J. Inorg. Biochem.*, **2007**, 101, 660-666; G. Garcia-Friaza, A. Fernandez-Botello, J. M. Perez, M. J. Prieto, V. Moreno, *J. Inorg. Biochem.*, **2006,** 100, 1368-1377; M. A. Galindo, D. Olea, M. A. Romero, J. Gomez, P. del Castillo, M. J. Hannon, A. Rodger, F. Zamora, J. A. R. Navarro, *Chem. Eur. J.,* **2007,** 13, 5075 – 5081.
16. H.G. Hansma, D.E. Laney, *Biophys. J.,* **1996**, 70, 1933-1939.
17. I. Horcas, R. Fernandez, J. M. Gomez-Rodriguez, J. Colchero, J. Gomez-Herrero, A. M. Baro, *Rev. Sci. Instrum.,* **2007,** 78, 013705.
18. V. A. Bloomfield, *Biopolymers*, **1997,** 44, 269–282.
19. M. J. Hannon, V. Moreno, M. J. Prieto, E. Moldrheim, E. Sletten, I. Meistermann, C. J. Isaac, K. J. Sanders, A. Rodger, *Angew. Chem. Int. Ed.,* **2001**, 40, 5, 879-884.
20. H. R. Drew, R. E. Dickerson, *J. Mol. Biol.,* **1981**, 151, 535-556.
21. H. G. Hansma, R. Golan, W. Hsieh, C. P. Lollo, P. Mullen-Ley, D. Kwoh, *Nucl. Acids Res.,* **1998,** 26, 2481–2487.
22. T. Mosmann, *J. Immunol. Meth.,* **1983,** 65, 55-63.
23. B. A. Teicher, P. A. Andrews, *Anticancer Drug Development Guide: Preclinical Screening, Clinical Trials and Approval, second edition*, New Jersey: Humana Press, **2004**.
24. Unpublished data from A. J. Pope, University of Birmingham.
25. A. C. G. Hotze, N. J. Hodges, R. E. Hayden, C. Sanchez-Cano, C. Paines, N. Male, M. K. Tse, C. M. Bunce, J. K. Chipman, M. J. Hannon, *Chem. Biol.*, **2008**, 15, 1258-1267.
26. D. A. Williams, T. L. Lemke, W. O. Foye, *Foye's principles of medicinal chemistry, sixth edition*, **2007,** Lippincott Williams & Wilkins.
27. K. Mortelmans, E. Zeiger, *Mutat. Res.,* **2000,** 455, 29–60; B. N. Ames, F. D. Lee, W. E. Durston, *Proc. Natl. Acad. Sci. USA.*, **1973,** 70, 3, 782-786.
28. S. Venitt, J. M. Parry, *Mutagenicity testing a practical approach,* Oxford: IRL Press., **1984**.

29. A. Hakura, S. Suzuki, T. Satoh, *Mutat. Res.,* **1999,** 438, 29–36.
30. http://www.mun.ca/biology/scarr/Bio4241_Ames_Test_2.html
31. D. M. Maron, B. N. Ames, *Mutat. Res.,* **1983,** 113, 173–215.
32. Z. Yan, G. W. Caldwell, *Optimization in Drug Discovery (Methods in Pharmacology and Toxicology),* Humana Press, **2004**.
33. O. Ostling, K. J. Johannson, *Biochem. Biophys. Res. Commun.,* **1984**, 123, 291-298.
34. N. P. Singh, M. T. McCoy, R. R. Tice, E. L. Schneider, *Exp. Cell Res.,* **1988,** 175, 184-91.
35. R. M. Green, *PhD Thesis,* University of Birmingham, **2008**.
36. J. Wierecky, C. Kollmannsberger, I. Boehlke, M. Kuczyk, J. Schleicher, N. Schleucher, B. Metzner, L. Kanz, J. T. Hartmann, C. Bokemeyer, *J. Cancer. Res. Clin. Oncol.*, **2005**, 131, 255-260; M. C. Escudero, A. Lassaletta, J. Sevilla, S. Fernandez-Plaza, A. Pérez, M. A. Diaz, L. Madero, *J. Pediatr. Hematol. Oncol.*, **2004**, 26, 454-456.

Chapter 4

Dinuclear Palladium(II) and Platinum(II) Pyridylimine Complexes

4.1 Introduction

Cis-platin is a potent anticancer drug widely used in the chemotherapeutic treatment of testicular and ovarian cancers.[1] The structure of cis-platin is shown in Figure 4.1 and its mode of action has previously been discussed in chapter 1 section 1.7.3.2.

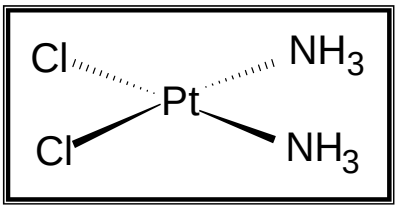

Figure 4.1. Structure of cis-platin.

Although cis-platin is an effective drug, its clinical utility is restricted by its toxic side effects which include kidney damage (nephrotoxicity), nervous system damage (neurotoxicity), nausea and vomiting.[2] Its usefulness is also limited by the development of acquired resistance and by the intrinsic resistance of cancerous tumors to the drug.[3] Therefore, much attention has been devoted to the development of new cis-platin type antitumor agents which portray fewer side effects, treat a broader spectrum of cancers and remain active against cis-platin resistant cells. In this context, tetravalent platinum(IV) complexes,[4] sterically hindered platinum(II) complexes,[5] carboxy-ligand derivatives[6] and Schiff base ligand derivatives[7] have been studied.

In 2006, Moreno *et al*. developed eight mononuclear palladium(II) and platinum(II) complexes based on four pyridylimine ligands (Figure 4.2).[8]

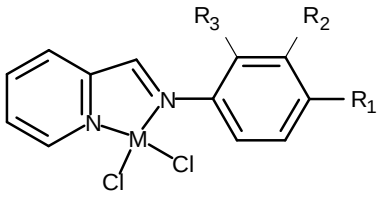

M= Pt(II) or Pd(II)

4-ime	R_1= CH_3; R_2=R_3=H
3-ime	R_2= CH_3; R_1=R_3=H
2-ime	R_3= CH_3; R_1=R_2=H
4-iol	R_1= OH; R_2=R_3=H

Figure 4.2. Moreno's palladium(II) and platinum(II) pyridylimine compounds.

Moreno reported the DNA-binding studies of these compounds and compared them to those of cis-platin. The cytotoxicity of the platinum(II) compounds was also investigated (Table 4.1).

	A2780	**A2780cr**
4-ime	9	52
3-ime	8	54
2-ime	9	50
4-iol	5	55
Cis-platin	2	38

Table 4.1. IC_{50} values (μM) of Moreno's platinum(II) pyridylimine compounds.

Although they are not as active as cis-platin, in the cell lines tested the pyridylimine based compounds still showed good activity. Unfortunately, the cytotoxic activity of the palladium(II) compounds was not reported.

4.1.1 Molecular Design

Hannon *et al*. have pioneered the use of pyridylimine ligands in the formation of a vast range of supramolecular architectures. A library of ligands has been synthesised by the simple, one-step reaction of an amine with an aldehyde. Due to the large number of inexpensive, commercially available starting materials, the ligands have proved to be versatile tools in the design of complex supramolecular structures.[9] Ligand **L^6** was first reported by Hannon in 1997 and has since been used in the synthesis of numerous dinuclear, metallo-supramolecular complexes (Figure. 4.3).[10]

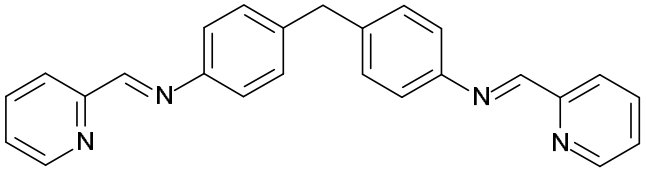

Figure. 4.3. Ligand **L^6**.

The ligand comprises of two pyridylimine binding units and is analogous to two of Moreno's 4-imine ligands bound together at the R_1 position (see Figure 4.2). The approach that was taken herein was to utilise **L^6** in the synthesis of dinuclear analogues of Moreno's palladium(II) and platinum(II) 4-imine compounds in hope of further enhancing their cytotoxic activities. The design approach is illustrated schematically in Figure. 4.4.

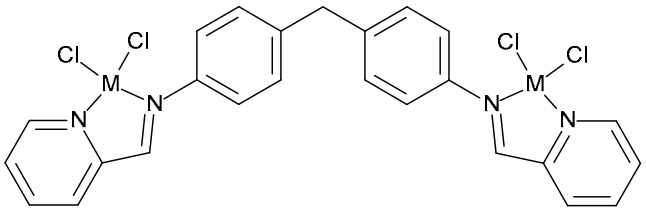

M= Pd(II) or Pt(II)

Figure 4.4. Design Approach.

In this chapter, the synthesis of palladium(II) and platinum(II) compounds of ligand **L^6** are reported and their DNA-binding potential investigated. The cytotoxicity of the novel compounds is also discussed. The techniques used in these investigations are circular and linear dichroism, gel electrophoresis and the MTT cytotoxicity assay.

4.1.2 Circular Dichroism Spectroscopy

Circular dichroism (CD) is a spectroscopic technique which measures the difference in absorption (A) of left and right-handed circularly polarised light. It is used to provide information about the chirality of optically active molecules and can be expressed by the equation:

$$\mathbf{CD = A_l - A_r}$$

Chiral refers to asymmetric objects which are non-superimposable on their mirror-images. A pair of chiral molecules are termed enantiomers. Enantiomers differ in their absorption of left and right circularly polarised light resulting in the occurrence of induced CD signals which are equal in magnitude but opposite in sign. Where a racemic (50:50) mixture is present, the CD signals of each enantiomer will cancel out the other and no signal will be seen on the spectrum. Therefore, CD is often used as an indication of enantiomeric purity or excess.

More recently, CD spectroscopy has been used to study the secondary structures of large biological molecules such as proteins and DNA. As discussed in chapter 1, DNA consists of a sugar-phosphate backbone and a combination of four aromatic bases. The phosphates and bases alone are achiral and do not produce a CD signal. However, on binding to the chiral sugars, all components of the DNA molecule inherit this chirality and a CD signal is produced. As discussed in chapter 1, DNA can portray several double helical conformations including A, B and Z-forms. Calf thymus (ct) DNA exhibits the typical characteristics of DNA with a B-conformation. A CD spectrum of ct-DNA is shown in Figure 4.5.

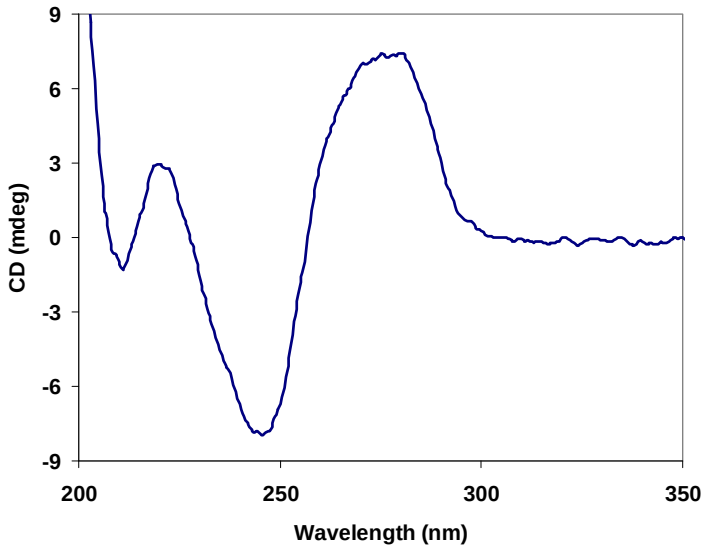

Figure 4.5. Circular dichroism spectrum of ct-DNA.

The CD signals below 190 nm are due to the sugar molecules of the DNA backbone. The negative band at ~245 nm is assignable to the right-handed helicity of the B-DNA and the positive band at ~275 nm arises from the stacking of the DNA bases. CD spectroscopy can be used for probing changes in DNA structure caused by the binding of DNA recognition agents.

4.1.3 Linear Dichroism Spectroscopy

Linear dichroism (LD) is a spectroscopic technique which measures the difference in absorption (A) of light linearly polarised parallel and perpendicular to the direction of an orientation axis:

$$\mathbf{LD = A}\parallel \mathbf{- A}\perp$$

To measure the LD of a sample the molecules within it must be oriented. Small molecules require the use of strong orienting methods such as stretched film LD. However, longer molecules are easier to align and can often be oriented by mere flow. DNA (minimum length ~250 base pairs) systems are commonly

studied by flow LD using a couette flow cell such as the one shown in Figure 4.6.

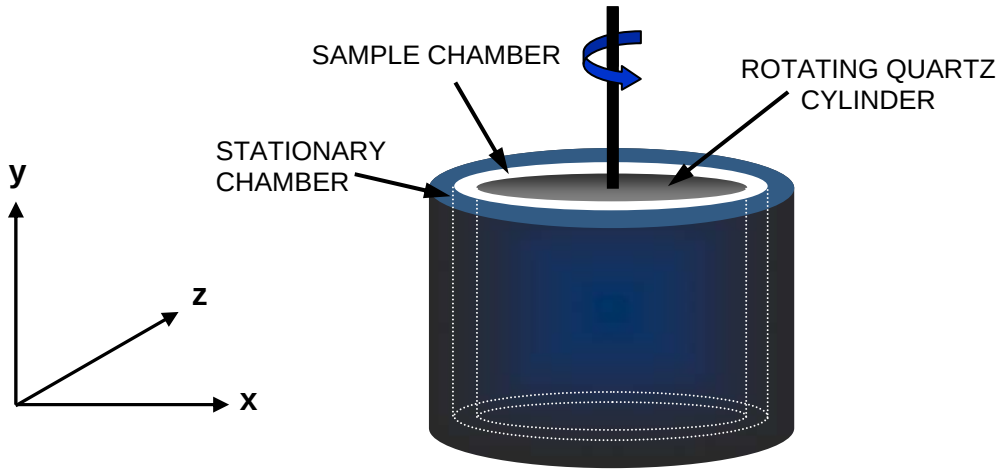

Figure 4.6. Schematic representation of a Couette cell.

A solution of the DNA is injected into the narrow channel between the rotating quartz cylinder and the stationary chamber. The viscous drag created in the channel results in the orientation of the DNA molecules in the same direction as the flow. An LD spectrum of ct-DNA is shown in Figure 4.7.

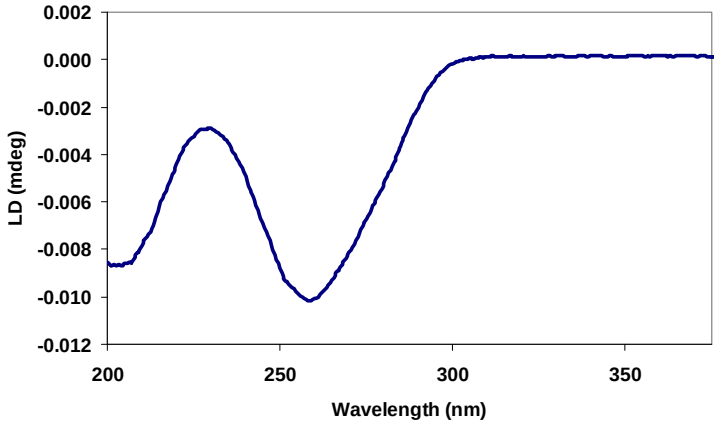

Figure 4.7. Linear dichroism spectrum of ct-DNA.

The LD signal at ~260 nm corresponds to the electron transitions between the DNA bases which lie approximately perpendicular to the orientation of the DNA double helix. Any coiling or kinking of the DNA caused by the binding of synthetic agents is observed by changes in the LD spectrum.

4.2 Results and Discussion

4.2.1 Ligand L^6

There is literature precedent for the use of this ligand in the successful synthesis of an array of metallo-supramolecular architectures.[9,10]

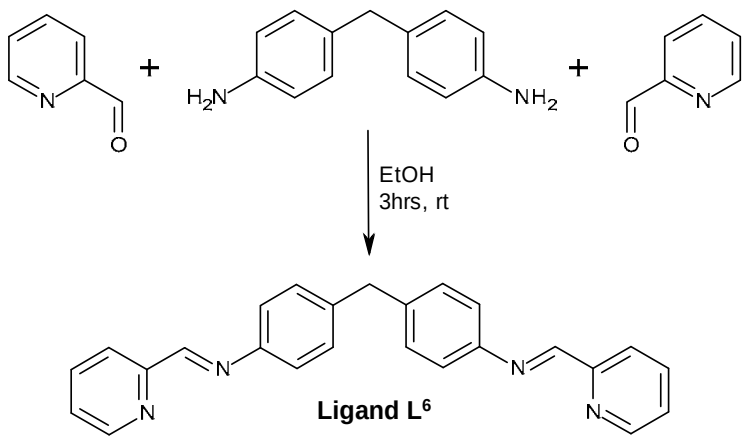

Scheme 4.1. Synthesis of Ligand **L^6**.

The ligand was synthesised in ethanol via a condensation reaction between two equivalents of 2-pyridine carboxaldehyde and one equivalent of 4,4'-methylenedianiline. The product precipitated as a white solid and was characterised by ^{1}H NMR, ^{13}C NMR, ESI mass spectrometry, FT-IR and elemental analysis (see experimental).

4.2.2 Synthesis of $Pd_2(L^6)Cl_4$

A DMSO solution of ligand **L^6** was heated at 90 °C with two equivalents of palladium(II) chloride for 30 minutes. On completion of the reaction a yellow solid was precipitated by the addition of a 1:1 chloroform:diethyl ether solution. The *crude* product was purified by washing with a range of organic solvents to give the pure compound in 83 % yield.

Partial microanalytical data are consistent with a formulation $\{Pd_2(C_{25}H_{20}N_4)Cl_4\}_n$ and the ESI mass spectrum shows peaks assignable to $\{Pd_2\mathbf{L^4}Cl_2\}^+$ and $\{Pd_2\mathbf{L^4}Cl\}^+$ indicating the formation of a single-stranded, dinuclear compound. The charge of these peaks suggests that on electrospray ionisation, the palladium(II) ion can become reduced to palladium(I). The solution behaviour of the complex was further investigated by ^{1}H NMR spectroscopy in *d*$_6$-DMSO (Figure 4.8).

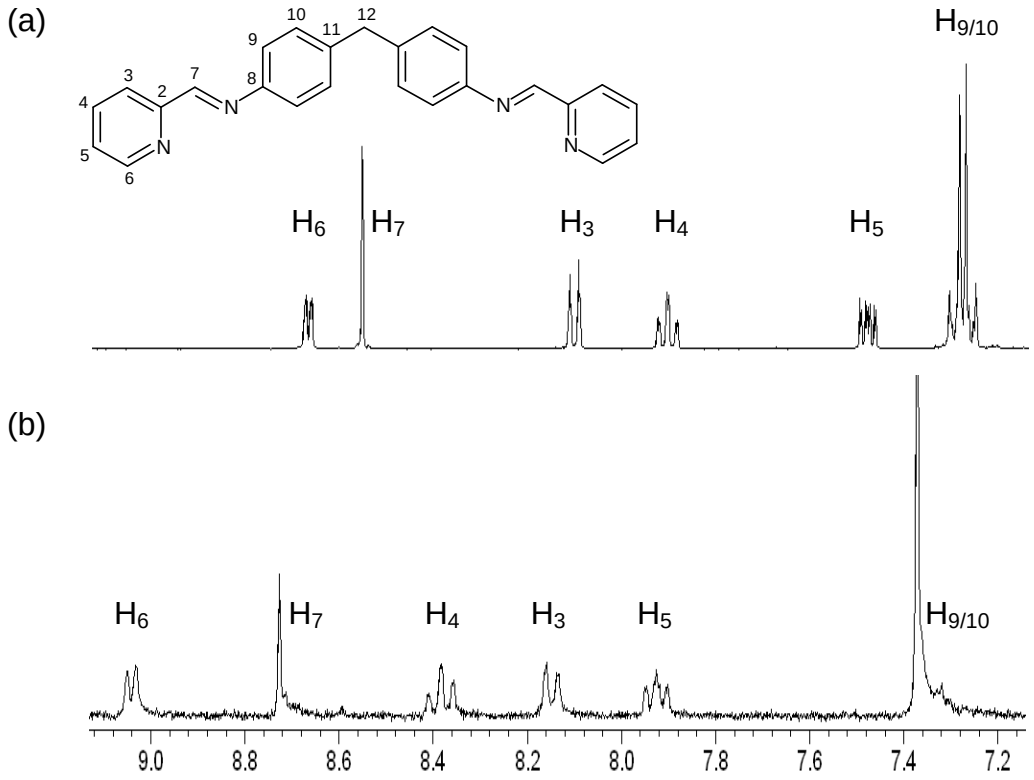

Figure 4.8. ^{1}H NMR spectra of the aromatic region of (a) Ligand **L^6** and (b) $Pd_2(\mathbf{L^6})Cl_4$ (300 MHz, *d*$_6$-DMSO, 298 K).

The ^{1}H NMR spectrum shows a single set of resonances. Unsurprisingly, the multiplicity and integration of the signals is the same as for the free ligand, however, the signals in the complex are significantly downfield shifted due to the effects of the metal-ligand coordination. Unfortunately, attempts to grow X-ray quality crystals of this complex have, so far, proved unsuccessful.

4.2.3 Synthesis of $Pt_2(L^6)Cl_4$

A methanolic solution of dichlorobis(dimethylsulphoxide)platinum(II)[11] was heated under reflux prior to the addition of ligand **L^6**. The solution was heated at 80 °C for a further hour after which it was cooled resulting in the precipitation of the desired product.

Elemental analysis data indicate that the complex has an empirical formula of $\{Pt_2C_{25}H_{20}N_4Cl_4\}_n$ and the ESI mass spectrum displays peaks corresponding to $[Pt_2\mathbf{L^6}Cl_2]^{2+}$ at *m/z* 419 and $[Pt_2\mathbf{L^6}Cl_4 + Na]^{+}$ at *m/z* 931. *D*$_6$-DMSO ^{1}H NMR spectra of the ligand **L^6** and $Pt_2\mathbf{L^6}Cl_4$ are shown in Figure 4.9. The spectrum of the complex displays a single set of signals which is consistent with the formation of a single solution species, symmetrically balanced through the central CH_2 constituent. Metal-ligand complexation is confirmed by the downfield shift of the proton signals relative to those in the uncoordinated ligand. The most predominant downfield shift is for H_6 and H_7, the protons which are adjacent to the coordinating nitrogen donors.

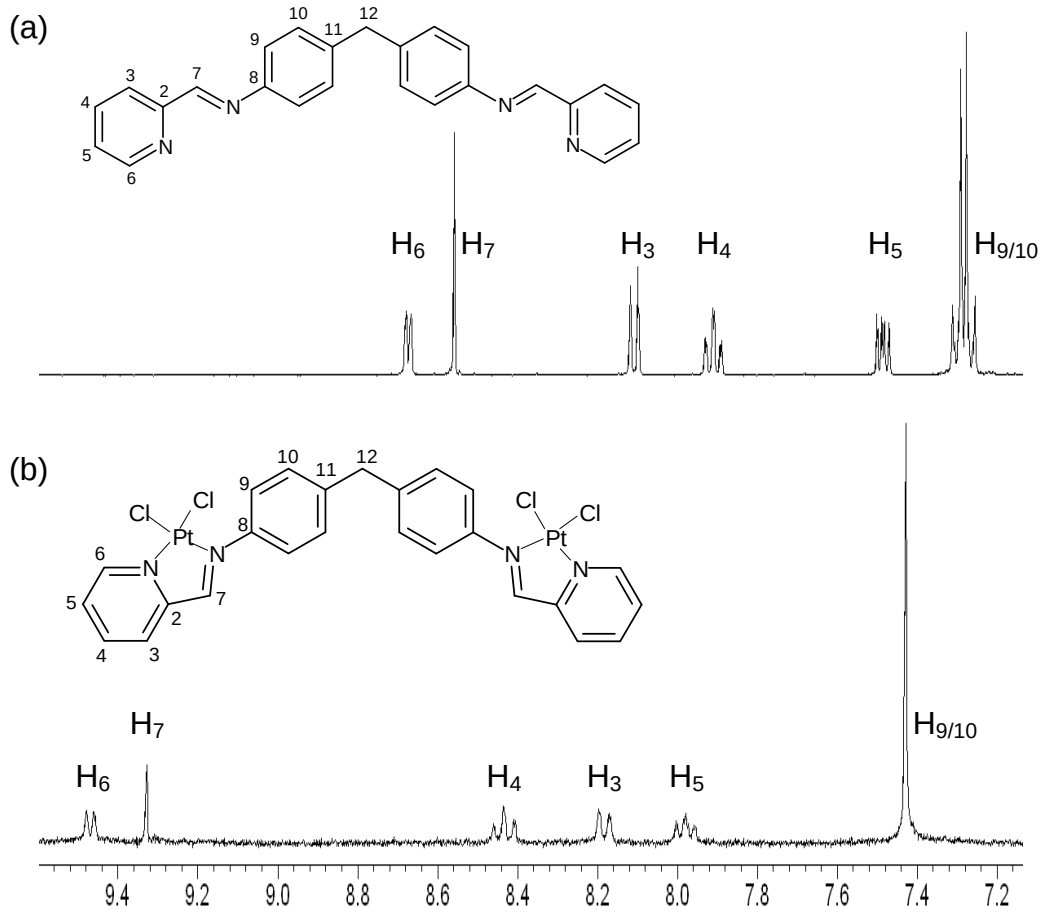

Figure 4.9. ^{1}H NMR spectra of the aromatic region of (a) Ligand **L^{6}** and (b) Pt_2(**L^{6}**)Cl_4 (300 MHz, d_6-DMSO, 298 K).

Despite making several attempts, we were unfortunately unable to obtain X-ray quality crystals of this complex.

4.3 Biological Studies

4.3.1 Circular Dichroism Spectroscopy

CD spectra of ct-DNA exhibit a positive signal at 275 nm due to the DNA base stacking and a negative signal at 240 nm which is characteristic of the right-handed B-conformation of the DNA double helix.

A CD titration experiment was carried out with ct-DNA as described in section 4.6.1. The concentration of the DNA (300 μM) was kept constant

throughout the experiment. The DNA was incubated with the compounds (DNA:compound ratios of 40:1, 20:1, 10:1 and 8:1) at 37 °C for 24 hours prior to measuring the CD spectra. The results of the titration are displayed in Figure 4.10.

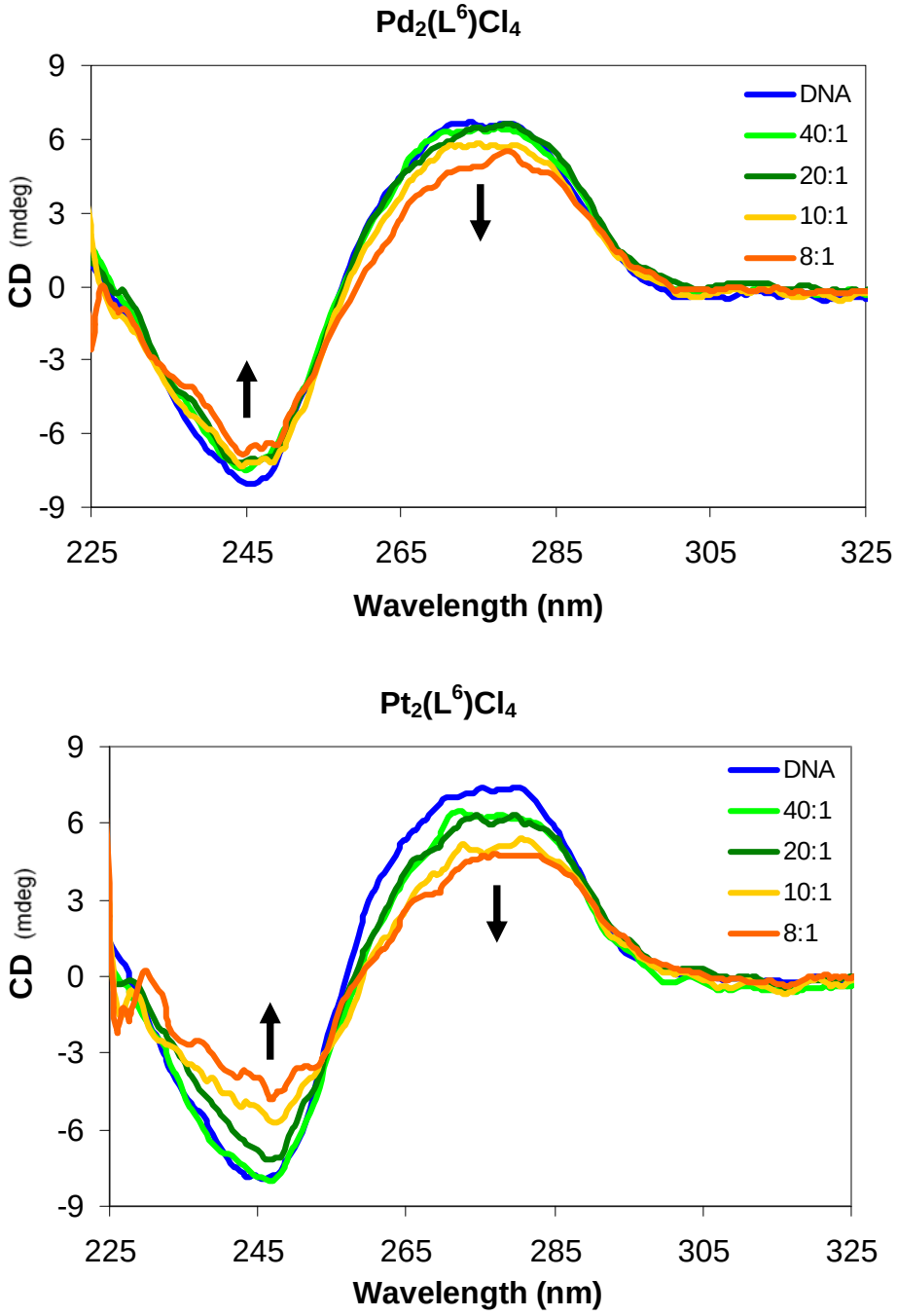

Figure 4.10. CD Spectra of ct-DNA in the presence of compounds $Pd_2(\mathbf{L^6})Cl_4$ and $Pt_2(\mathbf{L^6})Cl_4$.

The spectroscopy of the DNA appears altered by the addition of both $Pd_2(\mathbf{L^6})Cl_4$ and $Pt_2(\mathbf{L^6})Cl_4$. The basic shape of the B-DNA is retained. However, there is a decrease in the ellipticity of both the positive and negative bands. This is most dramatic for $Pt_2(\mathbf{L^6})Cl_4$ and indicates that the orientation and stacking of the base pairs has been perturbed as a result of the compounds binding to the DNA. This disturbance is most likely due to the binding of the compounds in the minor groove and/or the covalent binding of the compounds to the DNA bases.

4.3.2 Linear Dichroism Spectroscopy

A flow LD titration was conducted as described in section 4.6.1. The concentration of the ct-DNA was kept at 300 µM throughout the experiment. DNA:compound aliquots were made in ratios of 60:1 to 8:1 and were incubated at 37 °C for 24 hours prior to measuring the LD. The results of the experiments are shown in Figure 4.11.

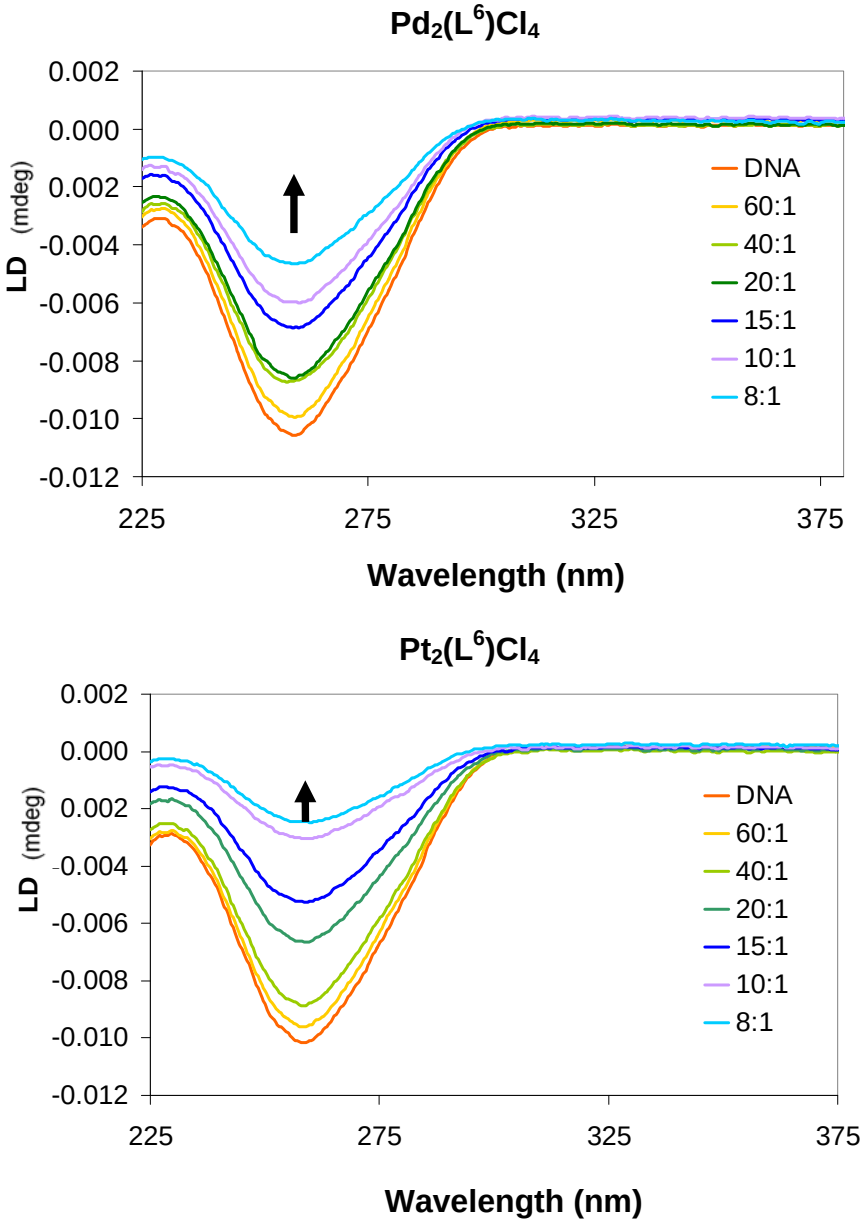

Figure 4.11. LD Spectra of ct-DNA in the presence of $Pd_2(\mathbf{L^6})Cl_4$ and $Pt_2(\mathbf{L^6})Cl_4$.

ct-DNA alone exhibits a negative signal at 260 nm. This band corresponds to the electron transitions between the DNA bases which lie approximately perpendicular to the orientation of the DNA double helix. The titration experiments reveal that on addition of increasing concentrations of $Pd_2(\mathbf{L^6})Cl_4$ and $Pt_2(\mathbf{L^6})Cl_4$, the magnitude of the negative band decreases. This indicates a loss of the DNA orientation which is consistent with compound-induced bending

or coiling of the DNA. The spectra of the compounds reveal that $Pt_2(\mathbf{L^6})Cl_4$ causes a greater decrease in the DNA signal than $Pd_2(\mathbf{L^6})Cl_4$, indicating that it has a higher coiling/bending effect on the DNA.

4.3.3 Agarose Gel Electrophoresis

Gel electrophoresis was used to probe whether the compounds alter the tertiary structure of DNA. A detailed description of this technique can be found in chapter 3. Due to the low solubility of the compounds, the stock solutions were made up in an aqueous solution of DMSO (5 %). The circular plasmid, pBR322, was mixed with different ratios of the compounds and $\mathbf{L^6}$ (Table 1) and incubated at 37 °C for 24 hours.

WELL	**1**	**2**	**3**	**4**	**5**	**6**
Base pairs: Compound	Control (5 % DMSO)	15/1	10/1	8/1	6/1	5/1
WELL	**7**	**8**	**9**	**10**	**11**	**12**
Base pairs: Compound	4/1	3/1	2/1	15/1 (ligand)	2/1 (ligand)	Control (no DMSO)

Table 1. Ratios of plasmid and compounds/ ligands used in gel electrophoresis studies

The wells were loaded with the samples and loading buffer and the gel was run at 180 V for 3 hours. Following electrophoresis, the gel was stained with ethidium bromide and visualised using a UVIPro Platinum 2.0 system at 312 nm. The resulting gels are shown in Figure 4.12.

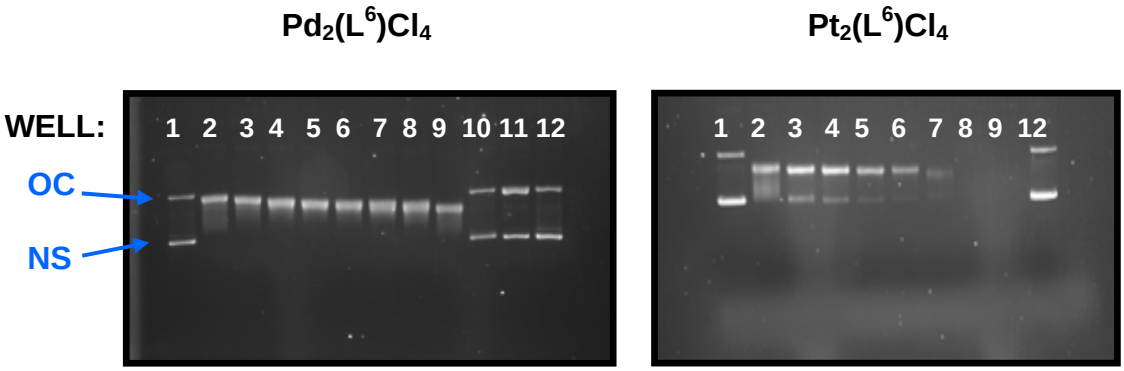

Figure 4.12. Agarose gel electrophoresis of pBR322 treated with ligand $\mathbf{L^6}$, $Pd_2\mathbf{L^6}Cl_4$ and $Pt_2\mathbf{L^6}Cl_4$.

It is evident that the ligands alone (wells 10 & 11) have no effect on the tertiary structure of the plasmid. However, on incubation with the compounds, the mobility of both the open circular (OC) and negatively supercoiled (NS) forms of the plasmid have significantly changed. On increasing the concentration, both compounds display an increase in the migration rate of the OC form and a decrease in that of the NS form. This suggests that on binding to the DNA, the compounds cause it to kink and bend leading to the positive supercoiling of the DNA double helix. This phenomenon would result in the uncoiling of the NS DNA and the positive supercoiling of the OC form. In the case of the platinum compound, at the highest concentrations (wells 8 and 9) the DNA band disappears altogether. This implies that compound binding may prohibit the intercalation of the ethidium bromide dye.

4.3.4 Cytotoxicity Testing

The anti-cancer properties of the compounds were tested via the MTT cell viability assay. The effect of the compounds were examined on the human breast cancer cell line T47D and the ovarian cancer cell lines A2780 and its cis-

platin resistant subline A2780cr. The IC_{50} values of the compounds are listed in Table 2 and are compared to those of cis-platin.

	A2780	**A2780cr**	**T47D**
$Pd_2(L^6)Cl_4$	54.0 ± 1.0	>100	75.2 ± 1.3
$Pt_2(L^6)Cl_4$	39 ± 1.9	>100	58.3 ± 1.1
Cis-platin	4.5 ± 0.8	16.0 ± 1.8	28.3 ± 1.7

Table 2. IC_{50} values (μM) of cis-platin and $Pd_2(\mathbf{L^6})Cl_4$ and $Pt_2(\mathbf{L^6})Cl_4$ in ovarian and breast cancer cell lines

In the A2780 and T47D cell lines, $Pt_2(\mathbf{L^6})Cl_4$ is the more active of the dinuclear compounds. However, in the A2780cr cell line, both compounds appear to be inactive. In all three cell lines, $Pd_2(\mathbf{L^6})Cl_4$ and $Pt_2(\mathbf{L^6})Cl_4$ are unfortunately less active than cis-platin. The activity of $Pt_2(\mathbf{L^6})Cl_4$ is also less than Moreno's Pt(4-imine)Cl_2 compound. This lower activity may be due to the compounds entering the cells via different mechanisms or because they have different modes of action.

4.4 Conclusions

Two novel dinuclear, cis-platin type compounds have been synthesised and characterised. The results of this study reveal that both $Pd_2(\mathbf{L^6})Cl_4$ and $Pt_2(\mathbf{L^6})Cl_4$ bind to ct-DNA, disturbing the orientation and stacking of the nucleotide base pairs. However, the B-conformation of the DNA is retained. Gel electrophoresis studies suggest that the compounds cause the DNA plasmid, pBR322, to kink and bend. At high concentrations, $Pt_2(\mathbf{L^6})Cl_4$ may also be intercalating between the DNA base pairs. The MTT assay showed that the compounds are active in the A2780 and T47D cell lines, although they were inactive in the cis-platin resistant cell line A2780cr. Unfortunately, the compounds proved less active than cis-platin in all three cell lines.

4.5 Experimental

4.5.1 General

All solvents and reagents were purchased from Aldrich, Fisher and Fluorochem and were used without further purification. ^{1}H NMR spectra were recorded on AC300, AV300 and AV400 Brüker spectrometers and processed using standard Brüker software. Infrared spectra were recorded from KBr pellets on a Perkin Elmer Paragon 1000 FTIR spectrometer. Electrospray Ionisation (ESI) spectra were recorded on a Micromass LCT Time of flight mass spectrometer in positive ionization mode**.** Microanalyses data were obtained using a CE Instruments EA1110 elemental analyser.

4.5.2 Synthesis of Ligand (L^{6})^{10}

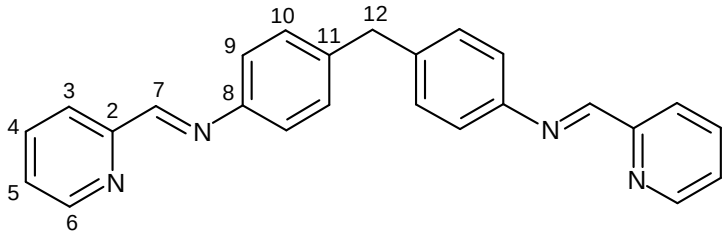

$C_{25}H_{20}N_4$
FW: 376.45

2-Pyridine carboxaldehyde (1.4 ml, 15.1 mmol) and 4,4'-methylenedianiline (1.50 g, 7.6 mmol) were stirred together in ethanol (28 ml) for 3 hours. The precipitate was isolated by vacuum filtration and washed with cold ethanol. The *crude* material was recrystallised from hot ethanol, filtered and dried *in vacuo* over P_4O_{10} to give the cream product (2.44 g, 86 % yield).

^{1}H NMR (300 MHz, $CDCl_3$, 298 K): δ 8.73 (2H, d, *J*= 4.5 Hz, H_6), 8.65 (2H, s, H_7), 8.23 (2H, d, *J*= 7.6 Hz, H_3), 7.83 (2H, td *J*= 7.6, 1.6 Hz, H_4), 7.39 (2H, ddd, *J*= 7.6, 4.5, 1.6 Hz, H_5), 7.29 (8H, m, $H_{9\ \&10}$), 4.07 (2H, s, H_{12}).

^{13}C NMR (400 MHz, $CDCl_3$, 300 K): δ 162.0 C_7, 156.6 $C_{2/8/11}$, 151.6 C_6, 151.0 $C_{2/8/11}$, 141.7 $C_{2/8/11}$, 138.6 C_4, 131.7 $C_{9/10}$, 127.0 C_5, 123.8 C_3, 123.3 $C_{9/10}$.

Mass Spectrum (E.S.I): *m/z* 377.0 $\{L + H\}^+$.

Elemental analysis (%) calculated for $C_{25}H_{20}N_4$: C: 79.8; H: 5.4; N: 14.9; Found: C: 79.9; H: 5.4; N: 14.8.

IR (KBr): ν= 3062(w), 2927(w), 1625(m), 1582(s), 1566(w), 1503(s), 1466(s), 1434(s), 828(s), 818(w), 784(s), 742(m) cm^{-1}.

4.5.3 Synthesis of $Pd_2(L^6)Cl_4$

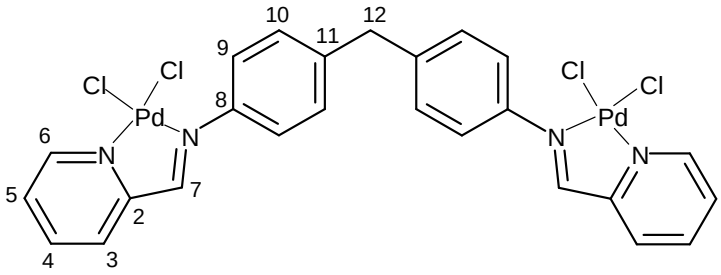

$Pd_2C_{25}H_{20}N_4Cl_4$
FW: 731.10

Ligand **L^6** (0.015 g, 0.04 mmol) and palladium(II) chloride (0.014 g, 0.08 mmol) were dissolved in DMSO (3 ml) and heated at 90 °C for 30 minutes. The solution was filtered and a yellow solid precipitated on the addition of a 1:1 solution of chloroform:diethyl ether. The *crude* product was washed with chloroform, methanol and diethyl ether and dried *in vacuo* over P_4O_{10} to afford the pure yellow compound (24 mg, 83 % yield).

^{1}H NMR (300 MHz, $(CD_3)_2SO$, 298 K): δ 9.05 (2H, d, *J*= 5.7 Hz, H_6), 8.73 (2H, s, H_7), 8.39 (2H, td, *J*= 8.0, 1.2 Hz, H_4), 8.15 (2H, d, *J*= 8.0 Hz, H_3), 7.95-7.90 (2H, m, H_5), 7.37-7.31 (8H, m, $H_{9\ \&\ 10}$), 4.04 (2H, s, H_{12}).

Mass Spectrum (E.S.I): *m/z* 660.0 $\{Pd_2LCl_2\}^+$, 625.0 $\{Pd_2LCl\}^+$.

Elemental analysis (%) calculated for $Pd_2C_{25}H_{20}N_4Cl_4$: C: 41.1; H: 2.8; N: 7.7; Found: C: 41.4; H: 2.8; N: 7.2.

IR (KBr): ν= 2921(w), 1637(m), 1618(s), 1598(m), 1501(s), 1474(w), 1445(w), 1416(w), 866(w), 821(w), 789(m), 775(s) cm^{-1}.

UV/Vis (DMSO): λmax (nm) = 257, 335.

4.5.4 Synthesis of $Pt_2(L^6)Cl_4$

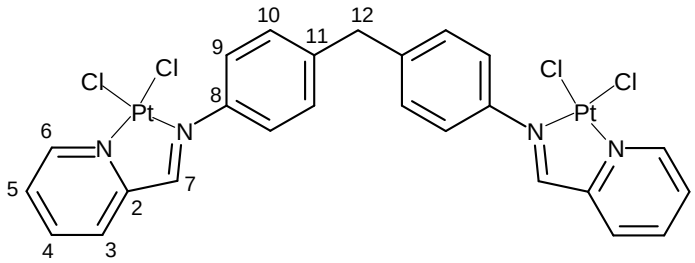

$Pt_2C_{25}H_{20}N_4Cl_4$
FW: 908.42

Dichloro(dimethylsulphoxide)platinum(II)[11] (0.034 g, 0.08 mmol) was dissolved in methanol (3 ml) and stirred under reflux for 1 hour. A methanolic solution (5 ml) of ligand **L^6** (0.015 g, 0.04 mmol) was added and the solution stirred at 80 ^oC for another hour. On cooling, an orange solid precipitated from the solution. The *crude* product was collected by vacuum filtration, washed with methanol, chloroform and diethyl ether and dried over P_4O_{10} (32 mg, 87 % yield).

^{1}H NMR (300 MHz, $(CD_3)_2SO$, 298 K): δ 9.46 (2H, d, *J*= 5.9 Hz, H_6), 9.33 (2H, s, H_7), 8.43 (2H, td, *J*= 7.7, 1.1 Hz, H_4), 8.18 (2H, d, *J*= 7.7 Hz, H_3), 8.01-7.94 (2H, m, H_5), 7.45-7.41 (8H, m, $H_{9\ \&\ 10}$), 4.10 (2H, s, H_{12}).

Mass Spectrum (E.S.I): *m/z* 931.0 $\{Pt_2LCl_4 + Na\}^+$, 418.7 $\{Pt_2LCl_2\}^{2+}$.

Elemental analysis (%) calculated for $Pt_2C_{25}H_{20}N_4Cl_4$: C: 33.1; H: 2.2; N: 6.2; Found: C: 32.9; H: 1.9; N: 5.9.

IR (solid): ν= 3429(br), 2919(w), 2850(w), 2360(w), 2343(w), 1625(s), 1582(s), 1566(m), 1503(s), 1467(s), 1434(s), 1384(m), 1348(m) cm^{-1}.

UV/Vis (DMSO): λmax (nm) = 258, 284, 330.

4.6 Experimental for Biological Testing

4.6.1 Circular Dichroism and Linear Dichroism

Ultra-pure (18.2 MΩ cm^{-1}) water was used in all CD and LD experiments. Highly polarised, ct-DNA (Sigma-Aldrich) was dissolved in ultra-pure water and the stock solutions kept frozen until the day of the experiment. The absorbance of the DNA was measured at 260 nm using UV-Vis spectroscopy and its concentration determined using the Beer-Lambert law (molar-extinction coefficient of 6600 $mol^{-1}\,dm^3\,cm^{-1}$ per DNA base).

Stock solutions of the compounds (300 μM) were made in 5 % DMSO/water and 1000 μl aliquots of ct-DNA (100 μM) were made using ultra-pure water, sodium chloride (20 mM) and sodium cacodylate buffer (0.89 mM, pH 6.8). Aliquots of the DNA and compound were mixed together in different ratios (DNA:compound of 60:1 to 8:1) and incubated at 37 ºC for 24 hours. Circular dichroism spectra were recorded on a Jasco J-810 spectropolarimeter using 1 cm pathlength cuvettes. Linear dichroism Flow spectra were collected in a Jasco J-715 spectropolarimeter adapted for LD measurements using a flow couette cell (Krometek) with a 1 mm pathlength. In between titrations the cuvette and couette cell were washed thoroughly with water and ethanol and dried well with a stream of nitrogen.

4.6.2 Gel Electrophoresis

Gel electrophoresis experiments were carried out using an Amersham Biosciences HE99X Max submarine kit. The agarose (Fisher) gel was prepared by heating 2 g of agarose (1 %) in 200 ml of TAE (1X) buffer (Sigma) until it dissolved. The gel then was allowed to cool in a gel tray (21-15 cm) containing

a 15-tooth comb which was used to form the wells. The plasmid pBR322 (New England Biolabs) was dissolved in ultra-pure water (1 μg/μl) and the compounds dissolved in 5 % DMSO/water solutions. Varying ratios of the plasmid and compound/ligand (base pairs:compound of 15:1 to 2:1) were mixed together (16 μl) and incubated at 37 ºC for 24 hours. 4 μl of loading buffer (30 % glycerol and 0.25 % bromophenol blue in ultra-pure water) was added to each mixture and 16 μl loaded onto the agarose gel. The gel was run in TAE (1X) electrophoresis buffer at 180 V and 125 mA for 3 hours. Gel staining was performed in the same buffer containing 1 ml of ethidium bromide solution (0.5 mg/ml). The gel was visualized using a UVIPro Platinum 2.0 system (UViDoc, Cambridge, UK) at 312 nm.

4.6.3 Cell Culture

Materials: The media were obtained from Invitrogen and the supplements were purchased from Sigma-Aldrich unless otherwise stated.

The A2780 (human ovarian carcinoma) and A2780cr (cis-platin-resistant) cell lines were cultured in Dulbecco's modified Eagle's medium (DMEM) and the T47D (human breast carcinoma) cell line was maintained in Roswell park memorial institute (RPMI-1640) medium. Both media were supplemented with 10 % FBS (Invitrogen), 1 % L-glutamine, 1 % hepes buffer, 1 % sodium pyruvate and an antibiotics-antimycotic solution (1X). All three cell lines were cultured in T_{25} flasks (Nunc) and kept in a humid, 5 % CO_2 atmosphere at 37 ºC. Cells were removed from confluent monolayers by trypsinisation with 1 % trypsin-EDTA in PBS. The trypan blue dye exclusion test was used to determine the cell viability.

4.6.3.1 Cytotoxcity Assay

Cells were seeded in 100 μl of complete medium in 96-well microtitre plates (Corning Costar®). 4,000 cells/well were seeded for A2780 and A2780cr and 25,000 cells/well were seeded for T47D. Before treating, the cells were allowed to adhere to the bottom of the wells by incubating the plates at 37 ºC for 24 hours. Due to the poor aqueous solubility of the compounds, the stock solutions of $Pd_2(\mathbf{L^6})Cl_4$ and $Pt_2(\mathbf{L^6})Cl_4$ were freshly prepared in solutions of 2 % DMSO and 98 % complete medium. Cis-platin was dissolved directly in complete medium. For each concentration, 100 μl of compound was added to the 100 μl of medium and cells in each well. In the control groups only complete medium or complete medium with 2 % DMSO was added. Each experiment was performed in quadruplicate and independently repeated at least three times. The plates were incubated under standard cell culture conditions for 72 hours. Cell proliferation was evaluated by the addition of 50 μl MTT (3-(4,5-dimethylthiazol-2-yl)-2,5-diphenyl-2H-tetrazolium bromide) solution (5 mg/ml in PBS) to each well and incubating the plates at 37 ºC for a further 2 hours. The medium was subsequently removed from the wells and the purple formazan crystals dissolved in 100 μl DMSO. The absorbance was measured at 590 nm using a microplate reader (Bio-Rad). IC_{50} values were obtained using GraphPad Prism software, version 3.05, 2000.

4.7 References

1. D. T. Sleijfer, S. Meijer, N. H. Mulder, *Pharm. Weekbl. Sci.,* **1985**, 7, 237-244.
2. B. J. S. Sanderson, L. R. Ferguson, W. A. Denny, *Mutat. Res.*, **1996**, 355, 59-70; T. Boulikas, A. Pantos, E. Bellis, P. Christofis, *Cancer Therapy,* **2007**, 5, 537-583.
3. C. A. Rabik, M. E. Dolan, *Cancer Treat Rev.,* **2007**, 33, 9-23; V. Brabec, J. Kasparkova, *Drug Resistance Updates,* **2005**, 8, 131–146; D. J. Stewart, *Crit. Rev. Oncol./Hematol*., **2007**, 63, 12–31.
4. G. N. Kaludjerović, D. Miljković, M. Momcilović, V. M. Djinović, M. Mostarica Stojković, T. J. Sabo, V. Trajković, *Int. J. Cancer,* **2005**, 116, 479–486; V. Horváth, O. Blanárová, L. Švihálková-Šindlerová, K. Souček, J. Hofmanová, P. Sova, A. Kroutil, P. Fedoročko, A. Kozubík, *Gynecol. Oncol.,* **2006**, 102, 32–40.
5. K. T. Flaherty, J. P. Stevenson, M. Redlinger, K. M. Algazy, B. Giantonio, P. J. O'Dwyer, *Cancer Chemother. Pharmacol.*, **2004**, 53, 404-408.
6. R. Canetta, M. Rozencweig, S. K. Carter, *Cancer Treat Rev.,* **1985,** 12, 125-36.
7. O. E. Offiong, E. Nfor, A. A. Ayi, S. Martelli, *Transition Met Chem.*, **2000**, 25, 369-373; M. A. Ali, A. H. Mirza, R. J. Butcher, M. T. H. Tarafder, T. B. Keat , A. M. Ali, *J. Inorg. Biochem,* **2002**, 92, 141-148.
8. G. García-Friaza, A. Fernández-Botello, J. M. Pérez, M. J. Prieto, V. Moreno, *J. Inorg. Biochem,* **2006**, 100, 1368-1377.
9. L. J. Childs, N. W. Alcock, M. J. Hannon, *Angew. Chem., Intl. Ed.*, **2001**, 40, 1079-1081; F. Tuna, J. Hamblin, G. Clarkson, W. Errington, N. W. Alcock, M. J. Hannon, *Chem., Eur. J.*, **2002**, 8, 4957-4964; F. Tuna, J. Hamblin, A. Jackson, G. Clarkson, N. W. Alcock, M. J. Hannon, *Dalton Trans.*, **2003**, 2141-2148; M. J. Hannon, L. J. Childs, *Supramol. Chem.*, **2004**, 16, 7-22; L. C. Childs, M. Pascu, A. J. Clarke, N. W. Alcock, M. J. Hannon, *Chem. Eur. J.*, **2004**, 10, 4291-4300; C. Uerpmann, J. Malina, M. Pascu, G. J. Clarkson, V. Moreno, A. Rodger, A. Grandas, M. J. Hannon, *Chem. Eur. J.*, **2005**, 11, 1750-1756; M. Pascu, G. J. Clarkson, B. M. Kariuki, M. J. Hannon,

Dalton Trans., **2006**, 22, 2635-2642; G. I. Pascu, A. C. G. Hotze, C. Sanchez Cano, B. M. Kariuki, M. J. Hannon, *Angew. Chem. Int. Ed.,* **2007**, 46, 4374-4378; A. C. G. Hotze, B. M. Kariuki, M. J. Hannon, *Angew. Chem., Int. Ed.*, **2006**, 45, 1. M. J. Hannon, L. Cardo, *Inorganica Chimica Acta.,* **2009**, 362, 784–792.

10. M. J. Hannon, C. L. Painting, A. Jackson, J. Hamblin, W. Errington, *Chem. Commun*., **1997**, 1807-1808.
11. J. H. Price, A. S. Williamson, R. F. Schramm, B. B. Wayland, *Inorg. Chem.*, **1972**, 11, 1280-1284.

Chapter 5

Silver(I) Supramolecular Polymers

5.1 Introduction

For almost half a decade, the principles of supramolecular chemistry have been employed in the design and synthesis of a multitude of complex molecular architectures. The approach exploits the self-assembly of small molecular subunits into larger arrays via non-covalent interactions such as hydrogen bonding, π-π stacking, van der Waals forces and metal-metal interactions.[1]

5.1.1 Research Aims

In chapter 2, the synthesis of a range of palladium(II) and platinum(II) supramolecular structures using bis-pyridyl ligands was described. The purpose of this chapter is to explore the coordination chemistry of silver(I) with three of these ligands- **L^1**, **L^2** and **L^5** (Figure 5.1).

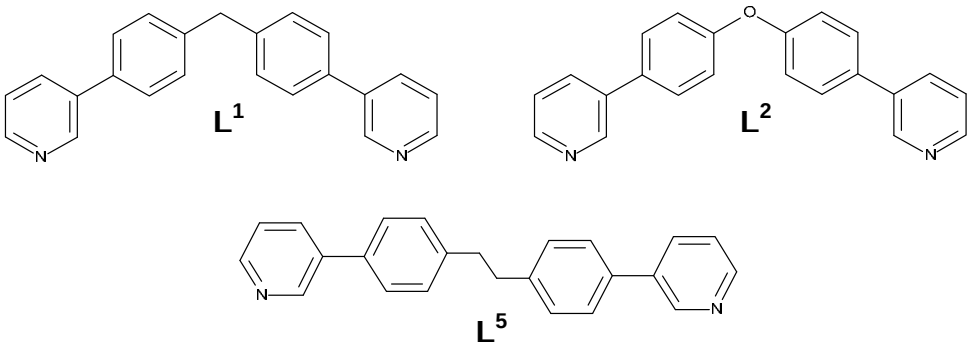

Figure 5.1. Bis-pyridyl ligands **L^1**, **L^2** and **L^5**.

Silver(I) is attractive as it can adopt various coordination numbers from two to six and is accompanied by a variety of coordination geometries such as linear, trigonal, tetrahedral and octahedral. However, this also makes it difficult to predict and control the structure of the resulting complexes. Therefore, the reaction of silver(I) with ligands **L^1**, **L^2** and **L^5** could result in the synthesis of discrete structures such as double, triple or quadruply-stranded helicates or

prismatic cages (discussed in chapter 1), or another possibility is the formation of metallo-supramolecular polymers.[2]

5.1.2 Metallo-Supramolecular Polymers

Metallo-supramolecular polymers (MSPs) are attracting a great deal of attention due to their potential to be used in a range of applications including electrical conductivity,[3] catalysis,[4] enantiomeric separation[5] and light-emitting devices[6]. They are formed by self assembly and consist of monomer units that are normally held together by reversible metal-ligand interactions (Scheme 5.1). This reversibility enables the polymers to lengthen, shorten and rearrange, making them potentially self-healing.[7]

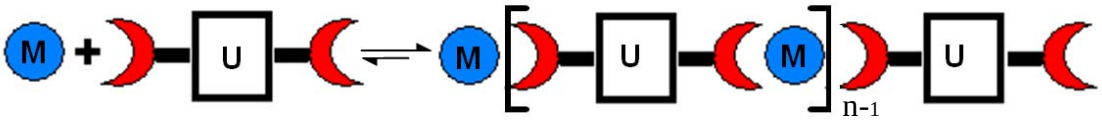

Scheme 5.1. Schematic representation of a metallo-supramolecular polymer. M represents a metal ion and U represents a monomer.

This chapter focuses on the reactions of silver(I) with ligands **L^{1}**, **L^{2}** and **L^{5}**, which might result in the formation of MSPs. To gain insight into the type of structures that could be formed, some examples of silver(I) supramolecular polymers generated from bis-pyridyl ligands are reviewed herein.

Zhao *et al.* have reported the synthesis of a heterocyclic ligand (**La'**) containing sulphur and nitrogen donor atoms (Figure 5.2).[8]

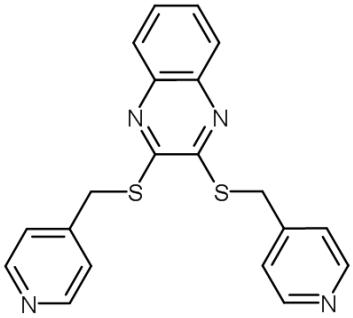

Figure 5.2. Zhao's Ligand **La'**.

On reaction of this ligand with silver(I), a cationic supramolecular polymer was formed. However, due to steric effects, the nitrogen atoms in the quinoxaline and the sulphur atoms do not coordinate to the metal ions. The pyridyl nitrogen atoms do coordinate and are forced to bind to two different silver(I) ions resulting in the formation of the polymer (Figure 5.3).

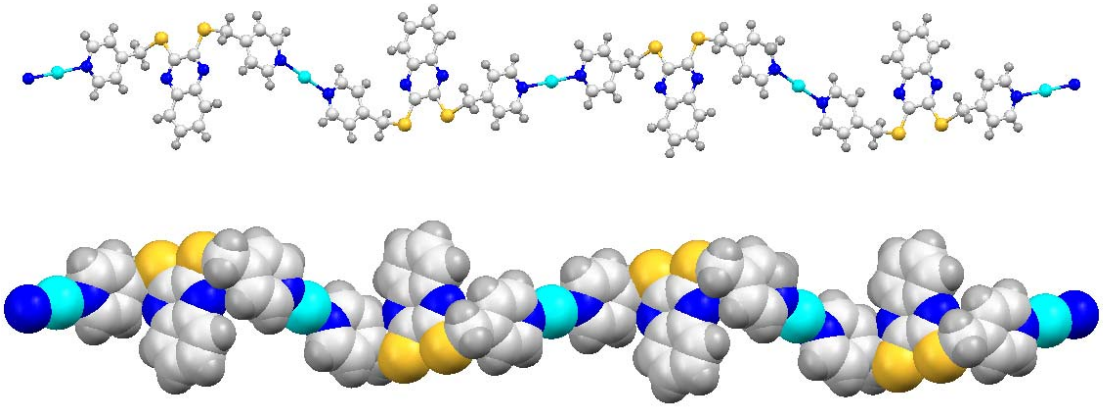

Figure 5.3. Zhao's silver(I) supramolecular polymer.

Kawano and co-workers have used ligand **Lb'** to generate a silver(I) supramolecular polymer. The rigid bis-pyridyl ligand adopts a trans orientation, resulting in the formation of a one dimensional chain with a helical conformation (Figure 5.4).[9]

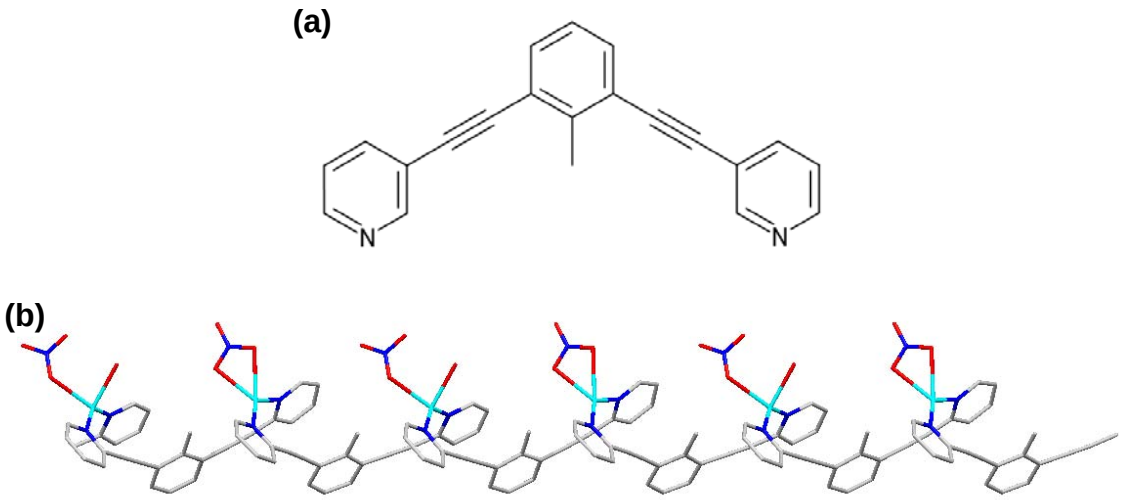

Figure 5.4. (a) Kawano's ligand **Lb'** and (b) Silver(I) supramolecular polymer.

The polymer consists of two types of silver(I) ions, one is bound to two pyridine nitrogen atoms and a nitrate anion and the other to two pyridine nitrogen atoms, a nitrate anion and a water molecule.

The bis-pyridyl ligand **Lc'**, reported by Hannon *et al*., is based on a 1,5-naphthalene spacer which sterically prevents the formation of dinuclear species with tetrahedral metal ions. On reaction of this ligand with silver(I) acetate a chiral isotactic polymer was formed (Figure 5.5).[10]

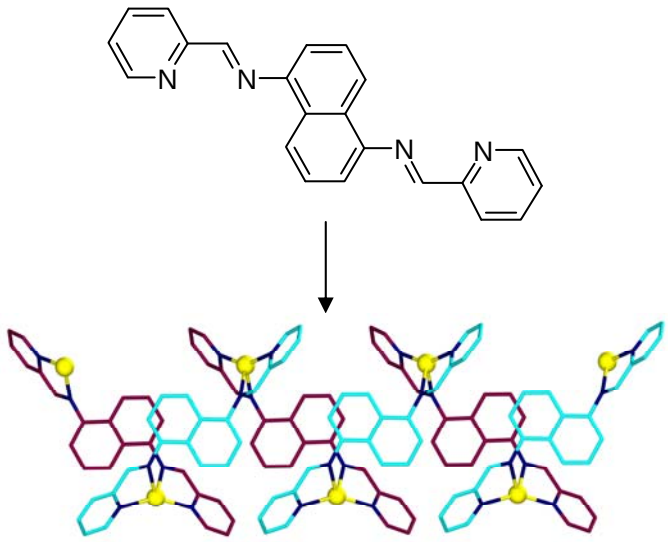

Figure 5.5. Hannon's silver(I) chiral isotactic polymer.

The counter-ion of this complex was exchanged for trifluoromethanesulfonate and on crystallisation, two types of crystals were observed. One of them corresponded to an isotactic polymer analogous to that shown in Figure 5.5 and the other corresponded to the achiral syndiotactic polymer shown in Figure 5.6. This shows that the counter-ion can play a vital role in determining the solid-state structure adopted.

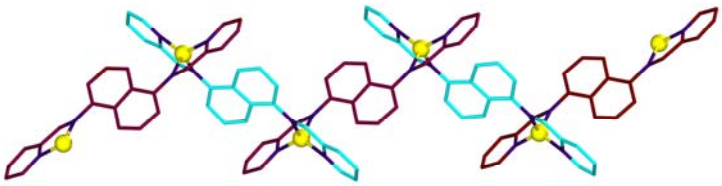

Figure 5.6. The X-ray crystal structure of
Hannon's silver(I) achiral syndiotactic polymer.

More recently, Paine and co-workers reported the synthesis and characterisation of three silver(I) polymers formed from ligands **Ld'**, **Le'** and **Lf'** (Figure 5.7).[11]

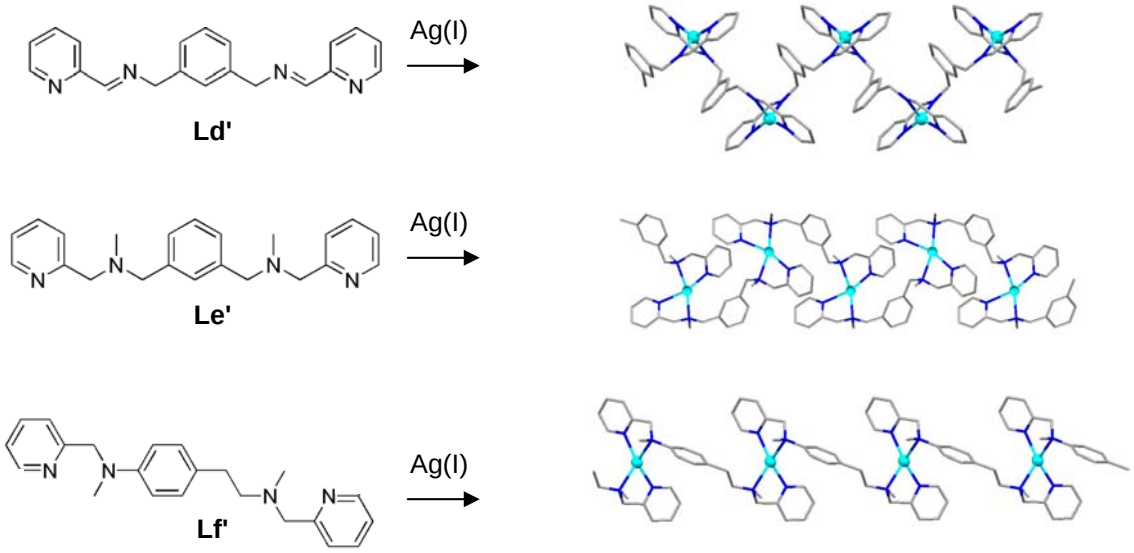

Figure 5.7. Paine's ligands and silver(I) supramolecular polymers.

The X-ray crystal structures showed that on reaction with silver(I), ligand **Ld'** had formed an achiral syndiotactic polymer analogous to Hannon's, whereas ligands **Le'** and **Lf'** had formed chiral isotactic polymers. These results demonstrate how changes in the structure of the ligand can have a big impact on the geometry of the final product.

5.2 Results and Discussion

5.2.1 Silver(I) complexes of L^1

Silver(I) was coordinated to ligand $\mathbf{L^1}$ by the reaction of silver(I) hexafluorophosphate with one equivalent of $\mathbf{L^2}$ for 3 hours. The reaction was conducted in the dark and resulted in the precipitation of the product in 73 % yield. The same product was also obtained from a 1:2 metal:ligand ratio reaction.

The FT-IR spectrum clearly shows an absorption band at 825 cm^{-1} which is characteristic of non-coordinated hexafluorophosphate vibrations. Elemental analysis data show that this complex has an empirical formula of $\{Ag(C_{23}H_{18}N_2)(PF_6)\}_n$. Unfortunately, despite trying several conditions, the ESI mass spectra from acetonitrile or nitromethane solutions were uninformative as the samples did not fly well. ^1H NMR spectra of the complex have been recorded in both deuterated acetonitrile and nitromethane solutions. At room temperature, a single set of resonances is observed in both solvents indicating the formation of a single solution species (Figure 5.8).

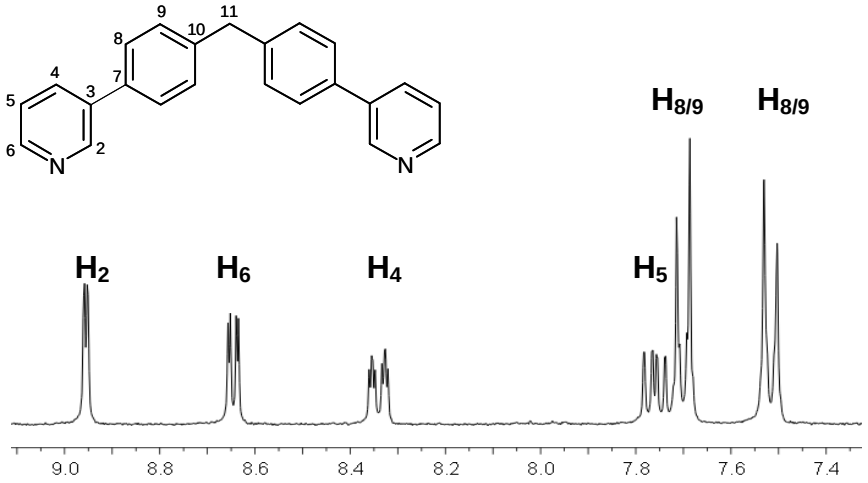

Figure 5.8. ^{1}H NMR spectrum of the aromatic region of $\{Ag(C_{23}H_{18}N_2)(PF_6)\}_n$ (300 MHz, d_3-nitromethane, 298 K).

The flexibility of the silver(I) coordination sphere leads to the formation of complexes with reversible Ag(I)-ligand interactions. This reversibility enables the resulting structures to lengthen, shorten and reorganize (potentially self-healing).[4] Low temperature NMR experiments were carried out to explore the possibility that the silver(I) complex of **L^1** contains more than one rapidly inter-converting species (Figure 5.9).

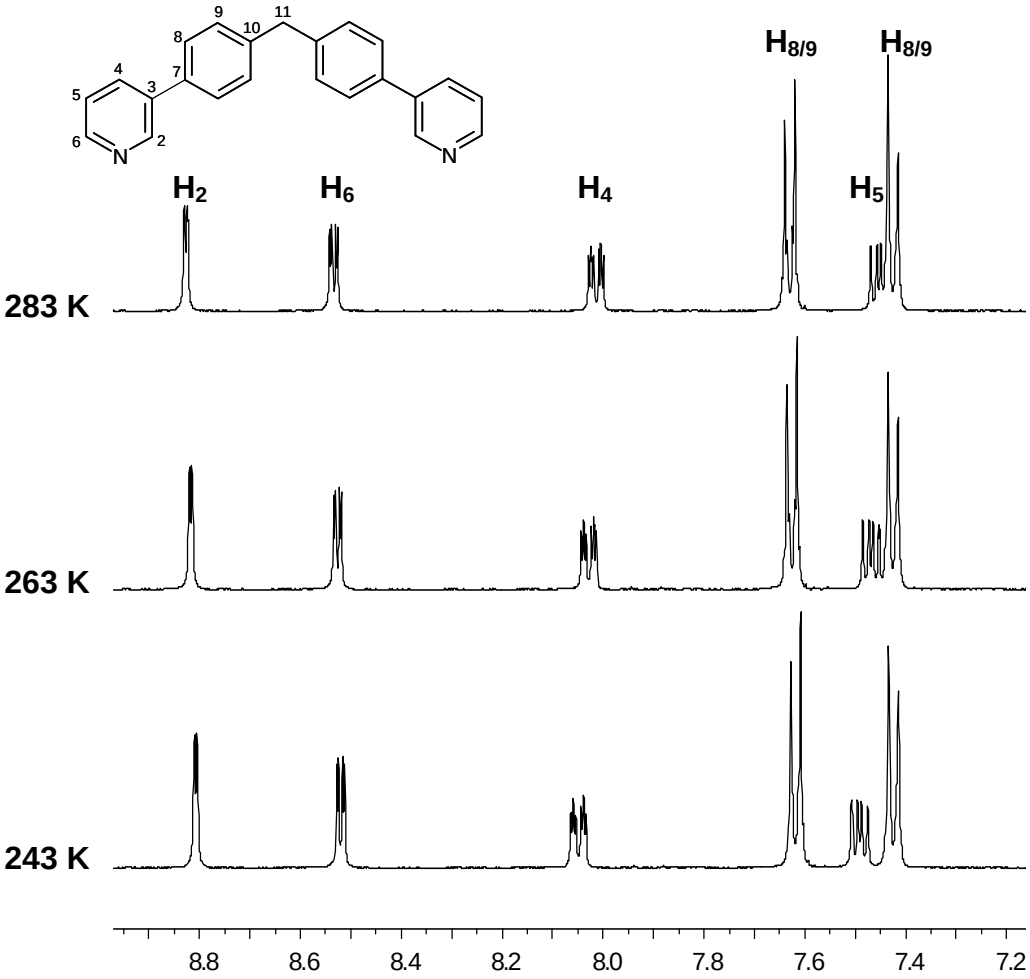

Figure 5.9. ^{1}H NMR spectra of the aromatic region of $\{Ag(C_{23}H_{18}N_2)(PF_6)\}_n$ at 243 K, 263 K and 283 K (400 MHz, d_3-acetonitrile).

The low temperature NMR spectra show a downfield shift of the **H_4** and **H_5** signals, however, this is probably because the rotation of the pyridine rings slows down on decreasing the temperature. Even at 243 K, the peaks remain sharp indicating that if more than one species is present, they are in rapid exchange on the NMR timescale.

Recrystallisation from acetonitrile by the slow diffusion of diethyl ether presented colourless crystals suitable for X-ray diffraction studies.[12] The crystal structure is shown in Figure 5.10. In contrast to what was seen in solution, the solid state structure reveals **two** distinct, cationic coordination polymers, P1 and P2.

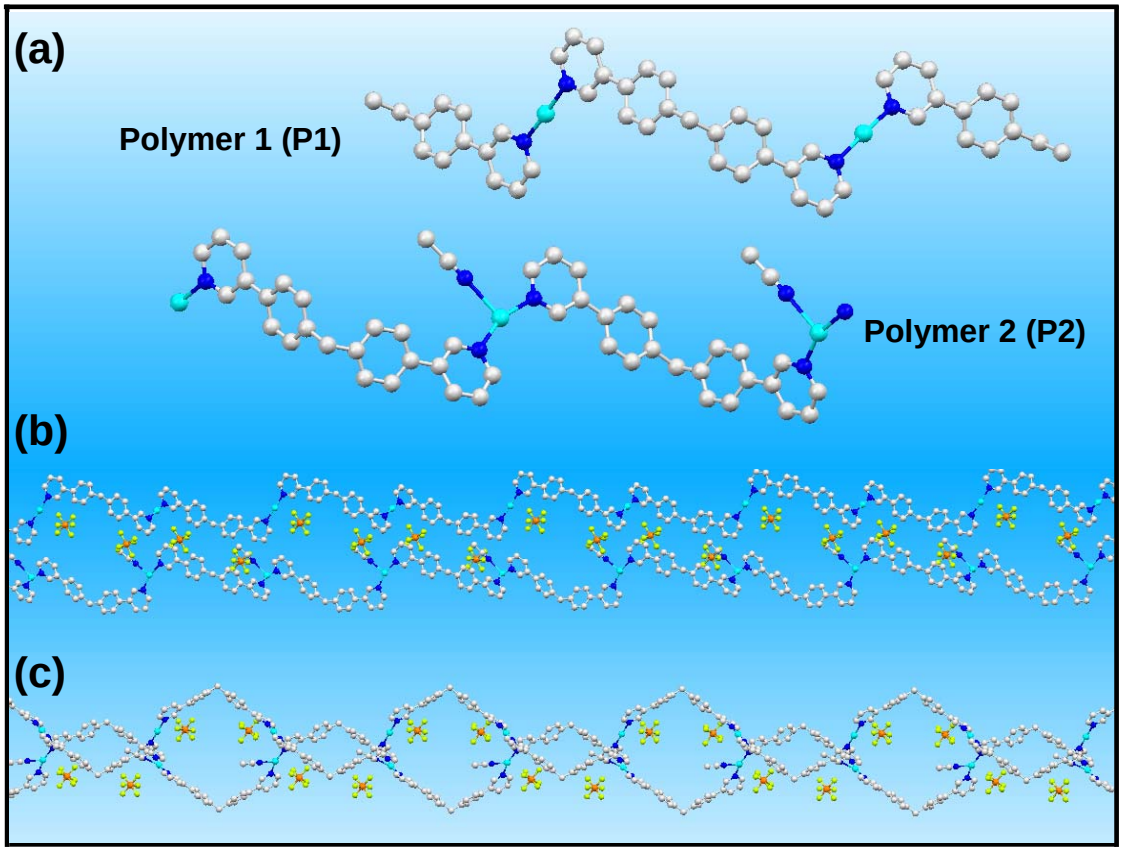

Figure 5.10. Silver(I) complex of **L**[1] (a) unit cell (b) polymeric chains (c) additional view exhibiting zigzag motif. Hydrogen atoms are omitted for clarity.

Both of the polymers display zigzag architecture but differ in their coordination environment. In P1, the metal centres adopt an almost linear (N_{py}-Ag-N_{py} = 176.97(13)°), two-coordinate environment with 1:1 metal:ligand stoichiometry. Each silver(I) ion is bound to two separate pyridyl ligands with typical Ag-N_{py} bond lengths of 2.133(3) Å and a Ag···Ag separation of 15.0 Å. The silver(I) ions also make weak contacts to the PF_6^- counter-ions (Ag···F 3.16 Å, Ag···F-P angle 162º). Conversely, the cationic chain of P2 is based on a $\{Ag(C_{23}H_{18}N_2)(CH_3CN)\}_\infty$ repeating unit in which the silver(I) centres occupy a three-coordinate, distorted trigonal planar geometry. The silver(I) ions are bound to two nitrogen atoms from the organic ligands (Ag-N_{py} = 2.159(3) Å) and one from an acetonitrile molecule (Ag-N_{MeCN} = 2.489(4) Å) resulting in a

N_{py}-Ag-N_{py} bond angle of 158.30(12)° and N_{py}-Ag-N_{MeCN} bond angles of 98.37(13)° and 103.11(13)°. As in P1, the bridging ligands separate the silver(I) ions by a distance of 15.0 Å. The crystal packing of the polymers is shown in Figure 5.11.

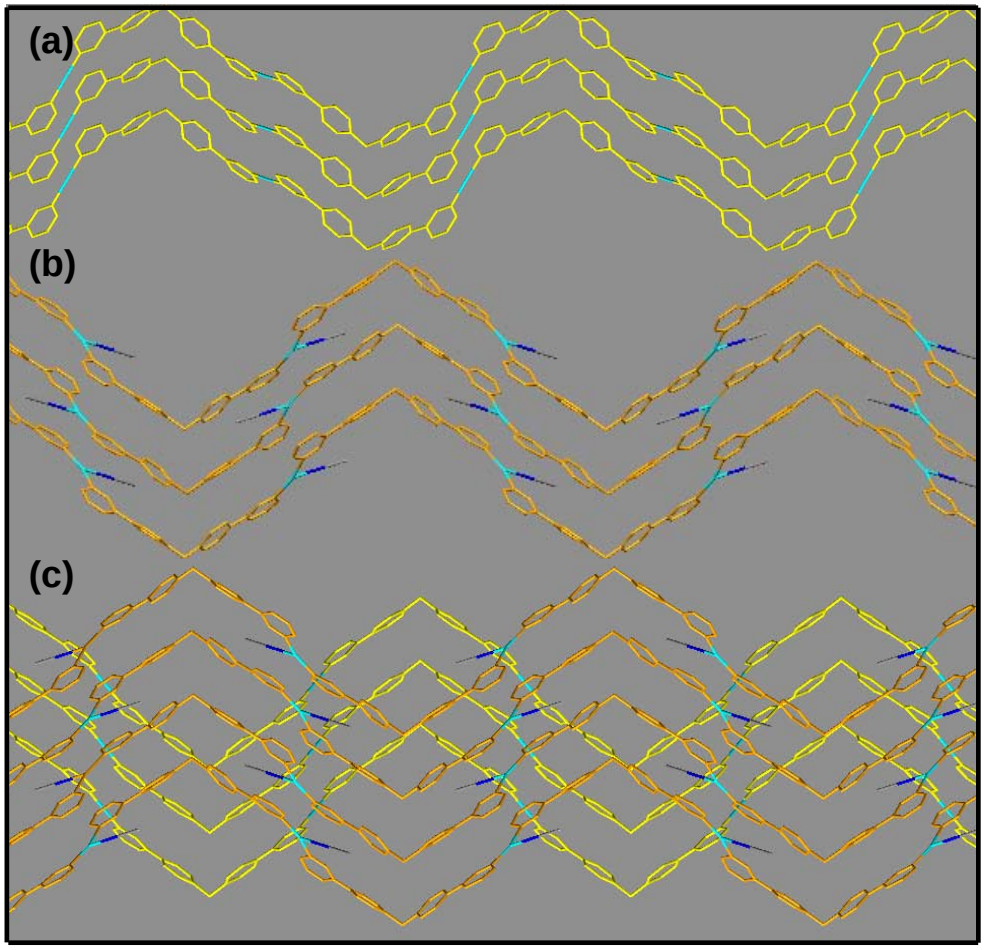

Figure 5.11. Packing in cationic sheets of (a) P1 (b) P2 and (c) P1 + P2
Hydrogen atoms, anions and solvent molecules have been omitted for clarity.

The polymeric chains are aggregated into two dimensional pleated sheets, each consisting of repeating units of P1 (Figure 5.11 (a)) or P2 ((Figure 5.11 (b)). These well-defined sheets run antiparallel to one another and the gaps between them are occupied by counter-ions and solvent molecules. There are also a number of short F···H contacts between the PF_6^- counter-ions and the protons of the organic and acetonitrile ligands (2.5-2.9 Å). Remarkably, despite the large

number of aromatic residues, there does not seem to be any significant π-π stacking interactions between the polymers (shortest π-π centroid-centroid distances are 4.3 Å in P1 and 3.8 Å in P2).[5]

5.2.2 Silver(I) complex of L^2

The silver(I) complex of Ligand **L^2** was self-assembled by the reaction of silver(I) hexafluorophosphate with one equivalent of the ligand in methanol:chloroform (1:1). The reaction took place over 3 hours with the exclusion of light.

In contrast to the silver(I) complex of **L^1** for which a mass spectrum could not be recorded, it was possible to record an ESI mass spectrum of this complex from an acetonitrile solution. The spectrum shows peaks corresponding to the dinuclear species $[Ag_2(\mathbf{L^2})_2(PF_6)]^+$ (*m/z* 1009) and the mononuclear species $[Ag(\mathbf{L^2})_2]^+$ (*m/z* 757) and $[Ag(\mathbf{L^2})(CH_3CN)]^+$ (*m/z* 472). Although this may indicate the presence of multiple distinct complexes in solution, the peaks may be due to fragmentation of a high molecular weight polymer. Partial microanalytical data are consistent with a formulation $\{Ag(C_{22}H_{16}N_2O)(PF_6)\}_n$ and a FT-IR spectrum confirms the presence of hexafluorophosphate anions by the occurrence of a strong absorption band at 836 cm^{-1}. ^1H NMR spectra of the complex have been recorded in both deuterated acetonitrile and nitromethane solutions. At room temperature, a single set of peaks were observed in each case. The 300 MHz ^1H NMR spectrum of this complex in d_3-nitromethane is shown in Figure 5.12. The spectrum is analogous to that of $\{Ag(\mathbf{L^1})(PF_6)\}_\infty$ with the pyridyl protons occurring at similar chemical shifts.

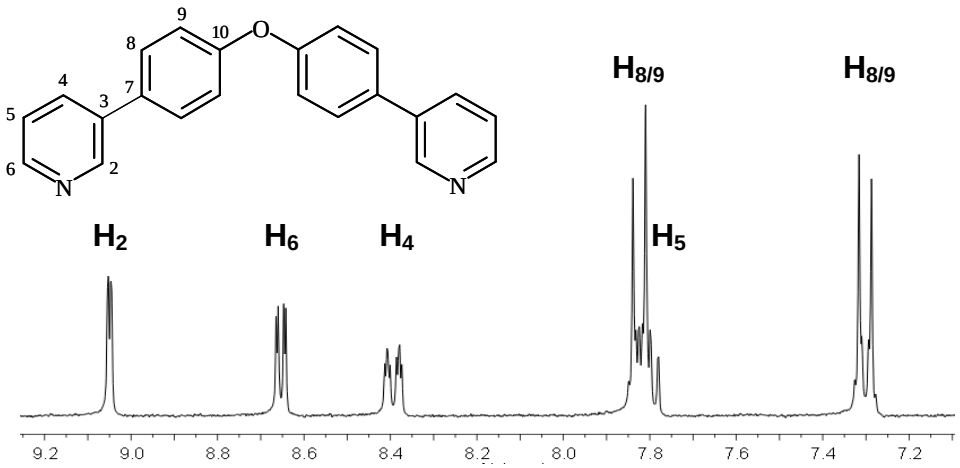

Figure 5.12. ^{1}H NMR spectrum of $\{Ag(C_{22}H_{16}N_2O)(PF_6)\}_n$ (300 MHz, d_3-nitromethane, 298 K).

The ESI mass spectrum of this complex suggested that multiple solution species might be present, this was investigated by carrying out low temperature NMR experiments in d_3-acetonitrile. At lower temperatures the peaks remain sharp, being consistent either with a single solution species or with the presence of multiple species inter-converting rapidly within the temperature range of this solvent (Figure 5.13).

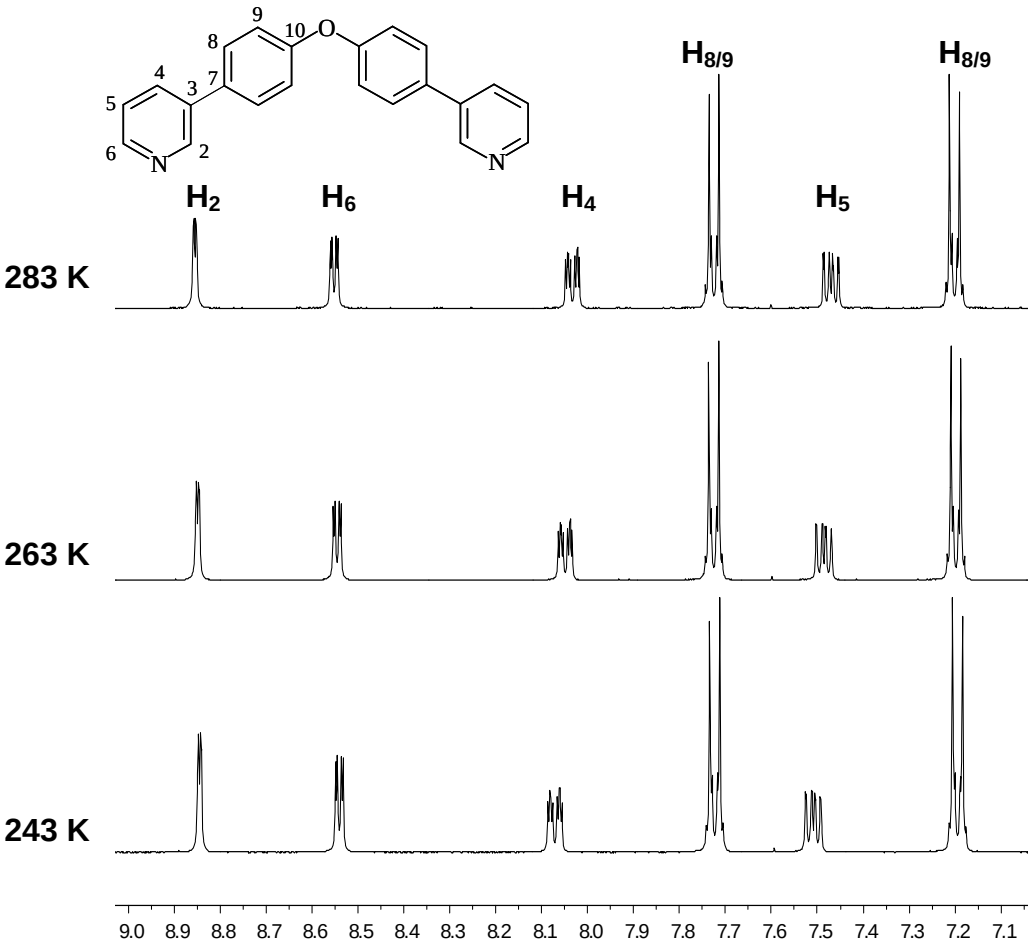

Figure 5.13. ^{1}H NMR spectra of the aromatic region of $\{Ag(C_{22}H_{16}N_2O)(PF_6)\}_n$ at 243 K, 263 K and 283 K (400 MHz, d_3-acetonitrile).

X-ray quality, colourless crystals were obtained by the slow diffusion of diethyl ether into an acetonitrile solution of this complex. The crystal structure revealed a linear polymeric chain with 1:1 metal:ligand stoichiometry (Figure 5.14).[12]

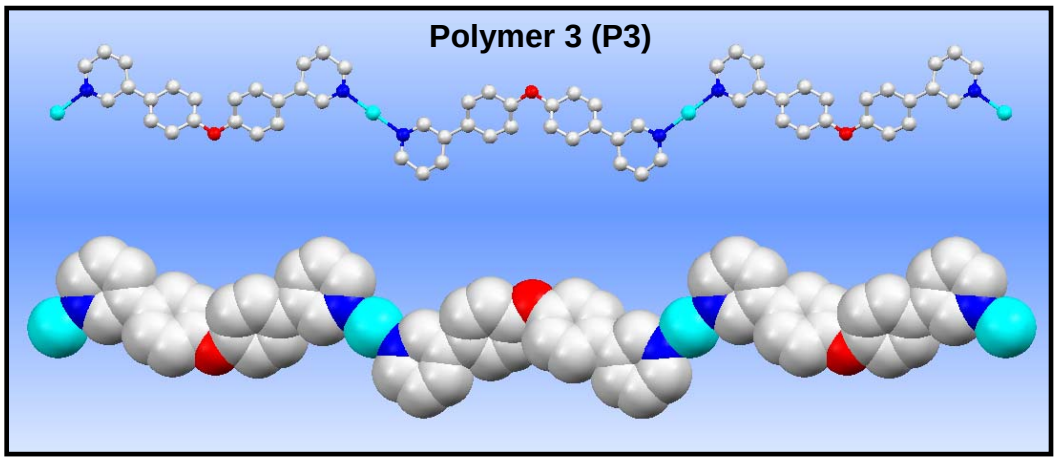

Figure 5.14. (a) Perspective view and (b) space-filling representation of polymer 3. Hydrogen atoms, solvent molecules and anions are omitted for clarity.

Polymer 3 is based on a $\{Ag(C_{22}H_{16}N_2O)(PF_6)\}$ repeating unit in which all of the silver(I) centres are equivalent and occupy a linear, two-coordinate environment. The silver(I) centres are bound to two pyridyl units from two separate ligands with inter-metallic distances of 18.4 Å. The N_{py}-Ag-N_{py} bonds of the polymer are perfectly linear with bond angles of 180.00(2)º and typical Ag-N_{py} bond lengths at 2.141(13) Å and 2.142(14) Å. The cationic chains are packed together as shown in Figure 5.15.

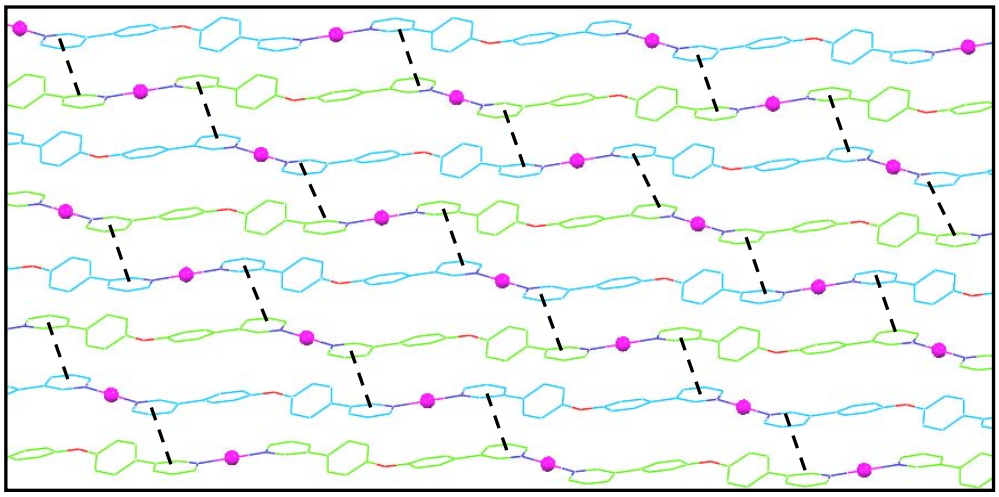

Figure 5.15. Packing diagram for polymer 3 showing the π-π stacking interactions between the phenyl rings. Hydrogen atoms, anions and solvent molecules have been removed for clarity.

The polymeric chains are interconnected into sheets supported by extensive face-to-face π-π stacking interactions. The interactions are between two parallel pyridyl rings from neighbouring chains with centroid-centroid distances of 3.6 Å. There are also secondary interactions between the phenyl rings of the spacers and the Ag(I) ions of the adjacent chains. As is typical for Ag···π interactions, η^2 rather than η^6 coordination is observed; however, the shortest Ag···C_{phenyl} distance (3.2 Å) is towards the long end of the range proposed for such interactions (Munakata *et al.* proposed an upper limit of 3 Å) and it is unclear whether this contributes significantly to the bonding. Disordered hexafluorophosphate counter-ions and non-coordinating solvent molecules are located in the channels between the polymer sheets.

In P3 the pyridyl binding sites adopt a *syn*-conformation and are oriented towards the central aromatic spacer (Figure 5.16 (a)). **L²** can also adopt two other conformations in the solid state, these are shown in Figure 5.16 (b) and (c).

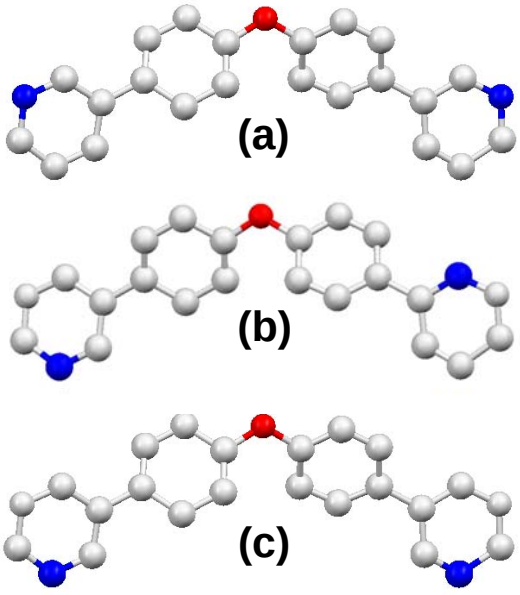

Figure 5.16. (a) *Syn*-orientation of ligand in silver(I) complex of **L²** (b) *anti*-conformation of **L²** (c) other *syn*-orientation of **L²**.

Contrary to what is seen in the crystal structure of P3, ligand **L^1** adopts an *anti*-conformation in P1 and P2. The conformational flexibility of these ligands arises from the rotation about the pyridyl-phenyl bond and plays an important role in enabling the analogous ligands **L^1** and **L^2** to bind to silver(I) with different orientations.

5.2.3 Silver(I) complex of L^5

One equivalent of ligand **L^5** was reacted with silver(I) hexafluorophosphate to afford a white solid in 68 % yield. FT-IR spectroscopy shows a strong absorption band at 821 cm^{-1}; this is characteristic of non-coordinated hexafluorophosphate anions. The elemental analysis data are consistent with a formulation $\{Ag(C_{24}H_{20}N_2)(PF_6)\}_n$ and the ESI mass spectrum is dominated by peaks corresponding to $[Ag_2L_2(PF_6)]^+$ (*m/z* 1033), $[AgL(CH_3CN)]^+$ (*m/z* 484) and $[AgL]^+$ (*m/z* 443). The ^{1}H NMR spectra in d_3-acetonitrile and d_3-nitromethane revealed one set of peaks indicating the formation of a single, symmetrical solution species. The ^{1}H NMR spectrum in d_3-acetonitrile is presented in Figure 5.17. The spectrum is similar to the room temperature spectra of $\{Ag(\mathbf{L^1})(PF_6)\}_\infty$ and $\{Ag(\mathbf{L^2})(PF_6)\}_\infty$ in this solvent and the pyridyl protons occur at almost exactly the same chemical shifts. This indicates that a polymeric structure may have also formed with Ligand **L^5**. On cooling the sample down to 243 K, a single, sharp set of resonances was still observed.

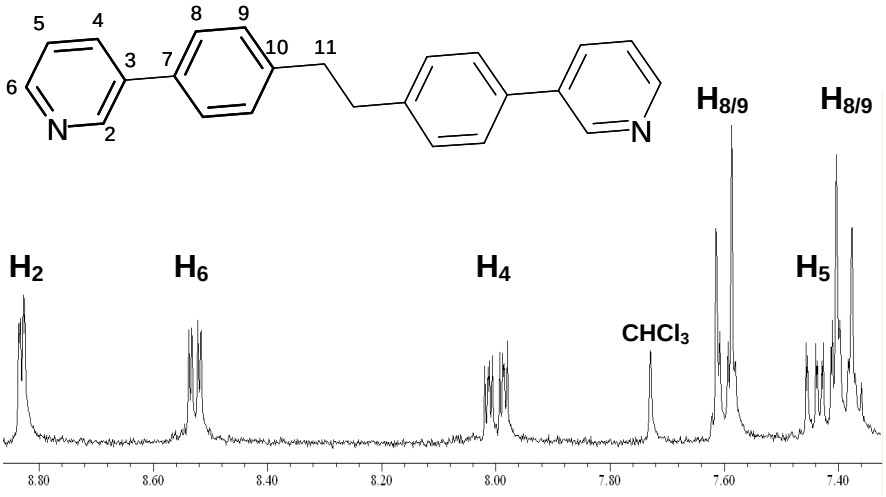

Figure 5.17. ^{1}H NMR spectrum of the aromatic region of $\{Ag(C_{24}H_{20}N_2)(PF_6)\}_n$ (300 MHz, d_3-acetontrile, 298 K).

Small, colourless crystals were obtained by the slow diffusion of diethyl ether into an acetonitrile solution of the complex. Single crystal X-ray diffraction analysis revealed a 1:1 metal:ligand zigzag coordination polymer (Figure 5.18).[12]

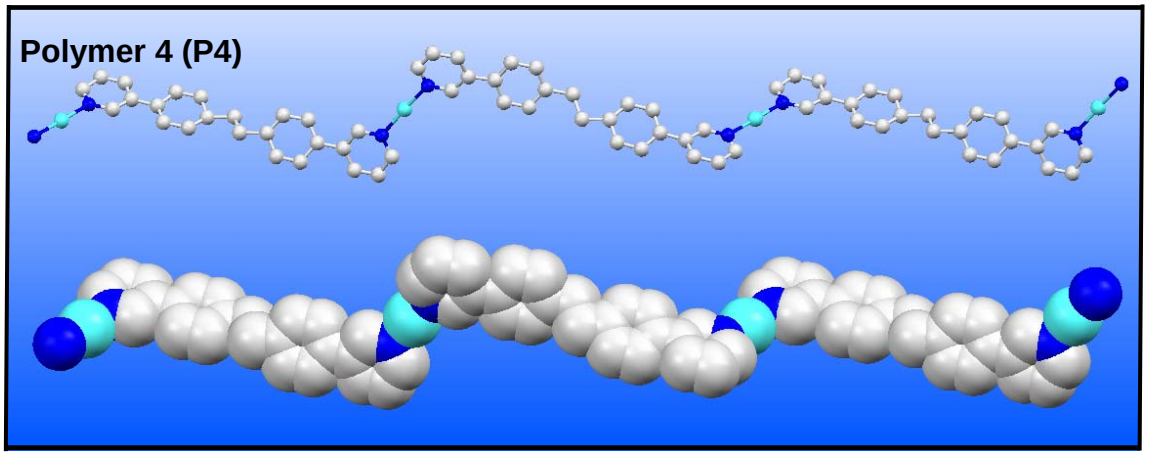

Figure 5.18. X-ray crystal structure of polmer 4.
Hydrogen atoms are omitted for clarity.

In P4, each silver(I) centre occupies a linear coordination environment (N_{py}-Ag-N_{py} = 179.0(4)º and 175.2(3)º) and is bound to pyridyl binding units from two different ligands. These bridging ligands separate the metal centres by a distance of 19.1 Å and the Ag-N_{py} bond lengths (2.120(8)-2.142(8) Å) are

unremarkable and analogous to those found in P1, P2 and P3. Within the ligands, the phenyl rings are twisted with respect to one another (46º and 47º) and with respect to the pyridine rings (6º, 17º, 21º, 28º). The zigzag chains pack together into layers as shown in Figure 5.19.

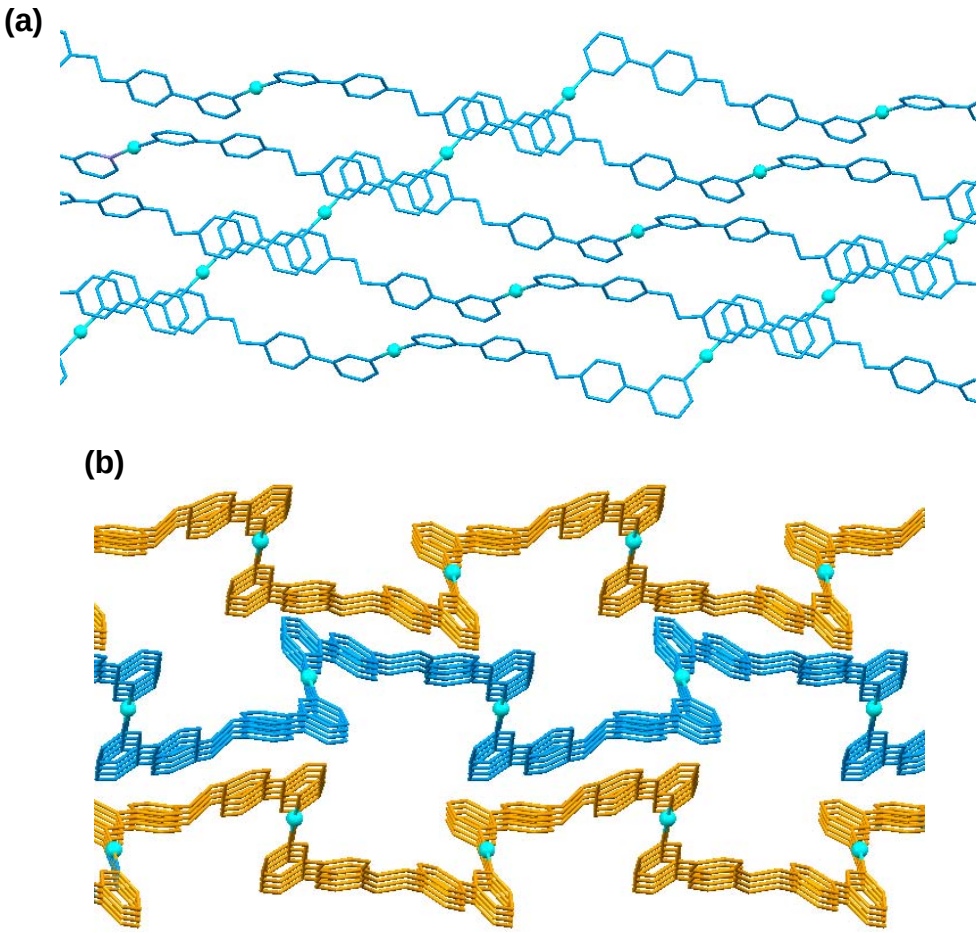

Figure 5.19. Crystal packing diagram for polymer 4 showing the packing in (a) one layer and (b) multiple layers (view approximately orthogonal to (a)). Hydrogen atoms, anions and solvent molecules have been removed for clarity.

The zigzag polymers pack together to form two dimensional layers (Figure 5.19 (a)). Within the layers the cationic chains are linked together by π-π stacking interactions (centroid-plane distance= 3.4 - 3.7 Å). Figure 5.19 (b) shows that the polymer layers pack together in a three dimensional network to form open channels. These channels are occupied by acetonitrile solvent molecules and

the PF_6^- counter-ions. The acetonitrile molecules interact with the silver(I) ions through weak Ag···N_{MeCN} contacts (3.3 Å). There are also a number of short F···H contacts between the counter-ions and the protons of the pyridine and phenyl rings (2.4-2.5 Å).

5.3 Summary

Four novel silver(I) supramolecular polymers have been described. Figure 5.20 shows the one dimensional structures of polymers 1-4. All of the polymers exhibit a zigzag geometry. In P2, the silver(I) ions occupy a trigonal coordination environment due to the incorporation of an acetonitrile molecule into the coordination sphere, however, in P1, P3 and P4 the metal centres are linear. The conformations of the ligands are susceptible to change and while **L^2** adopts a *syn*-conformation in P3, ligands **L^1** and **L^5** adopt an *anti*-conformation in P1, P2 and P4. The reason that the ligands adopt different conformations remains unclear as the only difference between them is the central linker and this does not appear to be implicated in any bonding or stabilising interactions in any of the three polymers.

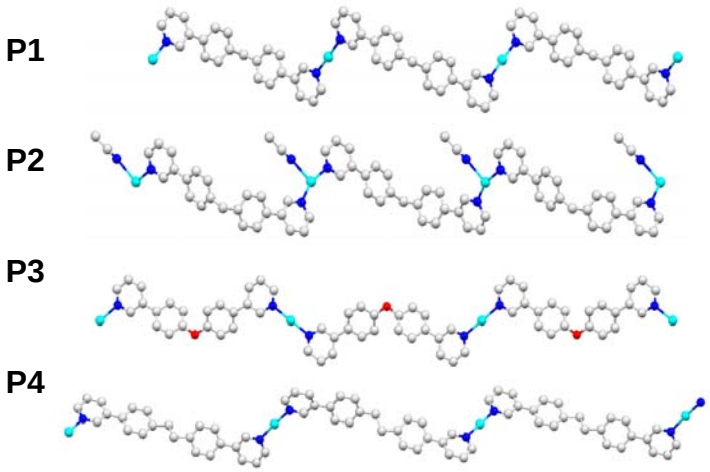

Figure 5.20. 1D structures of polymers 1-4.

5.4 Conclusion

In this chapter, the coordination chemistry of silver(I) hexafluorophosphate with ligands **L**^{1}, **L**^{2} and **L**^{5} was investigated. The results reveal the formation of four new supramolecular arrays, {Ag(**L**^{1})(PF_6)}$_\infty$, {Ag(**L**^{1})(CH_3CN)(PF_6)}$_\infty$, {Ag(**L**^{2})(PF_6)}$_\infty$ and {Ag(**L**^{5})(PF_6)}$_\infty$. The X-ray crystal structures of these complexes reveal one dimensional zigzag polymeric chains linked into two dimensional networks by Ag···N contacts, Ag···π interactions, F···H contacts and π-π stacking. The structure of the {Ag(**L**^{1})(CH_3CN)(PF_6)}$_\infty$ array demonstrates the flexibility of the silver(I) centre by the incorporation of a solvent molecule into the coordination sphere.

5.5 Experimental

5.5.1 General

All solvents and reagents were purchased from Sigma-Aldrich and were used without further purification. ^{1}H NMR spectra were recorded on AC300 and AV300 Brüker spectrometers and variable temperature experiments were performed by Dr Neil Spencer using an AV 400 Brüker spectrometer. NMR data were processed using standard Brüker software. Infrared spectra were recorded from KBr pellets on a Perkin Elmer Paragon 1000 FT-IR spectrometer. Electrospray Ionisation (ESI) spectra were recorded by Dr Peter Ashton on a Micromass LCT Time of flight mass spectrometer in positive ionization mode**.** Microanalyses data were obtained using a CE Instruments EA1110 elemental analyser.

5.5.2 Synthesis of silver(I) polymers of L^1

Ligand **L^1** (14.9 mg, 0.046 mmol) was dissolved in chloroform (5 ml) and excluding light, a solution of silver(I) hexafluorophosphate (11.6 mg, 0.046 mmol) in methanol (5 ml) was added. The reaction mixture was stirred for 3 hours after which an off white solid had precipitated. The *crude* product was collected by vacuum filtration, washed with chloroform (5 ml) and diethyl ether (5 ml) and dried *in vacuo* over P_4O_{10} (19.3 mg, 73 % yield).

^{1}H NMR (300 MHz, CD_3CN, 298 K): δ 8.82 (2H, dd, *J*= 2.4, 0.9 Hz, H_2), 8.52 (2H, dd, *J*= 4.9, 1.5 Hz, H_6), 7.99 (2H, ddd, *J*= 8.1, 2.4, 1.5 Hz, H_4), 7.62 (4H, d, *J*= 8.5, $H_{8/9}$), 7.43 (2H, ddd, *J*= 8.1, 4.9, 1.1 Hz, H_5), 7.41 (4H, d, *J*= 8.5 Hz, $H_{8/9}$), 4.09 (2H, s, H_{11}).

Elemental analysis (%) calculated for {Ag($C_{23}H_{18}N_2$)(PF_6)}: C: 48.0; H: 3.2; N: 4.9; Found: C: 48.0; H: 2.8; N: 5.0.

IR (Neat): ν= 1603(w), 1582(w), 1478(m), 1437(w), 1400(w), 1191(w), 1135(w), 1012(w), 825(s), 793(m), 763(m), 739(m), 700(m), 659(m), 621(m) cm^{-1}.

5.5.3 Synthesis of silver(I) polymer of L^2

Ligand **L^2** (15.0 mg, 0.046 mmol) was dissolved in chloroform (5 ml) and excluding light, a solution of silver(I) hexafluorophosphate (11.6 mg, 0.046 mmol) in methanol (5 ml) was added. The reaction mixture was stirred for 3 hours after which an off white solid had precipitated. The crude product was collected by vacuum filtration, washed with chloroform (5 ml) and diethyl ether (5 ml) and dried in vacuo over P_4O_{10} (20.3 mg, 77 % yield).

^{1}H NMR (300 MHz, CD_3CN, 298 K): δ 8.84 (2H, dd, *J*= 2.6, 0.7 Hz, H_2), 8.54 (2H, dd, *J*= 5.0, 1.7 Hz, H_6), 8.01 (2H, ddd, *J*= 8.1, 2.6, 1.7 Hz, H_4), 7.71 (4H, d, *J*= 8.8, $H_{8/9}$), 7.43 (2H, ddd, *J*= 8.1, 5.0, 1.1 Hz, H_5), 7.19 (4H, d, *J*= 8.8 Hz, $H_{8/9}$).

Mass Spectrum (E.S.I): *m/z* 1009.1 $\{Ag_2L_2 + PF_6\}^+$, 757.2 $\{AgL_2\}^+$, 472.1 $\{AgL + CH_3CN\}^+$,

Elemental analysis (%) calculated for {Ag($C_{22}H_{16}N_2O$)(PF_6)}: C: 45.8; H: 2.8; N: 4.9; Found: C: 45.7; H: 2.7; N: 4.9.

IR (Neat): ν= 1697(w), 1599(w), 1508(m), 1477(m), 1436(w), 1280(w), 1250(m), 1177(m), 836(s), 805(s), 703(m), 641(w) cm^{-1}.

5.5.4 Synthesis of silver(I) polymer of L^5

Ligand **L^5** (15.0 mg, 0.045 mmol) was dissolved in chloroform (5 ml) and excluding light, a solution of silver(I) hexafluorophosphate (11.3 mg, 0.045 mmol) in methanol (5 ml) was added. The reaction mixture was stirred for 3 hours after which an off white solid had precipitated. The *crude* product was collected by vacuum filtration, washed with chloroform (5 ml) and diethyl ether (5 ml) and dried *in vacuo* over P_4O_{10} (18.0 mg, 68 % yield).

^{1}H NMR (300 MHz, CD_3CN, 298 K): δ 8.83 (2H, dd, *J*= 2.4, 0.9 Hz H_2), 8.53 (2H, dd, *J*= 4.8, 1.8 Hz, H_6), 8.00 (2H, ddd, *J*= 8.1, 2.4, 1.7 Hz, H_4), 7.60 (4H, d, *J*= 8.5 Hz, $H_{8/9}$), 7.43 (2H, ddd, *J*= 8.1, 4.8, 0.7 Hz, H_5), 7.39 (4H, d, *J*= 8.5 Hz, $H_{8/9}$), 3.03 (2H, s, H_{11}).

Mass Spectrum (E.S.I): *m/z* 1033.2 $\{Ag_2L_2 + PF_6\}^+$, 779.3 $\{AgL_2\}^+$, 484.1 $\{AgL + CH_3CN\}^+$, 443.1 $\{AgL\}^+$.

Elemental analysis (%) calculated for $\{Ag(C_{24}H_{20}N_2)(PF_6)\}$: C: 48.9; H: 3.4; N: 4.8; Found: C: 48.8; H: 3.2; N: 4.8.

IR (Neat): ν= 1604(w), 1581(w), 1479(m), 1437(w), 1400(w), 1298(w), 1191(w), 1011(m), 821(s), 799(s), 739(m), 700(s) cm^{-1}.

5.6 References

1. J. M. Lehn, *Proc. Natl. Acad. Sci.,* **2002**, 99, 4763-4768; J. W. Steed, J. L. Atwood, *Supramolecular Chemistry*, John Wiley and Sons Ltd, **2000**; J. M. Lehn, *Supramolecular Chemistry: Concepts and Perspectives,* VCH, New York, **1995**.
2. E. C. Constable, *Aust. J. Chem.*, **2006**, 59, 1-2.
3. S. Delgado, P. J. Sanz Miguel, J. L. Priego, R. Jimenez-Aparicio, C. J. Gomez-García, F. Zamora, *Inorg. Chem*., **2008**, 47, 9128-9130; C. Janiak, *Dalton Trans*., **2003**, 2781–2804.
4. S. Kitagawa, R. Kitaura, S. I. Noro, *Angew. Chem. Int. Ed*., **2004**, 43, 2334 –2375.
5. M. Albrecht, M. Lutz, A. L. Spek, G. van Koten, G. *Nature,* **2000**, 406, 970-974.
6. Chi. C. Kwok, S. C. Yu, I. H. T. Sham, C. M. Che, *Chem. Commun*., **2004**, 2758–2759.
7. J.M. Lehn, *Chem. Eur. J.*, **1999**, 5, 2455-2463; J. B. Beck, J. M. Ineman, S. J. Rowan, *Macromolecules,* **2005**, *38,* 5060-5068; M. Burnworth, D. Knapton, S. J. Rowan, C. Weder, *J. Inorg*. *Organomet. Poly*. *Mat*., **2007**, 17, 91-103.
8. Y. J. Zhao, M. C. Hong, Y. C. Liang, W. P. Su, R. Cao, Z. Y. Zhou, A. S.C. Chan, *Polyhedron*, **2001**, 20, 2619–2625.
9. T. Kawano, C. X. Du, T. Araki, I. Ueda, *Inorg. Chem. Commun.*, **2003**, 6, 165–167.
10. F. Tuna, J. Hamblin, G. Clarkson, W. Errington, N. W. Alcock, M. J. Hannon, *Chem. Eur. J.*, **2002**, 8, 4957-4964.
11. P. Halder, E. Zangrando, T. K. Paine, *Dalton Trans.*, **2009**, 5386–5394
12. X-ray crystal data were collected and solved by Dr. Louise Male at the University of Birmingham.

Chapter 6

A Novel Azo Ligand System

6.1 Introduction

As discussed in chapter 4, the coordination chemistry of Hannon's ligand **L^{6}** has been extensively studied.[1] Ligand **L^{azo}** is an analogue of **L^{6}** in which the imine constituent has been replaced by an azo bond (Figure 6.1).[2] The azo bond is less susceptible to hydrolysis than the imine bond and so **L^{azo}** complexes should be more robust than their **L^{6}** analogues. The coordination chemistry of **L^{azo}** has also been previously investigated.[2,3]

(a)

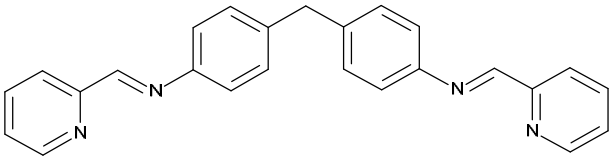

(b)

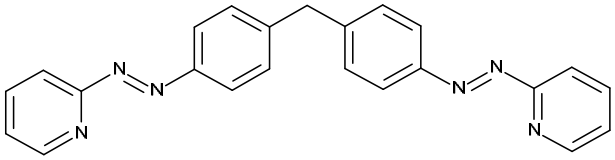

Figure 6.1. Hannon's (a) ligand **L^{6}** and (b) ligand **L^{azo}**.

6.1.1 Research Aims

In this chapter the effect of modification to the central spacer of **L^{azo}** is explored. A novel dinucleating ligand, **L^{7}**, is presented and its coordination chemistry investigated (Figure 6.2). **L^{7}** is very similar to Hannon's **L^{azo}** ligand except that the central methylene bridge has been replaced by a secondary amine.

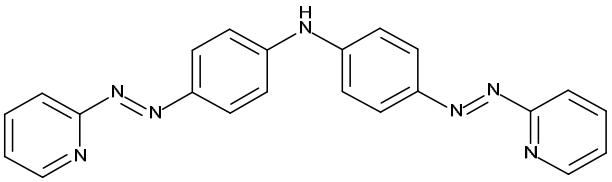

Figure 6.2. Ligand **L^{7}**.

It was anticipated that the amine bridge would not significantly affect the coordination chemistry and that the reaction of this ligand with four coordinate

metal ions would result in the formation of dinuclear $[M_2L_2]^{2+}$ species analogous to those formed with $\mathbf{L^{azo}}$ and $\mathbf{L^6}$.

6.2 Results and Discussion

6.2.1 Ligand $\mathbf{L^7}$

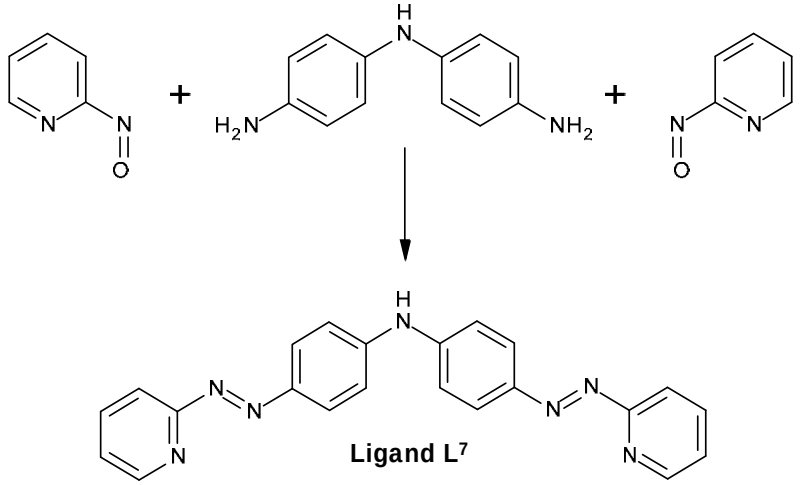

Scheme 6.1. Synthesis of Ligand $\mathbf{L^7}$.

2-Nitrosopyridine is not commercially available and was synthesized from 2-aminopyridine in the two step reaction outlined by Taylor *et al.*.[4] The 4,4'-diaminodiphenylamine spacer was also prepared using a literature procedure.[5] Ligand $\mathbf{L^7}$ was synthesized in 65 % yield by an acetic acid catalysed reaction between two equivalents of 2-nitrosopyridine and one equivalent of 4,4'-diaminodiphenylamine. A mixture of the ligand and half-ligand precipitated from the reaction mixture as a red powder. The *crude* product was purified by preparative RP-HPLC using a gradient of 100 % water to 100 % methanol over 40 minutes and the pure product was observed and collected at 38.10 minutes. Partial microanalytical data are consistent with the expected ligand formulation of $\{C_{22}H_{17}N_7\}$ and the ESI mass spectrum is dominated by two peaks corresponding to $[\mathbf{L^7} + H]^+$ (*m/z* 380) and $[\mathbf{L^7} + Na]^+$ (*m/z* 402). FT-IR

spectroscopy shows a broad band at 3425 cm^{-1} and a sharp one at 1409 cm^{-1} corresponding to the amine stretch and azo components, respectively. The ^1H NMR spectrum of the ligand has been assigned with the assistance of a 2D COSY and is shown in Figure 6.3.

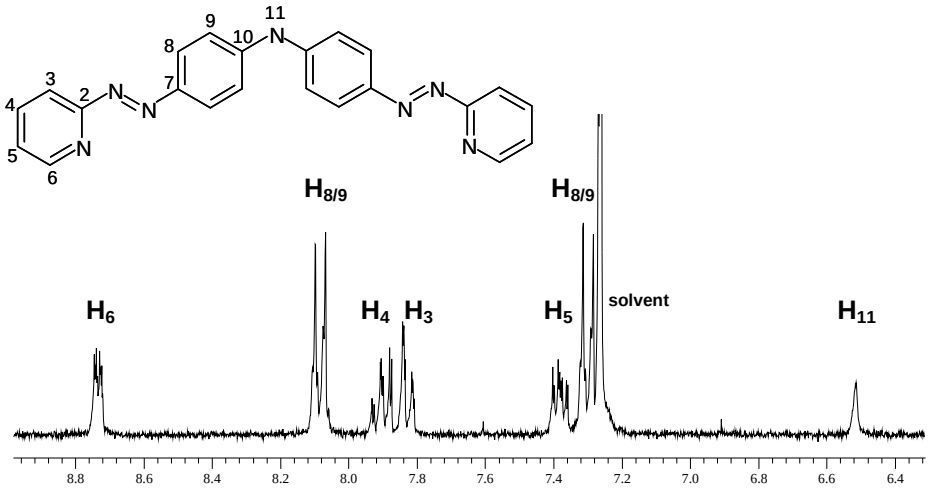

Figure 6.3. ^1H NMR spectrum of Ligand **L^7**
(300 MHz, d_3-chloroform, 298 K).

The resonances of the pyridine ring are readily identified from their distinctive splitting patterns. H_3 appears as a doublet and is coupled to H_4 with a coupling constant of ~8 Hz. The resonance corresponding to H_5 is observed as a doublet of doublets and is coupled to both H_4 and H_6 with coupling constants of ~7 Hz and ~5 Hz, respectively. The coupling with H_6 is smaller due to the presence of the adjacent electronegative nitrogen atom which also shifts the H_6 signal downfield to 8.73 ppm. The two doublets at 7.33 ppm and 8.08 ppm show a distinct roofing effect and correspond to H_8 and H_9 (J ~9 Hz). The signal for the amine proton (H_{11}) occurs as a singlet at 6.66 ppm.

Recrystallisation of this ligand from chloroform afforded red crystals suitable for X-ray diffraction analysis. The X-ray crystal structure of **L^7** is shown in Figure 6.4.[6]

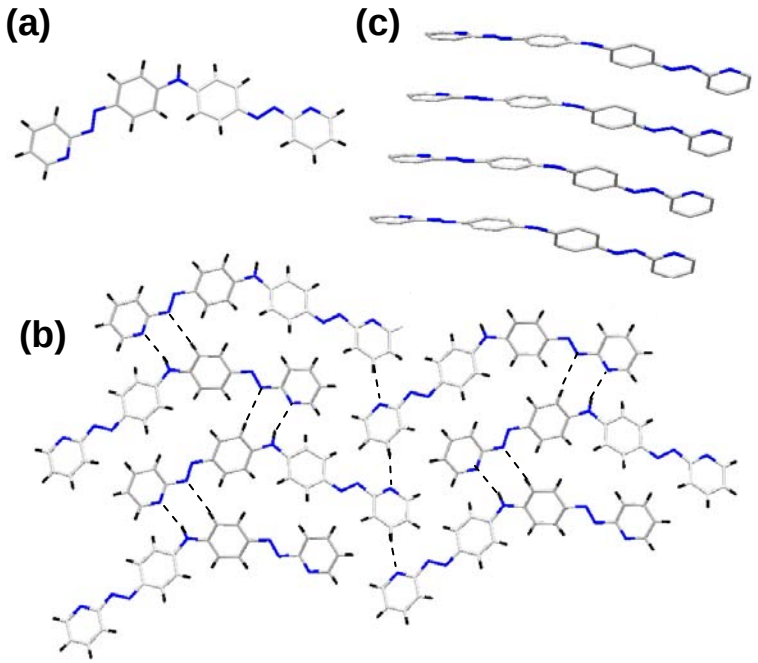

Figure 6.4. X-ray crystal structure of (a) Ligand **L**[7]
(b) H-bonded network and (c) π-π stacking interactions.

The free ligand adopts an *anti*-conformation with respect to the relative positions of the pyridyl nitrogen atoms (Figure 6.4 (a)). Therefore, the two pyridyl donors interact differently with their neighbours. The first forms N···H-N interactions with the central amine (H_{11}) proton (N_{py}···H 2.3 Å; N_{py}···H-N angle 153º) and the second with a pyridyl (H_4) proton (N_{py}···H 2.4 Å; N_{py}···H-C angle 169º). N···H-C interactions are also apparent between the azo nitrogen and the H_9 protons of the phenyl rings (N_{azo}···H 2.7 Å; N_{azo}···H-C angle 149º). These inter-molecular interactions result in the formation of a large H-bonded network (Figure 6.4 (b)). Within this network, the ligand molecules are arranged into columns which are held together by face-to-face π-π stacking interactions (Figure 6.4 (c)). The inter-planar distance between the stacked phenyl rings is 3.4 Å and the separation between the pyridyl rings is 3.3 - 3.5 Å.

In the following section the coordination chemistry of ligand **L^7** with silver(I), copper(I) and palladium(II) will be described. Each metal ion is expected to coordinate to a pyridylazo subunit from each ligand. Therefore, the reaction of each of these four coordinate metal ions with **L^7** is expected to result in the formation of a dinuclear $[M_2L_2]^{2+}$ species. Two conformations of the dimeric species are possible: the helix and the box (cyclophane).[2]

6.2.2 Silver(I) complex of L^7

Silver(I) acetate was added to a methanolic solution of ligand **L^7** and heated under reflux for 3 hours. Care was taken to exclude light from the reaction to prevent the reduction of the silver(I) starting material. On completion of the reaction, a red-brown solid was precipitated by the addition of methanolic ammonium hexafluorophosphate. The precipitate was isolated by vacuum filtration, washed with diethyl ether and dried *in vacuo* to give the pure product in 36 % yield.

Partial microanalytical data are consistent with a formula of $\{Ag(C_{22}H_{17}N_7)(PF_6)\}_n$ and infrared spectroscopy reveals bands at 850 cm^{-1} and 558 cm^{-1} due to the non-coordinated hexafluorophosphate counter-ions. The ESI mass spectrum displays peaks with the correct *m/z* ratios and isotope distribution to correspond to $[Ag_2L_2(PF_6)]^+$ (*m/z* 1119), $[AgL_2]^+$ (*m/z* 867) and $[Ag_2L_2]^{2+}$ (*m/z* 487). This indicates the presence of a monomeric and/or dimeric species in solution. The ^{1}H NMR spectrum of this complex is shown in Figure 6.5.

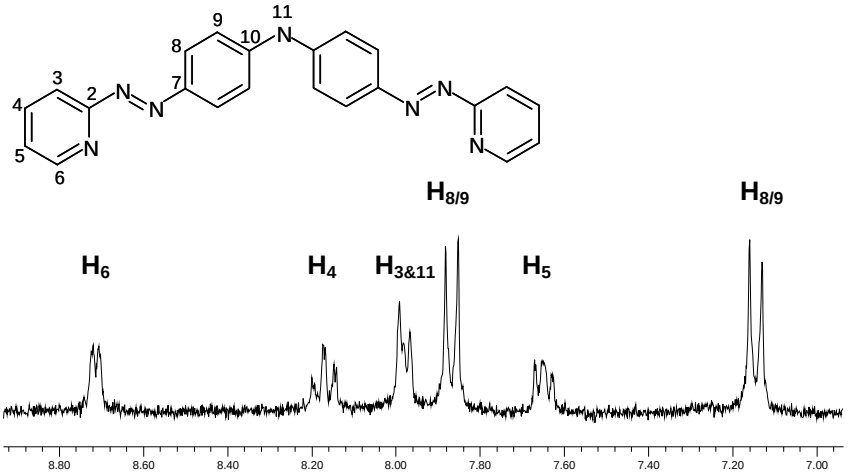

Figure 6.5. ^{1}H NMR spectrum of the silver(I) complex of **L^{7}** (300 MHz, *d*$_{3}$-acetonitrile, 298 K).

The spectrum consists of seven aromatic signals. At room temperature, a single set of well defined signals is displayed. On cooling to 233 K all of the signals remain sharp, suggesting that there is either a single species in solution or that any fluxional processes are rapid on the NMR timescale.

Red crystals suitable for X-ray diffraction were grown over a four week period by the slow diffusion of diethyl ether into an acetonitrile solution of the complex. Intriguingly, the X-ray crystal structure does not show the expected dimeric $[Ag_2(C_{22}H_{17}N_7)_2(PF_6)_2]$ species but instead reveals an infinite polymeric chain $\{Ag(\mathbf{L^7})(PF_6)\}_\infty$ (Figure 6.6).[7]

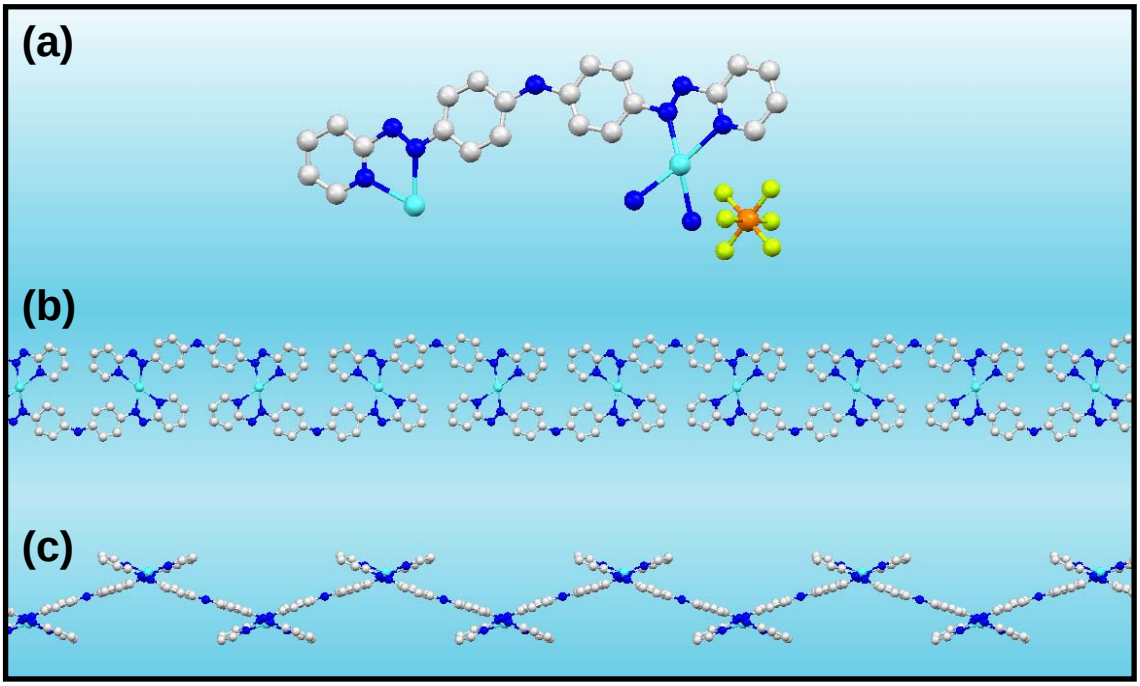

Figure 6.6. Silver(I) complex of **L**^{7} (a) unit cell (b) polymeric chain structure (c) additional view of polymer exhibiting zigzag motif. Hydrogen atoms are omitted for clarity.

The zigzag chain exhibits a 1:1 metal:ligand stoichiometry with the metal centres occupying a pseudo-tetrahedral, four-coordinate environment. Each silver(I) ion is bound to two separate ligands through Ag-N_{py} (2.33(3) - 2.36(2) Å) and Ag-N_{azo} (2.28(2) Å) bonds. The pyridylazo units are approximately coplanar (dihedral angles of 7.5º & 10.2º) and have N_{azo}-Ag-N_{py} bite angles of 67.1(9) - 67.8(9)º. The bridging ligands separate the silver(I) centres by a distance of 11.0 Å. In contrast to the free ligand which adopts an *anti*-conformation, a *syn*-conformation is seen in this complex as both pyridyl substituents are oriented in the same direction. The phenyl-phenyl (3.7º) and phenyl-pyridine rings (6.4º & 8.0º) are almost coplanar with respect to one another. The crystal packing of the polymer chains is shown in Figure 6.7.

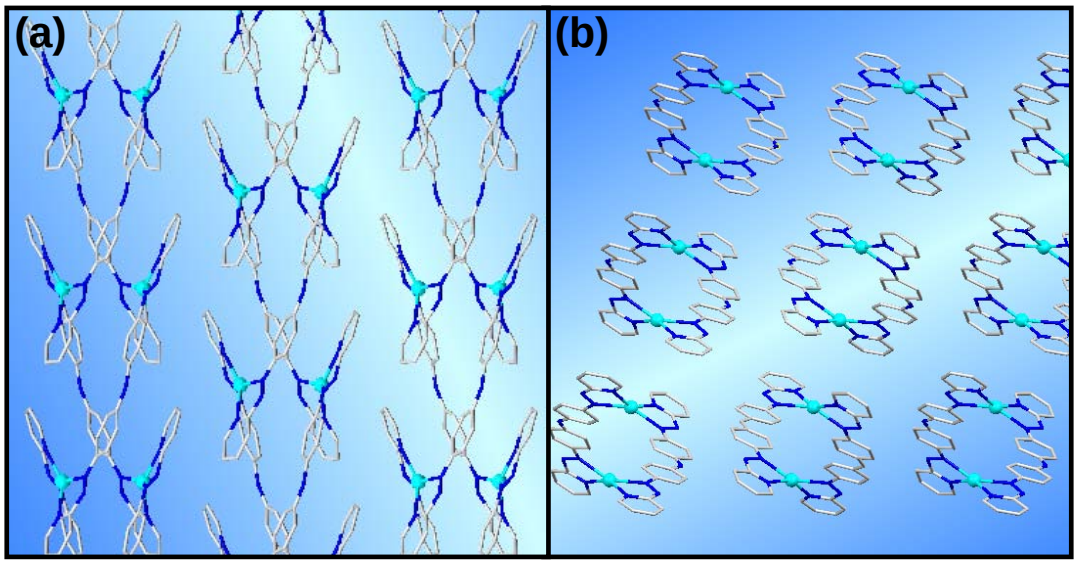

Figure 6.7. Packing diagrams for {Ag($\mathbf{L^7}$)(PF_6)}$_\infty$ showing (a) double-stranded helices (b) a view down the helical axis. Hydrogen atoms, anions and solvent molecules have been removed for clarity.

The packing diagram shows that the polymers pair up with one polymeric strand wrapping around the other to form a double-stranded helix. A racemic mixture is observed and the right- and left-handed helices are arranged into alternating rows (Figure 6.8).

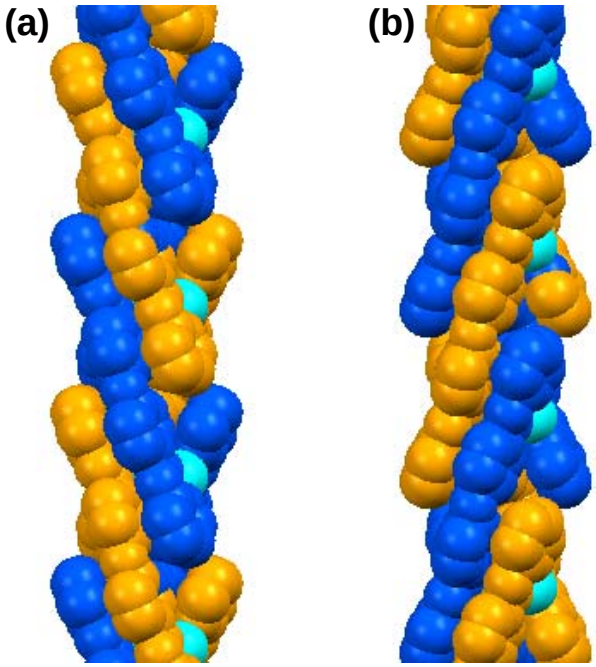

Figure 6.8. (a) Right- and (b) left-handed double helix of {Ag($\mathbf{L^7}$)(PF_6)}$_\infty$ Each polymer chain is shown in a different colour.

The helical pitch measures 21.3 Å in length and is defined as the distance between equivalent atoms when the double helix makes one complete turn about its axis. A hollow channel is formed along the helical axis with a Ag···Ag separation of 4.6 Å (no contact between the silver(I) ions). The driving force for the formation of these double-stranded helices seems to be a series of inter-polymer π-π stacking interactions between the phenyl and pyridine rings (centroid-plane distances of 3.3 – 3.9 Å). The counter-ions are located in the gaps between the helices. Each PF_6^- makes a weak F···Ag (3.2 Å) contact to a silver(I) ion and F···H contacts to an amine proton (F···H = 2.1 Å) and to the aromatic protons on six different ligands (F···H = 2.4 - 2.7 Å).

This result is very exciting because it represents a rare example of a supramolecular double-stranded helical polymer in which the polymer chains are held together through non-covalent interactions. Examples of supramolecular polymers formed from related pyridylimine ligands have already been discussed in chapter 5 (section 5.1.2), however, these single-stranded helical polymers are not intertwined. Numerous examples of other single-stranded helical polymers also exist[8] but only a few double-stranded polymeric helices have been reported.[9] An example of a silver(I) double-stranded polymer similar to the one discussed here was reported by Reger and co-workers in 2004 (Figure 6.9).[10]

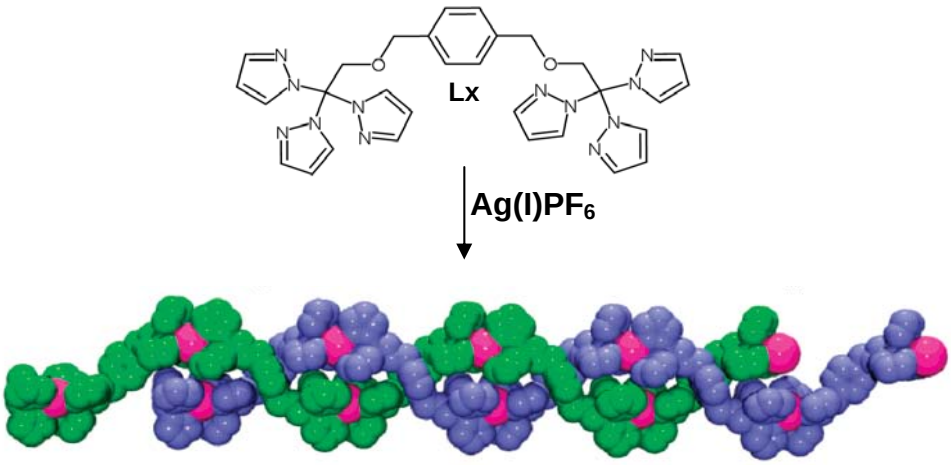

Figure 6.9. Reger's double-stranded helical polymer.[10]

Reger used ligand **Lx** and silver(I) to construct the double-stranded helix shown in Figure 6.9. The double-stranded architecture is made up of two intertwined single-stranded helices. The polymer was formed by the simple mixing of the ligand and silver(I) starting material in a similar way to $\{Ag(\mathbf{L}^{7})(PF_6)\}_{\infty}$ and gives an analogous double-stranded helix.

Another more sophisticated example is the double-stranded helical metallo-supramolecular polymer reported by Yashima *et al.* (Figure 6.10).[11]

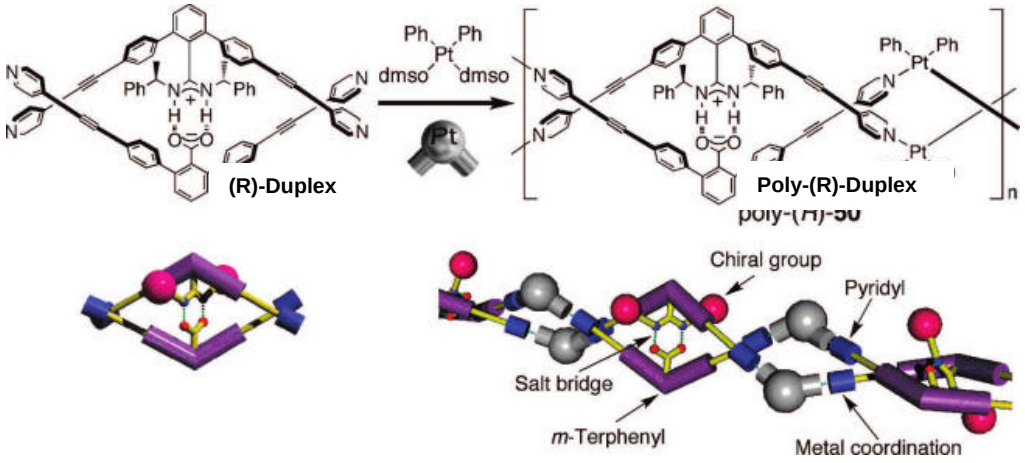

Figure 6.10. Yashima's double-stranded metallo-supramolecular helical polymer with complementary strands.[11]

This double-stranded polymer consists of two complementary metallo-polymer strands wrapped around each other in a helical fashion. The polymer is formed

from two different bis-monodentate ligands which are modified with either an amidinium group or carboxylate group. This is in contrast to $\{Ag(\mathbf{L^7})(PF_6)\}_\infty$ which is synthesised from a single bis-bidentate ligand. As shown in Figure 6.10, Yashima's helix is held together by chiral amidinium-carboxylate salt bridges and the helicity is controlled by the use of either (*R*)- or (*S*)-phenylethyl groups. It is formed by first synthesising the (R)-duplex structure and then carrying out the polymerisation reaction to form the double helical polymer. Yashima's system is more advanced than $\{Ag(\mathbf{L^7})(PF_6)\}_\infty$ because it does not form a racemic mixture but enables the helicity of the structures to be controlled.

The coordination chemistry of copper(I) with ligand $\mathbf{L^7}$ has also been investigated.

6.2.3 Copper(I) complex of $\mathbf{L^7}$

Coordination of $\mathbf{L^7}$ to copper(I) was achieved by the reaction of tetrakis(acetonitrile)copper(I) hexafluorophosphate with one equivalent of $\mathbf{L^7}$ in methanol. The reactants were heated under reflux for six hours whilst maintaining a nitrogen atmosphere. The resultant solution was concentrated under reduced pressure and the purple product precipitated in 98 % yield by the addition of diethyl ether.

Partial microanalytical data are consistent with a $\{Cu(C_{22}H_{17}N_7)(PF_6)\}_n$ formulation. The ESI mass spectrum of this complex is shown in Figure 6.11.

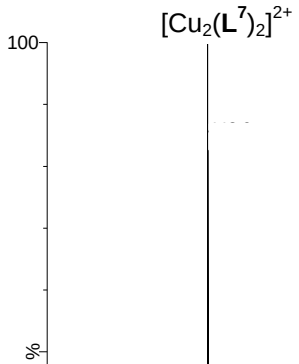

Figure 6.11. The ESI mass spectrum of $\{Cu(C_{22}H_{17}N_7)(PF_6)\}_n$.

The most abundant peak appears at *m/z* 442 and corresponds to the dimeric species $[Cu_2L_2]^{2+}$. A weak peak for the monomeric species $[CuL_2]^+$ (*m/z* 821) is also observed, however, this is probably formed by fragmentation during electrospray ionisation. Infrared spectroscopy reveals a strong peak corresponding to the non-coordinated PF_6^- counter-ions at 845 cm^{-1} and a broad band at 3429 cm^{-1} which is attributed to the central amine group. The ^1H NMR spectrum of this complex was recorded in d_3-acetonitrile and is presented in Figure 6.12.

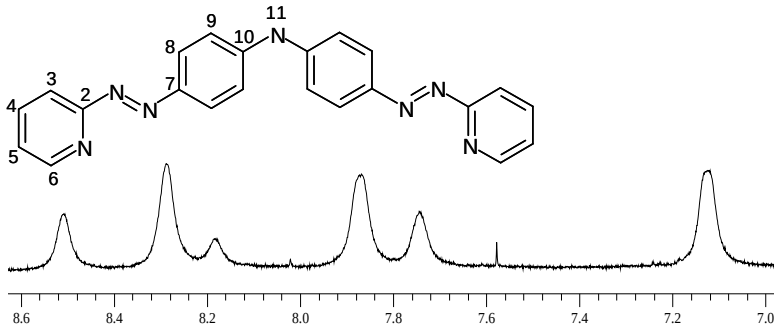

Figure 6.12. ^1H NMR spectrum of $\{Cu(C_{22}H_{17}N_7)(PF_6)\}_n$ (500 MHz, d_3-acetonitrile, 298 K).

The spectrum shows a single set of broad resonances. The NMR signals remain broad even on cooling down to 233 K. Broad room temperature spectra

were also obtained in d_6-dmso, d_4-methanol and d_3-nitromethane solutions. The mass spectrum results showed that each copper centre has a monocationic charge, however, the observed broadening could be due to the formation of a trace quantity of a copper(II) species from the oxidation of the metal centre.

Unfortunately, attempts to grow X-ray quality crystals of this complex proved unsuccessful. However, the structure of this complex is expected to be similar to that of Hannon's copper(I) complex formed from the analogous ligand $\mathbf{L^{azo}}$. In solution, the $\mathbf{L^{azo}}$ complex exists as a mixture of two dimeric isomers: a helicate and a box (Figure 6.13).[2,12]

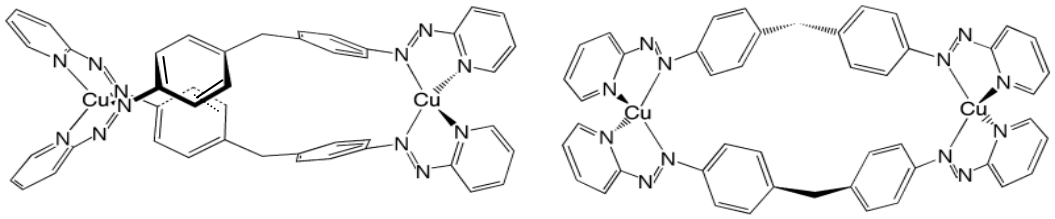

Figure 6.13. Representation of helix and box conformations of $[Cu_2(\mathbf{L^{azo}})_2]^{2+}$.

The coordination chemistry of ligand $\mathbf{L^7}$ has also been investigated with palladium(II).

6.2.4 Palladium(II) complex of L^7

The complex was prepared by stirring tetrakis(acetonitrile)palladium(II) tetrafluoroborate with one equivalent of ligand $\mathbf{L^7}$ under an argon atmosphere for 16 hours. The solvent was removed under vacuum and the *crude* material washed with methanol and diethyl ether to yield a dark blue solid in 78 % yield.

The FT-IR spectrum exhibits strong peaks at 1084 cm^{-1} and at 3438 cm^{-1}; These are characteristic of non-coordinated tetrafluoroborate anions

and secondary amines, respectively. The elemental analysis data are consistent with an empirical formula of $\{Pd(C_{22}H_{17}N_7)(BF_4)_2\}_n$. This complex does not fly well in electrospray mass spectrometry which could be consistent with a polymeric solution structure. However, the positive ion ESI mass spectrum does shows weak peaks corresponding to $[Pd_2L_2]^{2+}$ (m/z 485.0) and $[PdL_2 - H^+]^+$ (m/z 863.1). The charge of the mono-cationic peak implies that the central nitrogen can become deprotonated during electrospray ionization, thereby decreasing the overall charge of the cationic species. From previous studies it is also known that the palladium(II) ion can become reduced to palladium(I). While these results may indicate the presence of a dimeric and monomeric species, the observed peaks could be fragments of a higher mass polymeric species. The ^{1}H NMR spectrum of this complex has been recorded in d_3-acetonitrile, at 298 K. At this temperature a broad set of signals are observed. To investigate this further, a variable temperature ^{1}H NMR experiment has been performed in d_3-acetonitrile. Spectra were recorded from the same NMR sample at 298 K, 273 K and 233 K and are shown in Figure 6.14.

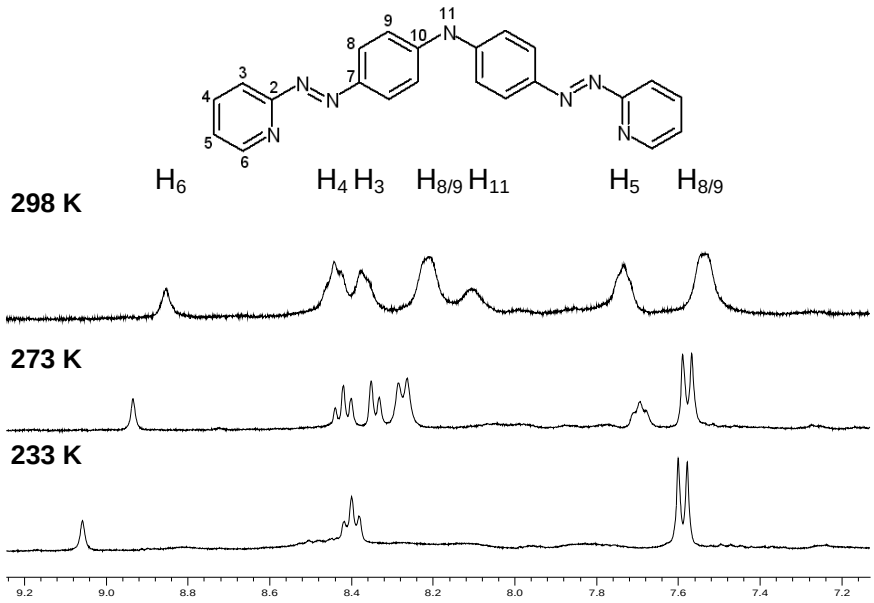

Figure 6.14. ^{1}H NMR spectra of the palladium(II) complex of **L^{7}** at 298 K, 273 K and 233 K (400 MHz, d_3-acetonitrile).

At room temperature, the ^{1}H NMR spectrum displays a broad set of signals. This broadening may arise from the presence of two or more, inter-changeable solution species or from the instability of the complex in solution. However, on cooling the sample down to 273 K, sharper signals were obtained and only a single set of resonances is seen. If multiple species had been present, cooling would normally slow down the inter-conversion of the species, resulting in an NMR spectrum with a set of signals for each species. Therefore, it is more probable that the ligands are in exchange with the d_3-acetonitrile solvent molecules than with each other. However, a ^{1}H NMR spectrum run in the non-coordinating, d_3-nitromethane, gave a similar broad spectrum. Further cooling to 233 K resulted in the coalescence of the phenyl peaks.

Numerous attempts were made to grow X-ray quality crystals of this complex. However, all attempts were unfortunately unsuccessful. Since it is unclear from the data obtained whether a discrete or polymeric species has been formed, the corresponding complex with the pyridyimine ligand **L^{6}** was

also prepared in hope that it might provide further insight. As discussed in section 6.1, ligand **L**^{6} is analogous to ligand **L**^{7}.

6.3 Palladium(II) complex of L^{6}

The synthesis of ligand **L**^{6} has already been described in chapter 4. The corresponding palladium(II) complex was formed by stirring a 1:1 ratio of **L**^{6} with tetrakis(acetonitrile)palladium(II) tetrafluoroborate under an argon atmosphere. After 16 hours, the solvent was removed under vacuum to yield an orange product. Attempts were made to purify this complex by washing with methanol, chloroform and diethyl ether.

To investigate the solution behaviour of this complex, ^{1}H NMR spectra were recorded in d_3-acetonitrile and d_3-nitromethane (Figure 6.15).

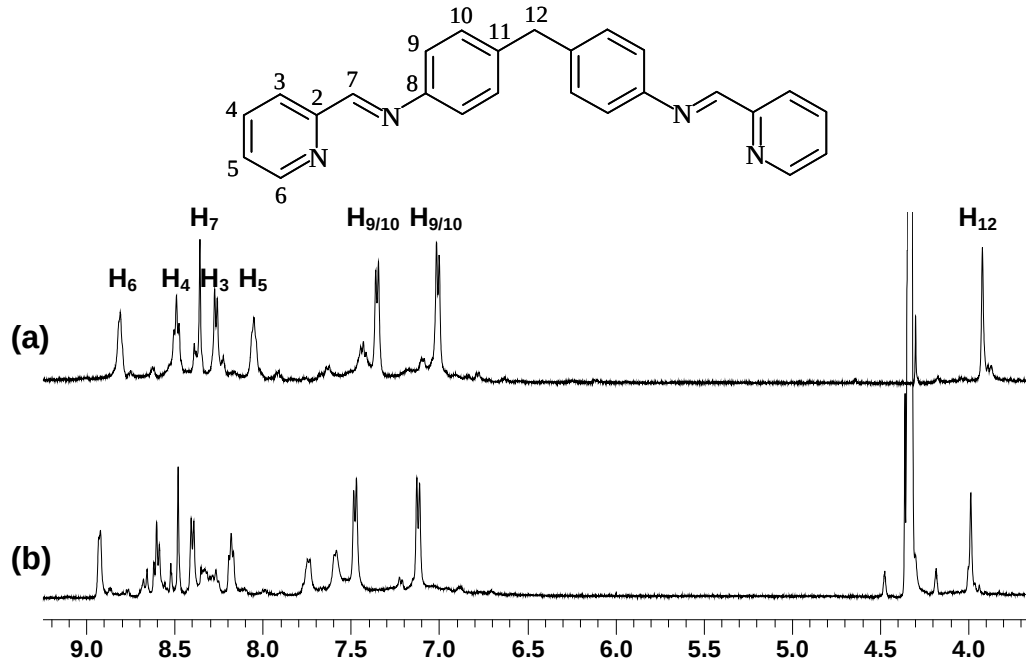

Figure 6.15. ^{1}H NMR spectra of the palladium(II) complex of **L**^{6} in (a) d_3-acetonitrile and (b) d_3-nitromethane solution (400 MHz, 298 K).

One main set of signals is observed in both spectra, however, numerous smaller resonances are also present. This indicates the presence of one major product and at least one minor product, possibly the box and helix

conformations that have already been discussed. Low temperature studies were carried out (Figure 6.16) and appear to show an increase in the ratio of the minor component(s) at low temperature. This would be consistent with a box-helix equilibrium in which the one species is enthalpically favoured and the other entropically favoured as is seen in cuprous box-helix equilibrium with this ligand.[12]

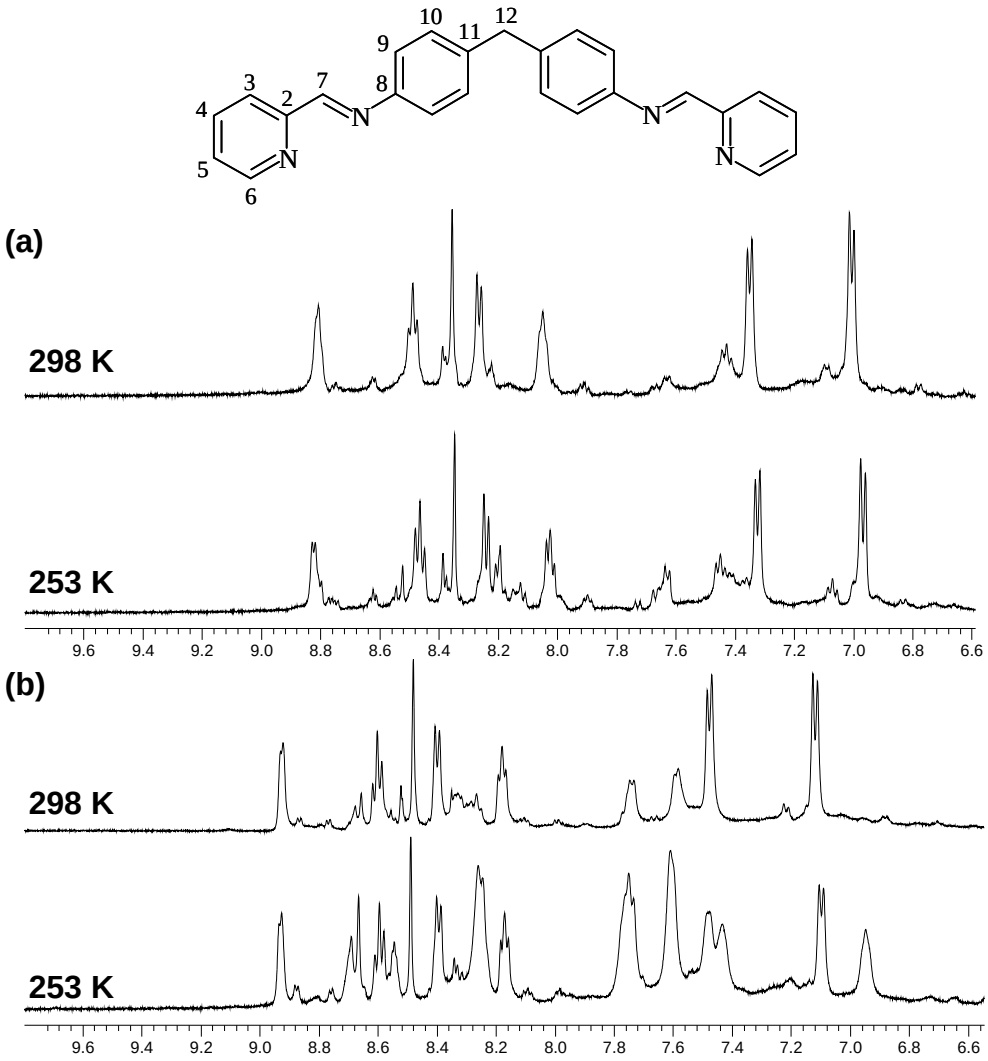

Figure 6.16. 500 MHz ^{1}H NMR spectra of the palladium(II) complex of **L^{6}** in (a) d_3-acetonitrile and (b) d_3-nitromethane solution

The ESI mass spectrometry results show the presence of a multitude of different solution species (Figure 6.17) indicating that the complex may be more complicated than a two species equilibrium or that it is not stable in solution.

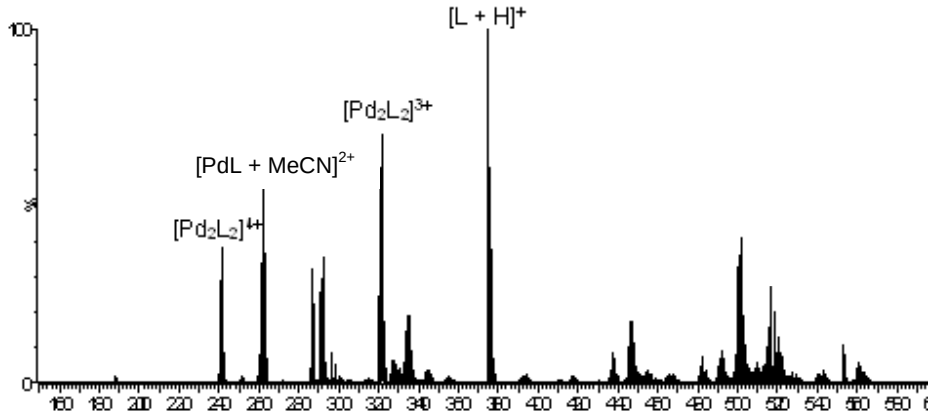

Figure 6.17. ESI mass spectrum of the palladium(II) complex of **L**^{6}.

Unfortunately, attempts to grow X-ray quality crystals of this complex were also unsuccessful.

6.4 Conclusions

In this chapter the synthesis and characterisation of a novel pyridylazo ligand (**L**^{7}) has been discussed. The ligand is analogous to Hannon's **L**^{azo} except that the spacer has been modified by exchanging the central methylene group for an amine substituent.

L^{7} has been utilized in the synthesis of three novel metallo-complexes. Surprisingly, the solid state structure of the silver(I) complex of **L**^{7} does not reveal the dimeric species seen for **L**^{azo} but instead shows it to have a polymeric $\{Ag(C_{22}H_{17}N_7)(PF_6)\}_\infty$ architecture. These polymer chains have been shown to pack together to form double-stranded helices that are held together by π-π stacking interactions.

With a M_2L_2 formulation, the copper(I) complex of **L**^{7} is analogous to the previously reported copper structures of **L**^{azo} and **L**^{6}.

The palladium(II) complex of **L**^{7} has a $\{Pd(C_{22}H_{17}N_7)(BF_4)_2\}_n$ formulation, however it remains unclear whether the complex formed has a dimeric or polymeric structure. The palladium(II) complex of **L**^{6} was prepared in hope that it might provide further insight. Data obtained for this complex indicated that the palladium(II) complexes may contain a number or inter-converting species or that they are not stable in solution.

6.5 Experimental

6.5.1 General

All solvents and reagents were purchased from Sigma-Aldrich and were used without further purification. ^{1}H NMR spectra were recorded on AC300 and DRX 500 MHz Brüker spectrometers and were processed using standard Brüker software. Variable temperature NMR experiments were performed by Dr Neil Spencer using a DRX 500 MHz Brüker spectrometer. Infrared spectra were recorded from KBr pellets on a Perkin Elmer Paragon 1000 FT-IR spectrometer. UV/Visible spectra were recorded using a Cary 5000 Varian spectrophotometer and quartz cuvettes. Electrospray Ionisation (ESI) spectra were recorded on a Micromass LCT Time of flight mass spectrometer in positive ionization mode**.** Microanalyses data were obtained using a CE Instruments EA1110 elemental analyser.

6.5.2 Synthesis of Ligand L^{7}

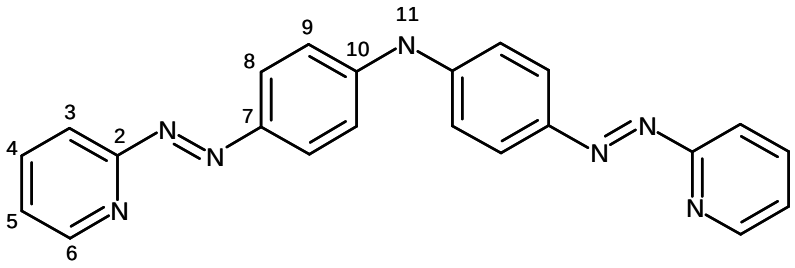

$C_{22}H_{17}N_7$
FW: 379.15

2-Nitrosopyridine[4] (0.150 g, 1.388 mmol), 4,4'-diaminodiphenylamine[5] (0.138 g, 0.694 mmol) and 2 drops of acetic acid were stirred together in dichloromethane (25 ml) for 48 hours. The red precipitate was filtered and washed with diethyl ether (8 ml). The *crude* product was purified by preparative RP-HPLC using a gradient of 100 % water to 100 % methanol over 40 minutes with a 10 minute

methanol wash. The product peak was observed and collected at 38.10 minutes (0.171 g, 65 % yield).

^{1}H NMR (300 MHz, $CDCl_3$, 298 K): δ 8.73 (2H, d, *J*= 4.8 Hz, H_6), 8.08 (4H, d, *J*= 8.8 Hz, $H_{8/9}$), 7.91 (2H, td, *J*= 7.8, 1.6 Hz, H_4), 7.83 (2H, d, *J*= 7.8 Hz, H_3), 7.38 (2H, dd, *J*= 7.8, 4.8 Hz, H_5), 7.33 (4H, d, *J*= 8.8 Hz, $H_{8/9}$), 6.66 (1H, s, H_{11}).

^{13}C NMR (400 MHz, $CDCl_3$, 300 K): δ 163.2 $C_{2/7/10,}$ 149.5 C_6, 147.4 $C_{2/7/10,}$ 145.3 $C_{2/7/10,}$ 138.2 $C_{4,}$ 125.8 $C_{8/9}$, 124.7 $C_{5,}$ 117.8 $C_{8/9}$, 115.4 C_3.

Mass Spectrum (ESI): *m/z* 402.1 $\{Ligand + Na\}^+$, 380.2 $\{Ligand + H\}^+$.

Elemental analysis (%) calculated for $C_{22}H_{17}N_7$: C: 69.6; H: 4.5; N: 25.8; Found: C: 69.6; H: 3.9; N: 25.2.

IR (KBr): ν= 3425(s), 1589(s), 1500(w), 1460(w), 1192(w), 1140(s), 829(w), 788(w), 741(w), 668(w) cm^{-1}.

6.5.3 Synthesis of silver(I) complex of L^7

Ligand **L^7** (0.010 g, 0.026 mmol) was dissolved in methanol (5 ml) to form an orange solution. Light was excluded from the reaction vessel and silver(I) acetate (0.004 g, 0.026 mmol) was added. The solution was heated under reflux for 3 hours resulting in the formation of a red solution. A red/brown solid precipitated on addition of methanolic ammonium hexafluorophosphate. The precipitate was isolated by filtration, washed with diethyl ether (5 ml) and dried *in vacuo* (12 mg).

^{1}H NMR (300 MHz, CD_3CN, 298 K): δ 8.71 (2H, d, *J*= 5.1 Hz, H_6), 8.17 (2H, td, *J*= 7.7, 1.6 Hz, H_4), 8.00-7.97 (3H, m, $H_{3\&11}$), 7.84 (4H, d, *J*= 8.9 Hz, $H_{8/9}$), 7.65 (2H, dd, *J*= 7.7, 5.1 Hz, H_5), 7.14 (4H, d, *J*= 8.9 Hz, $H_{8/9}$).

Mass Spectrum (ESI): *m/z* 1119.0 $\{Ag_2L_2 + PF_6\}^+$, 867.2 $\{AgL_2\}^+$, 487.0 $\{Ag_2L_2\}^{2+}$.

Elemental analysis (%) calculated for $[Ag(C_{22}H_{17}N_7)](PF_6)\cdot(CH_3CN)_{0.25}$: C: 42.1; H: 2.8; N: 15.8; Found: C: 42.5; H: 2.6; N: 15.4.

IR (KBr): ν= 3417(s), 2360(w), 1617(s), 1589(m), 1541(m), 1501(m), 1396(m), 1363(m), 1302(m), 1233(w), 1136(s), 850(s) cm^{-1}.

UV/Vis (CD_3CN): λmax (nm) = 268, 444.

6.5.4 Synthesis of copper(I) complex of L^7

Ligand **L^7** (0.015 g, 0.038 mmol) was dissolved in methanol (5 ml) and stirred under a nitrogen atmosphere. Tetrakis(acetonitrile)copper(I) hexafluorophosphate (0.015 g, 0.038 mmol) was added and the solution heated under reflux for 6 hours. The reaction mixture was allowed to cool and the volume of the filtrate was reduced under vacuum. Diethyl ether was added dropwise to precipitate the purple product. The *crude* product was washed with chloroform (3 ml) and diethyl ether (3 ml) and dried over P_4O_{10} (21 mg, 94 % yield).

^{1}H NMR (500 MHz, CD_3CN, 298 K): δ 8.51 (2H, bs), 8.29 (4H, bs), 8.18 (1H, bs), 7.87 (4H, bs), 7.74 (2H, bs), 7.12 (4H, bs).

Mass Spectrum (ESI): *m/z* 1029.1 $\{Cu_2L_2 + PF_6\}^+$, 442.0 $\{Cu_2L_2\}^{2+}$.

Elemental analysis (%) calculated for $[Cu(C_{22}H_{17}N_7)](PF_6)\cdot(CH_3O_2)_{0.5}$: C: 44.2; H: 3.1; N: 16.1; Found: C: 44.5; H: 2.9; N: 15.4.

IR (KBr): ν= 3429(br), 2919(w), 2360(w), 1582(s), 1529(w), 1500(w), 1443(w), 1303(m), 1242(w), 1203(w), 1141(s), 845(s) cm^{-1}.

UV/Vis (CD_3CN): λmax (nm) = 276, 486.

6.5.5 Synthesis of palladium(II) complex of L^7

Tetrakis(acetonitrile)palladium(II) tetrafluoroborate (0.017 g, 0.038 mmol) was added to a degassed suspension of ligand **L^7** (0.015 g, 0.038 mmol) in acetonitrile (6 ml). The solution immediately turned dark blue and was stirred overnight under an argon atmosphere. The solvent was removed under vacuum and the *crude* material washed with methanol (5 ml) and diethyl ether (5 ml) to yield a dark blue solid (19 mg, 76 % yield).

^{1}H NMR (400 MHz, CD_3CN, 273 K): δ 8.93 (2H, bs, H_6), 8.42 (2H, t, *J*= 7.9 Hz, H_4), 8.34 (2H, d, *J*= 7.9 Hz, H_3), 8.27 (5H, d, *J*= 8.7 Hz, $H_{8/9\&11}$), 7.71-7.68 (2H, m, H_5), 7.58 (4H, d, *J*= 8.7 Hz, $H_{8/9}$).

Mass Spectrum (ESI): *m/z* 863.1 $\{PdL_2 - H^+\}^+$, 485.0 $\{Pd_2L_2\}^{2+}$, 380.2 $\{L + H\}^+$.

Elemental analysis (%) calculated for $[Pd(C_{22}H_{17}N_7)][BF_4]_2$: C: 40.1; H: 2.6; N: 14.9; Found: C: 39.5; H: 2.9; N: 13.6.

IR (KBr): ν= 3438(br), 2360(m), 1582(s), 1530(m), 1494(m), 1462(w), 1305(s), 1242(s), 1140(b), 1084(s), 833(w) cm^{-1}.

UV/Vis (MeCN): λmax (nm) = 296, 614.

6.5.6 Synthesis of palladium(II) complex of L^6

Tetrakis(acetonitrile)palladium(II) tetrafluoroborate (0.031 g, 0.07 mmol) was added to a degassed suspension of ligand **L^6** (0.026 g, 0.07 mmol) in acetonitrile (4 ml). The solution immediately turned yellow and was stirred overnight under an argon atmosphere. The solvent was removed under vacuum to yield an orange solid. The crude product was washed with chloroform and diethyl ether, dissolved in nitromethane, filtered and then the solvent removed again to yield the yellow product (18 mg, 39 % yield).

^{1}H NMR (400MHz, CD_3NO_2, 298K): δ 8.94-8.92 (2H, m, H_6), 8.60-8.58 (2H, m, H_4), 8.49 (2H, s, H_7), 8.40 (2H, d, *J*= 7.3 Hz, H_3), 8.20-8.16 (2H, m, H_5), 7.45 (4H, d, *J*= 8.3 Hz, $H_{9/10}$), 7.11 (4H, d, *J*= 8.3 Hz, $H_{9/10}$), 3.98 (2H, s, H_{12}).

6.6 References

1. U. McDonnell, J. M. C. A. Kerchoffs, R. P. M. Castineiras, M. R. Hicks, A. C. G. Hotze, M. J. Hannon, A. Rodger, *Dalton Trans.*, **2008**, 667–675; M. J. Hannon, C. L. Painting, A. Jackson, J. Hamblin, W. Errington, *Chem. Commun.*, **1997**, 1807–1808; J. M. C. A. Kerckhoffs, J. C. Peberdy, I. Meistermann, L. J. Childs, C. J. Isaac, C. R. Pearmund, V. Reudegger, S. Khalid, N. W. Alcock, M. J. Hannon, A. Rodger, *Dalton Trans.*, **2007**, 734–742; G. I. Pascu, A. C. G. Hotze, C. Sanchez-Cano, B. M. Kariuki, M. J. Hannon, *Angew. Chem. Int. Ed.*, **2007**, 46, 4374–4378.
2. L. J. Childs, *PhD Thesis*, University of Warwick, **2002**.
3. A. C. G. Hotze, B. M. Kariuki, M. J. Hannon, *Angew. Chem. Int. Ed*., **2006**, 45, 4839 –4842.
4. E. C. Taylor, C. P. Tseng, J. B. Rampal, *J. Org. Chem.,* **1982**, 47, 552-555.
5. I. Kulszewicz-Bajer, I. Rozalska, M. Kuryłek, *New. J. Chem.*, **2004**, 28, 669–675.
6. X-ray crystal data were collected and solved by Dr. Louise Male at the University of Birmingham.
7. X-ray crystal data were collected and solved by Dr. Benson Kariuki at the University of Birmingham.
8. A. N. Khlobystov, A. J. Blake, N. R. Champness, D. A. Lemenovskii, A. G. Majouga, N. V. Zykand, M. Schröder, *Coord. Chem. Rev.,* **2001**, 222, 155–192; J. P. Zhang, Y. Y. Lin, X. C. Huang, X. M. Chen, *Chem. Commun*., **2005**, 1258–1260; X. D. Chen, T. C. W. Mak, *Dalton Trans*., **2005**, 3646–3652; K. Biradha, C. Seward, M. J. Zaworotko, *Angew. Chem. Int. Ed*., **1999**, 38, 492-495.
9. N. Ohata, H. Masuda, O. Yamauchi, *Angew. Chem. Int. Ed. Eng.,* **1996,** 35, 531-532; B. F. Abrahams, S. R. Batten, H. Hamit, B. F. Hoskins, R. Robson, *Chem. Commun.,* **1996**, 1313-1314; K. V. Domasevitch, I. Boldog, E. B. Rusanov, J. Hunger, S. Blaurock, M. Schröder, J. Sieler, *Z. Anorg. Allg. Chem.,* **2005**, *631*, 1095-1100; L. Han, H. Valle, X. Bu, *Inorg. Chem.*, **2007**, 46, 1511-1513.

10. D. L. Reger, R. F. Semeniuc, V. Rassolov, M. D. Smith, *Inorg. Chem.*, 43, **2004**, 537-554.
11. M. Ikeda, Y. Tanaka, T. Hasegawa, Y. Furusho, E. Yashima, *J. Am. Chem. Soc*., **2006**, 128, 6806-6807; E. Yashima, K. Maeda, Y. Furusho, *Acc. Chem. Res.*, **2008**, 41, 1166-1180.
12. L. J. Childs, M. Pascu, A. J. Clarke, N. W. Alcock, M. J. Hannon, *Chem. Eur. J*., **2004**, 10, 4291-4300.

Chapter 7

Conclusions and Future Work

As discussed in chapter 1, metallo-supramolecular chemistry is an attractive tool for the self-assembly of a range of different architectures. During this work to develop new metallo-supramolecular complexes, a number of novel organic ligands have been prepared.

In chapter 2, the synthesis of four palladium(II) and two platinum(II) tetra-stranded, dinuclear complexes has been described. To the best of our knowledge there are no other examples of similar tetra-stranded, dinuclear platinum(II) complexes reported in the literature. Biological investigations were carried out on four of the palladium(II) complexes. Gel electrophoresis and AFM experiments revealed that all four bind to DNA and promote localised changes in the DNA structure. Cytotoxicity experiments demonstrated that two of the cylinders showed good activity in a selection of cancer cell lines, while the other two were inactive. Preliminary results showed that the two active cylinders also proved to be non-mutagenic and non-genotoxic. The drawback of these complexes is that they are insoluble in water and only sparingly soluble in some water/solvent mixtures. Future work needs to focus on improving the aqueous solubility. Further biological testing also needs to be carried out to fully elucidate the mode of action of the cylinders. Due to time constraints the biological activities of the platinum(II) complexes were not studied and these also require investigation.

In chapter 4, the synthesis and characterisation of two new dinuclear cis-platin type compounds was discussed. Gel electrophoresis and CD and LD studies show that both of the compounds bind to DNA disturbing the orientation and stacking of the nucleotide bases. Cytotoxicity testing revealed that the compounds were active against A2780 and T47D cell lines but were less active

than cis-platin. Future work could involve reactions of the compounds with model bases to find out whether they bind to the bases of DNA. It would also be interesting to exchange the chlorine atoms for other ligands such as 2,2'-bipyridine and to investigate the biological activities of the resulting complexes.

In chapter 5, the coordination chemistry of silver(I) was investigated and resulted in the formation of four metallo-supramolecular polymers which were characterised crystallographically. The crystal structures highlight the importance of the conformation of the ligand and of inter-molecular interactions for linking the polymers together into two and three dimensional networks.

In chapter 6, a new pyridylazo ligand system was developed and the coordination chemistry of this ligand investigated. One of the complexes that was synthesised from this ligand was a silver(I) polymer. The solid state structure showed that the polymer chains pair up and intertwine to form a racemic mixture of double helices. This result is very interesting because it represents a rare example of a supramolecular double-stranded helical polymer, whereas Hannon's previously reported analogous ligands had formed double-stranded dinuclear complexes. This demonstrates that small changes in the ligand can result in dramatic changes in the resulting complexes. Future work would be to investigate the coordination chemistry of this ligand with other metal ions.